



University
of Glasgow

Facchini, Mark (2010) *A study of cobalt catalysts for Fischer-Tropsch synthesis*. MSc(R) thesis.

<http://theses.gla.ac.uk/2013/>

Copyright and moral rights for this thesis are retained by the author

A copy can be downloaded for personal non-commercial research or study, without prior permission or charge

This thesis cannot be reproduced or quoted extensively from without first obtaining permission in writing from the Author

The content must not be changed in any way or sold commercially in any format or medium without the formal permission of the Author

When referring to this work, full bibliographic details including the author, title, awarding institution and date of the thesis must be given

A Study of Cobalt Catalysts for Fischer-Tröpsch Synthesis

by

Mark Facchini ©

July 2010



University
of Glasgow

A thesis submitted for the degree of Master of
Science in the Faculty of Physical Sciences, University
of Glasgow.

Abstract

In the following study two 20 wt% Co/Al₂O₃ catalysts were characterised. The difference in activity, selectivity and deactivation of these two catalysts, under typical low-temperature Fischer- Tröpsch (LTFT) conditions, were studied. The effect of co-feeding different liquids: alcohols, alkanes and aromatics into the system were also studied. Techniques used in this study included Brunauer, Emmett, Teller (BET) surface area analysis, Thermo-gravimetric analysis (TGA), Temperature-programmed-reduction (TPR), powder X-Ray Diffraction (XRD), TPR-UV-vis-NIR spectroscopy and Transmission Electron Microscopy (TEM).

Table of contents

| | |
|---|-----------|
| Abstract | 2 |
| Table of contents | 3 |
| List of tables..... | 8 |
| List of figures..... | 9 |
| Acknowledgements..... | 15 |
| Declaration | 16 |
| 1 Introduction | 17 |
| 1.1 Background of current research | 17 |
| 1.2 The Fischer-Tröpsch Synthesis (FTS) Reaction | 20 |
| 1.3 Fischer-Tröpsch catalysts..... | 21 |
| 1.4 Deactivation methods for FTS catalysts | 26 |
| 1.4.1 Deactivation of cobalt based catalysts in Fischer-Tröpsch synthesis (FTS) | 28 |
| 1.4.1.1 Oxidation..... | 28 |
| 1.4.1.1.1 Thermodynamic analysis of bulk cobalt metal | 29 |
| 1.4.1.1.2 Unsupported cobalt catalysts | 30 |
| 1.4.1.1.3 Alumina, silica, and titania supported cobalt catalysts..... | 30 |
| 1.4.1.1.4 Silica supported cobalt catalysts | 32 |
| 1.4.1.1.5 Titania supported cobalt catalysts | 33 |
| 1.4.1.1.6 Comparisons between catalysts on different supports | 33 |
| 1.4.1.2 Sulfur poisoning | 34 |
| 1.4.1.3 Carbon deposition / fouling | 36 |
| 1.4.1.4 Sintering..... | 37 |
| 1.4.1.5 Formation of compounds between cobalt and supports | 38 |
| 1.5 Reaction Mechanisms in Fischer-Tröpsch | 39 |
| 1.5.1 Mechanisms involving hydrocarbon intermediates | 41 |
| 1.5.2 Mechanisms involving oxygenated intermediates | 42 |
| 1.5.3 Mechanism involving methylene and CO insertion | 44 |
| 1.6 Use of different species in the study of F-T | 46 |
| 1.6.1 Using alcohol as probes..... | 46 |
| 1.6.2 Using alkenes as probes | 47 |
| 1.6.3 C1 and C2 molecules as probes | 48 |

| | | |
|-----------|---|-----------|
| 1.7 | Project Aims..... | 49 |
| 2 | Experimental..... | 50 |
| 2.1 | Catalyst preparation | 50 |
| 2.1.1 | Support properties | 50 |
| 2.1.2 | Preparation via the nitrate method | 51 |
| 2.1.2.1 | Procedure | 51 |
| 2.1.3 | Preparation via the High Dispersion Cobalt (HDC) catalyst method..... | 51 |
| 2.1.3.1 | Procedure | 52 |
| 2.1.3.2 | Observations..... | 52 |
| 2.2 | Characterisation Techniques..... | 54 |
| 2.2.1 | BET Surface area analysis..... | 54 |
| 2.2.2 | Thermo-gravimetric analysis (TGA)..... | 55 |
| 2.2.3 | Hot stage powder X-ray diffraction (XRD) | 55 |
| 2.2.4 | TPR-UV-vis-NIR spectroscopy | 57 |
| 2.2.5 | Transmission Electron Microscopy (TEM)..... | 57 |
| 2.3 | Catalytic testing | 57 |
| 2.3.1 | Apparatus..... | 57 |
| 2.3.2 | Reaction Procedure | 58 |
| 2.3.3 | Gas Chromatography (GC) | 60 |
| 2.3.3.1 | Column conditions | 60 |
| 2.3.3.1.1 | Method 1 - Light hydrocarbons:..... | 60 |
| 2.3.3.1.2 | Method 2 - Heavy hydrocarbons: | 61 |
| 2.3.3.2 | Calibrations | 62 |
| 2.3.3.2.1 | Light hydrocarbons | 62 |
| 2.3.3.2.2 | Heavy molecular weight calibrations | 64 |
| 2.3.4 | Soxhlet extractions | 66 |
| 2.4 | Materials | 67 |
| 2.4.1 | Reactions | 67 |
| 2.4.2 | Product characterisation and analysis | 68 |
| 2.4.3 | Catalysts studied | 68 |
| 2.5 | Calculations | 69 |
| 2.5.1 | Conversion CO/H ₂ O | 69 |
| 2.5.2 | Selectivity | 69 |
| 2.5.3 | Anderson-Schulz-Flory (ASF) graph | 69 |
| 2.5.4 | Alpha value (α) | 69 |

| | | |
|----------|--|-----------|
| 2.5.4.1 | Background / theory of ASF and alpha plots for F-T..... | 69 |
| 3 | Design and Commissioning of Fischer-Tröpsch (F-T) reactor | 73 |
| 3.1 | Fischer-Tröpsch reactors | 73 |
| 3.1.1 | Circulating fluidised bed reactor (CFB) | 75 |
| 3.1.2 | Fixed fluidised bed reactor (FFB) | 75 |
| 3.1.3 | Slurry phase reactor | 75 |
| 3.1.4 | Tubular fixed bed reactor..... | 75 |
| 3.1.5 | Comparison of F-T reactors..... | 76 |
| 3.2 | Reactor design and build | 76 |
| 3.2.1 | Safety | 77 |
| 3.2.1.1 | Pressure | 77 |
| 3.2.1.2 | Temperature..... | 77 |
| 3.2.1.3 | Flow..... | 77 |
| 3.2.2 | Process..... | 78 |
| 3.2.2.1 | Gas feed..... | 78 |
| 3.2.2.2 | Liquid feed..... | 78 |
| 3.2.2.3 | Traps..... | 79 |
| 3.2.2.4 | Oven | 80 |
| 3.2.2.5 | Reactor | 81 |
| 3.2.2.6 | Silica lining | 82 |
| 3.2.3 | Conclusion..... | 82 |
| 4 | Results..... | 84 |
| 4.1 | Cobalt/alumina catalyst prepared via the nitrate method..... | 84 |
| 4.1.1 | Characterisation..... | 84 |
| 4.1.1.1 | Thermo-gravimetric Analysis (TGA) | 84 |
| 4.1.1.2 | BET Surface area analysis..... | 89 |
| 4.1.1.3 | Powder and hot stage powder X-ray diffraction (XRD) | 90 |
| 4.1.1.4 | TPR-UV-vis-NIR spectroscopy..... | 91 |
| 4.1.1.5 | Transmission Electron Microscopy (TEM) | 92 |
| 4.1.2 | Reaction at 210°C and 220°C | 93 |
| 4.1.2.1 | Reaction at 210°C..... | 94 |
| 4.1.2.2 | Reaction at 220°C..... | 99 |
| 4.1.2.3 | Post reaction analysis | 102 |
| 4.1.3 | Reaction with addition of octanol | 107 |
| 4.1.3.1 | Before octanol addition..... | 107 |

| | | |
|----------|--|------------|
| 4.1.3.2 | During octanol addition | 110 |
| 4.1.3.3 | Post reaction analysis | 118 |
| 4.1.4 | Reaction with addition of decanol then a mixture of naphthalene and dodecane | 123 |
| 4.1.4.1 | Before decanol addition | 123 |
| 4.1.4.2 | During decanol addition | 124 |
| 4.1.4.3 | After decanol feed turned off | 131 |
| 4.1.4.4 | Naphthalene and dodecane addition..... | 132 |
| 4.1.4.5 | Post reaction analysis | 132 |
| 4.2 | Cobalt/alumina catalyst prepared via High Dispersion Cobalt (HDC) catalyst method..... | 137 |
| 4.2.1 | Characterisation..... | 137 |
| 4.2.1.1 | Thermo-gravimetric Analysis (TGA) | 137 |
| 4.2.1.2 | BET Surface area analysis..... | 142 |
| 4.2.1.3 | Hot stage powder X-ray diffraction (XRD)..... | 143 |
| 4.2.1.4 | TPR-UV-vis-NIR spectroscopy..... | 145 |
| 4.2.1.5 | Transmission Electron Microscopy (TEM) | 145 |
| 4.2.2 | Reaction at 210°C | 146 |
| 4.2.2.1 | Post reaction analysis | 150 |
| 4.2.3 | Reaction with addition of octanol | 155 |
| 4.2.3.1 | Before octanol addition..... | 156 |
| 4.2.3.2 | During octanol addition | 159 |
| 4.2.3.3 | Post reaction analysis | 165 |
| 5 | Discussion..... | 169 |
| 5.1 | Characterisation | 169 |
| 5.1.1 | TGA..... | 169 |
| 5.1.2 | TPR/TPR..... | 171 |
| 5.1.3 | BET Surface area analysis..... | 172 |
| 5.1.4 | Transmission Electron Microscopy (TEM)..... | 172 |
| 5.1.5 | Powder and hot-stage powder X-ray diffraction (XRD) | 172 |
| 5.1.6 | TPR-UV-vis-NIR spectroscopy | 173 |
| 5.2 | Reaction chemistry | 174 |
| 5.2.1 | Reactions at 210°C (and 220°C in the case of Co/Al ₂ O ₃ (nitrate) catalyst) 174 | |
| 5.2.1.1 | Conversion | 174 |

| | | |
|----------|--|------------|
| 5.2.1.2 | Selectivity..... | 175 |
| 5.2.1.3 | Alpha value | 175 |
| 5.2.1.4 | Post reaction soxhlet extractions and TGA-DSC analysis..... | 176 |
| 5.2.2 | Reactions involving the co-feeding of octanol into the reactor ... | 177 |
| 5.2.2.1 | Conversion | 177 |
| 5.2.2.2 | Selectivity..... | 178 |
| 5.2.2.3 | Alpha value | 182 |
| 5.2.2.4 | Post reaction soxhlet extractions and TGA-DSC analysis..... | 182 |
| 5.2.3 | Reaction involving the co-feeding of decanol and 0.063M naphthalene solution into the reactor | 183 |
| 5.2.3.1 | Conversion | 184 |
| 5.2.3.2 | Selectivity..... | 184 |
| 5.2.3.3 | Alpha value | 185 |
| 5.2.3.4 | Post reaction soxhlet extractions and TGA-DSC analysis..... | 186 |
| 5.3 | Summary | 187 |
| 5.4 | Future work..... | 187 |
| 6 | References | 188 |

List of tables

| | |
|--|-----|
| Table 1-1 Comparison of the characteristic features of iron and cobalt F-T catalysts | 25 |
| Table 1-2 Influence of sulfur content of synthesis gas on the rate of activity decline for fluidised iron catalyst at about 320°C[70]. | 27 |
| Table 2-1 Support properties of HP14/150 gamma alumina | 50 |
| Table 2-2 Laboratory prepared catalysts | 53 |
| Table 2-3 Light hydrocarbons GC temperature ramp profile | 61 |
| Table 2-4 Heavy hydrocarbons GC temperature ramp profile | 62 |
| Table 2-5 Data table for light hydrocarbon calibrations..... | 63 |
| Table 2-6 Data table for heavy hydrocarbon calibrations (even carbon numbers) | 65 |
| Table 2-7 Data table for heavy hydrocarbon calibrations (odd carbon numbers) | 66 |
| Table 2-8 Materials used for reactions and GC analysis | 68 |
| Table 2-9 Materials used for characterisation and analysis | 68 |
| Table 2-10 Catalysts studied..... | 69 |
| Table 4-1 Surface area analysis of lab prepared Co/Al ₂ O ₃ (nitrate) catalyst..... | 89 |
| Table 4-2 Quantification of moles of octanol and tetradecanol in liquid organic phase | 114 |
| Table 4-3 Quantification of moles of octanol and tetradecanol in wax phase .. | 116 |
| Table 4-4 Selectivity differences between 408 and 432 hrs TOS | 118 |
| Table 4-5 Quantification of moles of octanol and decanol in light organic phase | 127 |
| Table 4-6 Quantification of moles of octanol and decanol in wax phase | 129 |
| Table 4-7 Surface area analysis of lab prepared Co/Al ₂ O ₃ (HDC) catalyst | 142 |
| Table 4-8 Quantification of moles of octanol and dodecane in light organic phase | 161 |
| Table 4-9 Quantification of moles of octanol, tetradecanol and dodecane in wax phase | 163 |
| Table 5-1 Mass balance data for Co/Al ₂ O ₃ (nitrate) catalyst..... | 179 |
| Table 5-2 Mass balance data for Co/Al ₂ O ₃ (HDC) catalyst | 180 |
| Table 5-3 Mass balance data for Co/Al ₂ O ₃ (nitrate) catalyst during addition decanol..... | 185 |

List of figures

| | |
|--|----|
| Figure 1-1 List of existing GTL/CTL plants and those under construction[7]..... | 19 |
| Figure 1-2 Principal process steps of GTL plant[9] | 19 |
| Figure 1-3 CO hydrogenation over Group VIII metals..... | 21 |
| Figure 1-4 Thermodynamic equilibrium constants for three selected cobalt oxidation reactions[11]. (Note: the thermodynamic equilibrium for the oxidation of cobalt to Co_3O_4 is about 4 orders of magnitude lower than that of the oxidation to CoO)..... | 29 |
| Figure 1-5 Conceptual model of fouling, crystallite encapsulation and pore plugging of a supported metal catalyst due to carbon deposition [37]..... | 36 |
| Figure 1-6 Hydrocarbon selectivity as a function as function of the chain growth probability factor, α [76]..... | 40 |
| Figure 1-7 Proposed alkyl scheme based on the carbide mechanism[78] | 42 |
| Figure 1-8 Hydroxycarbene scheme[89]..... | 43 |
| Figure 1-9 CO insertion mechanism [91] | 43 |
| Figure 1-10 Mechanism 1 (M = iron or cobalt)..... | 45 |
| Figure 1-11 Mechanism 2 (M = iron or cobalt)..... | 45 |
| Figure 2-1 Graph of pH vrs Time (mins) of the deposition process. | 53 |
| Figure 2-2 Schematic of hot stage X-ray chamber | 56 |
| Figure 2-3 Reactor setup | 58 |
| Figure 2-4 Reduction programme before reaction..... | 59 |
| Figure 2-5 Start-up procedure | 60 |
| Figure 2-6 Light hydrocarbons GC temperature ramp profile..... | 61 |
| Figure 2-7 Heavy hydrocarbons GC Temperature ramp profile | 62 |
| Figure 2-8 Calibration graph for light hydrocarbons | 63 |
| Figure 2-9 Calibration graph for heavy hydrocarbons (even carbon numbers) ... | 64 |
| Figure 2-10 Calibration graph for heavy hydrocarbons (odd carbon numbers) ... | 65 |
| Figure 2-11 Soxhlet apparatus..... | 66 |
| Figure 2-12 Graph of N_{max} vrs alpha value | 71 |
| Figure 2-13 Graph of weight distribution vrs carbon chain length | 71 |
| Figure 2-14 Graph of Weight Fraction vrs alpha value | 72 |
| Figure 3-1 Types of F-T reactor in commercial use[107] | 74 |
| Figure 3-2 Detailed schematic of Fischer-Tröpsch reactor | 83 |

| | |
|--|-----|
| Figure 4-1 TGA analysis (weight loss/derivative weight vs temperature) of Co/Al ₂ O ₃ (nitrate) catalyst under 2%O ₂ /Ar feed | 85 |
| Figure 4-2 TGA analysis (weight loss/heat flow vs temperature) of Co/Al ₂ O ₃ (nitrate) catalyst under 2%O ₂ /Ar feed..... | 85 |
| Figure 4-3 TGA analysis (weight loss/derivative weight vs temperature) of Co/Al ₂ O ₃ (nitrate) catalyst under 5%H ₂ /N ₂ feed | 86 |
| Figure 4-4 TGA analysis (evolution of water) of Co/Al ₂ O ₃ (nitrate) catalyst under 5%H ₂ /N ₂ feed | 87 |
| Figure 4-5 TGA analysis (uptake of hydrogen) of Co/Al ₂ O ₃ (nitrate) catalyst under 5%H ₂ /N ₂ feed | 87 |
| Figure 4-6 TGA analysis (evolution of nitric oxide) of Co/Al ₂ O ₃ (nitrate) catalyst under 5%H ₂ /N ₂ feed | 88 |
| Figure 4-7 TGA measurement (TPR/TPD) of Co/Al ₂ O ₃ (nitrate) catalyst | 89 |
| Figure 4-8 Powder XRD graph of calcined Co/Al ₂ O ₃ (nitrate) catalyst..... | 90 |
| Figure 4-9 Hot-Stage XRD graph of Co/Al ₂ O ₃ (nitrate) catalyst under H ₂ | 91 |
| Figure 4-10 TPR-UV-vis-NIR spectroscopy graph of Co/Al ₂ O ₃ (nitrate) catalyst under H ₂ | 92 |
| Figure 4-11 TEM image for Co/Al ₂ O ₃ (nitrate) catalyst | 93 |
| Figure 4-12 Conversion vs TOS of reaction at 210°C..... | 94 |
| Figure 4-13 Moles of carbon products in liquid phase at 48 hrs TOS..... | 95 |
| Figure 4-14 Gas chromatogram of light hydrocarbons at 48 hrs TOS | 95 |
| Figure 4-15 Moles of carbon products in wax phase at 48 hrs TOS..... | 96 |
| Figure 4-16 Typical chromatogram of heavy hydrocarbons | 97 |
| Figure 4-17 Moles of carbon products in both liquid and wax phase at 48 hrs TOS | 97 |
| Figure 4-18 Change in selectivity at 210°C | 98 |
| Figure 4-19 ASF plot at 210°C at 48 hrs TOS..... | 98 |
| Figure 4-20 Conversion vs TOS of reaction at 220°C..... | 99 |
| Figure 4-21 Moles of carbon products in liquid phase at 1274 hrs TOS | 100 |
| Figure 4-22 Moles of carbon products in wax phase at 1274 hrs TOS | 100 |
| Figure 4-23 Change in selectivity at 220°C | 101 |
| Figure 4-24 Typical ASF plot for reaction at 220°C | 102 |
| Figure 4-25 Post reaction soxhlet on a sample of catalyst | 103 |
| Figure 4-26 Post reaction soxhlet on a sample of alumina support | 103 |
| Figure 4-27 Post reaction TGA on Co/Al ₂ O ₃ (nitrate) catalyst under oxygen | 104 |

| | |
|---|-----|
| Figure 4-28 MS post reaction TGA on catalyst under oxygen..... | 105 |
| Figure 4-29 Post reaction TGA on alumina support under oxygen..... | 106 |
| Figure 4-30 MS post reaction TGA on alumina under oxygen..... | 106 |
| Figure 4-31 Conversion before octanol addition. | 108 |
| Figure 4-32 Moles of carbon products in liquid phase before octanol addition at 72 hrs TOS | 108 |
| Figure 4-33 Moles of carbon products in wax phase before octanol addition at 72 hrs TOS..... | 109 |
| Figure 4-34 Change in selectivity before octanol addition | 109 |
| Figure 4-35 Typical ASF plot before addition of octanol | 110 |
| Figure 4-36 Conversion during octanol addition | 111 |
| Figure 4-37 Moles of carbon products in liquid phase during octanol addition at 480 hrs TOS..... | 111 |
| Figure 4-38 Typical chromatogram of light hydrocarbons during octanol addition | 112 |
| Figure 4-39 Overlay of chromatograms of light hydrocarbons before and during octanol addition | 113 |
| Figure 4-40 Overlay of chromatograms of light hydrocarbons during octanol addition and C8, C10, C12, C14 and C16 alcohol mix..... | 113 |
| Figure 4-41 Moles of carbon products in wax phase during octanol addition at 480 hrs TOS..... | 114 |
| Figure 4-42 Typical chromatogram of heavy hydrocarbons during octanol addition | 115 |
| Figure 4-43 Overlay of chromatograms of heavy hydrocarbons before and during octanol addition | 115 |
| Figure 4-44 Overlay of chromatograms of heavy hydrocarbons during octanol addition and C8, C10, C12, C14 and C16 alcohols | 116 |
| Figure 4-45 Change in selectivity during octanol addition | 117 |
| Figure 4-46 Typical ASF plot during addition of octanol..... | 117 |
| Figure 4-47 Soxhlet post reaction on a sample of catalyst..... | 118 |
| Figure 4-48 Soxhlet post reaction on a sample of alumina support..... | 119 |
| Figure 4-49 Post reaction TGA on catalyst under oxygen gas | 120 |
| Figure 4-50 MS post reaction TGA on catalyst under oxygen gas..... | 121 |
| Figure 4-51 Post reaction TGA on alumina support under oxygen gas..... | 122 |
| Figure 4-52 MS post reaction TGA on alumina support under oxygen gas..... | 122 |

| | |
|---|-----|
| Figure 4-53 Conversion during decanol addition..... | 125 |
| Figure 4-54 Moles of carbon products in liquid phase during decanol addition at 311 hrs TOS..... | 125 |
| Figure 4-55 Gas chromatogram trace of light hydrocarbons during decanol addition | 126 |
| Figure 4-56 Overlay of chromatograms of light hydrocarbons during decanol addition and C8, C10, C12, C14 and C16 alcohol mix | 127 |
| Figure 4-57 Moles of carbon products in wax phase during decanol addition at 311 hrs TOS..... | 128 |
| Figure 4-58 Typical chromatogram of heavy hydrocarbons during decanol addition | 128 |
| Figure 4-59 Overlay of chromatograms of heavy hydrocarbons during decanol addition and C8, C10, C12, C14 and C16 alcohol mix | 129 |
| Figure 4-60 Change in selectivity during decanol addition | 130 |
| Figure 4-61 Typical ASF plot during addition of decanol | 131 |
| Figure 4-62 Moles of carbon products in liquid phase after decanol addition at 768 hrs TOS..... | 132 |
| Figure 4-63 Soxhlet post reaction on a sample of catalyst 3 rd reaction | 133 |
| Figure 4-64 Soxhlet post reaction on a sample of alumina support 3 rd reaction | 133 |
| Figure 4-65 Post reaction TGA (3 rd reaction) catalyst under oxygen gas | 134 |
| Figure 4-66 MS post reaction TGA (3 rd reaction) catalyst under oxygen gas..... | 135 |
| Figure 4-67 Post reaction TGA (3 rd reaction) Al ₂ O ₃ under oxygen gas | 136 |
| Figure 4-68 MS post reaction TGA (3 rd reaction) Al ₂ O ₃ under oxygen gas | 136 |
| Figure 4-69 TGA analysis (weight loss/derivative weight vs temperature) of Co/Al ₂ O ₃ (HDC) catalyst under 2%O ₂ /Ar feed | 138 |
| Figure 4-70 TGA analysis (weight loss/heat flow vs temperature) of Co/Al ₂ O ₃ (HDC) catalyst under 2%O ₂ /Ar feed..... | 138 |
| Figure 4-71 TGA analysis (weight loss/derivative weight vs temperature) of Co/Al ₂ O ₃ (HDC) catalyst under 5%H ₂ /N ₂ feed | 139 |
| Figure 4-72 TGA analysis (evolution of water) of Co/Al ₂ O ₃ (HDC) catalyst under 5%H ₂ /N ₂ feed | 140 |
| Figure 4-73 TGA analysis (uptake of hydrogen) of Co/Al ₂ O ₃ (HDC) catalyst under 5%H ₂ /N ₂ feed | 140 |
| Figure 4-74 TGA analysis (evolution of NO) of Co/Al ₂ O ₃ (HDC) catalyst under 5%H ₂ /N ₂ feed..... | 141 |

| | |
|---|-----|
| Figure 4-75 TGA measurement (TPR/TPD) of Co/Al ₂ O ₃ (HDC) catalyst..... | 142 |
| Figure 4-76 XRD graph of Co/Al ₂ O ₃ (HDC)..... | 143 |
| Figure 4-77 Hot-Stage XRD graph of Co/Al ₂ O ₃ (HDC) under H ₂ | 144 |
| Figure 4-78 TPR-UV-vis-NIR spectroscopy graph of Co/Al ₂ O ₃ (HDC) under H ₂ ... | 145 |
| Figure 4-79 TEM image for Co/Al ₂ O ₃ (HDC) catalyst..... | 146 |
| Figure 4-80 Conversion of reaction at 210°C | 147 |
| Figure 4-81 Moles of carbon products in liquid organic phase at 216 hrs TOS... | 148 |
| Figure 4-82 Moles of carbon products in wax phase at 216 hrs TOS | 148 |
| Figure 4-83 Selectivity over whole reaction | 149 |
| Figure 4-84 Typical ASF plot for Co(HDC) reaction at 210°C | 150 |
| Figure 4-85 Soxhlet results post reaction on a sample of catalyst | 151 |
| Figure 4-86 Soxhlet results post reaction on a sample of alumina support | 151 |
| Figure 4-87 Post-reaction TGA on catalyst under oxygen gas..... | 152 |
| Figure 4-88 MS post-reaction TGA on catalyst under oxygen gas..... | 153 |
| Figure 4-89 Post-reaction TGA on alumina support under oxygen gas..... | 154 |
| Figure 4-90 MS post-reaction TGA on alumina support under oxygen gas..... | 154 |
| Figure 4-91 Conversion before octanol addition | 156 |
| Figure 4-92 Moles of carbon products in liquid phase before octanol addition at 288 hrs TOS..... | 157 |
| Figure 4-93 Change in selectivity before octanol addition | 158 |
| Figure 4-94 Typical ASF plot before addition of octanol | 158 |
| Figure 4-95 Moles of carbon products in liquid phase during octanol addition at 480 hrs TOS..... | 159 |
| Figure 4-96 Typical chromatogram of light hydrocarbons during octanol addition | 160 |
| Figure 4-97 Overlay of chromatograms of light hydrocarbons during octanol addition and C8, C10, C12, C14 and C16 alcohol mix | 161 |
| Figure 4-98 Moles of carbon products in wax phase during octanol addition at 480 hrs TOS | 162 |
| Figure 4-99 Typical chromatogram of heavy hydrocarbons during octanol addition | 162 |
| Figure 4-100 Overlay of chromatograms of heavy hydrocarbons during octanol addition and C8, C10, C12, C14 and C16 alcohols | 163 |
| Figure 4-101 Change in selectivity during octanol addition..... | 164 |
| Figure 4-102 Typical ASF plot during addition of octanol | 165 |

| | |
|--|-----|
| Figure 4-103 Soxhlet results post reaction on a sample of catalyst (octanol run) | 165 |
| Figure 4-104 Soxhlet results post reaction on a sample of alumina (octanol run) | 166 |
| Figure 4-105 Post-reaction TGA on catalyst under oxygen gas (octanol run).... | 167 |
| Figure 4-106 MS post-reaction TGA on catalyst under oxygen gas (octanol run) | 167 |
| Figure 4-107 Post-reaction TGA on alumina under oxygen gas (octanol run).... | 168 |
| Figure 4-108 MS post-reaction TGA on alumina under oxygen gas (octanol run) | 168 |

Acknowledgements

First and foremost I would like to thank my supervisor, Professor S. David Jackson for his guidance, support and encouragement throughout this project. He was never too busy to discuss my work and I thank him for that.

Secondly, I would like to extend my gratitude to my industrial supervisors Dr. Gordon J. Kelly and Dr. C. Martin Lok of Johnson Matthey Catalysts for the opportunity to work on the project and for lending their support when needed. I am grateful that I was able to spend a short placement at JM laboratories in Billingham. Thanks go to Adel Neale, Jill Turner and Dr. John West from JM for their assistance.

I would also like to thank Ron Spence for his expertise in rig building; the rig could not have been built without you, Andrew Monaghan for running TGA and BET analysis throughout the project and Jim Gallagher for assisting with TEM analysis.

There are many people in the Catalysis group past and present that I would like to thank. Thank you to Sharon, Gemma, Claire, Lynsey, Fiona, Bilal, Javed, Anne-Marie, Liam and Dan for their help. Special thanks must go to Stuart, David and Graham who I hope to be friends with for life. They made every day enjoyable and the years we spent together were brilliant.

I cannot submit this thesis without thanking my parents, Lorraine and Cello, and my brother Paul. I am grateful for their constant love and support during the last four years. I would also like to give a heartfelt thanks to Claire for her love, support and encouragement throughout this project.

Declaration

This work contained in this thesis, submitted for the degree of Master of Science, is my own work except where due reference is made to other authors. No material within this thesis has been previously submitted for a degree at this or any other university.

© Mark Facchini

Signed

Date

Mark Facchini

July 2010

1 Introduction

1.1 Background of current research

Since oil was discovered in 1859 in USA, it has long been a source of cheap energy upon which the modern worldwide economy has been built [1, 2]. This relatively low price and the perceived long-term availability of crude oil has made the world extremely dependent on oil. However, recently there has been a major strain on the world's oil resources, due to the ever-increasing demand for oil, and this has led many to predict that oil production is peaking throughout the world[3]. The fears of oil running out[3], the growing demand in areas in South East Asia[4], driven by quick expansion, and the political unrest present in the major oil producing nations such as Iraq, Venezuela and Nigeria [4] has recently pushed oil prices to historic highs. The combination of these global forces and the large amount of natural gas reserves, which are spread relatively evenly (as compared to crude oil) around the world, has led to some people to comment that the 21st century will be the "Gas" century and will signal the end of "cheap" oil. This argument has created an overwhelming push for alternate fuels and the conversion of natural gas to liquid fuel, i.e. gas-to-liquid (GTL), via the Fischer-Tröpsch synthesis (FTS). The FTS stands out as the most promising and proven technology that has potential to revolutionize the fuel industry [4].

Currently there are many commercial gas-to-liquid (GTL)/ coal-to-gas (CTL) plants that are in operation and in construction. There has been a flurry of activity in this area in the last 15 yrs. PetroSA operates a 47,000 bbl/day GTL facility in Mossel Bay, South Africa[3]. Shell is operating a supported cobalt catalyst in a fixed bed reactor, as part of their 12,000 bbl/day Shell Middle Distillate Synthesis (SMDS) process in Bintula, Malaysia[4] and Sasol is currently operating a 34,000 bbl/day GTL plant in Ras Laffan, Qatar. Currently in construction is a large GTL facility by Shell-Qatar Petroleum Pearl which will have a capacity of 140,000 bbl/day. This plant is due to open late 2010. Gas-to-Liquid on a global scale is making its mark with many announcements made by the multi national oil companies to build large plants mainly in Qatar[3]. Figure 1-1 summarises the worldwide GTL/CTL plants in commercial use and

construction. The initial factors that stimulated interest in GTL and similar processes still remain valid[3, 5]:

- Global increase in energy demand. F-T based processes (GTL/CTL) are being employed and developed to meet this increased demand.
- High crude oil price that is expected to remain (FTS feasible at \$30/barrel).
- Large volumes of stranded gas, in remote areas like Alaska, have still to be unlocked and monetized[6].
- The need to reduce flaring of gas for a number of reasons: environmental, economic, and legal[7].

At the same time, certain factors have gained importance during recent years[7]:

- Current global security resource concerns given the present political climate. 40% of the world's gas reserves are in the Middle East- and coal, of which the US has the largest reserves.
- Current concern about the impact of climate change and the impact that CO₂ has on the environment. This has led to the exploration of a number of advancements in improving the efficiency of technology to enhance the efficiency of CO₂ capture.
- The increase market value of crude oil. Recently the oil price has reached nearly \$140/bbl in 2008 although the price has dropped considerably to around \$80/bbl[8].

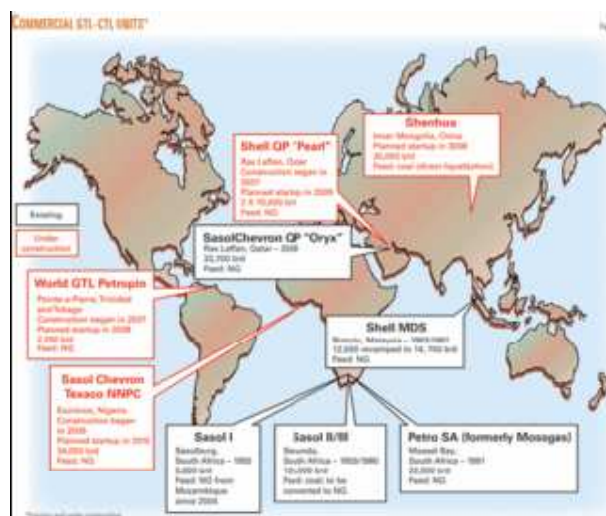


Figure 1-1 List of existing GTL/CTL plants and those under construction[7]

The principle process steps in a GTL plant is summarised below:

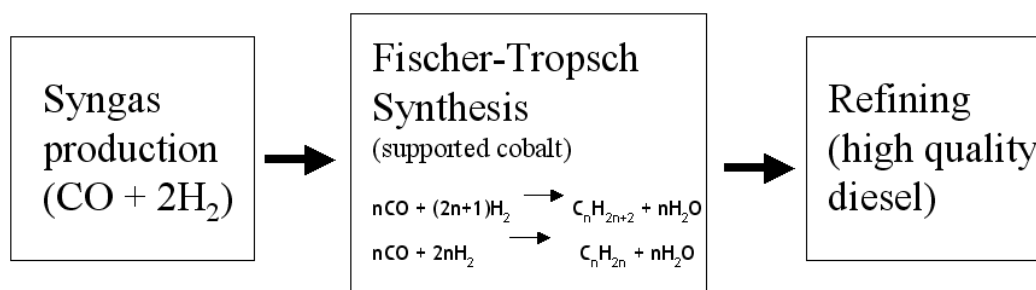


Figure 1-2 Principal process steps of GTL plant[9]

The most important part of the GTL process is the Fischer-Tröpsch synthesis (FTS) reaction. Although this has been studied intensively for many years, it is still being optimised further. FTS was discovered in 1925 by Frans Fischer and Hans Tröpsch and the two catalytic systems of choice were iron and cobalt[10]. The initial objective for the FTS process was gasoline production and this is still true today.

1.2 The Fischer-Tröpsch Synthesis (FTS) Reaction

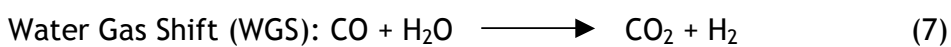
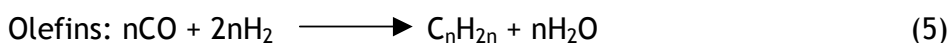
The Fischer-Tröpsch synthesis (FTS) is a process in which syngas, carbon monoxide (CO) and hydrogen (H₂) is catalytically converted into hydrocarbons (paraffins and olefins), and small amounts of oxygenated species. During FTS (CH₂)_{ads} monomers are formed by the dissociation and subsequent hydrogenation of adsorbed CO (equations 1 and 2), and the hydrocarbon products are formed by polymerisation. For each CO molecule that is converted to a CH_x species a residual oxygen atom remains on the cobalt surface which is then hydrogenated, in the case of cobalt catalysts, to form mostly water (CO₂ formation is negligible). The last step (equation 2), i.e. re-reduction of cobalt, is essential for regenerating the active site.



Sustained oxidation of cobalt can take place if CO dissociation proceeds rapidly so that reaction (2) can not compete with the amount of CoO formation or if the equilibrium of reaction 2 lies to the left due to the strength of the CoO bond and/or the ratio of the P_{H₂O}/P_{H₂} [11, 12]. Irreversible oxidation of cobalt will take place if cobalt metal reacts with the support (equation 3) to form cobalt aluminate [11].



A large number of reactions occur during the F-T reaction, the major ones are given below in equations 4-8 [13, 14]:



1.3 Fischer-Tröpsch catalysts

Group VIII metals such as iron, cobalt, ruthenium and nickel have measurable CO hydrogenation activity, the distinguishing feature being the product distribution (see Figure 1-3). The three most suitable metals for F-T synthesis are cobalt, iron, and ruthenium but even these three metals will produce a different spectrum of F-T products in terms of olefin content, branching of paraffins and amounts of oxygenated products produced. The high price and limited world resources of ruthenium exclude its industrial application. Nickel is not used as a F-T catalyst because it is a methanation catalyst which produces very little hydrocarbon products. Only iron and cobalt catalysts are currently used in industrial practice but the choice between using iron and cobalt-based catalysts is not so simple. Iron catalysts have been used by SASOL (South Africa Synthetic Oil Limited) since 1955 to yield a variety of fuels and chemicals from synthesis gas produced by the gasification of coal [15]. Currently, cobalt catalysts are used commercially in the Shell F-T plant in Malaysia and Syntroleum in Oklahoma. The commercial plant by SasolChevron in Qatar, ConocoPhillips, and Sasol/Qatar are all based on natural gas with cobalt catalysts [16].

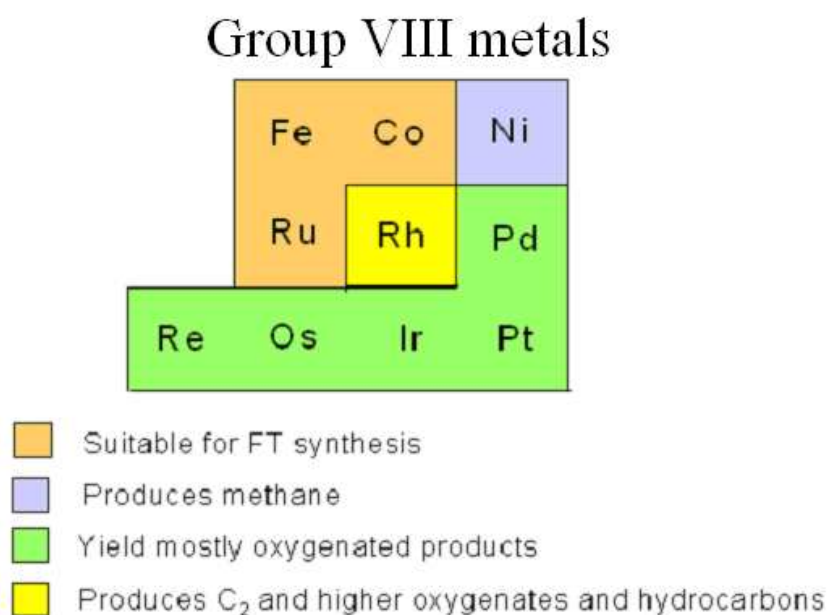


Figure 1-3 CO hydrogenation over Group VIII metals

Iron catalysts, usually used with addition of an alkali, preferably potassium oxide, are good water-gas shift (WGS) catalysts. Coal has a low hydrogen to carbon ratio, and the gasification of coal results in high ratios of CO to H₂. Since iron is a WGS catalyst, it would seem to be the preferred catalyst when coal is the source of syngas. With hydrogen-rich syngas, as produced from natural gas, iron is undesirable for F-T synthesis [17]. Iron catalysts prepared by precipitation or fusion are usually unstable and tend to gradually lose activity; they cannot be regenerated and must be replaced regularly [18]. Fused iron catalysts are the most suitable catalysts for the high temperature F-T process in circulating fluidized bed or fixed fluidized bed reactors to produce low molecular weight olefinic hydrocarbons. Many additives such as chemical promoters (usually K₂O) and structural promoters such as Al₂O₃ or MgO, have been added to iron catalysts to improve their mechanical and catalytic properties [17, 19]. After reduction with hydrogen, fused magnetite has low catalyst porosity with small pore diameters. Precipitated iron catalysts are used for wax production at low reaction temperatures. Typically, precipitated iron catalysts are obtained through precipitation from nitrate solutions. Alkali is an important promoter to attain high activity and stability; it modifies the adsorption of H₂ and CO, and increases selectivity to desired products [20, 21]. Copper promotes the reduction processes and decreases the temperature required for the activation of iron oxide [22]. SiO₂ or Al₂O₃ is added for structural promotion and possibly some manganese is applied for selectivity control (e.g. high olefinic products [18]).

Although iron catalysts are about 200 times cheaper than cobalt catalysts and have been studied in more detail, their structural instability restricts the attainable degree of conversion and leads to gas recycle operation. In many regions in the world there are cheap natural gas reserves. Due to iron's high WGS activity, it is undesirable for F-T plants to be based on natural gas feedstocks. Cobalt however, has low WGS activity, an advantage for such syngas. At present, essentially all new F-T plants, which are based on stranded natural gas to produce syngas at close to or higher than the F-T stoichiometric H₂/CO ratio, will use cobalt catalysts. Cobalt produces mainly straight-chain hydrocarbons and higher ratios of paraffins to olefins and fewer oxygenated products such as alcohols and aldehydes than iron catalysts [23]. Cobalt is

dispersed on high area stable supports such as alumina, silica, and titania, to maximize the available surface area of the metal [24-27] as a consequence of its high activity. Interaction with strong supports improves the strength of cobalt catalysts and results in better stability compared to iron catalysts. Cobalt catalysts are normally promoted with a noble metal in small amounts, e.g. platinum, ruthenium, rhodium which are reported to improve the reduction of cobalt by increasing hydrogen adsorption and improving regeneration of the deactivated catalyst [28]. However, it was found that the support has no effect on the turnover frequency of cobalt sites.

Both cobalt and iron catalysts synthesise products that are consistent with Anderson-Schulz-Flory (ASF) polymerization kinetics; however, there are some distinctive differences between these two catalysts in the F-T synthesis:

- (1) The metallic states of the two metals in FTS are very different. Iron catalysts, whether used in the reaction as iron metal or iron oxides, exist as a mixture of magnetite (Fe_3O_4), $\alpha\text{-Fe}$, and iron carbide under F-T reaction conditions. Although magnetite and iron carbide are formed rapidly and are both present in the F-T process, Fe_3O_4 is relatively inactive and iron carbide has been claimed to be the preferred route for F-T activity [29, 30]. The cobalt catalyst contains mainly the metallic phase [31].
- (2) Iron is extremely active in the WGS reaction in the presence of an alkali, which converts water and CO to H_2 and CO_2 , so that iron catalysts are suitable for coal-based synthesis gas with high CO/H_2 ratios. Unlike iron catalysts, cobalt catalysts have slight WGS activity, and are used when synthesis gas is produced from methane.
- (3) Cobalt is extremely expensive and has high F-T activity and therefore it is commonly supported on high area stable materials such as titania, silica, and alumina [24-27]. Cobalt catalysts are commonly promoted with a noble metal, like ruthenium, rhodium, and platinum. The amount of metal loading is high (> 85 wt%) with iron F-T catalysts,

with materials such as SiO_2 and Al_2O_3 used as structural promoters. Potassium is crucial for activity and chain growth for iron catalysts.

- (4) Cobalt catalysts can only be used for low temperature F-T (LTFT) processes, as they have been experimentally proved to form CH_4 in excess at high temperature. Iron catalysts that are prepared by precipitation methods can be used for low temperature F-T (LTFT) processes to produce wax products, while fused iron catalysts are used in high temperature F-T processes.
- (5) Cobalt catalysts produce mainly saturated hydrocarbons and a minimal amount of oxygenates, whereas iron-based F-T catalysts produce more olefinic hydrocarbons and oxygenated products. At present, cobalt catalysts are the preferred catalysts for the synthesis of high molecular weight products from natural gas based synthesis gas. Table 1.1 summarizes different properties of cobalt and iron catalysts:

| F-T catalyst | Cobalt | Iron |
|---|--|--|
| Price | 200 (high) | 1 (low) |
| Activity | Higher conversion rate | Lower conversion rate |
| Active phase | Cobalt metal | Iron carbides, oxides and oxycarbides |
| Source of carbon | Natural Gas; higher H ₂ /CO ratio | Coal; lower H ₂ /CO ratio |
| Catalyst life | Longer (~4 yrs) | Shorter (~4-8 wks) |
| Promoters | Ru, Rh, Pt | Alkalis (i.e. K) |
| Supports | Cobalt content: <20 wt%; alumina silica and titania | Iron content: >85 wt% alumina, silica as structural promoters |
| Hydrogenation activity | Higher hydrogenation activity Produce more CH ₄ at high temperature Produce more linear paraffins and branched hydrocarbons Produce lower oxygenates | Lower hydrogenation activity Less sensitive to reaction T and produces less CH ₄ Produce more olefins and oxygenated species |
| Water Gas Shift (WGS) activity (CO + H ₂ O → CO ₂ + H ₂) | Poor WGS catalyst Can operate at higher H ₂ :CO ratios Has higher C efficiency and H ₂ O is the principle oxygenate product | Good WGS activity Can operate at low H ₂ :CO ratios Has lower C efficiency and part of H ₂ O is converted to CO ₂ |

Table 1-1 Comparison of the characteristic features of iron and cobalt F-T catalysts

1.4 Deactivation methods for FTS catalysts

Decreasing the deactivation rates of cobalt and iron catalysts for Fischer-Tröpsch synthesis (FTS) has been one of the most important challenges that has faced the industrial development of these catalysts for the conversion of coal and natural gas to liquid fuels as alternative resources to crude oil.

The following factors are involved in the lowering of activity and the decline of F-T activity, of cobalt and iron based systems, with time on-stream[32]:

- The presence of high molecular mass waxes and or aromatic coke precursors on the catalyst pores.

These compounds lower the F-T conversion by reducing the rate of diffusion in and out of the catalyst particles. This should only occur with time on stream if there is a continuous build-up of these products in the catalyst pores.

- Fouling of the catalyst surface by coke deposits.

At higher temperatures, where the majority of the products exit the catalyst pores in the gas phase, build-up of heavy molecular weight hydrocarbons, e.g. coke precursors, could occur or the lay down of small carbon species on catalyst crystallite sites may occur.

- Poisons in the feed gas such as H₂S and organic sulfur compounds.

Fischer established long ago that sulfur compounds present in the synthesis gas feed resulted in rapid decline in activity of nickel, cobalt, and iron catalysts [33]. Fischer recommended that the sulfur content be kept below 2 mg m⁻³ but for current commercial operation this is too high. Sulphur compounds in the syngas feed stream poison all catalysts, at all FTS operating conditions. The following table illustrates the effect of various sulfur levels on the performance of a fluidised iron catalyst:

| Sulfur content of synthesis gas (mgS m ⁻³ _n) | Drop in % conversion per day |
|--|------------------------------|
| 0.1 | Very low |
| 0.4 | 0.25 |
| 2.8 | 2.0 |
| 28 | 33 |

Table 1-2 Influence of sulfur content of synthesis gas on the rate of activity decline for fluidised iron catalyst at about 320°C[34].

- Hydrothermal sintering

Sintering is thermally induced deactivation of catalyst by the loss of catalyst surface area by the crystallite growth in the catalytic phase or the loss of support area due to support collapse and of catalytic surface area, due to pore collapse on metal crystallites. This deactivation mechanism generally takes place at high reaction temperatures (> 500°C) and is generally accelerated in the presence of water.

- Oxidation of the active metal/carbide to the inactive oxide.

For iron based FTS the active phase is widely agreed to be a type of iron carbide and for cobalt based FTS the active site is cobalt metal. For cobalt based F-T reactions, under certain conditions, cobalt metal will oxidise readily to cobalt oxide or cobalt aluminate which speeds up deactivation.

1.4.1 Deactivation of cobalt based catalysts in Fischer-Tröpsch synthesis (FTS)

Supported cobalt catalysts have been one of the most important systems for Fischer-Tröpsch synthesis (FTS) over recent years and are the system of choice for the FTS because they have many advantages over iron based F-T catalysts (see table 1-1). Cobalt catalysts have lower water-gas-shift activity, they have higher hydrogenation activity and produce more saturated heavy molecular weight hydrocarbons (paraffins), and they are more resistant to deactivation that leads to longer time-on-stream.

However, as mentioned earlier, one of the major drawbacks of cobalt-based catalysts is their high cost, making catalyst replacement very undesirable. It is shown that a catalyst life span of four years is thought to be the minimum required for a viable fixed bed commercial process [35] and the need to have a high metal dispersion to remain economically feasible. Therefore it is of great importance to investigate the deactivation of cobalt catalysts, to extend the lifespan, and finally to cut down the cost of the catalyst.

Many studies have focused on the deactivation of cobalt catalysts[11, 26, 36-46]. The reasons for the deactivation of cobalt catalysts for FTS could be summarised as follows:

1.4.1.1 Oxidation

The oxidation of cobalt metal to cobalt oxide or cobalt aluminate (for alumina supported catalysts) by the product of water has been long postulated to be the major deactivation method of supported cobalt FTS catalysts. This is thought to be related to the cobalt crystallite size distribution [11, 12, 25, 47, 48].

Most authors agree that bulk oxidation of cobalt is not favourable under realistic FTS conditions and further concur on the size dependency of the oxidation behaviour of cobalt. It is also reported in literature that cobalt crystallites < 5-10 nm undergo oxidation during FTS.

Although there has been extensive research into the theory that oxidation is indeed a deactivation mechanism of cobalt based FTS catalysts, to date there is no consistent picture. Discussed below are some possible routes of deactivation by oxidation for cobalt based F-T catalysts.

1.4.1.1.1 Thermodynamic analysis of bulk cobalt metal

Van Berge et al. carried out a bulk phase thermodynamic evaluation of F-T catalysts to understand the effect of water on the oxidation behaviour of cobalt based F-T catalysts[11].

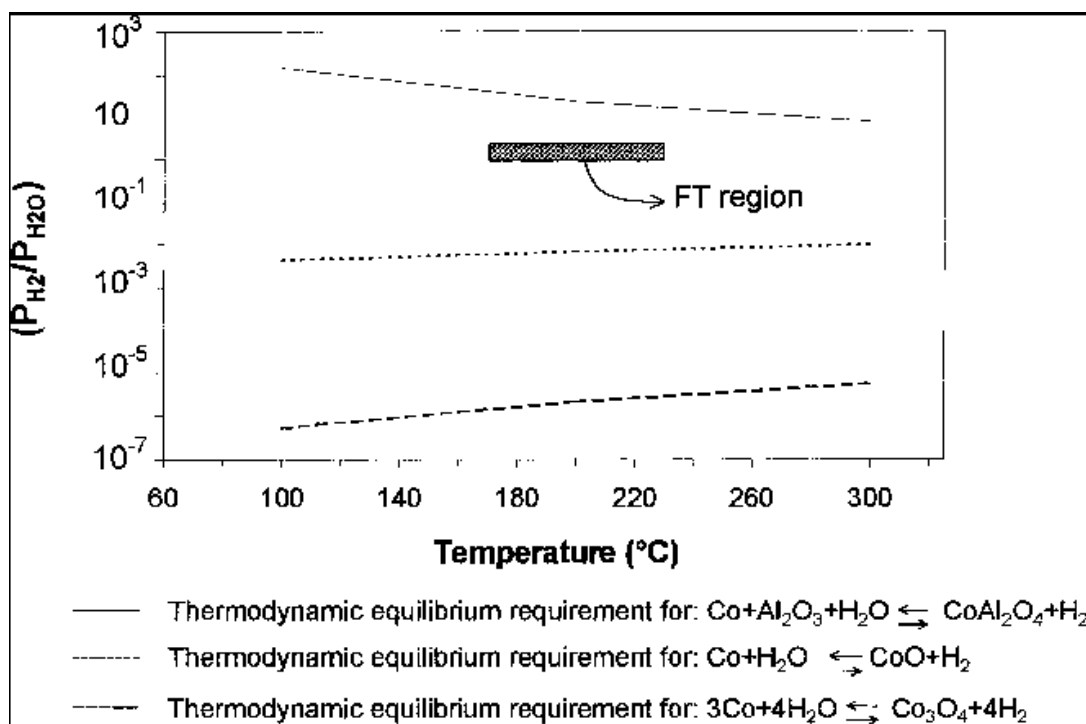
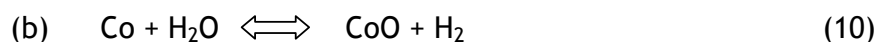
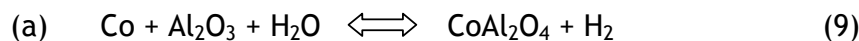


Figure 1-4 Thermodynamic equilibrium constants for three selected cobalt oxidation reactions[11]. (Note: the thermodynamic equilibrium for the oxidation of cobalt to Co_3O_4 is about 4 orders of magnitude lower than that of the oxidation to CoO).

The F-T region specified in Figure 1-4, was based on realistic conditions assuming a gradientless slurry phase reactor with the following conditions: reactor temperature of 170-240 $^{\circ}C$, reactor pressure of 20 bar, synthesis gas composition of 67 vol. % H_2 and 33 vol. % CO , and a $(H_2 + CO)$ conversion 50-70. These F-T conditions resulted in a hydrogen partial pressure between 6.5 and 9.2 bar, and a water partial pressure between 4.6 and 7.6 bar, resulting in a P_{H_2} / P_{H_2O} ratio between 0.86-2.00. The equilibrium constant (K_{eq}) versus temperature

curves of equations (a) and (b) from Figure 1-4 are in agreement with the following publication [49]:



Since these thermodynamic equilibrium constants (K_{eq}) for the chemical equilibria are both lower than typical $P_{\text{H}_2} / P_{\text{H}_2\text{O}}$ ratios observed during FTS, it can be concluded that the oxidation of bulk cobalt to CoO or Co_3O_4 is not spontaneous. In the case of Co/ Al_2O_3 catalysts, the oxidation of cobalt to the CoAl_2O_4 -spinel is thermodynamically favourable and it could therefore be postulated that the conversion of Co/ Al_2O_3 to CoAl_2O_4 -spinel needs to proceed via CoO as an intermediate product, thus: $\text{CoO} + \text{H}_2\text{O} \longrightarrow \text{CoO} + \text{H}_2$ followed by $\text{CoO} + \text{Al}_2\text{O}_3 \longrightarrow \text{CoAl}_2\text{O}_4$.

1.4.1.1.2 Unsupported cobalt catalysts

The addition of water to the synthesis gas feed at low CO conversions was reported by Kim [50, 51] to increase the activity of unsupported cobalt based Fischer-Tröpsch catalysts. Das et al. [52] similarly showed that the addition of water to the syngas feed increased the activity of an unsupported cobalt catalyst. Using isotopic labelling experiments, Bertole et al. [41] showed that water pressures of 4 and 8 bar decrease the FTS activity of unsupported cobalt catalysts irreversibly. The reason for this decrease in FTS activity was postulated as sintering. It is widely agreed that water at low partial pressures has a positive effect on unsupported catalysts with cobalt crystallites >ca. 30nm.

1.4.1.1.3 Alumina, silica, and titania supported cobalt catalysts

Huffman et al. [53] showed that a Co/ Al_2O_3 catalyst did not oxidise during FTS (at 190-200°C, 1 bar, $P_{\text{H}_2\text{O}} = 0.025$ bar, $\text{H}_2/\text{CO} = 3$). The addition of a K promoter was found to induce oxidation of the metallic cobalt at the same conditions.

Schanke et al. [38, 54] reported that oxidation of cobalt-to-cobalt oxide is a possible route of deactivation. They used Co/ Al_2O_3 catalysts with metal loadings between 18-30 wt%. They co-fed water during FTS in a fixed bed reactor and rapid deactivation was seen. This was attributed to surface oxidation of small cobalt crystallites.

A similar study to Schanke et al. [38, 54] was carried out by Hilmen et al. [39, 55, 56]. The deactivation mechanism of unpromoted and Re promoted Co/Al₂O₃ catalysts under model conditions using various techniques was studied. Both unpromoted and Re promoted Co/Al₂O₃ catalysts showed a decrease in FTS activity with an increase in water partial pressure. All the Co/Al₂O₃ catalysts showed surface oxidation and the re-oxidation of cobalt was found to increase with $P_{\text{H}_2\text{O}}$ and the $P_{\text{H}_2\text{O}} / P_{\text{H}_2}$ ratio. It can be stated from these experiments that small cobalt crystallites or surface oxidation of cobalt was responsible for the deactivation during FTS. However, an unpromoted Co/Al₂O₃ catalyst showed slight reduction under the following conditions; (250°C, 10 bar, $P_{\text{H}_2\text{O}} = 5$ bar, $\text{H}_2/\text{H}_2\text{O} = 10$).

Another group [57] tested the effect of introducing water during FTS on a number of active sites on Co/Al₂O₃ catalysts using steady-state isotopic transient kinetic analysis (SSITKSA). This resulted in lowering of the number of active sites during FTS and can be explained by surface oxidation of the metallic cobalt.

Van Berge and co-workers [11, 58, 59] showed that the addition of water under FTS conditions for a 20wt% Co/Pt/ Al₂O₃ catalyst brought about irreversible deactivation. This negative effect of water was thought to be the result of small cobalt crystallites. They also showed, using various techniques, that the degree of oxidation of these Pt promoted catalysts depended on the $P_{\text{H}_2} / P_{\text{H}_2\text{O}}$ ratio [11]. Van Berge et al. proposed that cobalt crystallites < 10 nm will oxidise during typical FTS conditions [60].

Another group, Jacobs et al. [61], found oxidation of a fraction of a spent Co/Ru/Al₂O₃ catalyst (cobalt size 6 nm) after FTS. The small cobalt crystallites oxidised during FTS to Co₃O₄ or cobalt aluminate. This was the first time that direct characterisation of the oxidation state of spent FTS catalysts was performed. They also studied unpromoted, platinum and ruthenium promoted Co/Al₂O₃ catalysts (cobalt size = 6nm) and found oxidation of a fraction of the catalyst to Co₃O₄ or cobalt aluminate [26]. The consensus was that the cobalt species that did oxidise were probably small cobalt clusters.

Li et al. [43] performed deactivation experiments of Pt promoted Co/Al₂O₃ catalysts (cobalt size = 6 nm) using the co-feeding of water into the reaction. The introduction of water into the FTS had a reversible effect even at low amounts ($P_{\text{H}_2\text{O}} / P_{\text{H}_2} = 0.5$). However, at higher $P_{\text{H}_2\text{O}} / P_{\text{H}_2} = 0.6$ an irreversible deactivation of the Pt promoted Co/Al₂O₃ catalyst was observed. So from this result and the increase in CO₂ production, the most likely cause of oxidation was metal cobalt oxidising to cobalt oxide or cobalt aluminate. Jacobs et al. [62] found similar results on Pt promoted Co/Al₂O₃ catalysts with similar cobalt size (cobalt size = 6 nm). Using XANES they came to the same conclusion as Li et al. [43].

In summary, most authors seem to agree that for alumina supported cobalt catalysts, the oxidation of surface cobalt or the oxidation of small cobalt crystallites plays a considerable role in the deactivation observed during typical Fischer-Tröpsch synthesis reactions. On the other hand, there is still debate on the threshold value above which cobalt is stable against oxidation. Many scientists believe that deactivation by oxidation is conditional on the $P_{\text{H}_2\text{O}} / P_{\text{H}_2}$ ratio and the total water pressure.

1.4.1.1.4 Silica supported cobalt catalysts

For a 44wt% Co/Re/SiO₂ catalyst with 5 nm cobalt crystallites, irreversible deactivation occurred during a typical F-T reaction (220°C, 20 bar, 94% synthesis gas conversion, $P_{\text{H}_2\text{O}} = 13.1$ bar, $P_{\text{H}_2} = 2.1$ bar, $P_{\text{CO}} = 0.4$ bar) [45]. The formation of cobalt silicate was detected but part of the deactivation was thought to be caused by sintering. Other groups while testing unpromoted Co/SiO₂ catalysts found the formation of cobalt silicates [63] and when water was introduced into the reaction stream, irreversible deactivation occurred [64]. Iglesia [47] found that cobalt crystallites below 5/6 nm would oxidise and quickly deactivate under typical FTS conditions.

Although many groups have postulated the negative effect that water partial pressure has on the oxidation of Co/SiO₂ catalysts in FTS activity, Krishnamoorthy et al [40] found that water partial pressure had no effect on the activity during FTS. This was also found by to be the case with Bian et al. [65] who found that Co/SiO₂ catalysts with cobalt crystallite sizes of 10 and 29 nm did not oxidise during FTS. It was reported by Li et al. [66] that higher activity

was seen with the introduction of water however, high water partial pressures did cause a negative effect on the FTS activity.

Although it is still unclear, authors believe that the water partial pressure and the cobalt crystallite size are the two factors that seem to affect the oxidation behaviour of silica supported catalysts.

1.4.1.1.5 Titania supported cobalt catalysts

The introduction of water into the synthesis gas feed at low CO conversions increased the activity of TiO₂ supported cobalt based Fischer-Tröpsch catalysts [50, 51]. It is thought that the positive effect of water is due to a reversal of the encapsulation of the cobalt crystal with titania [50, 51]. The effect of water on TiO₂ supported ruthenium promoted cobalt based FTS catalysts found that only reversible deactivation occurred in mild FTS conditions. When the FTS conditions were harsher irreversible deactivation did take place. Bertole et al. [41] found, from isotopic labelling experiments, that water partial pressures of 2 bar for TiO₂ supported rhodium promoted cobalt based Fischer-Tröpsch catalysts increased the FTS activity.

Unlike alumina supported cobalt based FTS catalysts titania supported cobalt based FTS catalysts, when undergoing the addition of to water, seem to experience an increase in FTS activity (at low conversions). This behaviour is similar to unpromoted and SiO₂ supported cobalt based FTS catalysts. Although, any increases in water partial pressures seem to be damaging to the activity. As mentioned earlier, a possible reason of the positive effect that water has on Co/TiO₂ catalysts is the reversal of the encapsulation of the cobalt crystal with titania [50, 51]. However, it is also possible that it is a crystallite size effect.

1.4.1.1.6 Comparisons between catalysts on different supports

Storsaeter et al. [67] studied the effect of introducing water into the syngas feed stream on unpromoted and Re promoted cobalt based FTS catalysts on the following supports; alumina, silica, and titania. For the Re promoted and unpromoted Co/Al₂O₃ catalysts water seemed to cause increased levels of deactivation. However, for the Re promoted and unpromoted Co/SiO₂ catalysts the introduction of water increased activity but also the deactivation. For unpromoted and Re promoted Co/TiO₂ catalysts the introduction of water

increased conversion and activity but the higher partial pressures of water resulted in decreased activity. These are in agreement with other studies on supported cobalt catalysts.

Li et al. [68] came to the conclusion that for the results found by the following groups [42, 61, 66], certain criteria have to be valid:

- (i) There is no effect on Co/TiO₂ catalysts with the introduction of water.
- (ii) There is improvement to Co/SiO₂ catalysts with the introduction of water.
- (iii) Co/Al₂O₃ catalysts decrease in activity when water is co-fed.

It has also been proposed that the ‘support effect’ might actually be down to a cobalt crystallite size effect, as the cobalt crystallite size is decreased in this order: SiO₂ (13.2 nm) > TiO₂ (8.5 nm) > Al₂O₃ (5.6 nm) [66].

The general consensus with authors is that bulk cobalt oxidation is not favourable under realistic Fischer-Tröpsch synthesis conditions and they further agree that oxidation of cobalt is related to cobalt crystallite size.

1.4.1.2 Sulfur poisoning

This occurs when there is a deactivation of active sites by strong chemisorption of species on catalytic sites, thereby blocking sites for catalytic reaction.

It is widely regarded in literature that S-compounds that are present in coal or natural gas are poisonous to Fischer-Tröpsch synthesis catalysts [17, 36, 69-71]. Even very low levels of S (a few ppm) can limit the life of a catalyst to a few hrs or days[69].

Liu et al. [70] studied the poisoning of iron promoted Cu/K catalyst by COS in syngas for realistic FTS. They found that the levels of deactivation of the iron catalyst varied with different COS concentration syngas. The selectivity to CH₄ and C₂-C₄ hydrocarbons seen in the product stream increased with increased levels of S fed to the catalyst. They also found C⁵⁺ fractions in the product

rapidly decreased with increased levels of S. This suggests that there is a shift to lower hydrocarbons in the product distribution. They concluded the catalyst resistance to S increased with higher temperatures. Bartholomew et al. [69] also found that there was a rapid decline of CO hydrogenation activity with Co/SiO₂ and Fe/SiO₂ under exposure to H₂S. They also saw an increase in C₄+ production with Co/SiO₂ catalyst. They concluded that this might be due to adsorption on metal sites that usually adsorb hydrogen, thus creating a poor hydrogen surface. It may also relate to the increase in water production seen, thus limiting the selectivity.

However, Bartholomew et al. [69] also saw opposite effects to Liu et al.[70]. They found that potassium or boron promoted iron FTS catalysts exposed to 0.5 ppm H₂S levels resulted in an increase in activity.

Investigations of the effects of S involving cobalt-based FTS catalysts are quite rare [69, 72, 73], in particular there does not seem to be many studies involving alumina-supported samples. Curtis et al. [73] found that when Co/TiO₂ and Co/SiO₂ FTS catalysts were introduced to S before calcination and reduction procedures, the S seemed to inhibit CO adsorption onto the surface of cobalt catalysts. They proposed this was possibly due to (i) site blockage and (ii) inhibited reduction of the catalysts. Sulfur also affected the Co/TiO₂ and Co/SiO₂ FTS catalysts during the F-T reaction.

It is believed and widely acknowledged that the effect of S-poisoning on both catalyst selectivity and activity is extremely complex and depends on the concentration of sulphur. It has been suggested that in order to minimise the deactivation of both iron and cobalt-based industrial Fischer-Tröpsch catalysts, the sulphur content of syngas should not exceed 0.02 mg/m³[17].

1.4.1.3 Carbon deposition / fouling

Carbon deposition/fouling is the lay down of carbonaceous species onto the catalyst surface that results in blockage of active sites or pores thus decreasing activity (see Figure 1-5). In severe deposition/fouling, the disintegration of catalyst particles and plugging of the reactor voids may occur.

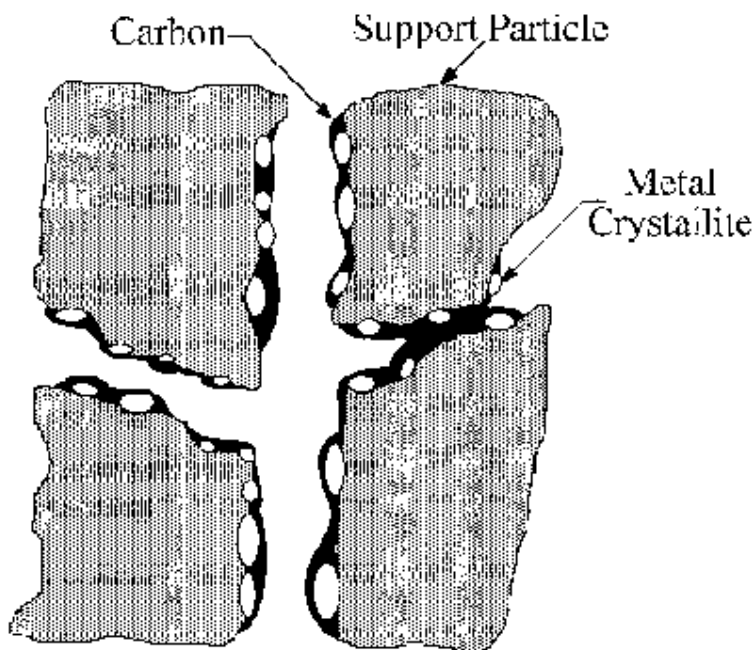


Figure 1-5 Conceptual model of fouling, crystallite encapsulation and pore plugging of a supported metal catalyst due to carbon deposition [37].

Bartholomew [37] reported that cobalt-based Fischer-Tröpsch synthesis was a coke-intensive reaction. Freide et al.[46] studied the effect of co-feeding CO_2 into the gas feed stream of a cobalt on zinc oxide catalyst during realistic FTS conditions. Although the catalyst system was very stable over 1000 h TOS, the catalyst inevitably underwent slow deactivation and needed mild regeneration. XRD measurements showed that the cobalt crystallite size remained unchanged after 100 h TOS even though the activity of the catalyst had decreased. It was discovered that the mechanism of deactivation was due to very small levels of carbon, deposited on the cobalt crystallite sites. It is extremely difficult to remove this carbon without damaging the catalyst morphology, thus making the catalyst useless.

1.4.1.4 Sintering

Sintering is the aggregation of small metal particles of the catalytic phase reducing the catalyst surface area. Sintering can also be the reduction of support area due to support collapse and of catalytic surface area, due to pore collapse on metal crystallites [9]. Sintering generally takes place at high reaction temperatures and is generally accelerated in the presence of water.

Bertole et al. [41] showed that unsupported cobalt based FTS catalysts underwent sintering when they were subjected to high water partial pressures. They found 'crowding' of the surface by active carbon. Similarly Bartholomew [37] stated that water vapour also increases the rate of sintering but on supported metals.

Jacobs et al. [42] studied unpromoted and Pt promoted Co/Al₂O₃ catalysts under realistic FTS conditions with the introduction of water. Catalysts with cobalt cluster sizes 5-6 nm and >10 nm were investigated. It was found that the catalysts with smaller cluster sizes reacted with the alumina support to form cobalt aluminate-like species. They were also more sensitive to permanent deactivation from water. However, the catalysts with larger cluster sizes deactivated by surface oxidation to form cobalt oxide. They found the clusters sintered by an oxidation-reduction cycle and suggested the oxidation of cobalt clusters to cobalt oxide was due to the interaction of the cobalt clusters and support.

Das et al. [74] also found that rhodium promoted cobalt alumina catalysts sintered. They observed an increase in cobalt-cobalt coordination for the cobalt metallic phase during the early part of the deactivation. Although this did not cause a change in the deactivation rate for CO conversion, they still postulate that a main reason for this deactivation was sintering.

1.4.1.5 Formation of compounds between cobalt and supports

The formation of species interacting between cobalt phase and Al_2O_3 support during realistic Fischer-Tröpsch synthesis has been reported [39, 44]. Jacobs et al. [26] studied the deactivation of unpromoted and noble metal-promoted cobalt Al_2O_3 catalysts. They found that the catalysts tested showed a fraction of cobalt reacting with the Al_2O_3 support to produce cobalt aluminate, thus accelerating deactivation via oxidation. Promoting the Al_2O_3 catalysts with a noble metal allowed for easier reducibility. These noble metal catalysts displayed higher initial activity due to the increased reducibility but, the rate of deactivation for these catalyst was more severe than for unpromoted catalysts.

Li et al. [43] performed similar experiments to Jacobs et al. [26]. They studied the effect of water on the deactivation of unpromoted and Pt promoted cobalt Al_2O_3 catalysts. Similarly they found that Pt promoted cobalt Al_2O_3 catalysts had easier reducibility compared with the unpromoted catalysts.

Authors do differ in the explanation for the exact species that interact but most agree that they are small cobalt species with different degrees of interaction with the support, that hinder their reduction to cobalt metal.

Kiss et al. [45] found that a needle-like crystalline cobalt-silica mixed oxide was formed at high water partial pressures, created by high CO conversion or steam cofeeding in Fischer-Tröpsch synthesis, which caused an increase in deactivation of the catalyst. Chen et al. [75] studied the deactivation of $\text{Co}/\text{ZrO}_2/\text{SiO}_2$ catalyst for Fischer-Tröpsch synthesis under hydrothermal conditions. They found that the silicates species in the $\text{Co}/\text{ZrO}_2/\text{SiO}_2$ catalyst were enhanced under these conditions, thus possibly being responsible for the irreversible deactivation of the catalyst.

1.5 Reaction Mechanisms in Fischer-Tröpsch

Many authors have reviewed the mechanism of the F-T synthesis reaction but it has been the subject of much debate since Fischer and Tröpsch discovered the reaction in 1923. It is widely accepted that the FTS is a polymerisation-like process with the following steps [76]:

1. Reactant adsorption
2. Chain initiation
3. Chain growth
4. Chain termination
5. Product desorption
6. Readsorption and further reaction

The plots of $\log(W_n/n)$ against carbon number n yield straight lines over a fairly large range of products. These plots will give the product distribution of the F-T reaction and can be described by the Anderson-Schulz-Flory (ASF) equation:

$$W_n = n(1-\alpha)^2 \alpha^{(n-1)} \quad (11)$$

Where W_n is the mass fraction of the carbon-atoms with a chain containing n carbon-atoms. The chain growth probability, α , is independent of n and W_n is the mole fraction of a hydrocarbon with chain length n . The growth probability factor, α , is the ratio of the chain propagation rate constant to the chain propagation plus the termination rate constants defined by [76]:

$$\alpha = \frac{R_p}{R_p + R_t} \quad (12)$$

where R_p and R_t are the rates of propagation and termination, respectively. α determines the total carbon-number distributions of the F-T products (see Figure 1-6). The ASF equation predicts the selectivities towards the following products that are produced in the FTS reaction: methane, gasoline, diesel and waxes. Under certain FTS reaction conditions methane can be produced in 100%

selectivity; with all other products having a well-defined maxima of selectivities shown in Figure 1-6[76]. The highest selectivities that can be achieved by the F-T synthesis are, in wt%, methane 100; ethylene 30; gasoline (C_5-C_{11}) 48; diesel fuel ($C_{12}-C_{18}$) 25.

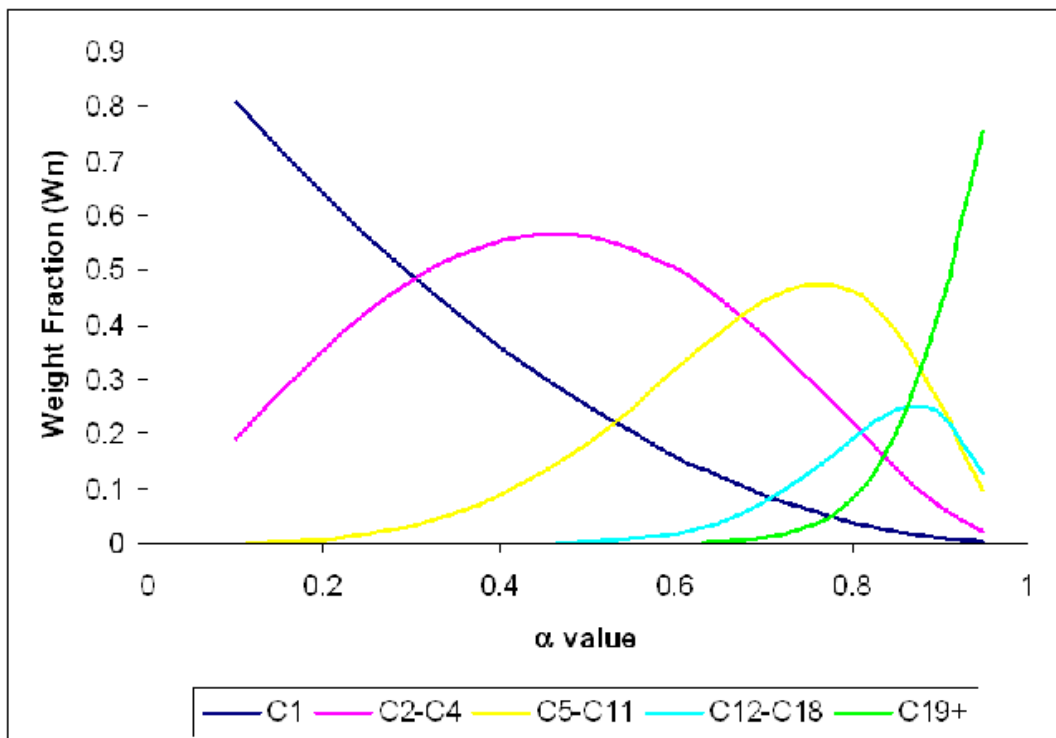


Figure 1-6 Hydrocarbon selectivity as a function as function of the chain growth probability factor, α [76].

It is possible to increase the chain growth probability, α , by using the following parameters [76]:

1. Choice of active phase (Co, Ru, Fe)
2. Addition of promoter (eg. K for Fe)
3. Increase pressure
4. Decrease temperature
5. Decrease $H_2:CO$ ratio

As the F-T process involves many intermediates, there have been numerous proposed schemes of F-T reactions, since the discovery of FTS process. The initial scheme, proposed by Fischer and Tröpsch in 1926, suggested that through

a carbide intermediate, chain growth occurred [77]. Later Brady and Petit suggested that methylene addition to a growing chain could be a possible mechanistic route [78]. Another proposed route involving oxygenate intermediates was suggested by Elvins and Nash [79] while other groups proposed chain growth was accomplished via insertion of undissociatively adsorbed CO [80].

1.5.1 Mechanisms involving hydrocarbon intermediates

The first mechanism proposed by Fischer in 1926 [77] where the F-T synthesis forms products through a metallic carbide scheme was improved by Craxford et al. [81]. They proposed in more detail that the F-T synthesis might proceed by these steps: (1) chemisorption of CO; (2) formation of carbide by reaction of chemisorbed CO and H₂; (3) the formation of CH₂ groups by carbide and H₂. They believe that selectivity to CH₂ and higher hydrocarbons is established by the amount of H₂ chemisorbed; CH₂ association to produce higher molecular weight hydrocarbons; (4) the higher molecular mass hydrocarbons cracking; (5) the desorption to produce olefins and paraffins.

Investigations on iron based F-T catalysts for the formations of metal carbides as the active sites for F-T reactions have been widely reported [29, 82]. Cobalt based F-T catalysts normally stay in the metallic phase during F-T synthesis however, low concentrations and small sizes of cobalt carbide particles have been detected. These small particles are unstable and decompose to metallic cobalt and carbon.

Different studies have been used to test the carbide theory. Biloen et al. [83] proposed that chain growth proceeds via CH_x species. Other investigations by Young et al. [84] demonstrated that a methylene group could be inserted into a M-C bond. The carbide theory was questioned by Eidus [85] who treated the carbide intermediate with CO and did not produce any liquid hydrocarbons and this was mirrored by Kummer et al. [86] who determined that bulk phase carbide does not participate in the F-T synthesis over iron catalysts.

Brady and Petit [78, 87] proposed an alkyl scheme based on the carbide mechanism (Figure 1-7). They believe M-hydride bonds initiate the polymerisation and chain propagation occurs via CH₂ insertion into M-hydride bond.

This scheme does not explain the formation of branched hydrocarbons, the small volumes of C₂ molecules or β-elimination of M-hydrides.

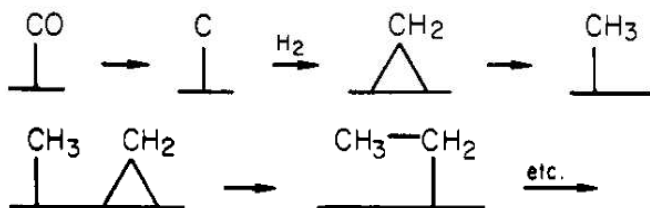


Figure 1-7 Proposed alkyl scheme based on the carbide mechanism[78]

1.5.2 Mechanisms involving oxygenated intermediates

As mentioned earlier, the carbide theory does not support the formation of oxygenated products. It was thought that an oxygen intermediate might be involved in the mechanism for FTS. Emmett et al.[88] supported the theory that chain growth follows via a condensation reaction involving two hydroxycarbene species with the elimination of water. They added various alcohols to the syngas feed and passed this over a iron catalyst. They found primary alcohols adsorbed on the catalysts and might have acted as propagators in the formation of higher molecular weight hydrocarbons. They also concluded that isopropyl alcohol was adsorbed in smaller amounts. They concluded that the adsorbed species (OH-containing complexes) could be formed from CO and H₂ during FTS and might be behaving as intermediates in the formation of products during FTS. Figure 1-8 represents the proposed scheme by Kummer et al. They suggest that the species attaches to the surface via M-C bond.

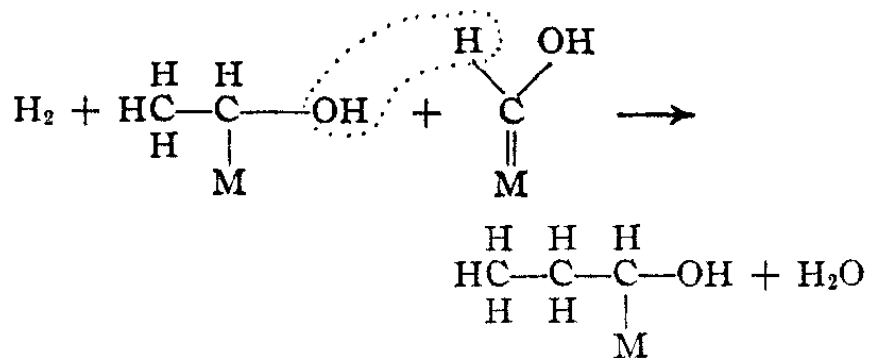


Figure 1-8 Hydroxycarbene scheme[89]

Blyholder et al. [90] later suggested that the complex might attach via both the M-C and M-O bond. Another proposed mechanism was that chain propagation proceeds via CO insertion into M-H (initiation) and M-alkyl (chain growth) bonds [80] as shown in Figure 1-9 [91].

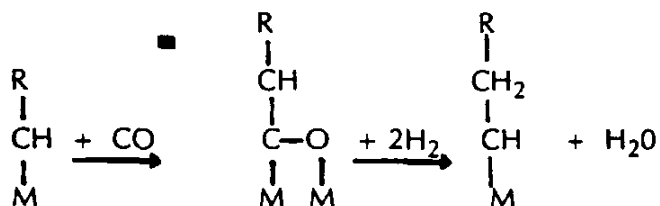


Figure 1-9 CO insertion mechanism [91]

1.5.3 Mechanism involving methylene and CO insertion

Many believe the CH₂ insertion mechanism to be the dominant mechanism for F-T synthesis but it does not explain how oxygenated products are formed. It is widely assumed that the formation of oxygenates proceeds via the CO insertion mechanism. Dry [92] proposed a mechanism that included CH₂ and CO as active surface intermediates. Gaube et al. [93] studied the reaction mechanism of F-T synthesis on iron and cobalt catalysts. They used co-feeds of various alkenes and alcohols and came up with two schemes Figures 1-10 and 1-11. Mechanism 1 (Figure 1-10) shows the possible reaction scheme for chain growth by initiation of the CH₂ monomer. Mechanism 2 (Figure 1-11) shows the reaction scheme for chain growth by initiation of the CO monomer. The co-feeding experiments presented by Gaube et al. shows without exception the theory that two contrary mechanisms involving both CH₂ and CO monomers are possible in the chain growth of FTS.

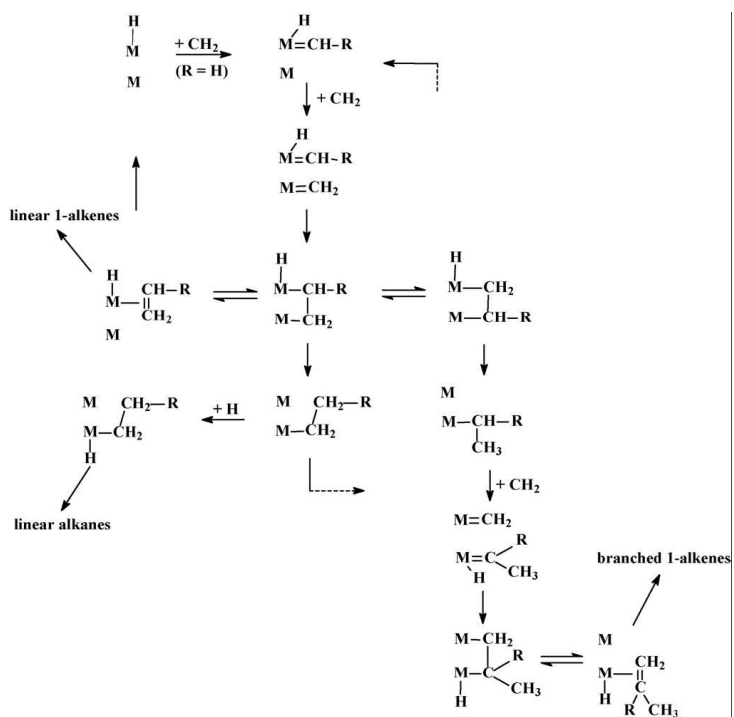


Figure 1-10 Mechanism 1 (M = iron or cobalt)

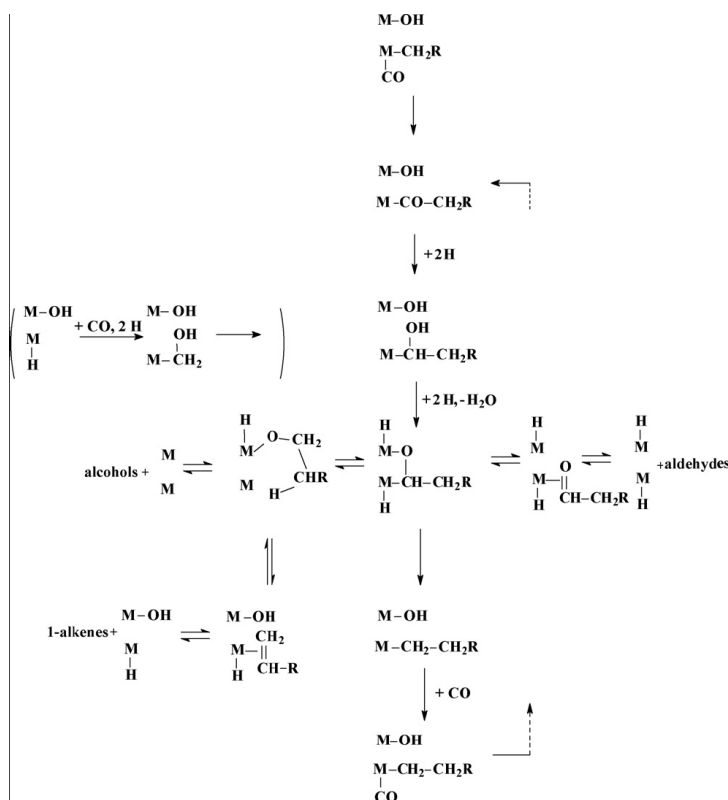


Figure 1-11 Mechanism 2 (M = iron or cobalt)

1.6 Use of different species in the study of F-T

It is difficult to identify reaction intermediates and various methods have been used over the years. An important role in the understanding of the F-T mechanism is the use of probe molecules that can interact with one or more intermediates to produce distinctive products. If these probe molecules resemble active species then they should be incorporated into the reaction [94]. Probe molecules such as olefins, to alcohols, and to C1 and C2 molecules have been used in mechanistic FTS studies.

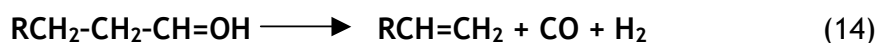
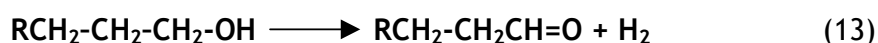
1.6.1 Using alcohol as probes

An early study by Emmett and coworkers [89] found the alcohols acted as chain propagators when co-feeding syngas with ^{14}C labelled alcohols over iron catalysts at a pressure of 1 bar and a reaction temperature of 235°C , while Blyholder et al. [90] studied the co-feeding of labelled ethanol over cobalt-based F-T catalysts. There were three differences:

- 1) CH_4 activity was high for cobalt catalysts but not for iron catalysts.
- 2) Roughly 35% of products originated from the ethanol over iron catalysts and chain initiation occurred at the C-atom to which the OH was attached. For cobalt catalysts the incorporation of ethanol was much lower.
- 3) Cobalt catalysts produced far more C_2 products than iron catalysts which suggests that the intermediates are different between cobalt and iron. Cobalt dehydrated ethanol to ethylene but it was proposed that this alcohol might be an intermediate for chain propagation in iron catalysts.

Davis et al. [95] also agreed with the earlier studies of Emmett et al. [89] that ethanol started chain growth but did not serve as a propagator. When Davis et al. [95] co-fed 1-propanol and 2-propanol over iron catalysts they found that 10-20% 1-propanol incorporated into straight chain products but only 1-3% 2-propanol incorporated into branched products. It was proposed that alkenes were intermediates formed via alcohol dehydrogenation but this was contested by Davis et al. [95] due to the dehydration of alcohols to alkenes was very low

for the same C number. It was decided that the route of alkene products for iron catalyst in FTS was not by alcohols [96]. They thought that alkenes, produced through two steps with inclusion of alcohols, serve as chain initiators. Aldehydes can be formed by the dehydrogenation of alcohols (equation 13). They could then change to terminal olefins with one less C-atom (equation 14) but this cannot be achieved with ethanol as it converts to CH₄ and CO.



From literature it can be concluded that alcohols are intermediates that are involved to some extent in the production of hydrocarbons for iron catalysts. It is clear that iron and cobalt FTS reactions do not follow the same pathways and oxygenate intermediates are not important with cobalt catalysts.

1.6.2 Using alkenes as probes

As early as 1930 alkenes were added to the FTS reaction [97]. Hydrogenation is an important reaction when alkenes react under FTS conditions. Gibson [98] studied the hydrogenolysis of ethylene over cobalt catalysts and found that C₁ molecules from ethylene seemed to serve as monomers for chain growth. When ethylene was passed over iron catalysts under normal FTS conditions a small volume of CH₄ was found but on increase in reaction temperature this amount of CH₄ increased [99].

Adesina et al. [100] found that ethylene was a chain initiator over cobalt catalysts under realistic FTS conditions. They found that C₃-C₅ products increased from 40-160% and C₆-C₈ products increased by 50%. They also commented that the alpha value was not changed which implies that ethylene in large-scale propagation is not probable; it is just present as a chain initiator. This observation was also found for iron catalysts [101] where it was established that ethylene in concentrations > 5 mol% suppressed CH₄ formation.

Schulz et al. [102] studied the addition of alkenes of different chain lengths over cobalt catalysts and found that incorporations of 29% ethylene, 31% propene, and 6% 1-hexadecene occurred. For cobalt catalysts hydrogenolysis of ethylene occurred but less hydrogenolysis was seen using iron catalysts. The reactions that occurred with these additions were hydrogenation and isomerization and it was commented that co-feeding of alkenes is not a reasonable mechanism for changing the alpha value.

The incorporation of ethylene into F-T products over iron catalysts is small, as most authors report. Snel et al. [101] observed a larger incorporation of ethylene on iron-calcium catalysts. They found up to 66% of ethylene was incorporated into larger molecular weight hydrocarbon products. Snel et al. [101] believed the different results they obtained was due to the method of catalyst preparation and the low H₂ to CO ratio. Boelee et al. [103] carried out numerous co-feeding experiments of ethylene for FTS. They concluded that the outcome of ethylene additions was down to two factors: (1) C₂H₄/CO ratio (competitive adsorption) and (2) CO conversion (activity).

Hydrogenation is the main reaction for co-fed alkenes under FTS conditions. Alkenes are incorporated into higher molecular weight products under cobalt-based FTS catalysts. Hydrogenation and isomerization of alkenes were also detected. Iron-based FTS catalysts seem to show less incorporation but it is widely thought that alkenes serve as chain initiators.

1.6.3 C1 and C2 molecules as probes

Brady and Petit [78, 87] co-fed methylene groups into hydrocarbon chains. They studied the products of diazomethane (CH₂N₂), C1 probe, over various metals. They found that products with similar molecular weights (ASF distribution) were formed with higher alpha values than with normal FTS using only syngas. They proposed that these experiments followed an alkyl mechanism of insertion.

Long et al. [104] conducted experiments that co-fed vinyl bromide (C₂H₃Br) and ethyl bromide (C₂H₅Br) over Ru/SiO₂ catalysts under realistic FTS conditions to see the effect of C2 probe molecules. They found that C2 species formed from

vinyl bromide were easily incorporated into F-T products but the species formed from ethyl bromide only incorporated into C2 fraction of the products, thus providing proof that unsaturated C2 units are crucial for chain initiation.

From literature it can be concluded that C1 and C2 species can be incorporated into F-T synthesis products. C1 species are chain initiators and building blocks to produce longer hydrocarbon chains whereas C2 unsaturated species only play a role in chain initiation.

1.7 Project Aims

The aim of the project was to:

- 1) Characterise two 20 wt% Co/Al₂O₃ catalysts, that were prepared by two different techniques, for use in low-temperature Fischer- Tröpsch Synthesis.
- 2) Investigate the difference in activity, selectivity, and deactivation between these two catalysts under typical low-temperature Fischer-Tröpsch conditions.
- 3) Investigate the effect of co-feeding different liquids: alcohols, alkanes, and aromatics, into the Fischer- Tröpsch reaction.

2 Experimental

The following chapter describes the experimental techniques utilised throughout the course of this study. Included are any equations or calculations that were used during the treatment of the results. The actual results and discussion of results are described in chapter four.

2.1 Catalyst preparation

For catalytic testing, two transition metal catalysts were prepared, both over alumina support, with 20% metal loadings. These catalysts were prepared by two different methods described below in sections 2.1.2 and 2.1.3. The first method was via the nitrate route and the second method via the HDC catalyst route. The two cobalt catalysts were prepared at the laboratories of Johnson Matthey PCT in Billingham.

2.1.1 Support properties

The support chosen for the catalysts was Puralox HP14/150 gamma alumina. The support properties are shown in table below, and were provided by Adel Neale from Johnson Matthey:

| | |
|---------------------------------------|------|
| Average pore diameter (Å) | 282 |
| Pore volume (cm ³ / g) | 1.04 |
| BET surface area (m ² / g) | 148 |

Table 2-1 Support properties of HP14/150 gamma alumina

2.1.2 Preparation via the nitrate method

This catalyst was prepared by impregnating the support to incipient wetness with an aqueous solution containing the precursor salt. The wet catalyst was then oven dried prior to calcination. The metal precursor of the catalyst was cobalt (II) nitrate hexahydrate supplied by Shepherd Widness.

To ensure uniform and maximum metal dispersion throughout the support precursor was dissolved in a volume of water equal to the pore volume of the support.

2.1.2.1 Procedure

50.0g of alumina was weighed out into a plastic bag. 62.56g of cobalt nitrate feed was weighed out into a beaker along with 12.38g of water. This was then heated and stirred until the cobalt nitrate went into solution. Once into solution the cobalt nitrate was added to the alumina in small aliquots. Between each addition the bag was sealed, shaken and kneaded from the exterior to obtain as near as possible to a free flowing uniformed powder (incipient wetness). This was then repeated for another 50g of alumina. The impregnated samples were then mixed and placed on a glass tray. They were dried and calcined in an oven, which was heated to 120°C in 45mins, and held for 3hours then heated to 200°C in 40mins and held for an hour.

2.1.3 Preparation via the High Dispersion Cobalt (HDC) catalyst method

High-Dispersion-Cobalt (HDC) catalysts are prepared for improved FT productivity. They are produced to try to manufacture catalysts with dispersions at, or close to, the postulated optimum dispersion compared with the nitrate route.

These catalysts are made by a single deposition step by deposition-precipitation of cobalt compounds at high pH via cobalt ammine complexes. This leads to

uniform distribution of cobalt crystallites of 3-5nm. Due to high dispersion and cobalt loadings, the catalysts have high weight and volume activity.

2.1.3.1 Procedure

A 2000 ml solution was prepared for the HDC preparation. 99.0g of ACC ammonium carbonate chips, 95.0g ml 30% NH₃ solution, 93g ml demineralised water and 98g Cobalt Basic Carbonate (Co BC) were added together in a beaker and stirred for 1 hour. 26 ml of 30% H₂O₂ was added over 19mins. This was used as an oxidiser. Then the mixture was stirred for a further 18mins. This solution was filtered and stored overnight.

1925ml -2.9 w/w% cobalt hexamine solution was added to a 5000 ml round bottomed flask (this was the solution that was prepared earlier), filled with a reflux condenser, pH probe and mechanical stirrer. The stirrer was set at 450rpm and alumina support (156.3g) was slowly added to the stirred solution. The reaction mixture was refluxed until all the ammonia distilled off and metal deposition was complete (visible by a change in colour of the solution).

2.1.3.2 Observations

The solution was dark mauve to start but when metal deposition was complete the solution was black. The pH of the solution was continually monitored throughout the reaction. Reflux was continued for 15 mins to age the reaction mixture. The reaction mixture was then filtered via Buchner flask to collect the catalyst. The catalyst was washed with demineralised water and left to dry on the Buchner flask for 30 mins. The sample was dried at 105°C overnight (12 hrs). When the Co/Al₂O₃ (HDC) catalyst had dried, it was then filtered through a sieve (1000 microns) to break the sample up as it had clumped together during drying.

When preparing HDC catalysts there is always a change in pH and usually a change in colour. The depositions were carried out under high pH conditions to facilitate strong interaction between positive metal ions and negative alumina support material. The pH decreased over the first 30 mins (see Figure 2-1) of the deposition process as ammonia was distilled off. During the synthesis of the

HDC catalyst a colour change was observed during the precipitation process (metal deposition). The cobalt solution went from mauve to black, which is due to a change in oxidation state of the cobalt ions.

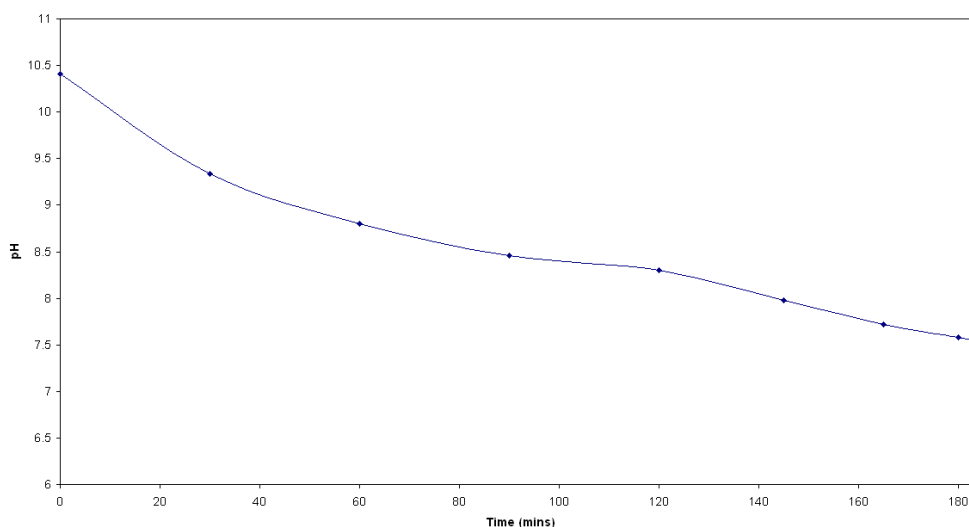


Figure 2-1 Graph of pH vrs Time (mins) of the deposition process.

A table of the prepared catalysts are shown below:

| Catalyst |
|---|
| 20 % CoNIT/Al ₂ O ₃ |
| 20 % CoHDC/Al ₂ O ₃ |

Table 2-2 Laboratory prepared catalysts

2.2 Characterisation Techniques

As the condition of the catalyst surface plays an important role in heterogeneous catalysis, a number of techniques were used to investigate the materials and their surfaces. These techniques included BET surface area, Thermo-gravimetric analysis (TGA) temperature-programmed-reduction (TPR), powder X-Ray Diffraction (XRD), TPR-UV-vis-NIR spectroscopy and Transmission Electron Microscopy (TEM). The results of these techniques are detailed in section 4.

2.2.1 BET Surface area analysis

The total surface area of the catalyst was determined by Brunauer, Emmett, Teller (BET) analysis (Equation 15). This process uses the physisorption of nitrogen to determine the surface area of solids. Surface area measurements for all of the catalysts prepared were determined using a Micromeritics Gemini III 2375 Surface Area Analyser. Approximately 0.04g of each sample was weighed into a glass sample tube and purged in a flow of N₂ overnight at 383K before the measurement was carried out to remove any adsorbed species from the surface. The evacuation rate used was 4.0x10⁴ Pa min⁻¹ (300 torr min⁻¹).

$$\frac{p}{V(p_0-p)} = \frac{1}{V_m c} + \frac{(c-1)}{V_m c} \cdot \frac{p}{p_0}$$

Equation 15 Brunauer, Emmett and Teller (BET) equation

where V = amount of gas adsorbed at equilibrium pressure P

V_m = amount of gas in a monolayer

p_0 = saturation pressure

$V \longrightarrow \infty$ at $P = P_0$

c = BET constant defined as:

$$c = \exp[(\Delta H_1 - \Delta H_L)/RT]$$

H_1 and H_L are the adsorption enthalpy of first and subsequent layers

2.2.2 Thermo-gravimetric analysis (TGA)

Thermo-gravimetric analysis was performed on pre and post reaction catalysts using a combined TGA/DSC SDT Q600 thermal analyser coupled to an ESS mass spectrometer for evolved gas analysis. Samples were heated from 30°C to 1000°C using a heating ramp of 10°Cmin⁻¹. This temperature profile was employed using O₂/Ar, H₂/Ar or Ar at a flow rate of 100ml min⁻¹. For mass spectrometric analysis, various relevant mass fragments were followed such as 28 (CO) and 44 (CO₂). The sample loading was typically 10-15mg.

2.2.3 Hot stage powder X-ray diffraction (XRD)

To obtain information concerning the phase composition and the distribution of the crystallite size of the catalyst, XRD studies were performed using a Siemens D5000 X-ray diffractometer (40kV, 40mA) using monochromatic CuK alpha X-ray source (1.5418Å). The scanning range used was $5 < 2\theta < 85^\circ$ with a scanning rate of 1 second / step and a step size of 0.02°. The fresh samples were examined as well as a selection of post-reaction samples to determine any changes in catalyst morphology.

In situ hot-stage comprises of a water-cooled, vacuum tight, stainless steel chamber with a beryllium window shown in Fig. 2-2. The internal fittings were mounted on the front flange, which was inserted into the rear part of the chamber attached to the goniometer.

The samples were heated at 12°C / min and scans taken at 30°C, 100°C and then at 100°C increments thereafter to 900°C. At each stage the sample was held for 15mins at the desired temperature before the scan was taken, with each scan lasting 115 minutes.

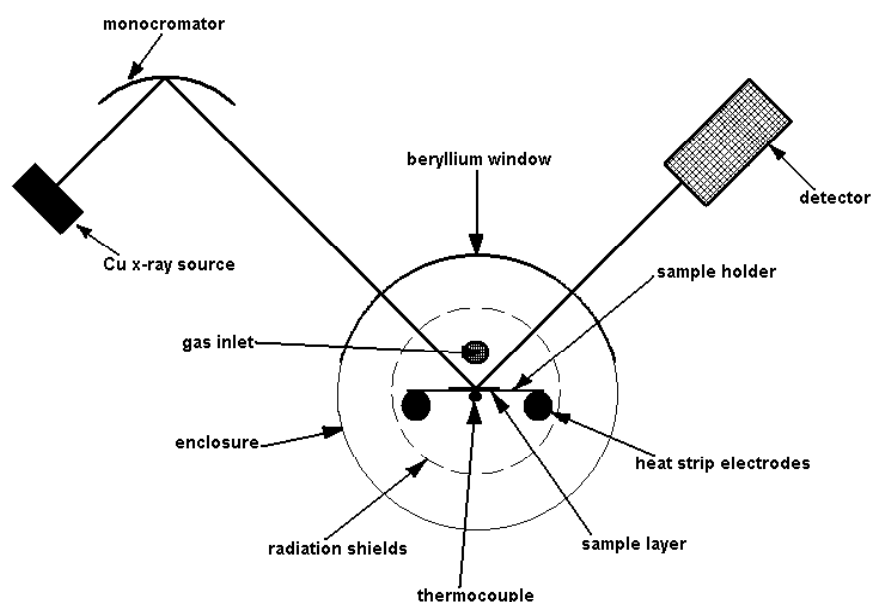


Figure 2-2 Schematic of hot stage X-ray chamber

Where possible, the Scherrer Equation was used to determine the average crystallite size by using the line-width of the strong signals in each sample.

$$d = \frac{k \lambda}{B \cos\theta} \quad (16)$$

Equation 16 The Scherrer Equation[105]

where

- d = particle size diameter / Å
- k = constant / 57.2978°
- λ = wavelength of X-ray source / 1.5418
- B = full width at half maximum / degrees
- θ = diffraction angle / degrees

This is only an approximate method since the results can be influenced by various factors such as lattice distortion as well as instrumental parameters.

2.2.4 TPR-UV-vis-NIR spectroscopy

Solid-state UV-vis-NIR spectroscopy of the powdered catalysts was carried out using a Praying Mantis Diffuse Reflectance Accessory, equipped with a temperature controlled reaction chamber connected to a gas dosing system, on the Varian Cary 500 Scan spectrometer. Two hemispherical mirrors positioned above the sample collected the light reflected by the sample/reference. The light collected was then projected onto the instrument detectors. The advantage of using this attachment was that very small solid samples could be analysed, without reducing the wavelength that could be examined. Baselines were collected using BaSO₄ as a reference. The spectra were recorded between 800 nm to 200 nm with baseline correction. For the catalysts, fresh samples were heated from 30°C to 600°C using a heating ramp of around 5°C min⁻¹.

2.2.5 Transmission Electron Microscopy (TEM)

High-Resolution Transmission Electron microscopy (TEM) was performed on a Jeol 1200EX instrument equipped with a tungsten source, at 80kV, with a point-to-point resolution of 0.3nm. Samples were then deposited on copper grids with a holey-carbon-film support. Magnification and camera constants were calibrated using appropriate standards in the same electrical-optical conditions.

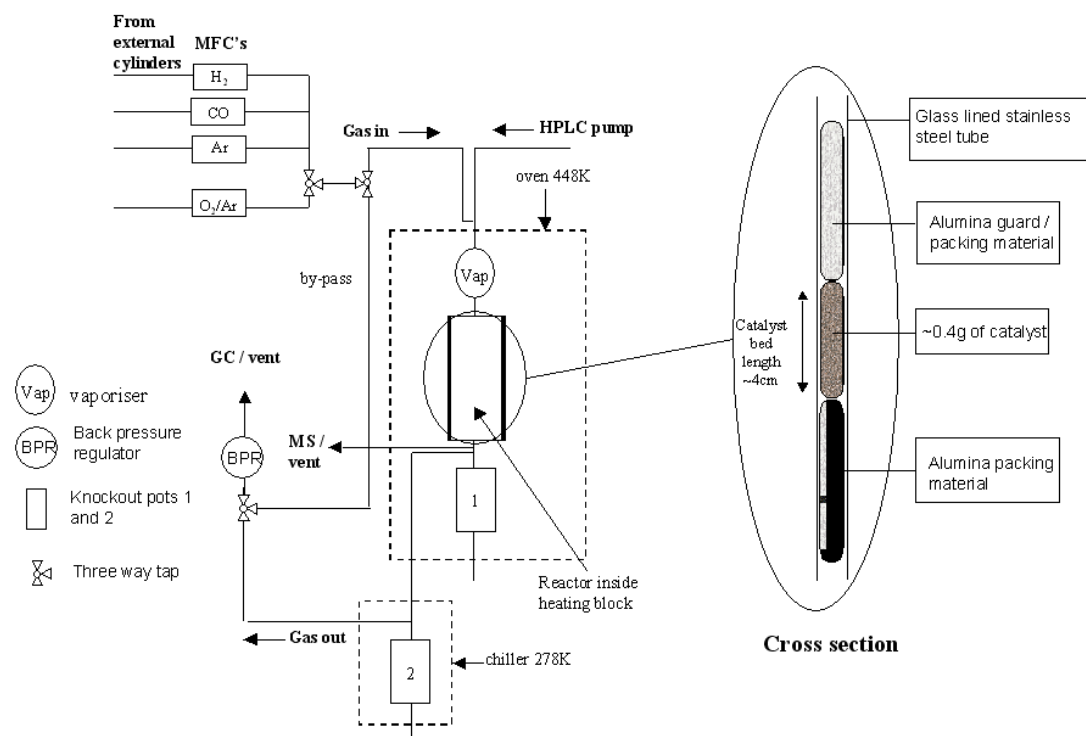
2.3 Catalytic testing

2.3.1 Apparatus

Catalytic tests were carried out in a high-pressure rig with a fixed-bed reactor depicted in Fig. 2-3. Gases could be fed into the reactor via mass flow controllers and pressures up to 20 bar could be achieved. Liquid feeds could be introduced into the system prior to the reactor via the use of an HPLC pump. The feeds were vaporised inside a stainless steel bulb to insure laminar flow into the reactor. Certain parts of the rig are housed inside a large oven that is heated to 448K. This is to prevent some products from solidifying and blocking up in the rig.

The rig is complicated and was built purposely for these sets of FT reactions. Because the rig was built from new this build is explained in more detail in section three.

Figure 2-3 Reactor setup



2.3.2 Reaction Procedure

The reactor was charged with a fixed bed of packing material, the same gamma alumina that is used as support, on top of which sits the catalyst. Roughly 0.4g of catalyst was weighed out and placed in the reactor. More gamma alumina is placed on top of the catalyst to fill the reactor tube. Prior to reaction the catalyst was reduced in H₂, at atmospheric pressure, *in-situ* at 47ml/min (5000GHSV) (Fig 2-4). The catalyst was heated from room temperature to 393K at 3°C / min and dwelled for 2 hrs. Then it was heated to 698K at 3°C / min and dwelled for 9 hrs. It was then allowed to cool overnight in flowing H₂ to 423K.

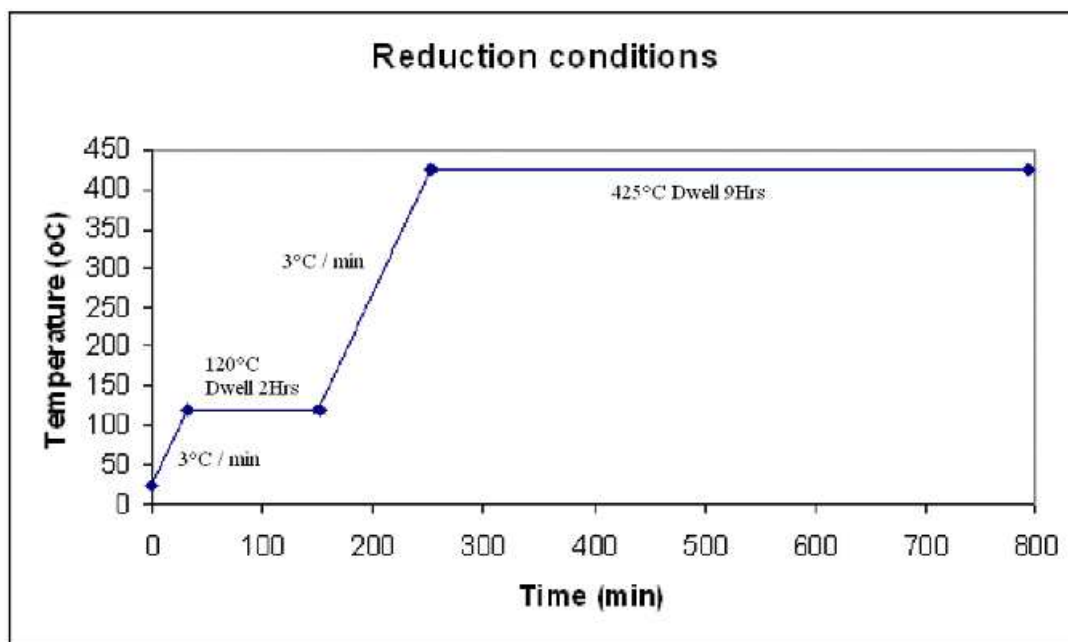


Figure 2-4 Reduction programme before reaction

The catalyst was then introduced to a flow of the desired reaction gas mix. A 2.1:1 ratio of $H_2:CO$ at 47ml/min (5000GHSV) was used for each experiment. The pressure in the reactor was built up to 20 bar using the backpressure regulator. Once this had been reached the start-up procedure began (Figure 2-5). The temperature was increased from 423K to 463K at $1^\circ C / min$ and dwelled for 30mins to stabilise, then increased to 483K at $0.1^\circ C / min$. Once reaction temperature was reached the analysis began.

Some experiments involved the introduction of a liquid feed prior to the reactor via the use of a HPLC pump. The desired liquid was introduced into the reactor via the HPLC pump with flows between 0.01 - 5.0 ml / min. The HPLC pump was pressurised up to ~50 bar then introduced into the reactor via opening of a two-way tap. The liquid was pumped into the reactor at 5.0 ml / min for a period of 10mins. This was to fill the dead space before the reactor with liquid. The flow was then reduced to 0.02 ml / min.

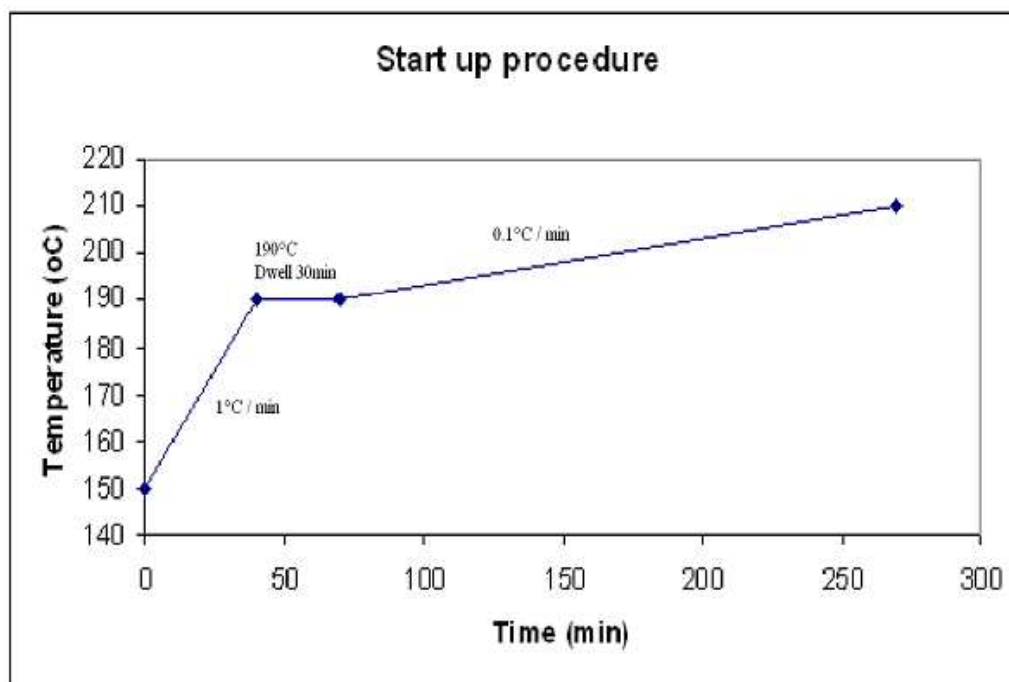


Figure 2-5 Start-up procedure

2.3.3 Gas Chromatography (GC)

Product analysis was carried out by offline Gas Chromatography (G.C.). The ThermoFinnigan Focus GC was fitted with a Chrompack column (CP-Sil 5CB), length 50 meters and internal diameter 0.25mm. It is a capillary column with 100% dimethylpolysiloxane phase.

2.3.3.1 Column conditions

Analysis was carried out on liquid (light hydrocarbons) and wax (heavy hydrocarbon) products therefore two different GC methods were used.

2.3.3.1.1 Method 1 – Light hydrocarbons:

Injector temperature - 613K

Carrier gas - Hydrogen with 2.0 ml / min flow

The column heating profile is shown below:

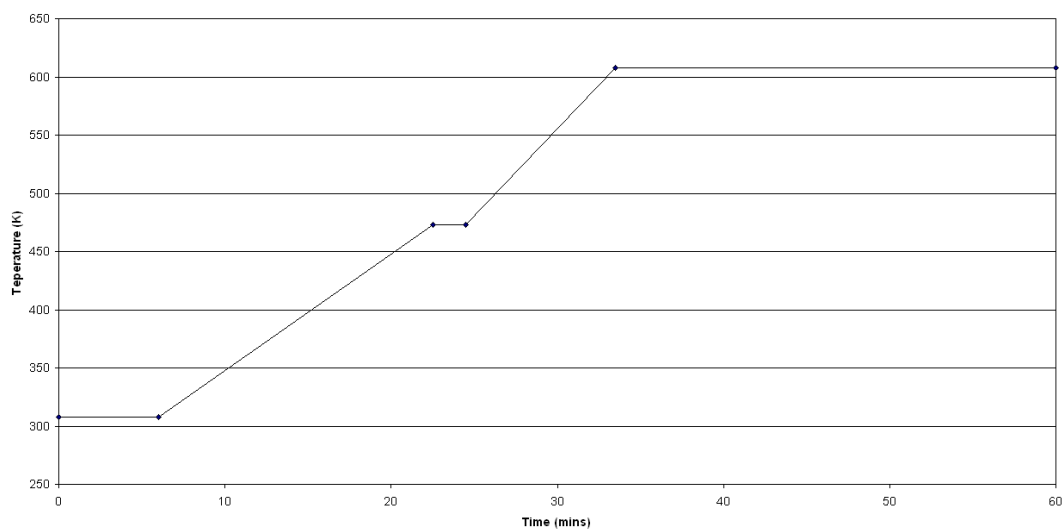


Figure 2-6 Light hydrocarbons GC temperature ramp profile

| Time (mins) | Temperature (K) |
|-------------|-----------------|
| 0 - 6 | 308 |
| 6 - 22.5 | 308 - 473 |
| 22.5 - 24.5 | 473 |
| 24.5 - 33.5 | 473 - 608 |
| 33.5 - 60 | 608 |

Table 2-3 Light hydrocarbons GC temperature ramp profile

2.3.3.1.2 Method 2 – Heavy hydrocarbons:

Injector temperature - 613K

Carrier gas - Hydrogen with 6.0 ml / min flow

The column heating profile is shown below:

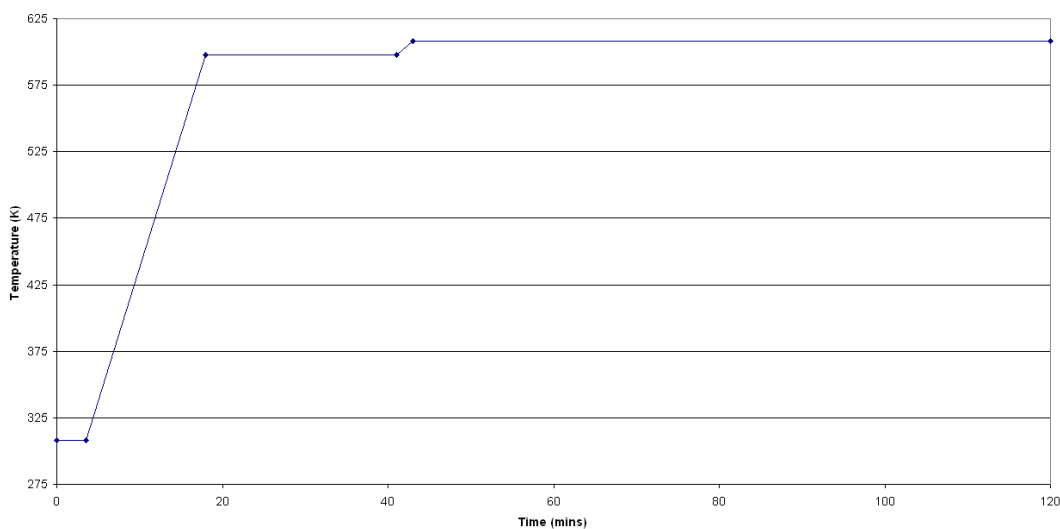


Figure 2-7 Heavy hydrocarbons GC Temperature ramp profile

| Time (mins) | Temperature (K) |
|-------------|-----------------|
| 0 – 3.5 | 308 |
| 3.5 - 18 | 308 - 598 |
| 18 – 41 | 598 |
| 41 - 43 | 598 - 608 |
| 43 – 120 | 608 |

Table 2-4 Heavy hydrocarbons GC temperature ramp profile

2.3.3.2 Calibrations

2.3.3.2.1 Light hydrocarbons

Calibration standards for C5, C6, C7, C8, C10, C12, and C16 alkenes were prepared in 50ml volumetric flasks, using an appropriate diluent. A 1µl sample

was injected into the GC and ran through the light hydrocarbon GC method. From the peak area responses, linear calibration plots were obtained.

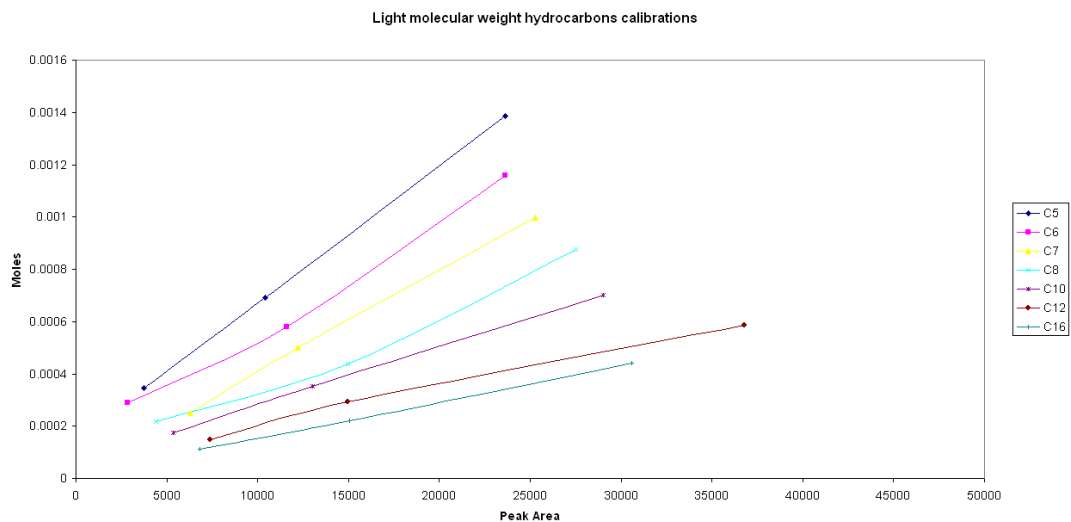


Figure 2-8 Calibration graph for light hydrocarbons

| Carbon number | Equation of trendline | R ² value |
|---------------|--|----------------------|
| 5 | $y = 5.22\text{E-}08x + 1.51\text{E-}04$ | 1.00 |
| 6 | $y = 4.22\text{E-}08x + 1.41\text{E-}04$ | 0.90 |
| 7 | $y = 3.92\text{E-}08x + 9.67\text{E-}06$ | 0.99 |
| 8 | $y = 2.86\text{E-}08x + 6.39\text{E-}05$ | 0.98 |
| 10 | $y = 2.22\text{E-}08x + 5.87\text{E-}05$ | 1.00 |
| 12 | $y = 1.46\text{E-}08x + 5.40\text{E-}05$ | 0.99 |
| 16 | $y = 1.40\text{E-}08x + 1.35\text{E-}05$ | 1.00 |

Table 2-5 Data table for light hydrocarbon calibrations

2.3.3.2.2 Heavy molecular weight calibrations

The GC responses to various higher molecular weight alkenes were calibrated using a standard solution of C₁₀ and C₂₀₋₄₀ alkenes diluted to various concentrations. A 1µl sample was injected into the GC and ran through the heavy hydrocarbon GC method. From the peak area responses, linear calibration plots were obtained.

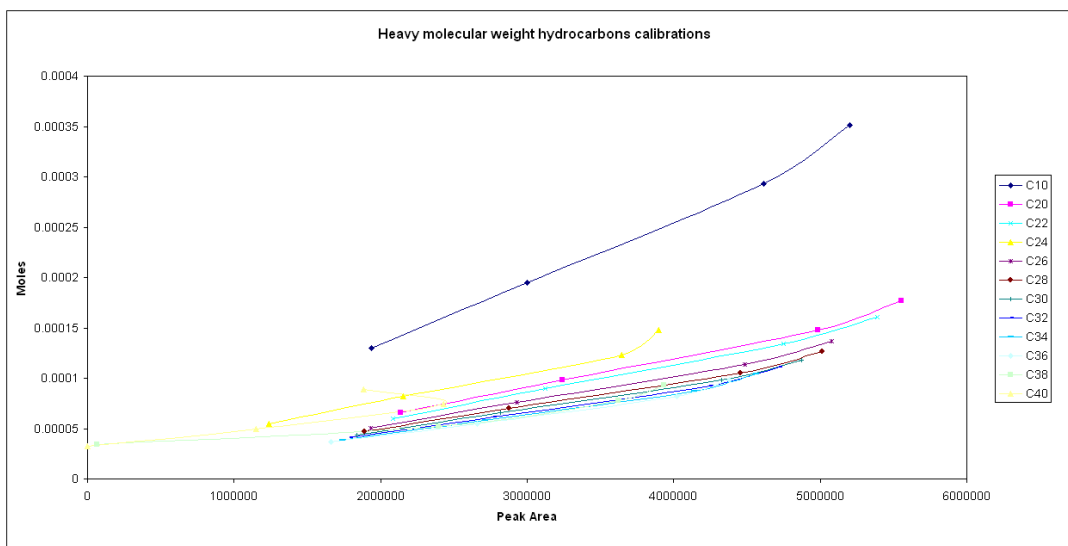


Figure 2-9 Calibration graph for heavy hydrocarbons (even carbon numbers)

| Carbon number | Equation of trendline | R ² value |
|---------------|----------------------------|----------------------|
| 10 | $y = 6.59E-11x - 8.72E-07$ | 0.99 |
| 20 | $y = 3.14E-11x - 2.92E-06$ | 0.99 |
| 22 | $y = 2.99E-11x - 3.72E-06$ | 0.99 |
| 24 | $y = 3.25E-11x - 1.31E-05$ | 0.97 |
| 26 | $y = 2.65E-11x - 1.69E-06$ | 0.99 |
| 28 | $y = 2.47E-11x - 7.09E-07$ | 0.99 |

| | | |
|----|----------------------------|------|
| 30 | $y = 2.38E-11x - 1.02E-06$ | 0.99 |
| 32 | $y = 2.30E-11x - 1.30E-06$ | 0.99 |
| 34 | $y = 2.24E-11x - 1.55E-06$ | 0.99 |
| 36 | $y = 2.19E-11x - 1.56E-06$ | 0.98 |
| 38 | $y = 1.41E-11x + 2.91E-05$ | 0.89 |
| 40 | $y = 2.09E-11x + 3.27E-05$ | 0.77 |

Table 2-6 Data table for heavy hydrocarbon calibrations (even carbon numbers)

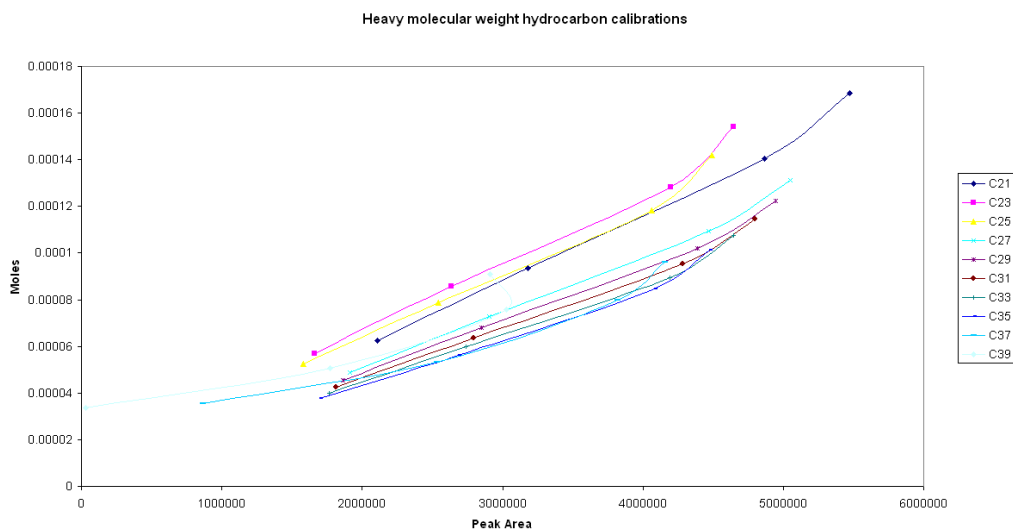


Figure 2-10 Calibration graph for heavy hydrocarbons (odd carbon numbers)

| Carbon number | Equation of trendline | R ² value |
|---------------|----------------------------|----------------------|
| 21 | $y = 3.06E-11x - 3.35E-06$ | 0.99 |
| 23 | $y = 3.11E-11x + 4.11E-06$ | 0.99 |
| 25 | $y = 2.93E-11x + 4.80E-06$ | 0.99 |
| 27 | $y = 2.56E-11x - 1.18E-06$ | 0.99 |

| | | |
|----|----------------------------|------|
| 29 | $y = 2.43E-11x - 8.69E-07$ | 0.99 |
| 31 | $y = 2.34E-11x - 1.17E-06$ | 0.99 |
| 33 | $y = 2.27E-11x - 1.43E-06$ | 0.99 |
| 35 | $y = 2.21E-11x - 1.57E-06$ | 0.98 |
| 37 | $y = 1.75E-11x + 1.64E-05$ | 0.94 |
| 39 | $y = 1.71E-11x + 2.97E-05$ | 0.86 |

Table 2-7 Data table for heavy hydrocarbon calibrations (odd carbon numbers)

2.3.4 Soxhlet extractions

Soxhlet equipment was used to extract soluble species from the catalyst surface post-reaction. A small amount of sample was placed in the glass thimble. The thimble was placed in the soxhlet chamber and the equipment set up as shown:

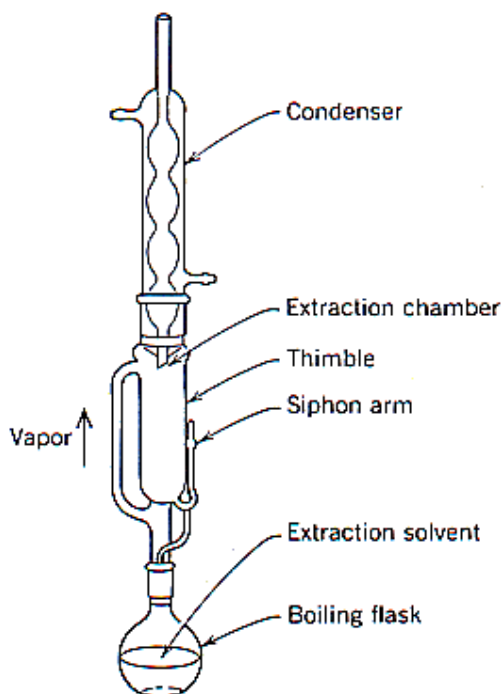


Figure 2-11 Soxhlet apparatus

The solvent, n-heptane, was poured into the still pot along with boiling chips. The solvent was heated to reflux using an oil bath. Solvent vapour travels up the distillation arm, reaches the condenser and drips back down into the soxhlet chamber. The thimble fills with the solvent and any soluble material is extracted. When the chamber is nearly full, the chamber is automatically emptied via the siphon side arm and the solvent drains back down into the still pot.

The process is left to repeat itself overnight to ensure all soluble material is extracted from the catalyst sample. Post extraction a sample is injected into the GC for analysis.

2.4 Materials

2.4.1 Reactions

The following materials were used for reactions and GC analysis of products.

| Material | Purity (%) | Supplier |
|-------------------|------------|-------------------------|
| Carbon Monoxide | 99.99 | BOC |
| Hydrogen | 99.995 | BOC |
| Argon | 99.995 | BOC |
| 2% Oxygen / Argon | 99.99 | BOC |
| Helium | 99.997 | BOC |
| 1 - Octanol | 99+ | Sigma Aldrich |
| 1 - Decanol | 99 | Sigma Aldrich |
| Dodecene | 99 | Sigma Aldrich |
| Napthalene | > 98 | Laboratory Chemicals |

| | | |
|--------------------------|-------|-------------------|
| n - hexane | 99 | Fisher Scientific |
| Dichloromethane (DCM) | 99.99 | Fisher-Scientific |
| n - heptane | 99.86 | Fisher-Scientific |

Table 2-8 Materials used for reactions and GC analysis

2.4.2 Product characterisation and analysis

The following materials were used to characterise and analyse products using the following techniques: BET surface area, Thermo-gravimetric analysis (TGA) temperature-programmed-reduction (TPR), powder X-Ray Diffraction (XRD) and TPR-UV spectroscopy.

| Material | Purity (%) | Supplier |
|---------------------------|-------------------|-----------------|
| Argon | 99.995 | BOC |
| 2% Oxygen / Argon | 99.99 | BOC |
| 5% Hydrogen / Nitrogen | 99.99 | BOC |

Table 2-9 Materials used for characterisation and analysis

2.4.3 Catalysts studied

BET surface area, Thermo-gravimetric analysis (TGA) temperature-programmed-reduction (TPR), powder X-Ray Diffraction (XRD) and TPR-UV spectroscopy were performed on the following catalysts:

| Catalyst |
|---|
| 20 % CoNIT/Al ₂ O ₃ |
| 20 % CoHDC/Al ₂ O ₃ |

Table 2-10 Catalysts studied

2.5 Calculations

The following calculations were used to evaluate the results obtained from the high-pressure rig:

2.5.1 Conversion CO/H₂O

$$\text{Conversion} = [(\text{volume H}_2\text{O (ml)} / 18) / (0.975)] * 100 \quad (17)$$

2.5.2 Selectivity

$$\text{Selectivity} = [(\text{moles of carbon number (C}_n) * C_n) / (C_n * \text{total moles of all C}_n)] * 100 \quad (18)$$

2.5.3 Anderson-Schulz-Flory (ASF) graph

$$\text{Plot } C_n \text{ vs } \ln(\text{mass of } C_n / C_n) \quad (19)$$

2.5.4 Alpha value (α)

$$\alpha \text{ value} = (1 / \text{exponential of gradient of ASF graph}) \quad (20)$$

2.5.4.1 Background / theory of ASF and alpha plots for F-T

n = carbon chain length

α = chain growth probability

W_n = mass fraction of the C-atoms with a chain containing n C-atoms

$$\frac{W_n}{n} = a^{n-1}(1-a)^2 \quad (21)$$

To calculate α log or ln versions of this equation are used as follows

$$\ln\left(\frac{W_n}{n}\right) = (n-1)\ln a + \ln(1-a)^2 \quad (22)$$

or re-arranging

$$\ln\left(\frac{W_n}{n}\right) = n\ln a + \ln\frac{(1-a)^2}{a} \quad (23)$$

or using logs

$$\log\left(\frac{W_n}{n}\right) = n\log a + \log\frac{(1-a)^2}{a} \quad (24)$$

Plotting $\log\left(\frac{W_n}{n}\right)$ versus n gives a plot with

gradient = $\log\alpha$

intercept = $\log\frac{(1-a)^2}{a}$

Both the gradient and the intercept can be used to calculate α .

Differentiation wrt to n and re-arrangement of equation (21) gives the following

$$N_{\max} = \frac{-1}{\ln a} \quad (25)$$

Where N_{\max} is the carbon chain length with the highest weight frequency.

High α figures >0.9 are required to produce appreciable amounts of larger hydrocarbon products as seen by Figures 1-9 and 1-10.

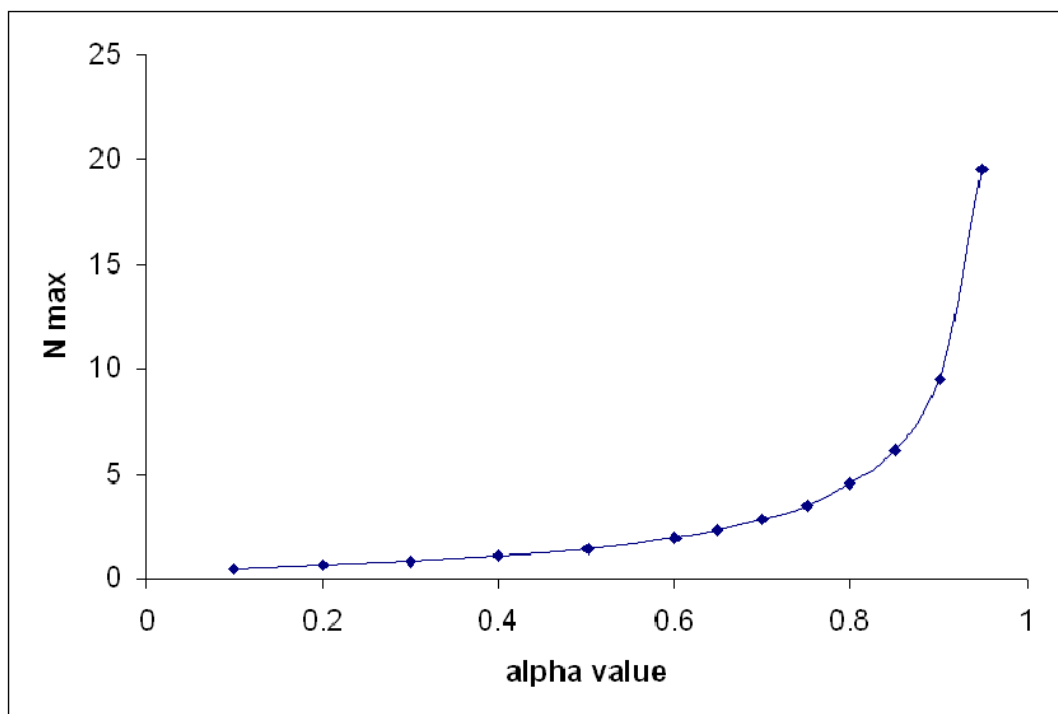


Figure 2-12 Graph of N_{\max} vrs alpha value

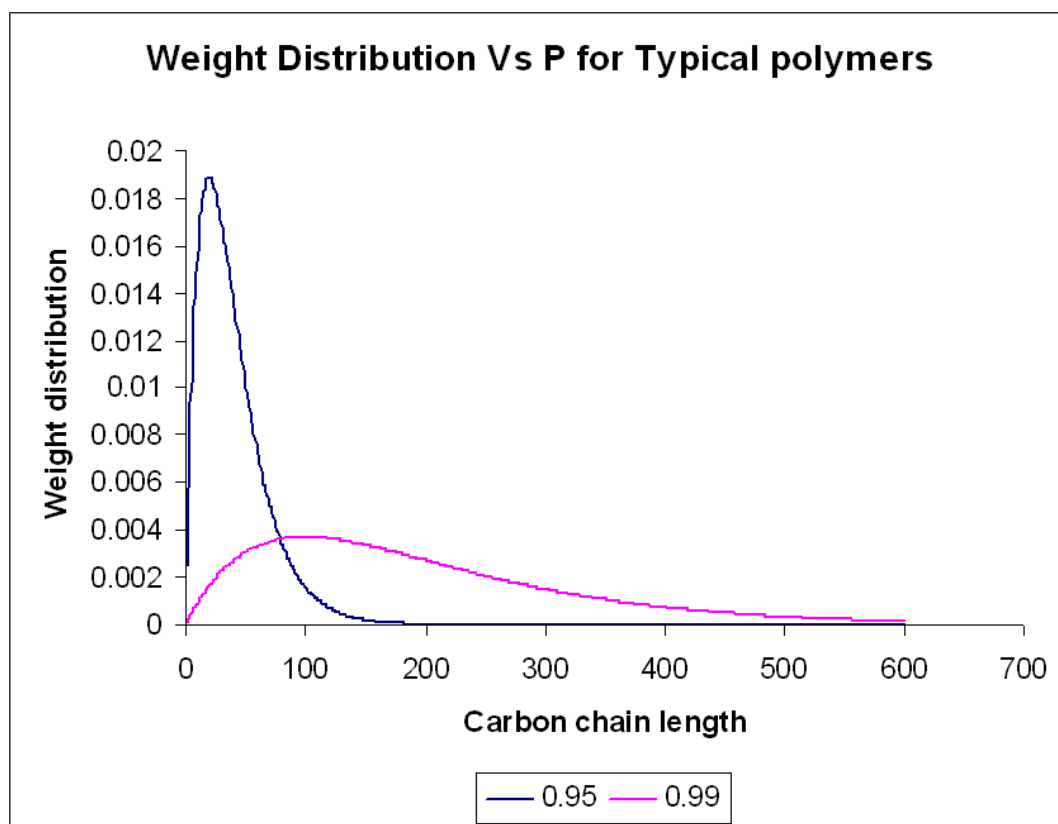


Figure 2-13 Graph of weight distribution vrs carbon chain length

Typical representations of alpha vrs product distribution are seen below:

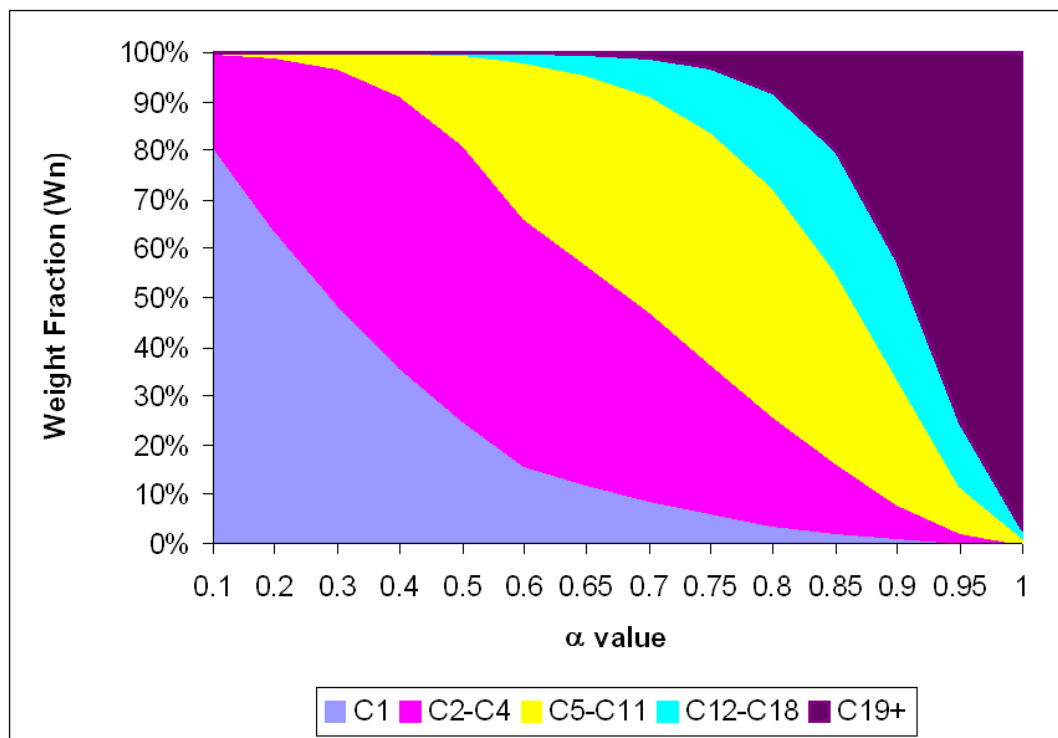


Figure 2-14 Graph of Weight Fraction vrs alpha value

3 Design and Commissioning of Fischer-Tröpsch (F-T) reactor

3.1 Fischer-Tröpsch reactors

Reactor design is often not straightforward. In many cases, various characteristics of a chemical process impose conflicting requirements on the selection of a reactor. The resulting reactor is often a compromise, which is not optimal for all process characteristics. The Fischer-Tröpsch synthesis (FTS) is a good example of a process where a large variety of reactors have been proposed and even commercially applied since its discovery in the 1930s[106]. All of these reactors can be considered as nonoptimal compromises.

There are four types of Fischer-Tröpsch (F-T) reactor in commercial use at present illustrated below. Three broad categories of catalyst are used in these reactors: fused iron, precipitated iron and supported cobalt. The four types of reactor are:

- Circulating fluidised bed reactor (CFB)
- Fixed fluidised bed reactor (FFB)
- Slurry phase reactor
- Tubular fixed bed reactor

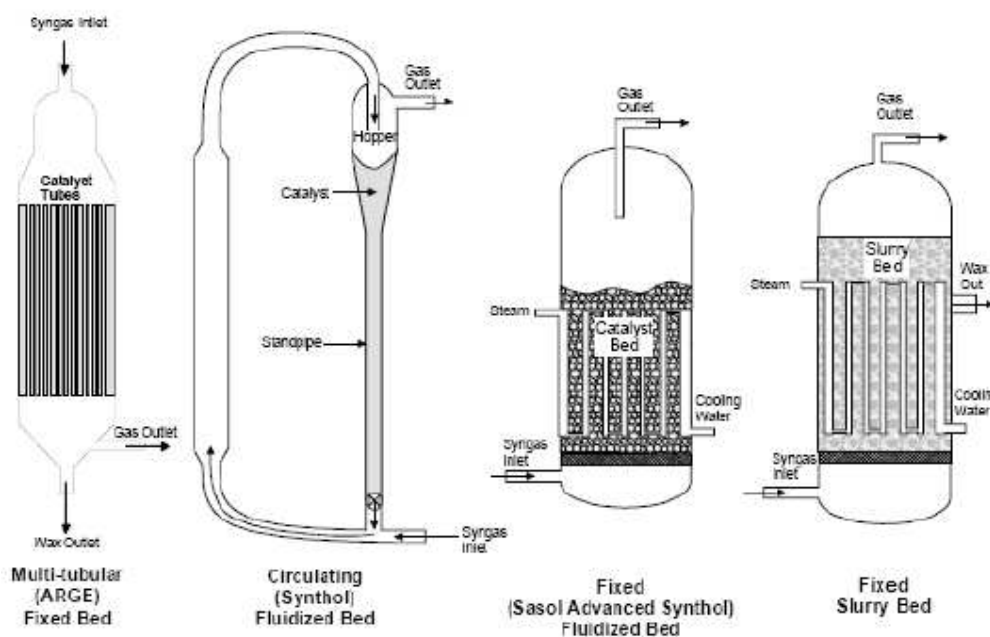


Figure 3-1 Types of F-T reactor in commercial use[107]

Currently there are two F-T operating modes. The high-temperature Fischer-Tröpsch (HTFT) (300-350°C) process with iron-based catalysts is used for the production of gasoline and linear low molecular mass olefins. In industry the HTFT operation uses FFB and CFB reactors. The low-temperature Fischer-Tröpsch (LTFT) (200-240°C) process with either iron or cobalt catalysts is used for the production of high molecular linear waxes and mainly uses slurry phase and tubular fixed bed reactors.

Compared to many industrial operations the F-T reaction is highly exothermic. The average heat released per 'CH₂' formed is about 145kJ[108]. It is vitally important to quickly remove the heat of reaction from the catalyst particles as any increase in the operating temperature of the F-T synthesis will result in an undesirable increase in the production of methane and may increase the rate of deactivation due to sintering and fouling. High rates of heat transfer are obtained by forcing the syngas through long narrow tubes, at high linear velocities, packed with catalyst particles to achieve turbulent flow (tubular fixed bed reactor), or better, by operating in fluidised catalyst bed reactor (CFB, FFB and slurry reactor)[17].

The major distinguishing feature between the HTFT and LTFT reactors is the fact that there is no liquid phase present outside the catalyst particles in the HTFT reactors.

3.1.1 Circulating fluidised bed reactor (CFB)

These reactors are entrained bed reactors. The combined feed (fresh plus recycle) enters at the bottom. The catalyst and this feed flow upward co-currently in a pipe reactor and high velocity. The reactor is cooled by heat exchangers that remove around one third of the heat of reaction[91].

3.1.2 Fixed fluidised bed reactor (FFB)

These reactors have a stationary bed with internal heat exchangers. The heat is removed by cooling tubes inside the reactor. The syngas enters at the bottom and passes through the fluidised bed.

3.1.3 Slurry phase reactor

Synthesis gas is bubbled through a slurry of heavy liquid products and catalyst particles. Unreacted syngas and light products leave the reactor in the gas phase, while liquid products are removed as a part of the slurry. Heat is removed by cooling coils mounted inside the reactor.

3.1.4 Tubular fixed bed reactor

The preferred fixed bed reactor type is multi-tubular with the catalysts placed inside the tubes and a cooling medium of water. Syngas enters from the top of the reactor with products being removed at the bottom of the system[32].

3.1.5 Comparison of F-T reactors

Advantages of FFB over CFB reactors are as follows[17]:

- Cheaper construction / running costs
- Easier to cool
- At any given time all of the catalyst participates in the reaction.
- Less erosion / maintenance

Advantages of slurry over multitubular reactors are as follows[17]:

- Lower capital / operating costs.
- Very efficient heat transfer and uniform temperature
- High catalyst efficiency / performance
- Longer reaction runs because of online removal / addition of catalyst

3.2 Reactor design and build

As mentioned earlier, this reactor was built purposely for these sets of F-T reactions and it was constructed from new. Johnson Matthey sponsored the project and the design of the reactor system was constructed in conjunction with this sponsor.

The set-up of a F-T reactor system is complicated. The F-T reaction produces a very large range of products from C1 to C40 and above, therefore there are three product phases: wax (heavy molecular weight hydrocarbons), liquid (lighter molecular weight hydrocarbons) and gas (C1-C6 hydrocarbons). The design of the reactor had to incorporate the collection of these three product phases.

The set-up used for this project was a single tube fixed bed high-pressure reactor see figure 3.2.

3.2.1 Safety

Many safety measures were taken to insure a safe working rig to industrial standards was achieved.

3.2.1.1 Pressure

There was a pressure relief valve connected just after the mass flow controllers. If the pressure increased above a certain pressure this valve would release pressure from the reactor. A variable pressure regulator was used to set the desired pressure of the reactor. Swagelok pressure gauges were used to monitor the reactor pressure.

3.2.1.2 Temperature

The reactor had various N-type thermocouples that were connected to West temperature controllers, which allowed temperature programs to be set and executed. These controllers had the function to programme temperature trips. If the temperature of the reactor increased above a certain temperature, these trips would over-ride the current temperature program and shut off any power to the reactor. In the event of overheating, the flammable gases would shut down.

3.2.1.3 Flow

The reactor was housed in a cabinet that contained an extractor fan, hydrogen and carbon monoxide detectors. In the event of a leak of carbon monoxide or hydrogen these detectors would sound and the gases would be shut off.

A Hurricane 2156 SIP compressor was used to keep air driven activators open. If any of the gas cylinders attached to the rig failed these activators would shut down stopping the gas flow through the mass flow controllers and into the reactor.

3.2.2 Process

3.2.2.1 Gas feed

The flow rates of the gases entering the reactor were controlled using Brooks 5805S mass flow controllers that allowed gas flows between 5 and 250cm³ / min and a swagelok pressure gauge was fitted to monitor reactor pressure. A filter was fitted before the gas entered the oven and reactor to stop any particles from entering the reactor tube and contaminating the reaction.

A three-way tap labelled '1' in Figure 3.2 was in place to avoid mixing of oxidising (O₂) and reducing (H₂) gases. While the oxidising gas was flowing, tap 1 blocked the path from the reducing gas and vice versa.

The gases could be directed through the reactor tube in the direction indicated by the arrow labelled 4 in Figure 3.2 or the three-way taps 5 and 6 could be changed to isolate the reactor and direct the flow through the by-pass.

3.2.2.2 Liquid feed

Liquid feeds could be introduced into the system prior to the reactor via the use of a Gilson 307 HPLC pump with flows between 0.001 - 5.0 ml / min achievable. Above the reactor was a stainless steel bulb (vaporiser) that contained glass beads. This insured that any liquid feeds introduced were mixed and vaporised to insure laminar flow into the reactor.

A major problem was encountered regarding the co-feeding of liquids into the F-T reactor. 1-propanol was decided as the first liquid to add to the F-T reaction. When 1-propanol was fed into the system, via the HPLC pump, this liquid did not reach the reactor tube. It was discovered that this was due to a slight design fault. The reactor was under 20 bar of pressure and the oven temperature was 448K. The distance between the HPLC pump and the reactor was roughly 2.5mtrs and the volume of liquid that was introduced into the system was 0.02ml/min. The boiling point of 1-propanol is 370K and it was introduced into the reactor as a liquid at 1 bar before vaporising. Because of the small flow rate, long length of tube leading from HPLC pump to vaporiser, boiling point of

1-propanol, pressure, and temperature of the reactor, the 1-propanol liquid vaporised as soon as it entered the oven and not in the vaporiser as intended. It was calculated that it would take a long period of time for the small volume of 1-propanol liquid that was pumped to fill the long length of tubing, to vaporise into the gas phase and build up to 20 bar (in the gas phase) before it would be introduced to the reactor tube. Because of this design flaw, the HPLC pump could not force any liquids, at a small flow rate, with a boiling point of less than 448K into the reactor. Any liquid being introduced into the system has to have a boiling point of higher than 448K, due to it being introduced to a system at 20 bar and 448K.

A possible improvement to the rig could be to shorten the length of piping between the HPLC pump and oven, which would reduce the dead space in the pipe prior to the oven, thus reducing wasting any expensive liquid feeds that are introduced into the system.

3.2.2.3 Traps

As mentioned earlier, the F-T reaction produces a wide range of hydrocarbon products. The three product phases wax, liquid, and gas had to be collected using three different traps. These traps were heated/cooled at different temperatures to knockout the desired product phase.

The first knockout pot was heated to 448K and was used to collect wax products (heavy hydrocarbons) that were in liquid phase at 448K. An external tap, labelled 2 in figure 3.2 was fitted to open a needle valve to allow sampling of heavy hydrocarbons during a reaction. This external tap kept coming loose from the needle valve, even during mid-reaction. This resulted in the inability to open the valve that was used to sample the waxy hydrocarbons. This external tap had to be tightened and fixed so the collection pot did not fill up with waxes and spill into other parts of the reactor, i.e. down-stream. This was done either at the end of the reaction or if this occurred during a run, the oven had to be opened and the needle valve had to be mended at 448K.

This again seemed to be a slight design flaw with the rig as the external tap and needle valve could have been welded together rather than screwed together. However, the reason they were screwed together was so they could be dismantled and both removed from the oven to make future modifications to the apparatus easier.

The lighter hydrocarbon products formed during the reaction were collected in a second knockout pot, which was cooled in a chiller to 278K. To ensure the temperature stayed constant a TC Ltd. N-type thermocouple was positioned inside the chiller and both the thermocouple and chiller were linked via a West 6100 temperature controller. A two-way valve labelled 3 in figure 3.2 was fitted to allow sampling of light hydrocarbons during a reaction. A swagelok pressure gauge was fitted after the chiller to monitor pressure. A Platon 250 cc/min AIR rotameter was fitted after this pressure gauge as the first sign of a blockage could be detected in a drop in gas flow.

Any gas products formed during the reaction were to be analysed online using a HP 5890 series II GC with a Thermal Conductivity Detector (TCD) and 4 columns: DC200, UCW982, HayeSep Q and Mol Sieve 13X. The GC was connected to a PC via a Varian Star 800 module interface (integrator) using the computer program Varian Star Workstation version 6.41. As the F-T reaction produces high molecular weight hydrocarbons, there is a chance that these products will travel further down the reactor into the GC. Two filters were fitted to minimise this; the first after the 2nd knockout pot and the second just before the gas products enter the GC.

3.2.2.4 Oven

The design of the reactor was changed, on a number of occasions, as problems were encountered. The main change in design came with the introduction of an oven. On discussion with the sponsors of the project they made aware the many problems they encountered building their F-T reactor. They found that the heavy molecular weight hydrocarbons formed during the F-T reaction would solidify, build up in the piping and eventually block the reactor. Initially trace heating was proposed, as the method of keeping the relevant parts of the

reactor warm, so that the wax products formed would be kept in the molten state. However, Johnson Matthey had found that with trace heating, cold spots were common and even these small cooler sections of the rig would get blocked.

The following parts: vaporiser, reactor tube, heater block, first knockout pot and all piping were encased in an LTE OP-250 oven with a TLK 49 temperature controller. The oven was heated to 448K to avoid any products from solidifying and blocking up in the rig.

3.2.2.5 Reactor

The reactor consists of a 0.455cm inside-diameter glass lined metal reactor tube positioned within an aluminium/bronze heater block. Two TC Ltd. N-type thermocouples were positioned inside the heating block in such a way that the tips of each thermocouple sat at the middle of the catalyst bed and monitored the temperature of the heating block. These thermocouples and the heater block were linked via a West 4400 temperature controller, which allowed temperature programs to be set and executed. The reactor tube was operational up to +773K.

The exact temperature of the catalyst bed had to be monitored to ensure there were no temperature gradients within the reactor tube. A small groove was scored into the section of the heater block where the reactor tube sat so that a TC Ltd. N-type thermocouple could be placed directly on the outside of the reactor tube where the mid-point of the catalyst bed would be. This work was carried out by the metal workshop at the University of Glasgow. It was decided to place the thermocouples on the outside of the reactor tube instead of placing them inside, as this would stop any iron carbonyl or nickel carbonyl being formed and contaminating the reaction.

The total pressure in the apparatus was controlled with a Tescom 250 variable pressure regulator and the system was operational up to a maximum of 20 bar. Below the reactor was a valve that opened to connect to a Minitorr quadrupole mass spectrometer (MS). The computer software used was from ESS. The MS

was attached to carry out online temperature programmed oxidation (TPO) experiments in real-time.

3.2.2.6 Silica lining

The rig was constructed of 316 stainless steel with all stainless steel leading up to, and including the reactor, silica lined. This was to minimise the formation of iron carbonyl or nickel carbonyl, which is a major source of deactivation for this reaction. The steel required to be silica lined was sent to Thames Restek UK Ltd.

3.2.3 Conclusion

In conclusion the design of the high-temperature reactor does work and experiments can be operational over a number of hours with no problems.

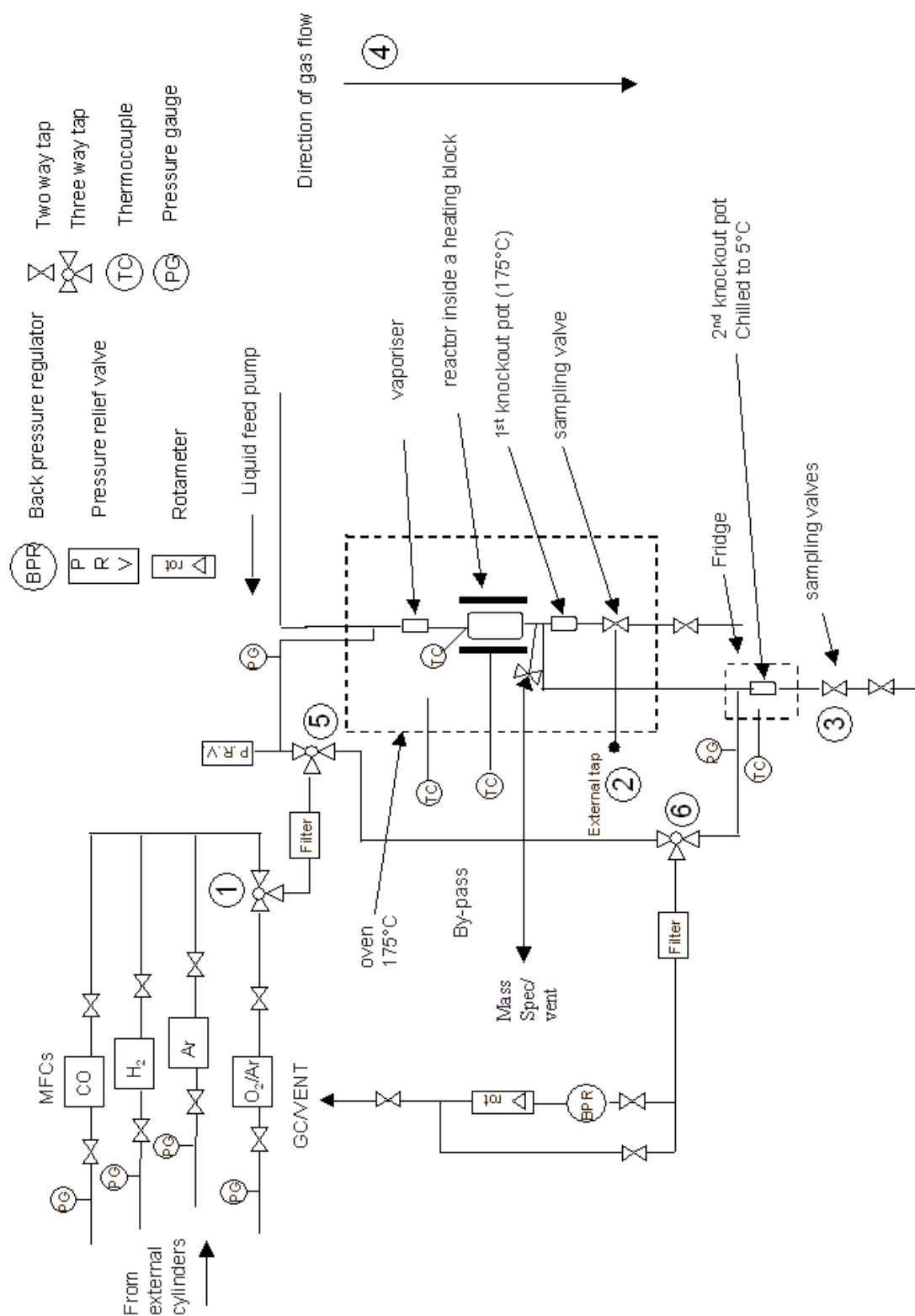


Figure 3-2 Detailed schematic of Fischer-Tröpsch reactor

4 Results

4.1 Cobalt/alumina catalyst prepared via the nitrate method

4.1.1 Characterisation

All catalysts were characterised using thermogravimetric analysis (TGA), Brunauer, Emmett, Teller (BET) analysis, X-ray diffraction (XRD), TPR-UV-vis-NIR spectroscopy, and Transmission Electron Microscopy (TEM) prior to catalytic testing.

The efficient control of cobalt reducibility through calcinations is a key issue in the design of Co/Al₂O₃ supported catalysts.

4.1.1.1 Thermo-gravimetric Analysis (TGA)

TGA can be used to determine the temperature of calcination and reduction. Usually these temperatures need to be determined experimentally. However, as this was an industrial catalyst produced at Johnson Matthey, they had already determined that the calcination temperature of the catalyst should be 200°C. Therefore the following analyses were performed on a pre-calcined catalyst. Calcination is the process whereby the catalyst precursor, in this case the nitrate, is converted to the oxide by heating in air[109]. This was desirable as the ultimate goal is to reduce the transition metal oxide to the metallic phase.

TGA analysis in oxygen

From the weight and derivative weight profiles, shown in Figure 4-1, it appeared that the calcination procedure at 200°C does not fully decompose the nitrate. The decomposition of cobalt nitrate has been investigated previously [110] and shows a similar decomposition profile to that shown in Fig 4-1. The cobalt nitrate decomposition in oxygen mainly occurs as several broad events below 310°C with a sharp weight loss at 248°C. There is a further high temperature weight loss at 749°C. From the heat flow data, Figure 4-2, it can be seen that

the weight loss was an exothermic event occurring at 258°C, which suggests the nitrate precursor, was breaking down to form the oxide.

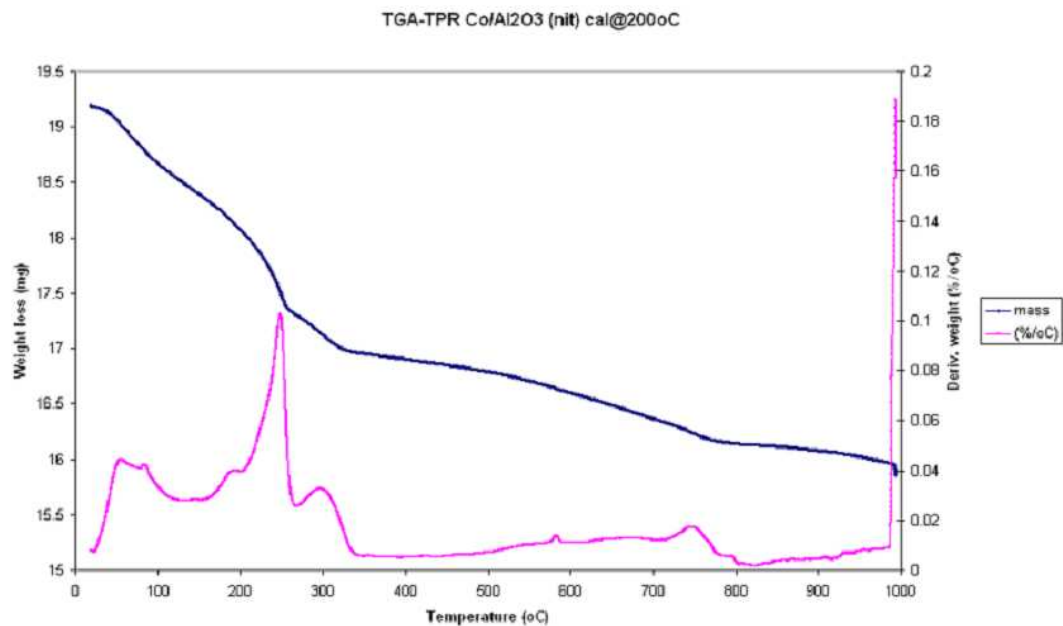


Figure 4-1 TGA analysis (weight loss/derivative weight vs temperature) of Co/Al₂O₃ (nitrate) catalyst under 2%O₂/Ar feed

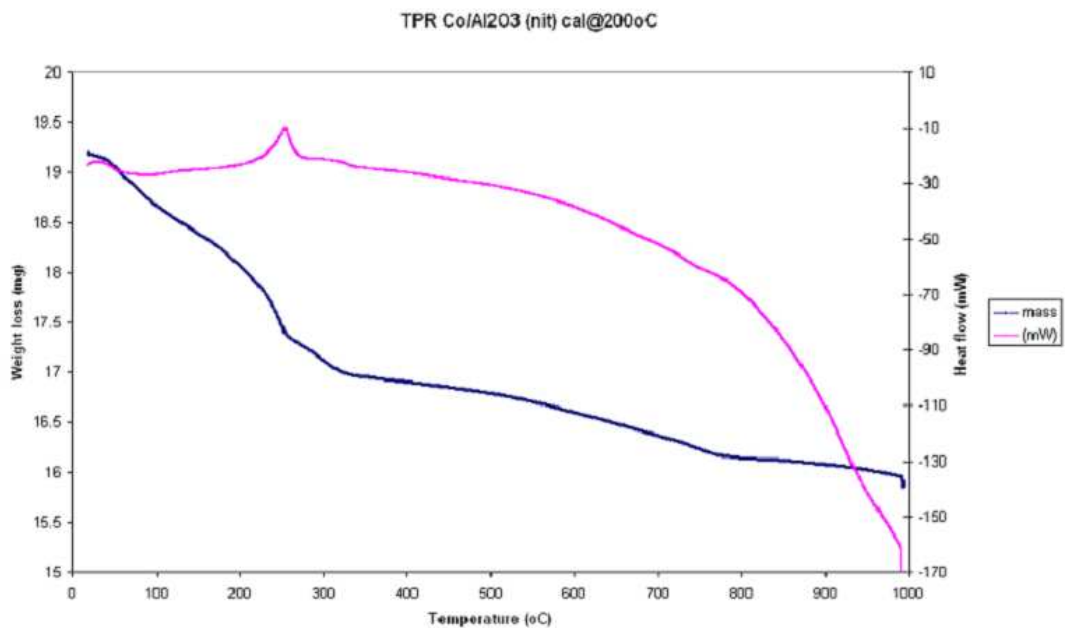


Figure 4-2 TGA analysis (weight loss/heat flow vs temperature) of Co/Al₂O₃ (nitrate) catalyst under 2%O₂/Ar feed

TGA analysis in hydrogen

The graph below shows the weight loss and derivative weight profile for the Co/Al₂O₃ (nitrate) catalyst under a reducing atmosphere. From Figure 4-3, it can be seen that the weight loss occurs over four events at 62°C, 250°C, 304°C and 750°C.

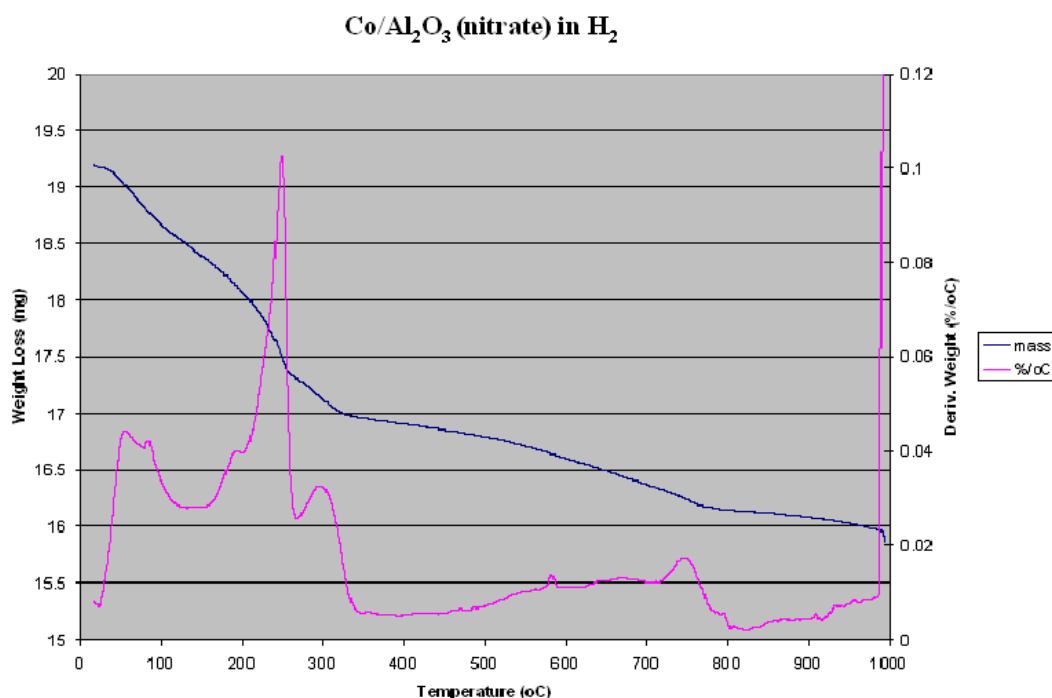


Figure 4-3 TGA analysis (weight loss/derivative weight vs temperature) of Co/Al₂O₃ (nitrate) catalyst under 5%H₂/N₂ feed

Mass spectrometry data, Figure 4-4, showed that the weight losses at 62°C, 256°C and 307°C correspond to the loss of water and the peak at 62°C represents physisorbed water on the catalyst surface. These evolutions mirror the hydrogen uptake peaks of Figure 4-5. The uptake of H₂ and release of H₂O however is most likely due to the reduction of the cobalt oxide. There was an evolution of nitric oxide at 251°C, Figure 4-6, indicating that not all of the nitrate precursor had been converted to the oxide in the calcination stage in agreement with the O₂ TGA. The catalyst was calcined at higher temperatures, 250°C, 300°C, 350°C, and 400°C to see if this increase in temperature would decompose all of the nitrate precursor. It was found that temperatures of 350°C and above are

needed to remove any nitrates still present and the higher the calcination temperature, the higher the temperature needed to reduce cobalt oxide.

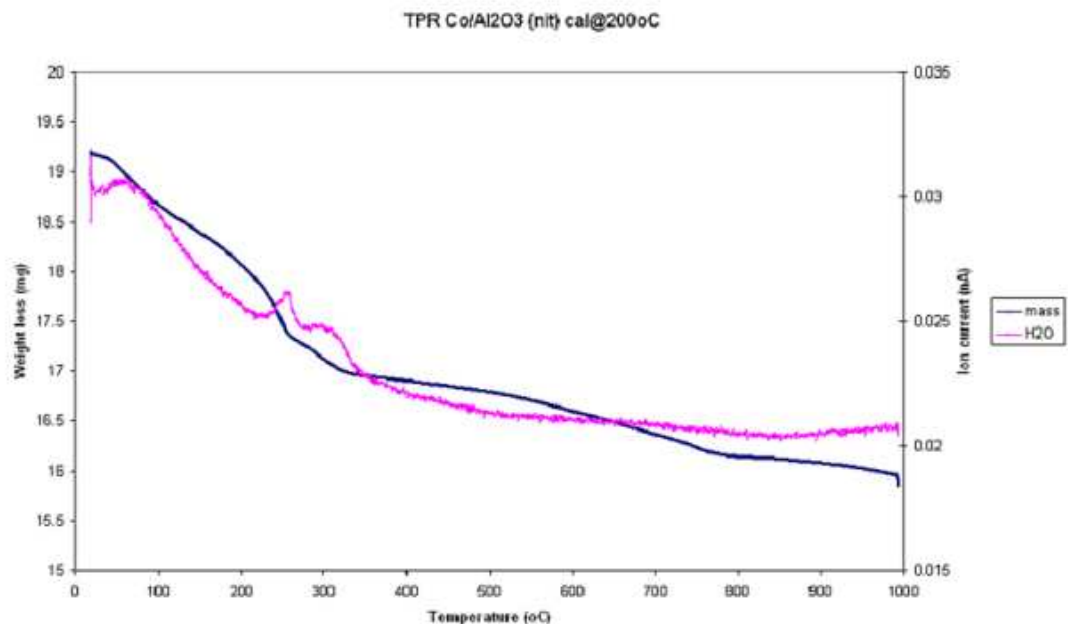


Figure 4-4 TGA analysis (evolution of water) of Co/Al₂O₃ (nitrate) catalyst under 5%H₂/N₂ feed

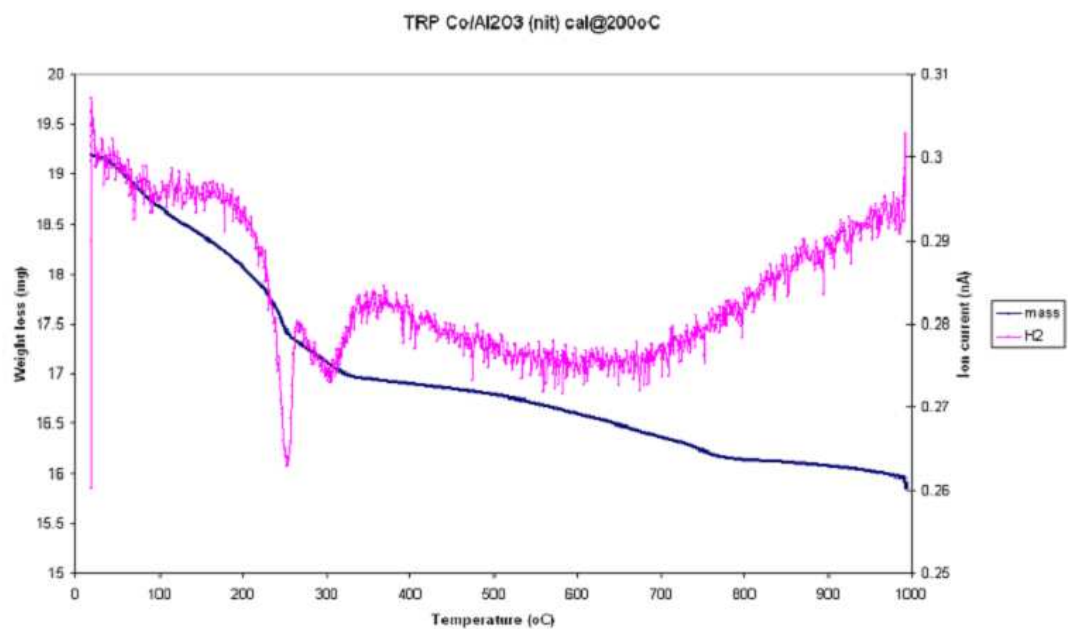


Figure 4-5 TGA analysis (uptake of hydrogen) of Co/Al₂O₃ (nitrate) catalyst under 5%H₂/N₂ feed

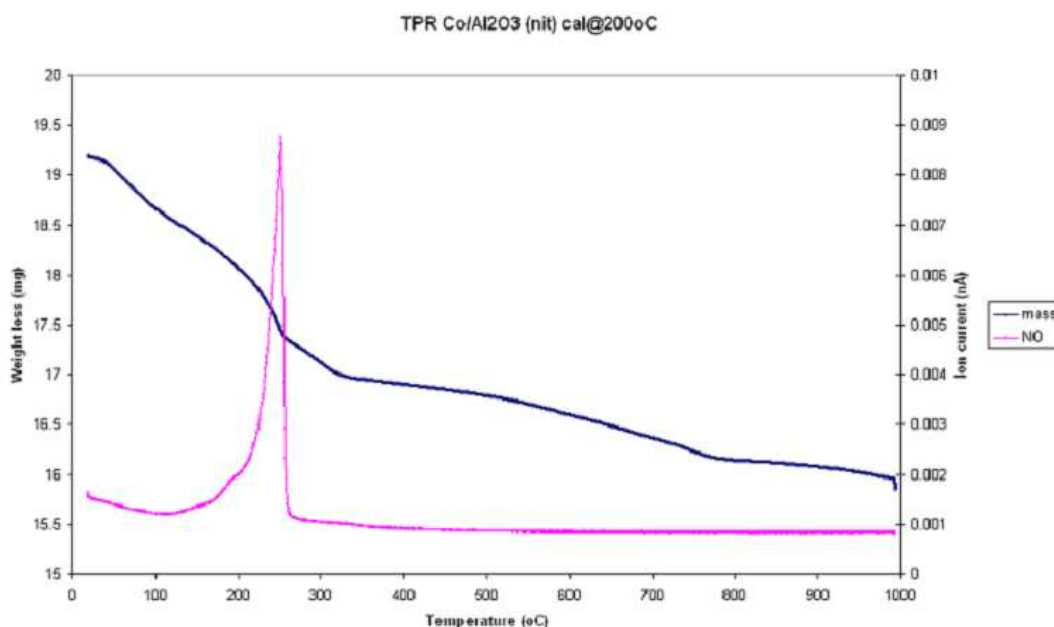


Figure 4-6 TGA analysis (evolution of nitric oxide) of Co/Al₂O₃ (nitrate) catalyst under 5%H₂/N₂ feed

Studying the TGA data it can be seen that the peaks are reasonably broad which indicates the catalyst reduction is over a broad temperature range.

The graph below represents a TPR/TPD measurement of the Co/Al₂O₃ (nitrate) catalyst. Jill Turner from Johnson Matthey carried out this procedure. It is widely acknowledged that reduction of unsupported cobalt oxide (Co₃O₄) occurs as a two stage process [111, 112] which can be ascribed to successive reduction of Co₃O₄ to CoO and then to Co [113, 114]. The first low temperature peak at 246°C corresponds to any nitrate precursor that is still present after calcination and this is in agreement with the TGA data showing the release of nitric oxide at 251°C. The second low temperature peak at 292°C represents Co₃O₄ being reduced to CoO and then to Co with the third peak at 614°C representing the final reduction of CoO to Co and any alumina interaction species. The final peak at 914°C represents any cobalt aluminate species which always occur with alumina supported cobalt catalysts [43]. These species are very difficult to reduce even at temperatures of >1000°C[43]. These peaks are in agreement with the derivative weight plot, Figure 4-3, and also with literature. Jacobs et al [25] and Bechara et al. [115] have typically assigned the reduction of surface

Co₃O₄ phase (Co³⁺ to Co²⁺ to Co) between 260-450°C. The high temperature peaks between 450-750°C are attributed to the reduction of cobalt oxide and alumina interaction species.

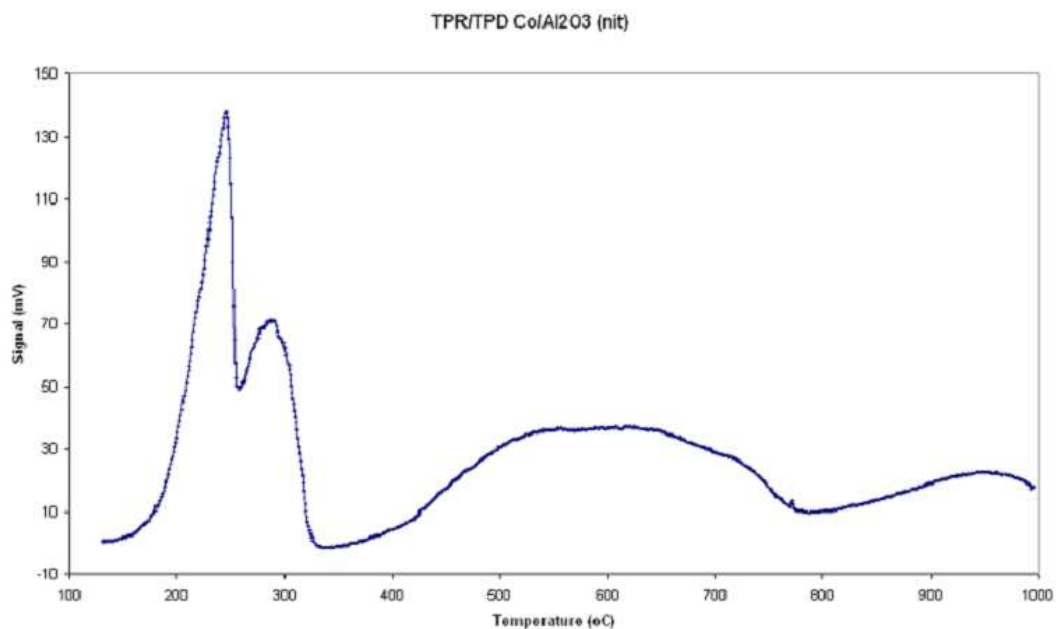


Figure 4-7 TGA measurement (TPR/TPD) of Co/Al₂O₃ (nitrate) catalyst

4.1.1.2 BET Surface area analysis

The table below represents surface area analysis of Co/Al₂O₃ (nitrate) catalyst. The analysis was carried out by the procedure covered in section two.

| Catalyst | Surface Area (m ² / g) | Pore Diameter (Å) | Pore Volume (cm ³ / g) |
|---|-----------------------------------|-------------------|-----------------------------------|
| Co/Al ₂ O ₃ (nitrate) | 108 | 240 | 0.64 |

Table 4-1 Surface area analysis of lab prepared Co/Al₂O₃ (nitrate) catalyst

4.1.1.3 Powder and hot stage powder X-ray diffraction (XRD)

X-ray diffraction can provide information regarding a materials crystal structure, degree of crystallinity and crystallite size. Although unable to detect all aspects of the active phase of a catalyst, XRD can be used to gain information about materials with long range order. It is particularly useful for characterising materials with well ordered structures such as zeolites[116, 117]. Although materials such as alumina (the support for the catalysts) can be amorphous, XRD can still be used to gain information regarding the active species on the support if it exists in a crystalline phase.

Powder XRD was used to determine if any phase changes occurred upon reduction. Identification of the species present on the support was made by comparison with the Powder Diffraction Database[118]. The graph below represents the XRD pattern for the calcined cobalt/alumina (nitrate) catalyst. It can be seen that the crystalline phases present are Co_3O_4 and gamma alumina support. The peak at 37 (2θ) represents Co_3O_4 spinel and the crystal size was calculated as 28nm using the Scherrer equation.

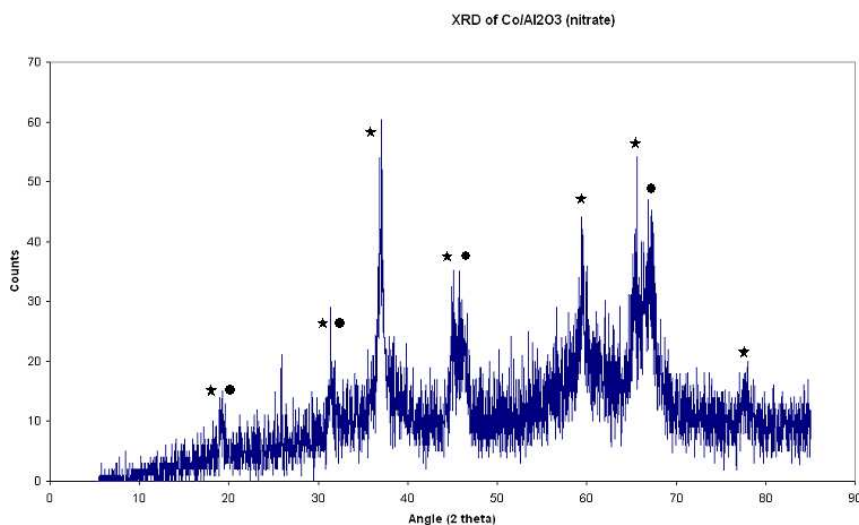


Figure 4-8 Powder XRD graph of calcined $\text{Co}/\text{Al}_2\text{O}_3$ (nitrate) catalyst
Phases denoted are (★) Co_3O_4 and (●) gamma Al_2O_3

Figure 4-9 shows the hot-stage XRD pattern for cobalt/alumina (nitrate) catalyst under reducing conditions. The reduction of the sample took place *in-situ* inside the XRD diffractometer using the conditions defined in the section two.

The graph below shows the reduction of Co_3O_4 (Co^{3+}) to CoO (Co^{2+}) to Co metal (Co^0). As the temperature increases, the cobalt oxide is being reduced to cobalt metal but even at 800°C there is still cobalt oxide present. Not all of the oxide is being reduced to the metal. There is also CoAl_2O_4 (cobalt aluminate) spinel present, which is virtually irreducible even at high temperatures [43]. The peaks at higher temperatures are sharper than those at lower temperatures which indicates an increase in crystallinity upon reduction. The peak at 43 (2θ) at 800°C represents cobalt metal phase and the crystal size was calculated at $\sim 20\text{nm}$ using the Scherrer equation.

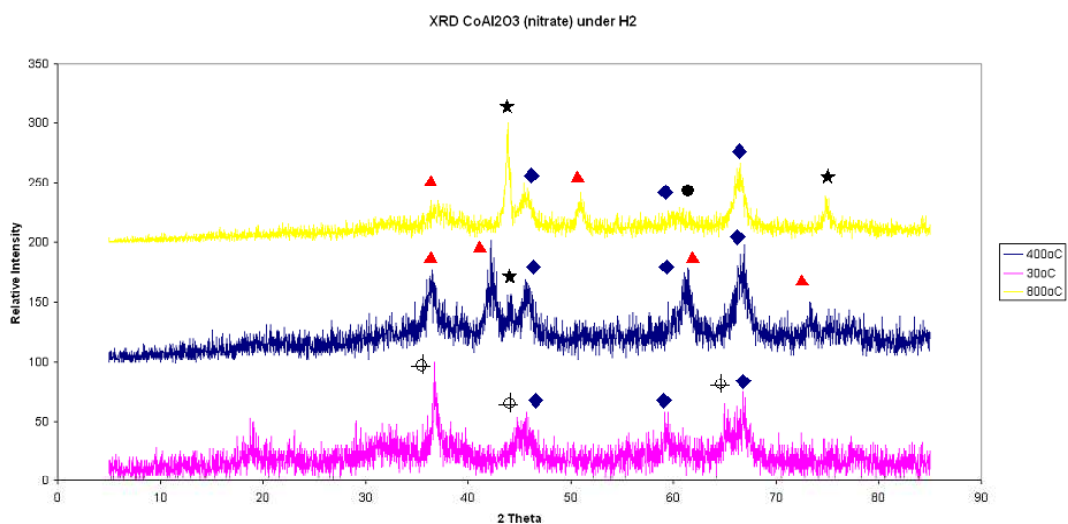


Figure 4-9 Hot-Stage XRD graph of $\text{Co}/\text{Al}_2\text{O}_3$ (nitrate) catalyst under H_2

Phases denoted are (★) Co , (▲) CoO (⊕) Co_3O_4 , (●) CoAl_2O_4 and (◆) $\gamma\text{-Al}_2\text{O}_3$

4.1.1.4 TPR-UV-vis-NIR spectroscopy

The graph below represents the UV-spectrum of cobalt/alumina (nitrate) catalyst under reducing conditions at different temperatures. At 302°C we get an absorption band starting at 510nm which is attributed to a ${}^4\text{T}_{1g}(\text{F}) \rightarrow {}^4\text{T}_{1g}(\text{P})$ transition in octahedral high-spin Co^{2+} complexes [119]. This corresponds with the TPR/TRP graph, Figure 4-8, which shows Co^{3+} being reduced to Co^{2+} at 292°C .

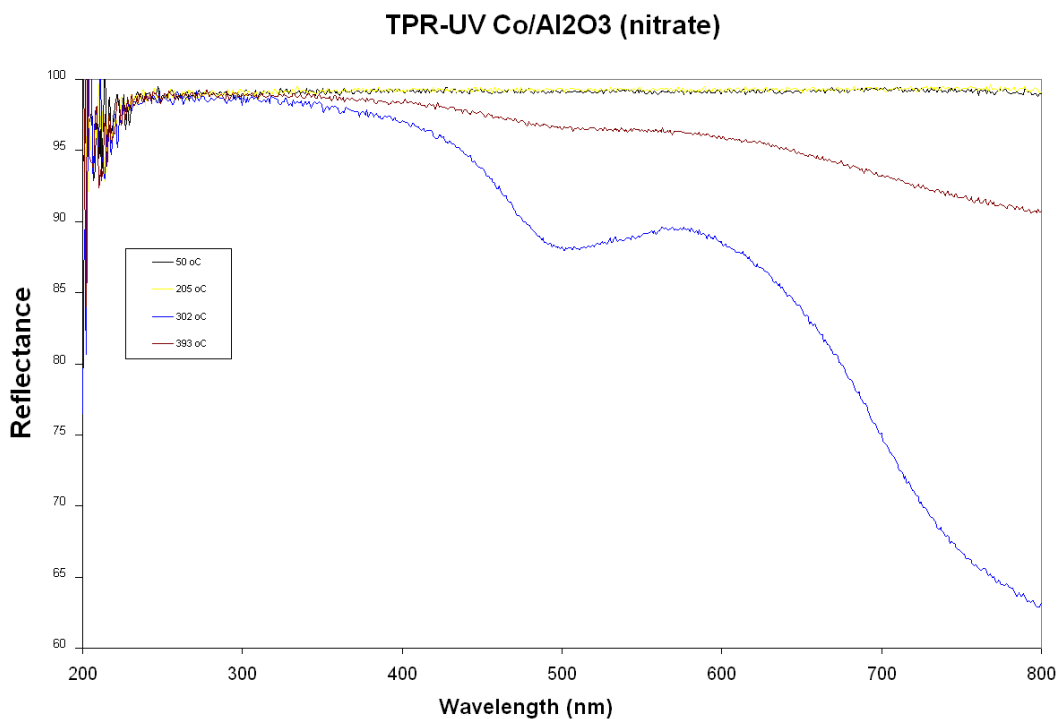


Figure 4-10 TPR-UV-vis-NIR spectroscopy graph of Co/Al₂O₃ (nitrate) catalyst under H₂

4.1.1.5 Transmission Electron Microscopy (TEM)

Figure 4-11 represents a TEM image of the calcined Co/Al₂O₃ (nitrate) catalyst. In the literature there have been a number of studies using TEM on silica and titania supported cobalt catalysts [120-123] but not as much on alumina supported cobalt catalysts. From the literature it has been found that with an increase in metal loading there is an increase in aggregation of cobalt oxide clusters and the cobalt species are not homogeneously distributed on silica support [123]. They appear as near spherical aggregates of Co₃O₄ particles inside the pores and on the surface of the support. The aggregates can form different sizes from single Co₃O₄ particles to larger clusters[123]. In Figure 4-11 the dark areas represent Co₃O₄ particles or clusters with the lighter areas representing alumina support. From the image it can be seen that the structure consists mostly of clusters of cobalt oxide (Co₃O₄) on the alumina support with some smaller clusters or single particles. The size of cobalt clusters or particles range from roughly 20nm to larger clusters of 150nm in diameter.

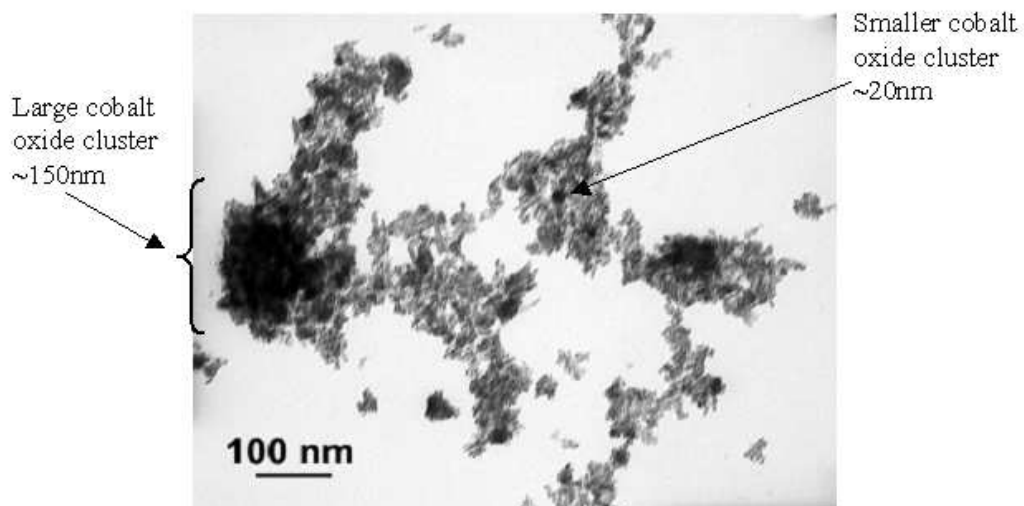


Figure 4-11 TEM image for Co/Al₂O₃ (nitrate) catalyst

4.1.2 Reaction at 210°C and 220°C

The FT activity of this catalyst was investigated at 210°C and 220°C using the following conditions:

| | |
|------------------------------------|---------------------------|
| • Reaction Temperature (°C) | 210 then increased to 220 |
| • Pressure (barg) | 20 |
| • Gas Flow (ml min ⁻¹) | 46.88 |
| • Catalyst Volume (ml) | 0.5626 |
| • Catalyst weight (g) | 0.399 |
| • GHSV (hr ⁻¹) | ~5,000 |
| • Residence time | 0.72 s ⁻¹ |

The synthesis feed gas composition employed was 31.76ml min⁻¹ H₂ and 15.12ml min⁻¹ CO. This equated to a molar ratio of 2.1:1 H₂:CO which was ideal for FTS.

Prior to reaction, the catalyst was reduced *in situ* in the reactor under 46.88ml min⁻¹ flowing hydrogen using the reduction conditions stated earlier in section two. Once the reduction programme was complete the catalyst was brought on-

line very slowly and gently, as this F-T catalyst is easily damaged if brought on-line too harshly.

4.1.2.1 Reaction at 210°C

The reaction temperature used at the start of this reaction was 210°C as this is a common temperature used commercially for FTS.

The graph below represents carbon monoxide conversion over the first ~900 hrs TOS. The conversion dropped from ~23% to ~8% in this time period. The reaction seems to have reached steady state and clear deactivation has occurred. The deactivation profile suggests exponential decay has taken place. The 1st order deactivation constant was calculated over this time period as 0.0014 hr^{-1} .

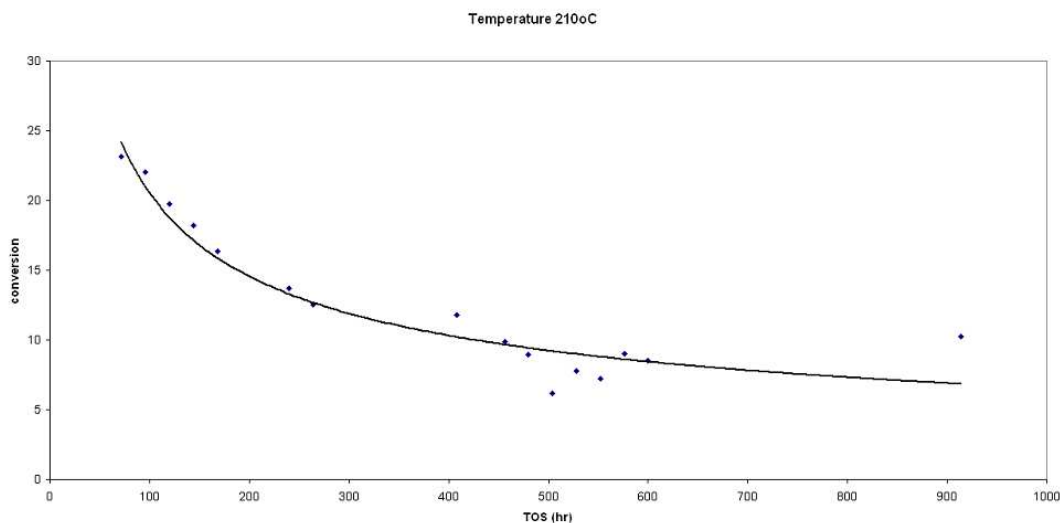


Figure 4-12 Conversion vs TOS of reaction at 210°C

The graph below represents the number moles, in the light organic phase at 48 hrs TOS, of each hydrocarbon formed during the reaction. From the graph it can be seen that a broad range of hydrocarbons are formed. The selectivity seems to peak at carbon number nine. As the reaction proceeds the volume of liquid organics produced decreases as expected from the deactivation profile.

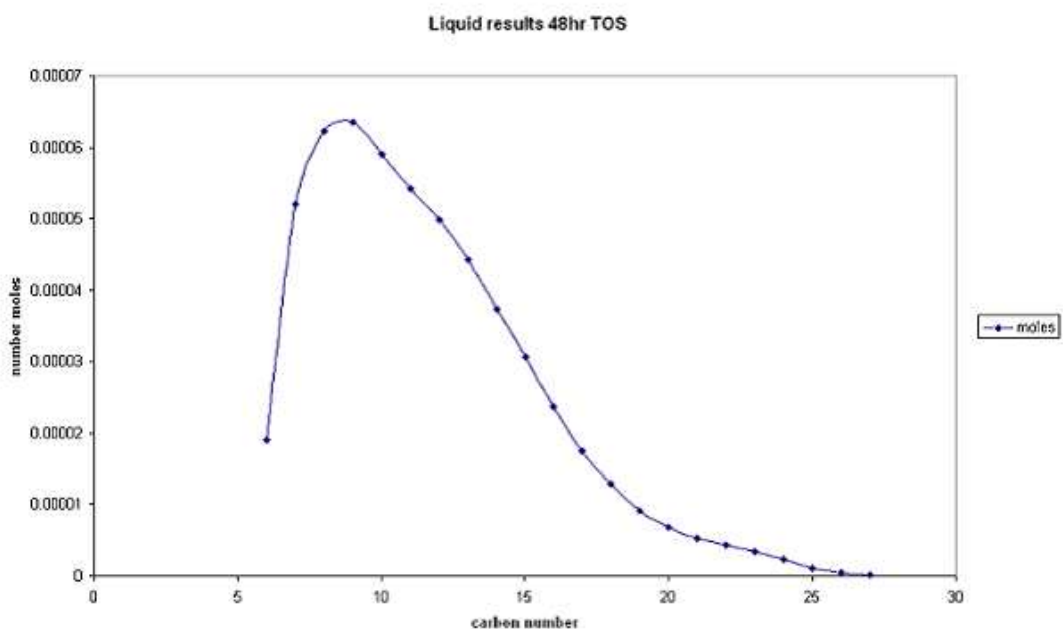


Figure 4-13 Moles of carbon products in liquid phase at 48 hrs TOS

The graph below represents the gas chromatogram trace for the light organic phase at 48 hrs TOS. From the graph it can be seen that there are distinct and regular main peaks with smaller peaks surrounded around these main peaks. The larger peaks represent the alkane products (C6 - C25). The F-T reaction under the conditions stated above will produce mainly alkanes with a small amount of alkenes and oxygenate species. The smaller peaks are believed to be a mixture of these minor products.

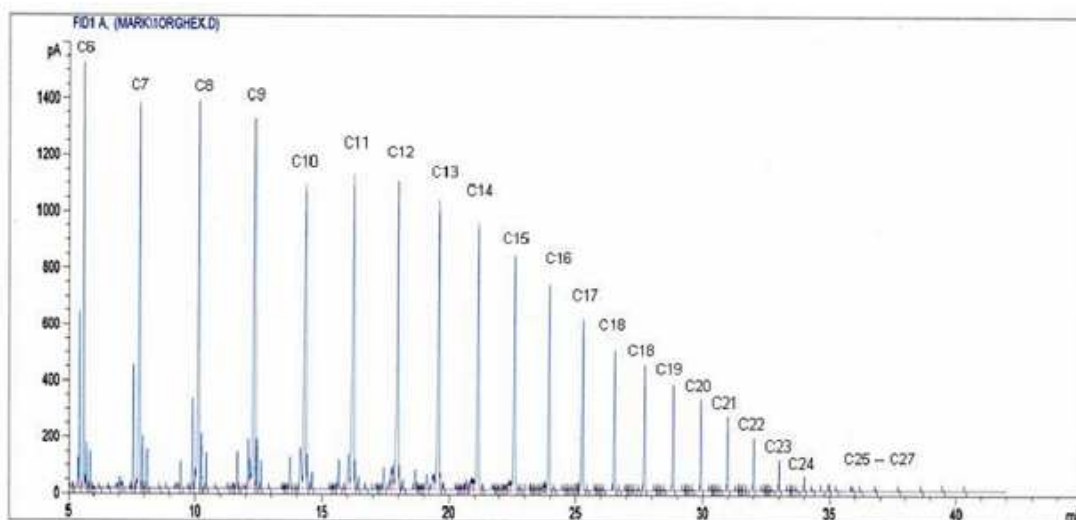


Figure 4-14 Gas chromatogram of light hydrocarbons at 48 hrs TOS

The graph below represents the number moles, in the wax phase at 48 hrs TOS, of each hydrocarbon formed during the reaction. The wax phase contains an even broader range of hydrocarbons than in the light phase. Similarly to the light hydrocarbon phase, as the reaction proceeds the mass of heavy hydrocarbons produced decreases as expected from the deactivation profile.

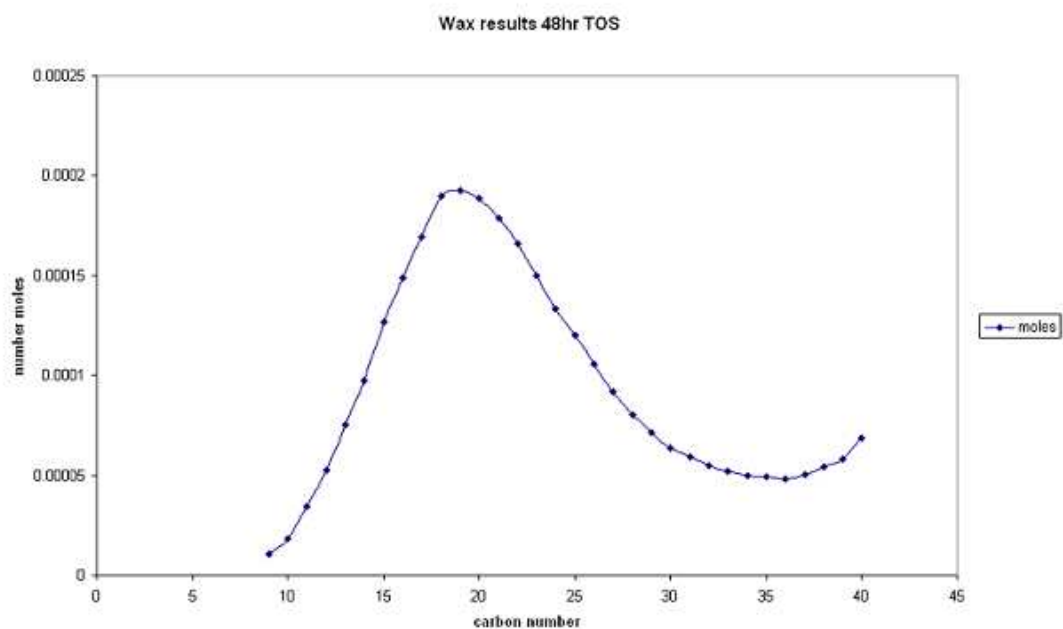


Figure 4-15 Moles of carbon products in wax phase at 48 hrs TOS

The graph below represents the gas chromatogram trace of wax phase at 48 hrs TOS. From the graph it can be seen that there are distinct and regular main peaks. In the light phase it was clear that there were additional products other than alkanes being produced but they seem to be produced in smaller quantities in the heavy hydrocarbon phase. The larger peaks represent the alkane products (C9 - C40). The F-T reaction under the conditions stated above will produce mainly alkanes with a small amount of alkenes and oxygenate species. The smaller peaks are believed to be a mixture of these minor products.

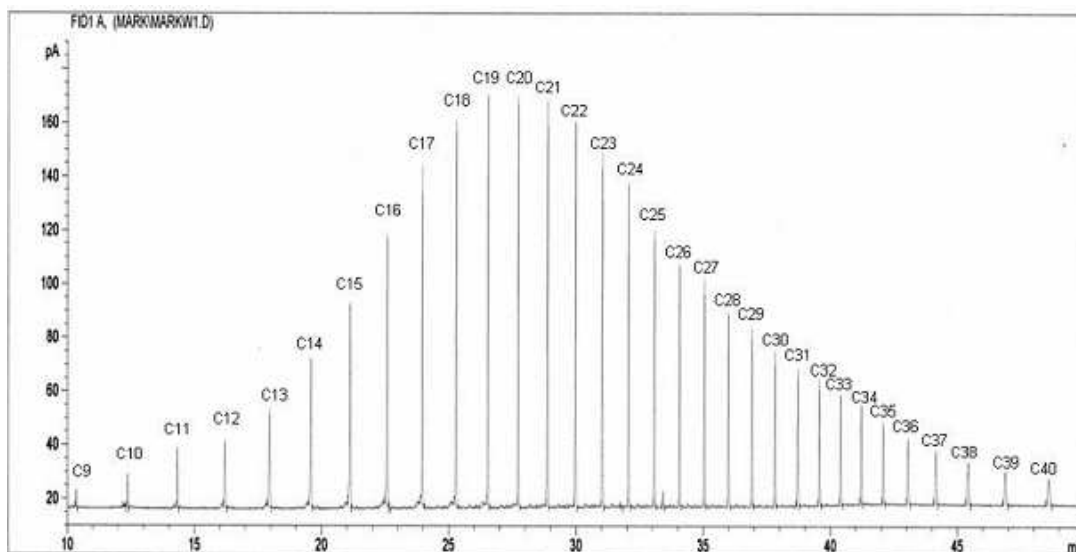


Figure 4-16 Typical chromatogram of heavy hydrocarbons

The graph below represents an overlay of the number moles of each hydrocarbon formed during the reaction in both the liquid and wax phases at 48 hrs TOS. From the graph it can be seen that there is a large overlap of hydrocarbons and this requires a careful analysis and summation of yield in both traps.

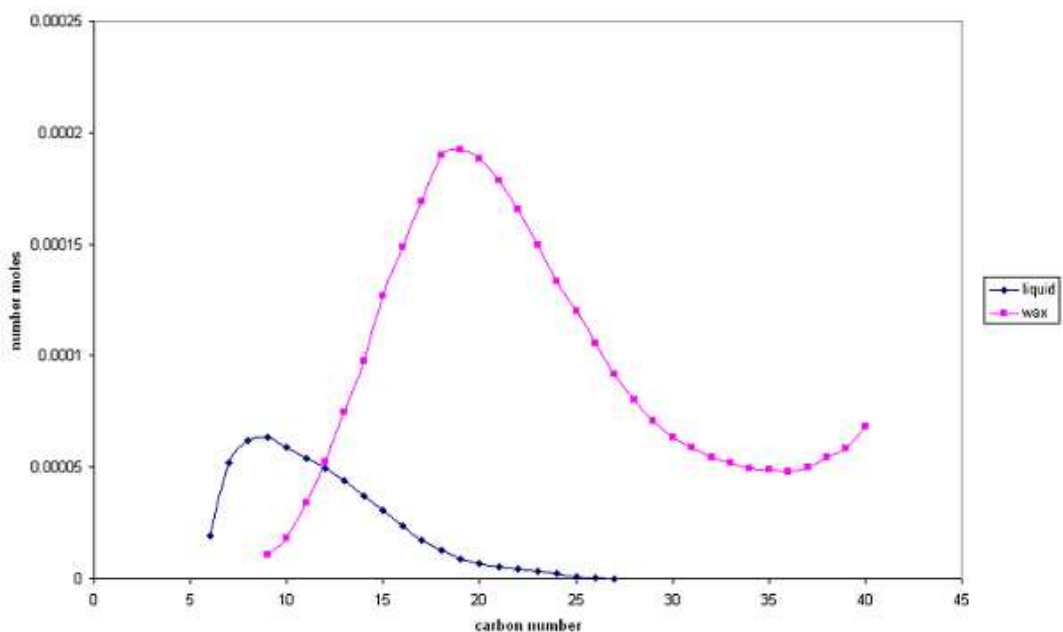


Figure 4-17 Moles of carbon products in both liquid and wax phase at 48 hrs TOS

The graph below represents the change in selectivity of the hydrocarbon products as TOS increases. It can be seen that as the reaction proceeds, the selectivity shifts slightly to higher carbon numbers.

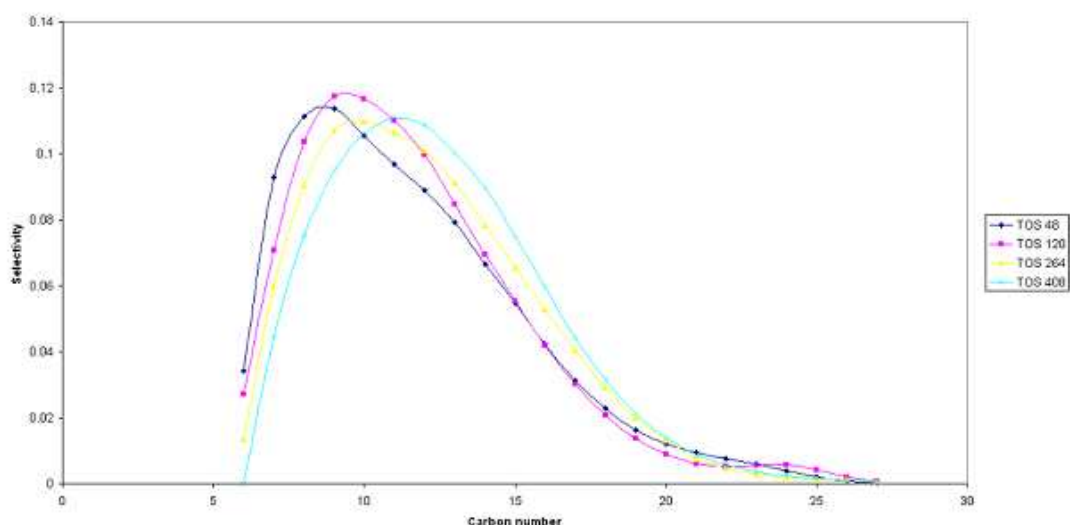


Figure 4-18 Change in selectivity at 210°C

The graph below represents the Anderson-Shultz-Flory plot for the reaction at 210°C at 48 hrs TOS. The alpha value at 48 hrs TOS was calculated at 0.881 for carbon numbers 25-35. The overall average alpha value for the reaction at 210°C was 0.91 ± 0.02 (C25-35).

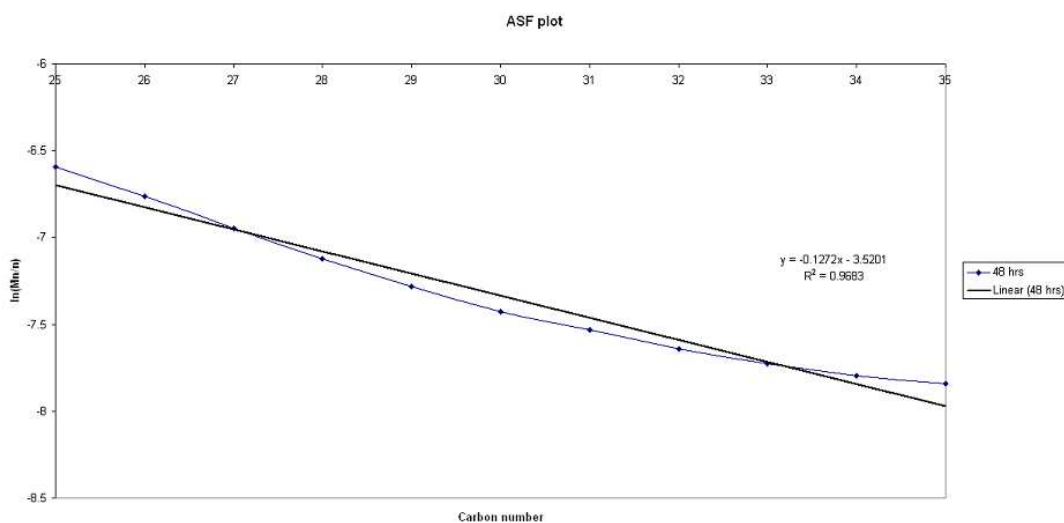


Figure 4-19 ASF plot at 210°C at 48 hrs TOS

4.1.2.2 Reaction at 220°C

The reaction temperature was then increased to 220°C at 480 hrs TOS at a ramp rate of 1°C/min. This was to investigate the effect of increase temperature on the reaction profile.

The graph below represents carbon monoxide conversion over the next ~700 hrs at the elevated reaction temperature. The conversion rose from ~8 to ~12% on the increase in temperature then dropped at a much slower rate to ~9%. The reaction seemed to deactivate linearly at a slow rate and this is shown by the smaller 1st order deactivation constant of 0.0004 hr⁻¹.

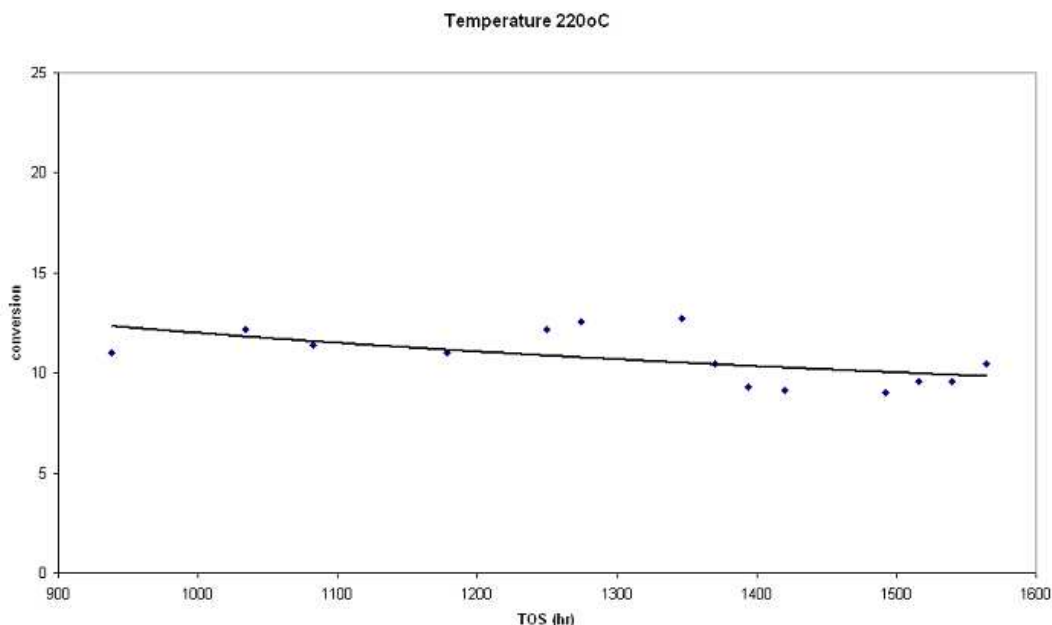


Figure 4-20 Conversion vs TOS of reaction at 220°C

The graph below represents the number moles, in the light organic phase at 220°C and 1274 hrs TOS, of each hydrocarbon formed during the reaction. From the graph it can be seen that a broad range of hydrocarbons are formed. The selectivity seems to peak at carbon number eleven which is slightly higher than at 210°C. As the reaction proceeds the volume of liquid organics produced again decreases as expected from the deactivation profile.

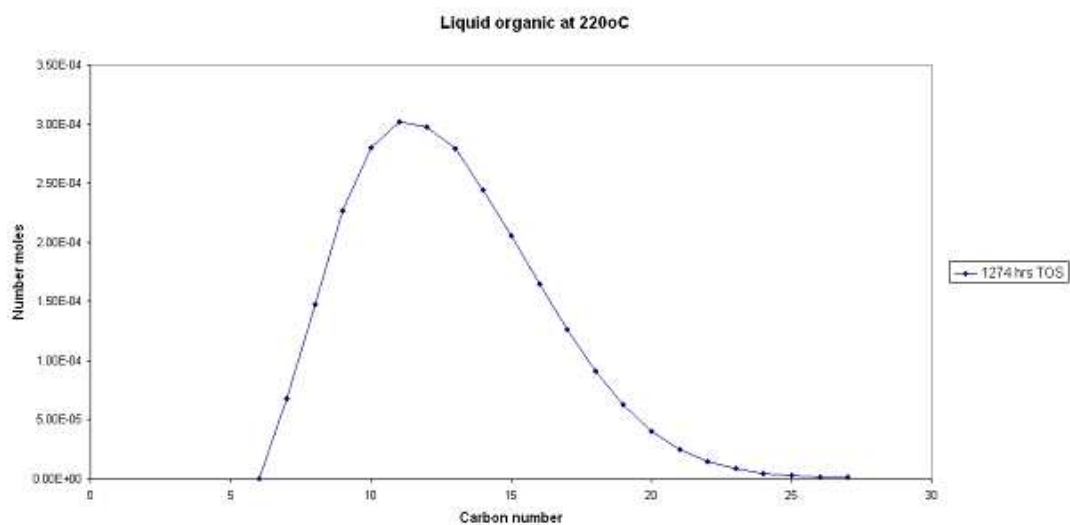


Figure 4-21 Moles of carbon products in liquid phase at 1274 hrs TOS

The graph below represents the number moles, in the wax phase at 220°C and 1274 hrs TOS, of each hydrocarbon formed during the reaction. The selectivity again seems to peak slightly higher than at 210°C at carbon number twenty-one. Similarly to the light hydrocarbon phase, as the reaction proceeds the mass of heavy hydrocarbons produced decreases again supporting the deactivation profile.

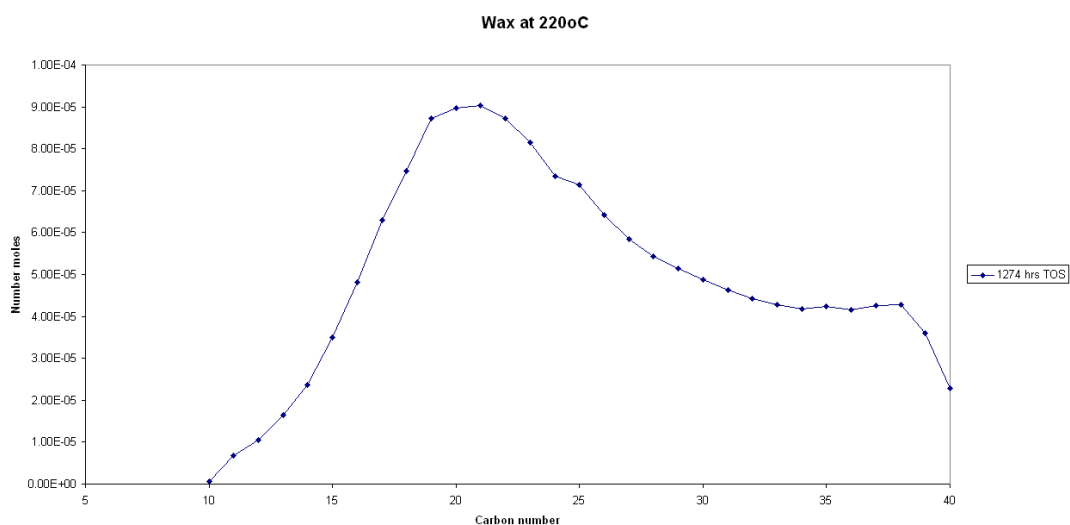


Figure 4-22 Moles of carbon products in wax phase at 1274 hrs TOS

The graph below represents the change in selectivity of the hydrocarbon products as TOS increases. The catalyst has reached steady state therefore no change in selectivity is expected.

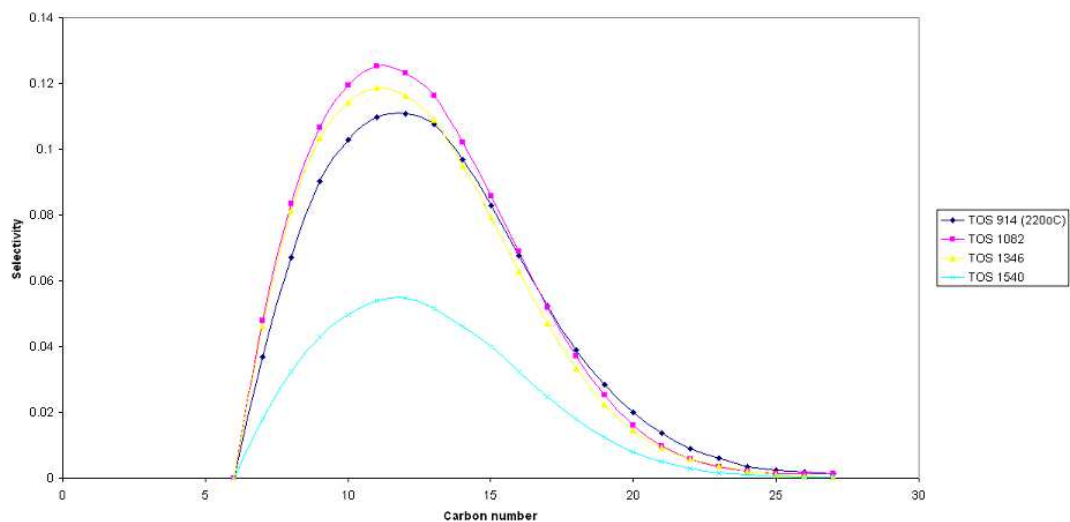


Figure 4-23 Change in selectivity at 220°C

The graph below represents the Anderson-Shultz-Flory plot for the reaction at 220°C and 1346 hrs TOS. The alpha value at 1346 hrs TOS was calculated at 0.931 for carbon numbers 25-35. The overall average alpha value for the reaction at 220°C was 0.92 ± 0.01 (C25-35).

There is no statistical difference between the α value for the reactions at 210°C and 220°C.

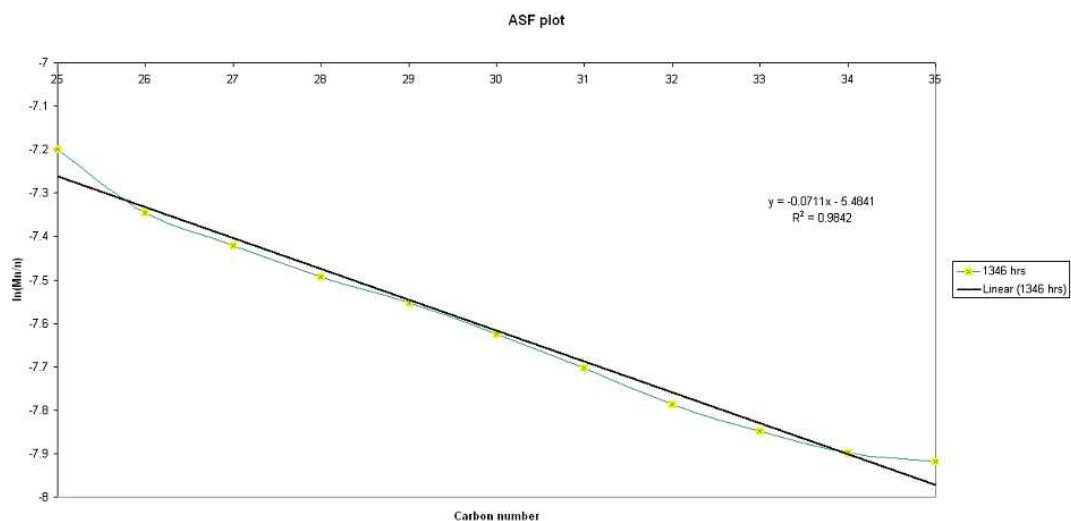


Figure 4-24 Typical ASF plot for reaction at 220°C

4.1.2.3 Post reaction analysis

To get full post reaction analysis on the catalysts it was decided not to use the online mass spectrometer for temperature-programme-oxidations. If the mass spectrometer was used the catalyst samples would be fully oxidised online (*in-situ*) and this would limit any other post reaction analysis to be carried out.

The graphs below, Figures 4-25 and 4-26, represent soxhlet analysis of the post-reaction catalyst and gamma alumina. From the graphs it can be seen that a broad range of hydrocarbons are deposited on both these materials with selectivity towards higher molecular weight hydrocarbons. Although not shown below, both materials contain hydrocarbons of C40+ with the gamma alumina containing heavier molecular weight hydrocarbons than the catalyst.

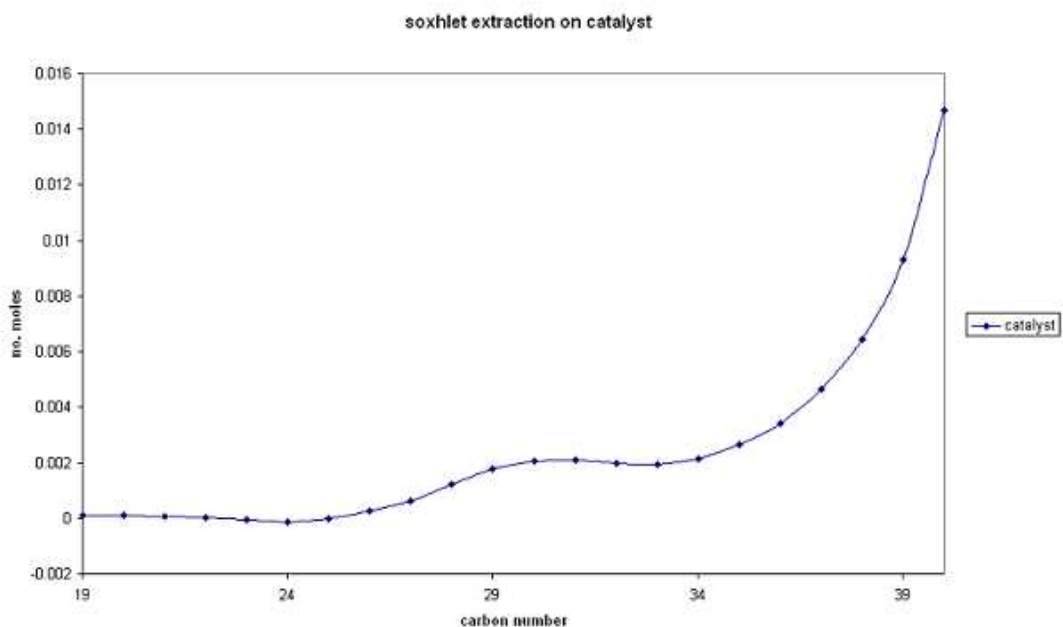


Figure 4-25 Post reaction soxhlet on a sample of catalyst

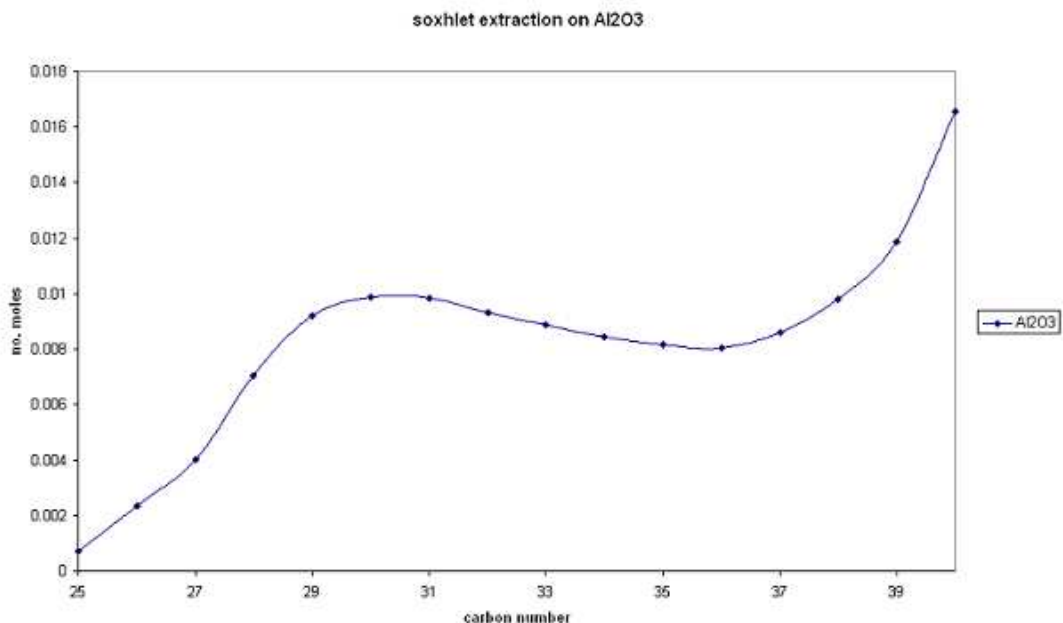


Figure 4-26 Post reaction soxhlet on a sample of alumina support

To determine as to whether carbon laydown had occurred on the surface of the catalyst, a temperature programmed oxidation (TPO) was performed on a sample of the post reaction catalyst. Any carbonaceous species deposited on the surface of the catalyst would be removed in the form of CO₂.

The graph, Figure 4-27, shows that the weight loss occurred over 3 distinct events at 53°C, 364°C and 445°C. From the weight loss curve it was calculated that the weight loss of the catalyst was ~15%. Graph, Figure 4-28, shows that CO₂ evolution occurred over a broad temperature range (200°C-580°C). A DSC trace showed that the evolutions were exothermic, confirming that the burn off of carbonaceous species was likely.

An unusual feature of the temperature programmed oxidation was that there was a slight weight increase upon exposure to the 2%O₂/Ar gas. This was most likely due to the high levels of cobalt oxide that were present in the catalyst prior to reaction. Upon reduction of the catalyst and under the CO/H₂ feed employed during the experiment, the cobalt oxide will have been reduced to metallic cobalt. Upon performing the TPO the cobalt in the catalyst re-oxidised to cobalt oxide. The weight increase in the sample indicates that only ~0.8% of the cobalt was re-oxidised. However prior to the TPO being performed the catalyst was exposed to air upon opening of the reactor lid and therefore its probable that the majority of the cobalt had been oxidised during this instance.

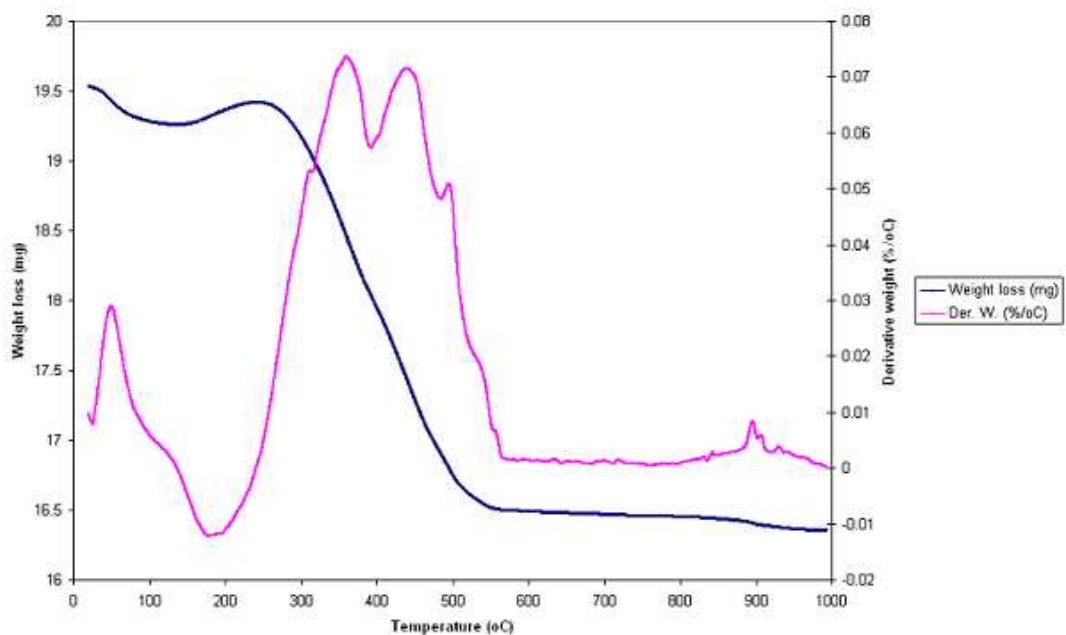


Figure 4-27 Post reaction TGA on Co/Al₂O₃ (nitrate) catalyst under oxygen

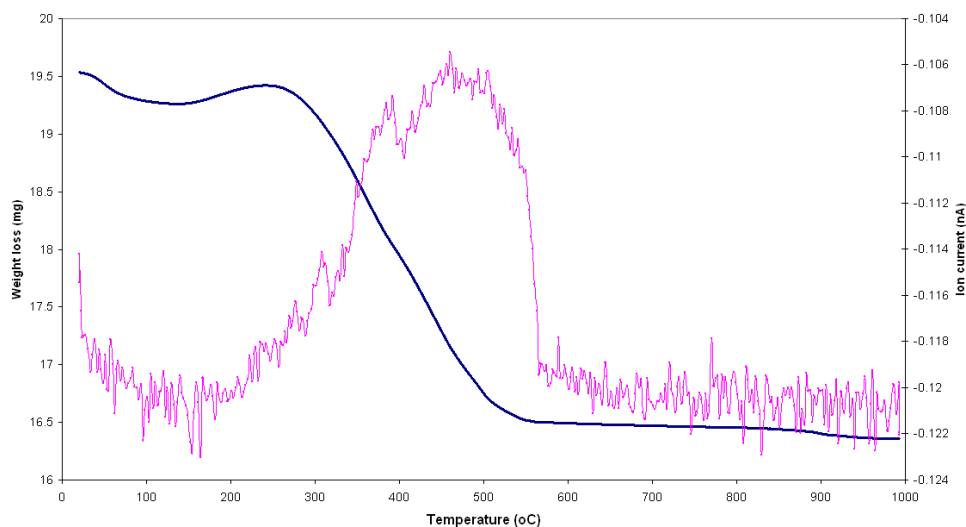


Figure 4-28 MS post reaction TGA on catalyst under oxygen

To determine as to whether carbon laydown had occurred on the surface of the gamma alumina packing material, a temperature programmed oxidation (TPO) was performed on a sample of the post reaction gamma alumina packing material. Any carbonaceous species deposited on the surface of the catalyst would be removed in the form of CO₂.

The graph, Figure 4-29, shows that the weight loss occurred over one broad temperature range between 200°C- 470°C with a small weight loss at a higher temperature of 600°C. From the weight loss curve it was calculated that the weight loss of the alumina was ~40%. Graph, Figure 4-30, shows that CO₂ evolution occurred over a broad temperature range (200°C+). A DSC trace showed that the evolution was exothermic, confirming that the burn off of carbonaceous species was likely.

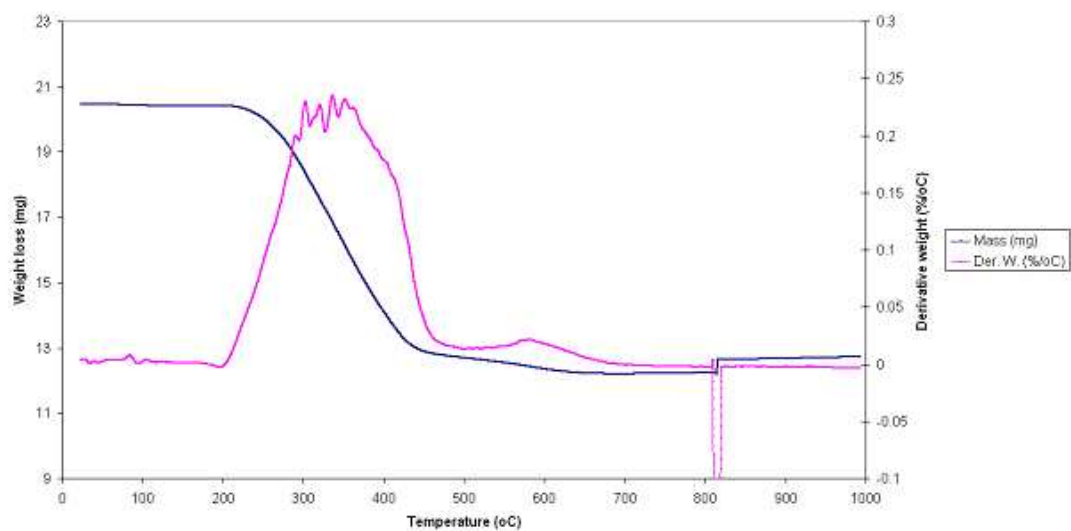


Figure 4-29 Post reaction TGA on alumina support under oxygen

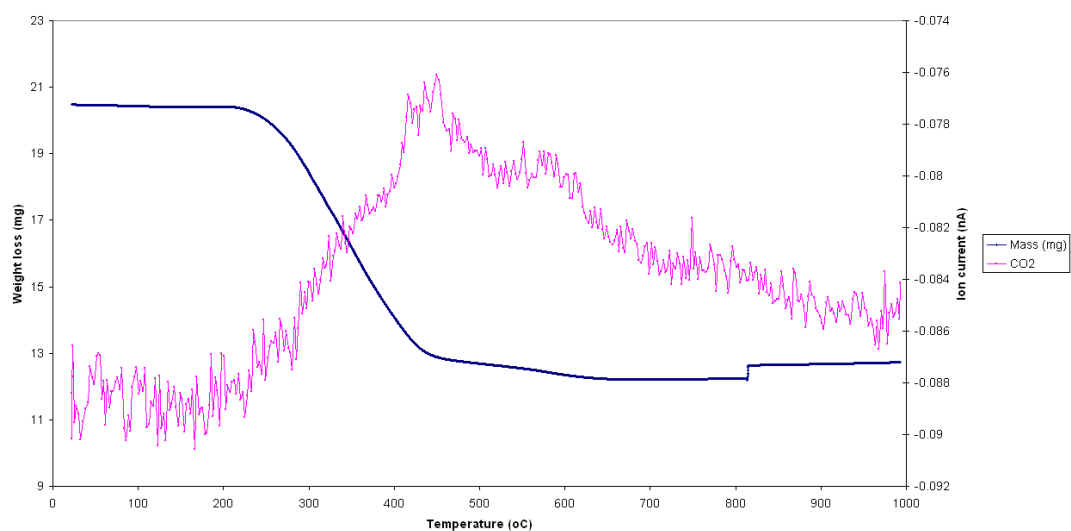


Figure 4-30 MS post reaction TGA on alumina under oxygen

4.1.3 Reaction with addition of octanol

The FT activity of this catalyst was investigated at 210°C with the addition of an octanol feed using the following conditions:

| | |
|------------------------------------|----------------------|
| • Reaction Temperature (°C) | 210 |
| • Pressure (barg) | 20 |
| • Gas Flow (ml min ⁻¹) | 47 |
| • Catalyst Volume (ml) | 0.5641 |
| • Catalyst weight (g) | 0.4001 |
| • GHSV (hr ⁻¹) | ~5,000 |
| • Residence time | 0.72 s ⁻¹ |
| • Octanol introduced | 0.02 ml / min |

The synthesis feed gas composition employed was 31.84ml min⁻¹ H₂ and 15.16ml min⁻¹ CO. This equated to a molar ratio of 2.1:1 H₂:CO which was ideal for FTS.

Prior to reaction, the catalyst was reduced *in situ* in the reactor under 47ml min⁻¹ flowing hydrogen using the reduction conditions stated earlier in section two. The catalyst was reduced in flowing hydrogen using the reduction conditions stated earlier in section two. Once the reduction programme was complete the catalyst was brought on-line very slowly and gently, as this F-T catalyst is easily damaged if brought on-line too harshly. During the reaction octanol was co-fed into the reactor to investigate the effect this had on the reaction profile.

4.1.3.1 Before octanol addition

The graph below represents carbon monoxide conversion before the addition of octanol. The conversion dropped from ~35% to ~21% in this time period compared with the drop of ~23%-11% with the 1st reaction at 210°C. Clear deactivation has occurred and the deactivation profile suggests linear decay has taken place. The 1st order deactivation constant was calculated over this time period as 0.0015 hr⁻¹ which is very similar to the 1st reaction at 210°C.

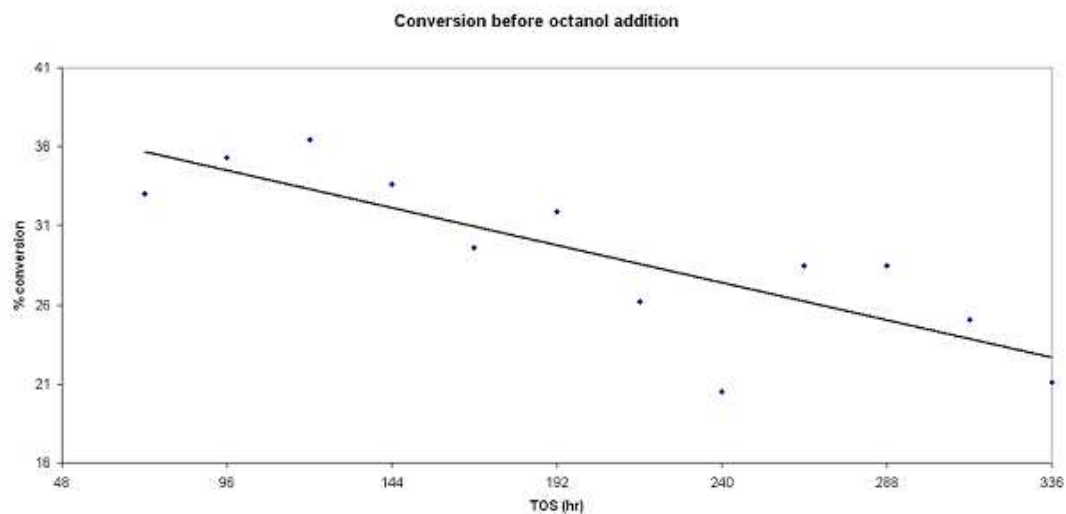


Figure 4-31 Conversion before octanol addition.

The graph below represents the number moles, in the light organic phase before octanol addition at 72 hrs TOS, of each hydrocarbon formed during the reaction. From the graph it can be seen that a broad range of hydrocarbons are formed. The selectivity seems to peak at carbon numbers nine-to-eleven which is similar to 1st reaction at 210°C. As the reaction proceeds the volume of liquid organics produced again decreases as expected from the deactivation profile.

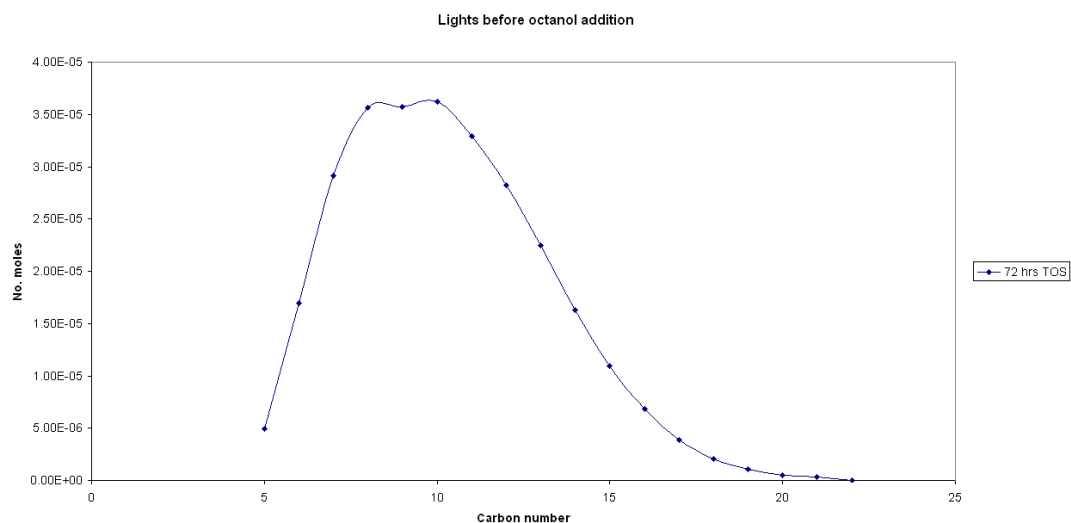


Figure 4-32 Moles of carbon products in liquid phase before octanol addition at 72 hrs TOS

The graph below represents the number moles, in the wax phase before octanol addition at 72 hrs TOS, of each hydrocarbon formed during the reaction. The selectivity peaks at the same hydrocarbon number to the 1st run at 210°C.

Similarly to the light hydrocarbon phase, as the reaction proceeds the mass of heavy hydrocarbons produced decreases again supporting the deactivation profile.

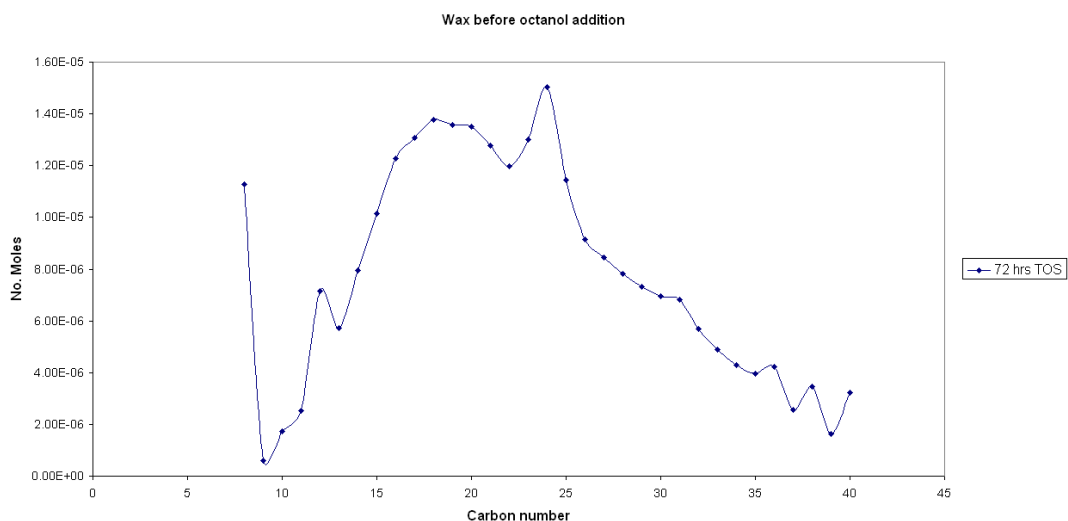


Figure 4-33 Moles of carbon products in wax phase before octanol addition at 72 hrs TOS

The graph below represents the change in selectivity of the hydrocarbon products as TOS increases. It can be seen that as the reaction proceeds, the selectivity shifts slightly to higher carbon numbers.

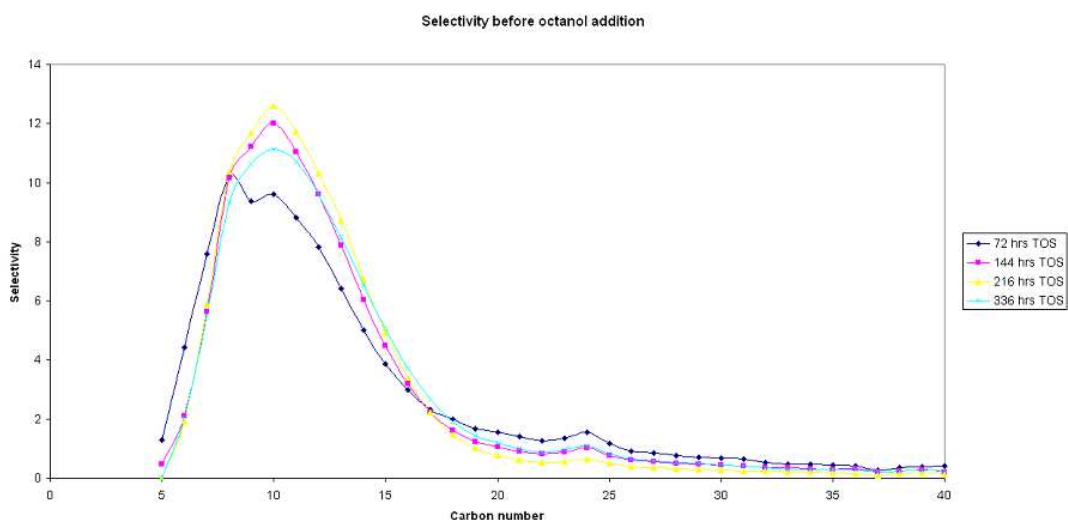


Figure 4-34 Change in selectivity before octanol addition

The graph below represents the Anderson-Shultz-Flory plot for the reaction at before octanol addition at 312 hrs TOS. The alpha value at 312 hrs TOS was

calculated at 0.913 for carbon numbers 25-35. The overall average alpha value for the reaction before the introduction of octanol was 0.915 ± 0.01 (C25-35) which is within experimental error to the 1st reaction at 210°C.

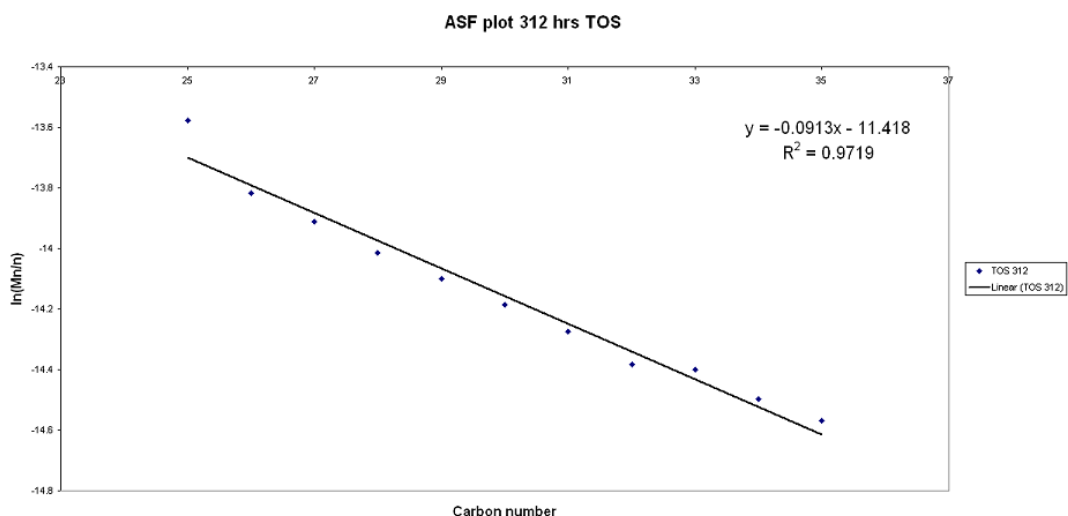


Figure 4-35 Typical ASF plot before addition of octanol

The selectivity and alpha values confirm that the catalyst is behaving as previously observed so the system is reproducible.

4.1.3.2 During octanol addition

The graph below represents carbon monoxide conversion during the co-feeding of octanol. The conversion dropped from ~21% to ~7% in this time period. Clear deactivation has occurred and the deactivation profile suggests linear decay has taken place. On the introduction of octanol into the system, an increased deactivation is seen and this is shown by the doubling of the 1st order deactivation constant which was calculated as 0.0032hr^{-1} compared without octanol addition.

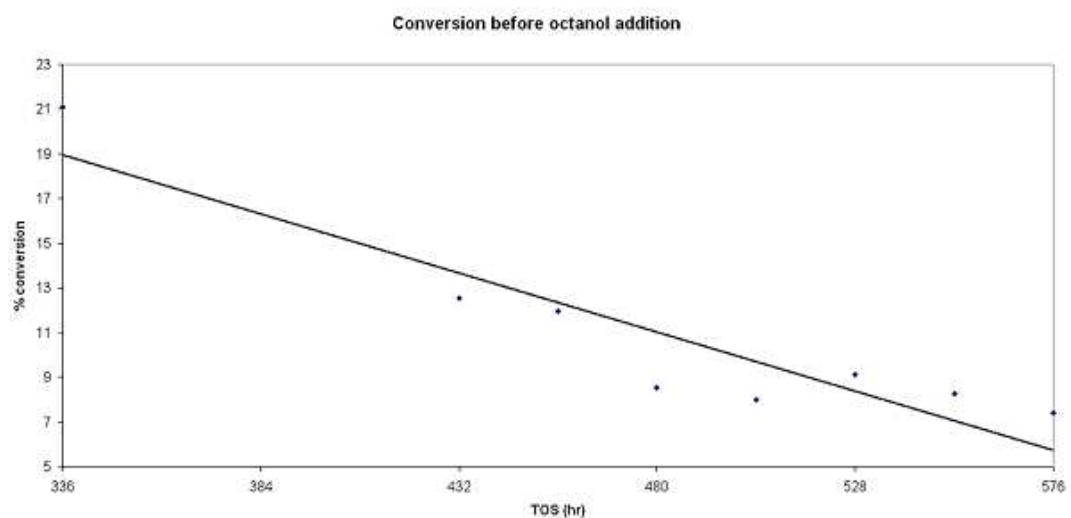


Figure 4-36 Conversion during octanol addition

The graph below represents the number moles, in the light organic phase during octanol addition at 480 hrs TOS, of each hydrocarbon formed during the reaction. From the graph it can be seen that a broad range of hydrocarbons are formed. The selectivity peaks at carbon number seven which is slightly lower than before the introduction of octanol. It is clear that a totally different profile is observed to the profile without octanol addition.

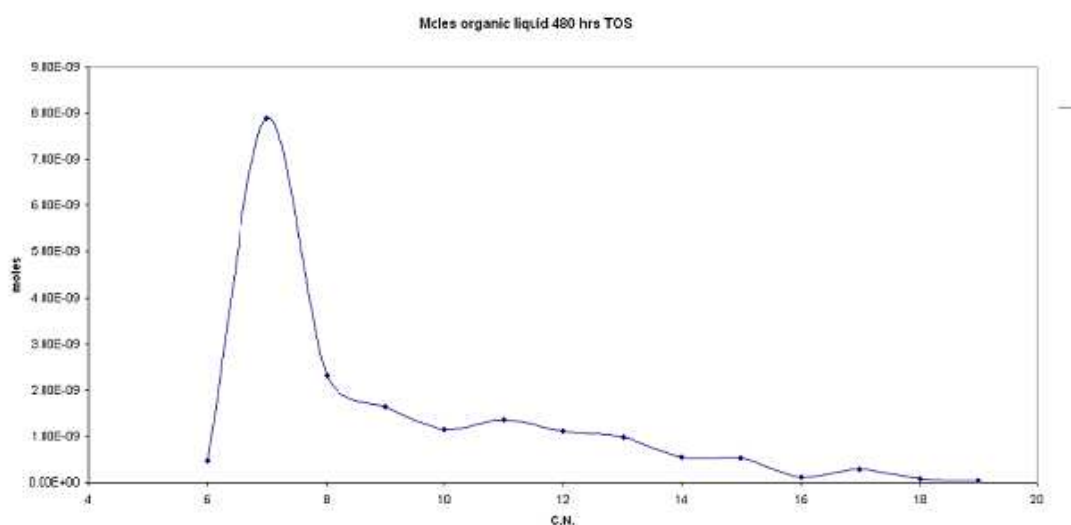


Figure 4-37 Moles of carbon products in liquid phase during octanol addition at 480 hrs TOS

The figure below represents the gas chromatogram trace for the light organic phase during octanol addition at 480 hrs TOS. From the trace it can be seen that linear alkanes are still present but there are two very distinct large peaks that appear that were not present before the addition of octanol. There also seems to be more oxygenates or alkenes present.

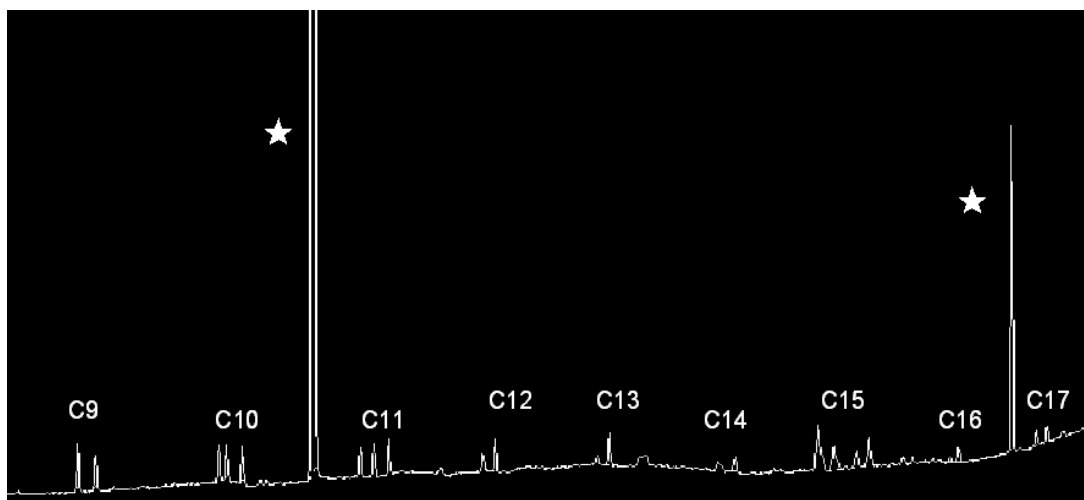


Figure 4-38 Typical chromatogram of light hydrocarbons during octanol addition

The figure below represents the overlay of the gas chromatogram traces for the light organic phase before and during octanol addition. From the trace it can clearly be seen that the two extra peaks are not linear alkanes, appear in large quantities and were not present before the addition of octanol.

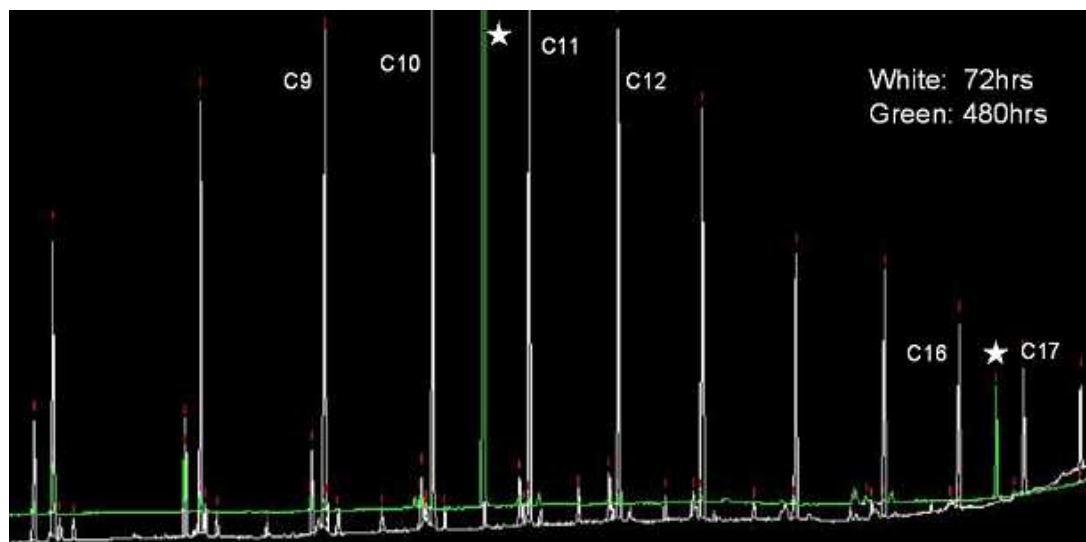


Figure 4-39 Overlay of chromatograms of light hydrocarbons before and during octanol addition

The figure below represents the overlay of the gas chromatogram traces for the light organic phase during octanol addition and a mixture of C8, C10, C12, C14 and C16 alcohols. From the trace it can clearly be seen that the two extra peaks represent octanol and tetradecanol.

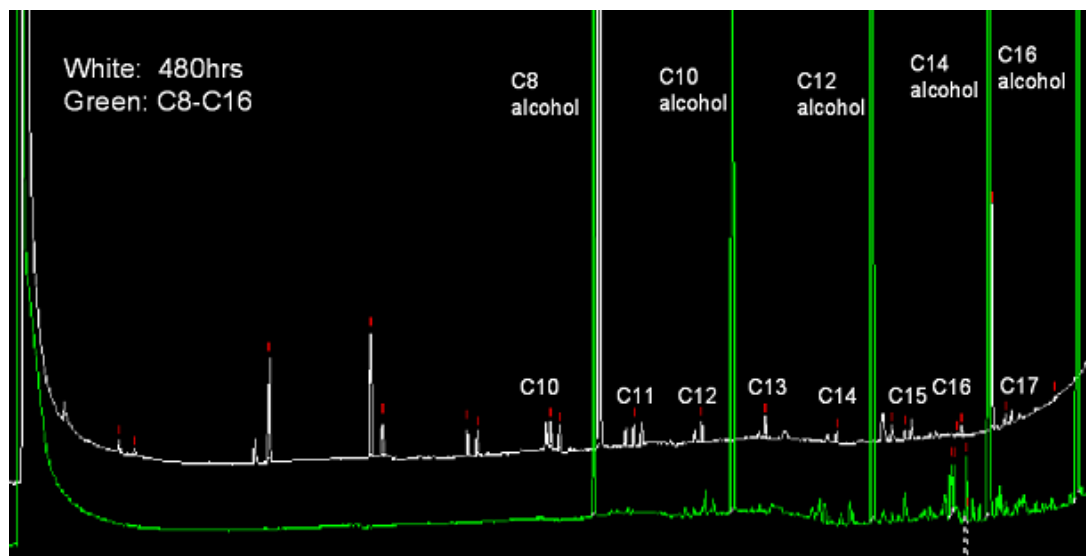


Figure 4-40 Overlay of chromatograms of light hydrocarbons during octanol addition and C8, C10, C12, C14 and C16 alcohol mix

The table below represents the quantification of octanol and tetradecanol within the light organic phase during octanol addition:

| Time period (hrs) | Moles of octanol | Moles of tetradecanol | Factor |
|-------------------|------------------|-----------------------|--------|
| 24 | 6.99E-2 | 4.42E-3 | 15.8 |
| 48 | 7.06E-2 | 4.71E-3 | 15.0 |
| 72 | 1.06E-1 | 5.39E-3 | 19.7 |
| 96 | 1.47E-1 | 6.00E-3 | 24.5 |

Table 4-2 Quantification of moles of octanol and tetradecanol in liquid organic phase

The graph below represents the number moles, in the wax phase during octanol addition at 480 hrs TOS, of each hydrocarbon formed during the reaction. Unlike the light organic phase where there was a clear change in profile, the profile for the wax phase is not dramatically changed.

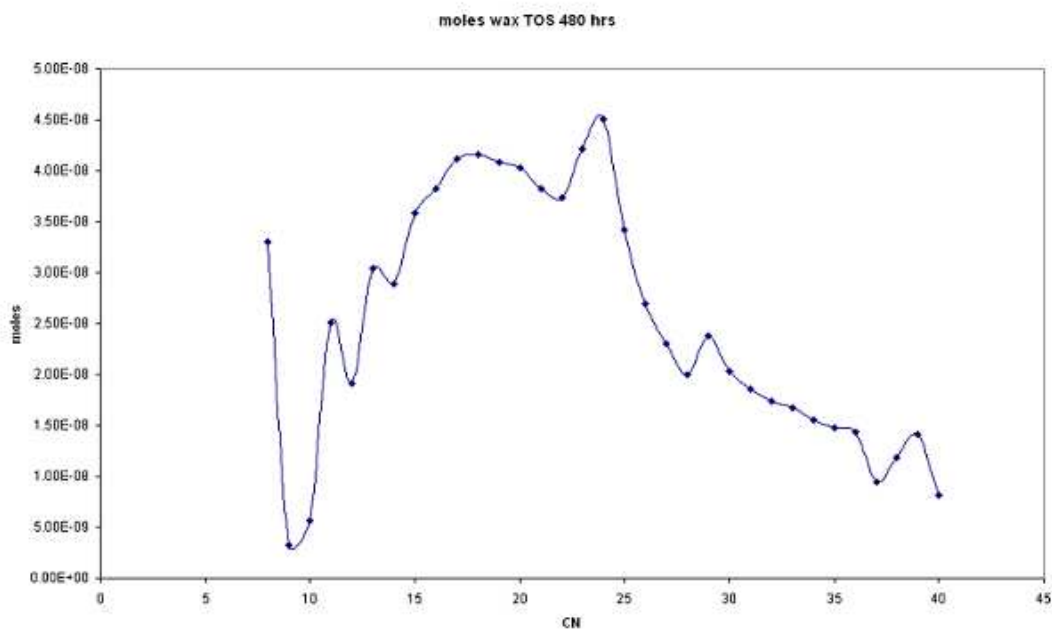


Figure 4-41 Moles of carbon products in wax phase during octanol addition at 480 hrs TOS

The figure below represents the gas chromatogram trace for the wax phase during octanol addition at 480 hrs TOS. From the trace it can be clearly seen that linear alkanes are still present but again there are two very distinct large peaks that appear that were not present before the addition of octanol.

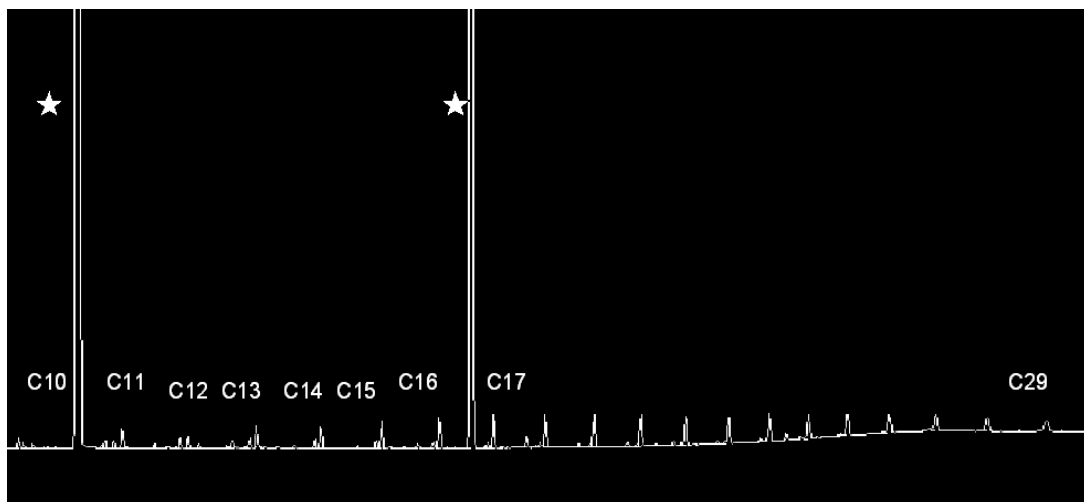


Figure 4-42 Typical chromatogram of heavy hydrocarbons during octanol addition

The figure below represents the overlay of the gas chromatogram traces for the wax phase before and during octanol addition. Again from the trace it can clearly be seen that the two extra peaks are not linear alkanes, appear in large quantities and were not present before the addition of octanol.

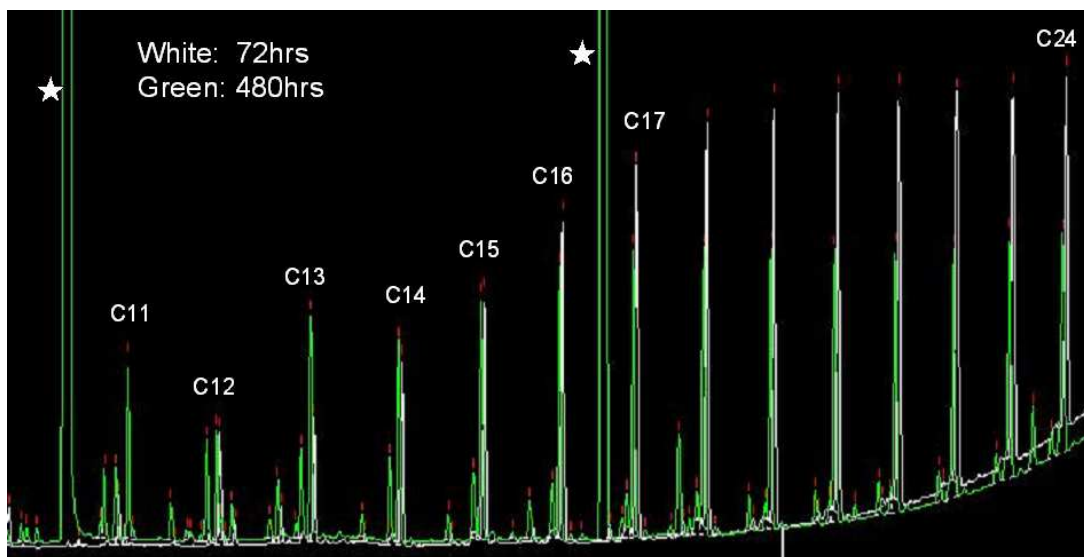


Figure 4-43 Overlay of chromatograms of heavy hydrocarbons before and during octanol addition

The figure below represents the overlay of the gas chromatogram traces for the wax phase during octanol addition and a mixture of C8, C10, C12, C14 and C16

alcohols. From the trace it can clearly be seen that the two extra peaks represent octanol and tetradecanol.

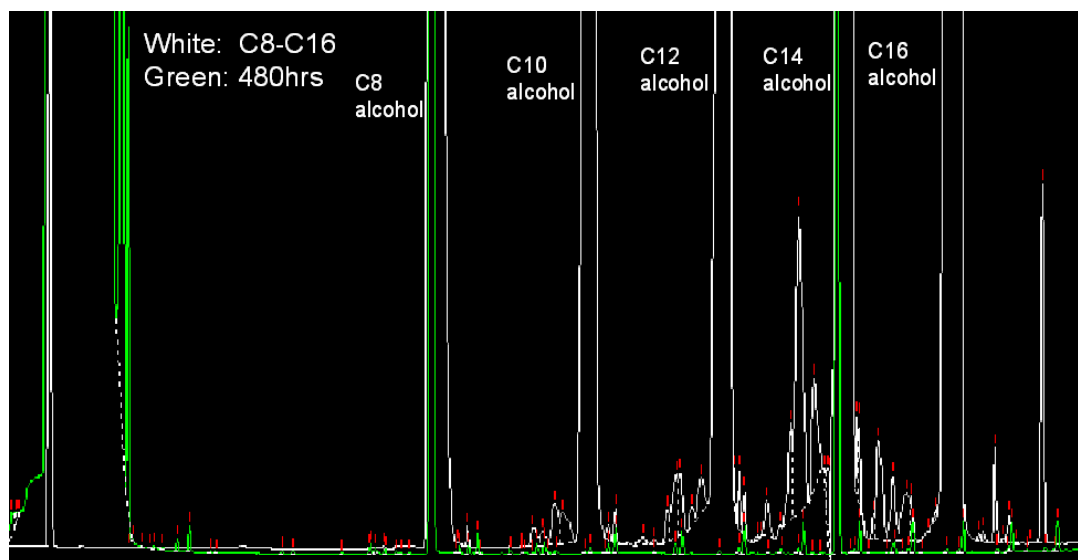


Figure 4-44 Overlay of chromatograms of heavy hydrocarbons during octanol addition and C8, C10, C12, C14 and C16 alcohols

The table below represents the quantification of octanol and tetradecanol within the wax phase during octanol addition:

| Time period (hrs) | Moles of octanol | Moles of tetradecanol | Factor |
|-------------------|------------------|-----------------------|--------|
| 24 | 1.42E-2 | 3.46E-3 | 4.0 |
| 48 | 1.43E-2 | 4.72E-3 | 3.0 |
| 72 | 1.6E-2 | 5.32E-3 | 3.0 |
| 96 | 1.73E-2 | 5.35E-3 | 3.2 |

Table 4-3 Quantification of moles of octanol and tetradecanol in wax phase

The graph below represents the change in selectivity of the hydrocarbon products as TOS increases. What appears to be happening is a situation where the initial effect of octanol inhibits polymerisation and over time the polymerisation seems to increase.

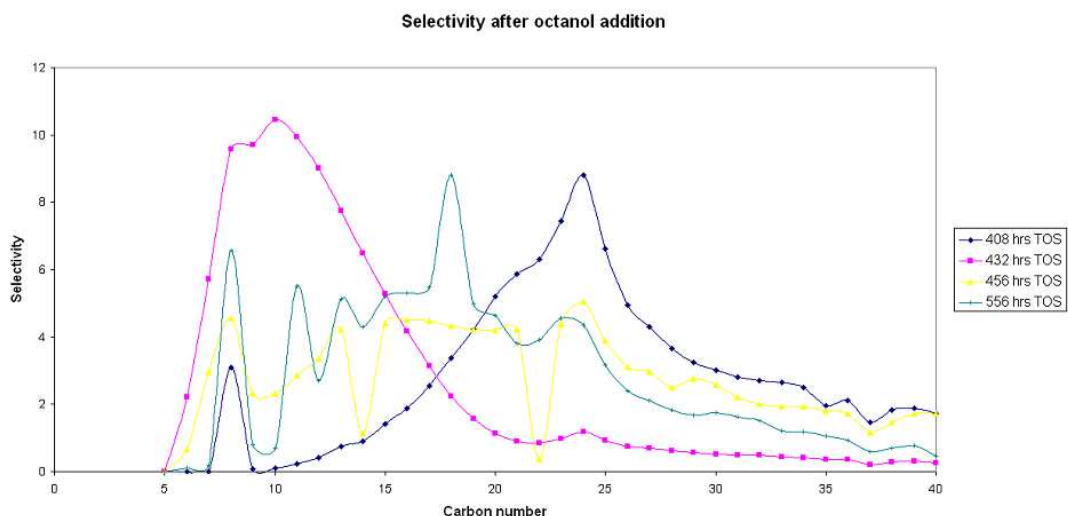


Figure 4-45 Change in selectivity during octanol addition

The graph below represents the Anderson-Shultz-Flory plot for the reaction during octanol addition at 408 hrs TOS. The alpha value at 408 hrs TOS was calculated at 0.905 for carbon numbers 25-35. The overall average alpha value for the reaction during the introduction of octanol was 0.921 ± 0.01 (C25-35).

There is no statistical difference between the α value for the reactions before and during the addition of octanol. However if we compare the C12+ and C20+ selectivity we can see the impact of the octanol (see table below).

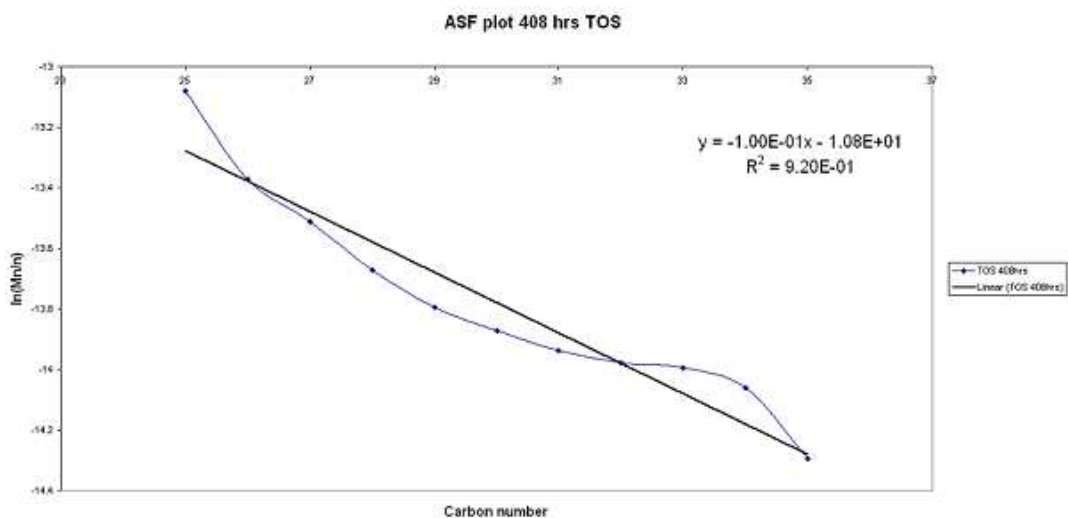


Figure 4-46 Typical ASF plot during addition of octanol

| TOS (hrs) | C12+ selectivity | C20+ selectivity |
|-----------|------------------|------------------|
| 408 | 96.51 | 86.02 |
| 432 | 52.39 | 12.72 |

Table 4-4 Selectivity differences between 408 and 432 hrs TOS

4.1.3.3 Post reaction analysis

The graphs below, Figures 4-47 and 4-48, represent soxhlet analysis of the post-reaction catalyst and gamma alumina. From the graphs it can be seen that a broad range of hydrocarbons are deposited on both these materials with selectivity towards higher molecular weight hydrocarbons. Although not shown below, both materials contain hydrocarbons of C40+ with the gamma alumina containing heavier molecular weight hydrocarbons than the catalyst which is in agreements with the previous experiment.

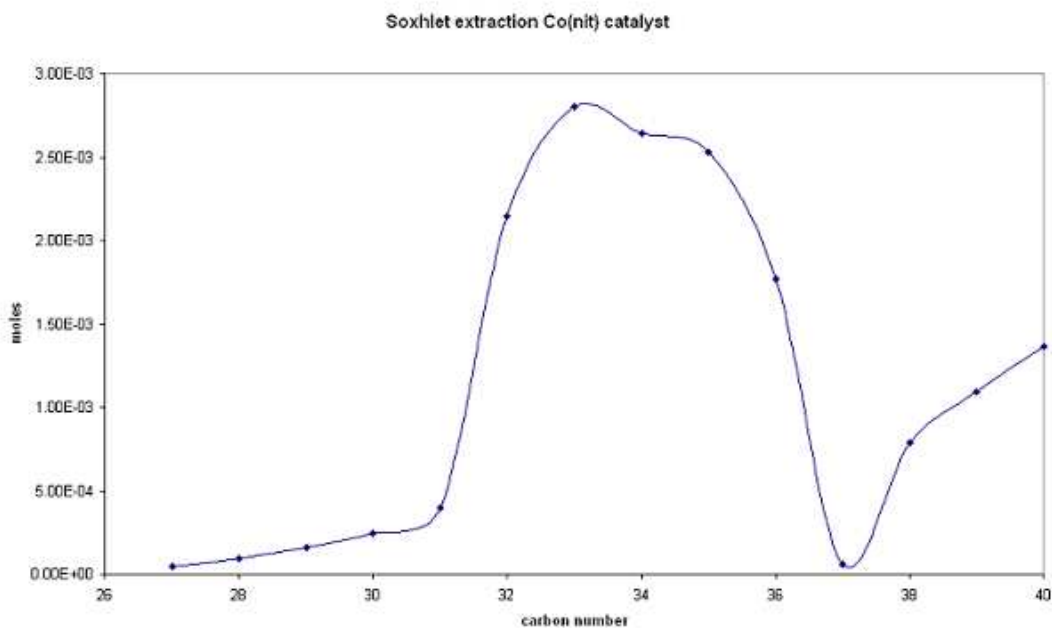


Figure 4-47 Soxhlet post reaction on a sample of catalyst

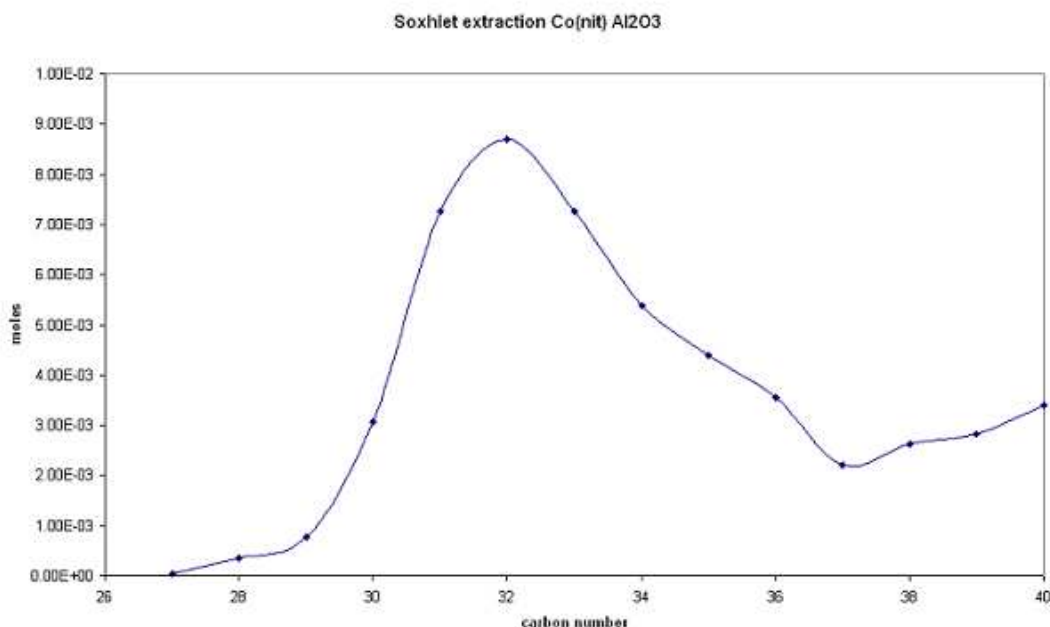


Figure 4-48 Soxhlet post reaction on a sample of alumina support

To determine as to whether carbon laydown had occurred on the surface of the catalyst, a temperature programmed oxidation (TPO) was performed on a sample of the post reaction catalyst. Any carbonaceous species deposited on the surface of the catalyst would be removed in the form of CO_2 .

The graph, Figure 4-49, shows that the weight loss occurred over 3 distinct events: one broad peak between 45°C - 200°C , and two further peaks at 311°C and 375°C . There was even a small weight loss at higher temperature of 930°C . From the weight loss curve it was calculated that the weight loss of the catalyst was $\sim 6.5\%$. Graph, Figure 4-50, shows that CO_2 evolution occurred over a broad temperature range (200°C - 500°C). A DSC trace showed that the evolutions were exothermic, confirming that the burn off of carbonaceous species was likely.

An unusual feature of the temperature programmed oxidation was that there was a slight weight increase upon exposure to the $2\%\text{O}_2/\text{Ar}$ gas. This was most likely due to the high levels of cobalt oxide that were present in the catalyst prior to reaction. Upon reduction of the catalyst and under the CO/H_2 feed employed during the experiment, the cobalt oxide will have been reduced to metallic cobalt. Upon performing the TPO the cobalt in the catalyst re-oxidised to cobalt oxide. The weight increase in the sample indicates that only $\sim 0.7\%$ of

the cobalt was re-oxidised. However prior to the TPO being performed the catalyst was exposed to air upon opening of the reactor lid and therefore its probable that the majority of the cobalt had been oxidised during this instance.

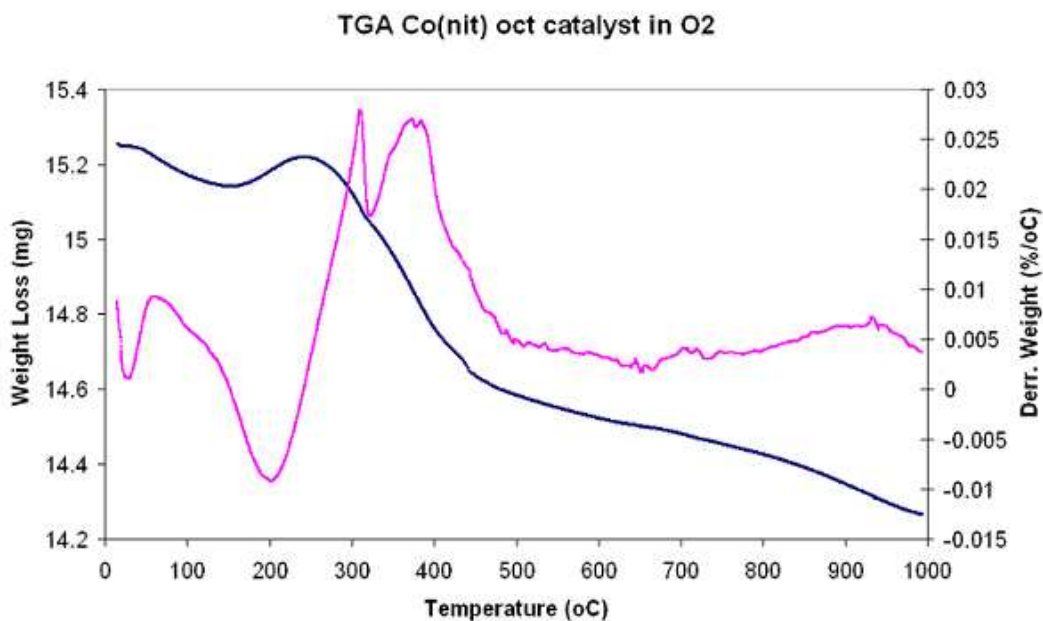


Figure 4-49 Post reaction TGA on catalyst under oxygen gas

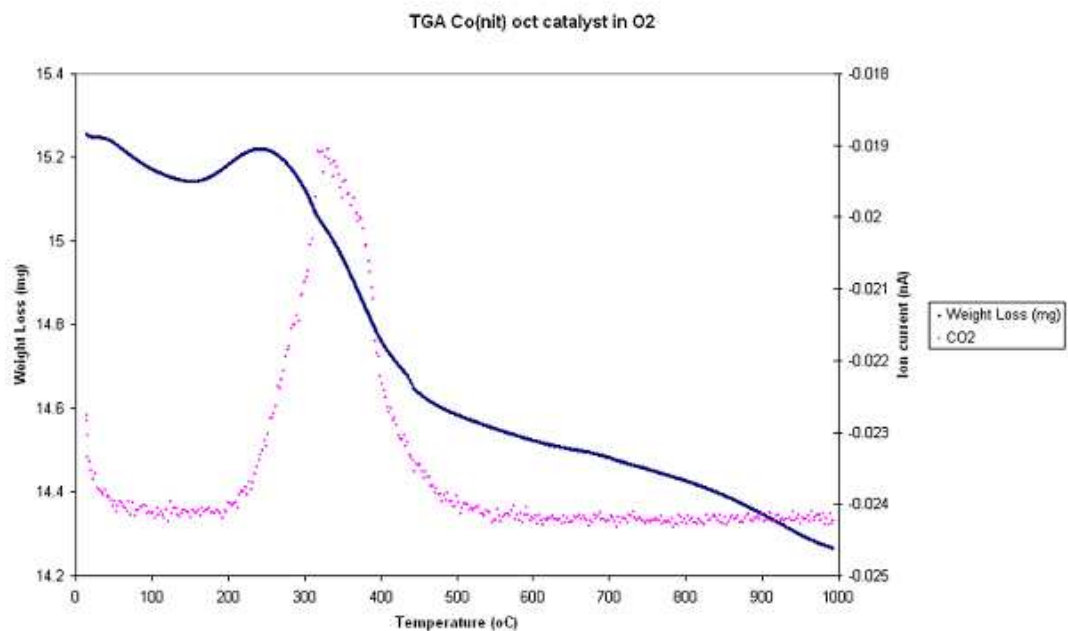


Figure 4-50 MS post reaction TGA on catalyst under oxygen gas

To determine as to whether carbon laydown had occurred on the surface of the gamma alumina packing material, a temperature programmed oxidation (TPO) was performed on a sample of the post reaction gamma alumina packing material. Any carbonaceous species deposited on the surface of the catalyst would be removed in the form of CO₂.

The graph, Figure 4-51, shows that the weight loss occurred over a broad temperature range between 35°C- 150°C with two further weight losses at higher temperatures of 380°C and 419°C. From the weight loss curve it was calculated that the weight loss of the alumina was ~11%. Graph, Figure 4-52, shows that CO₂ evolution occurred over a broad temperature range (280°C - 550°C). A DSC trace showed that the evolution was exothermic, confirming that the burn off of carbonaceous species was likely.

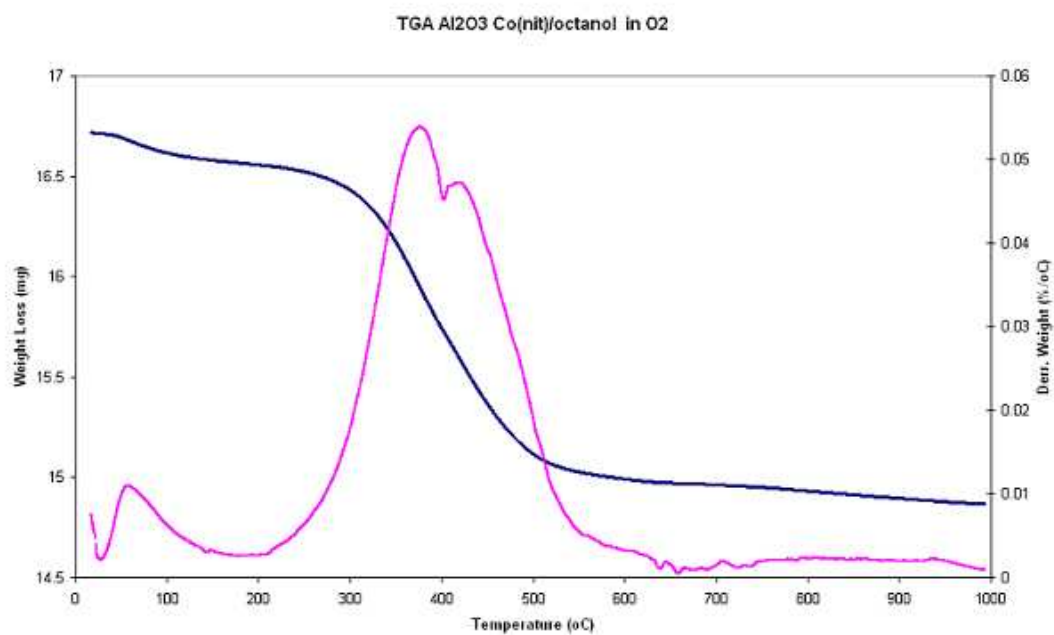


Figure 4-51 Post reaction TGA on alumina support under oxygen gas

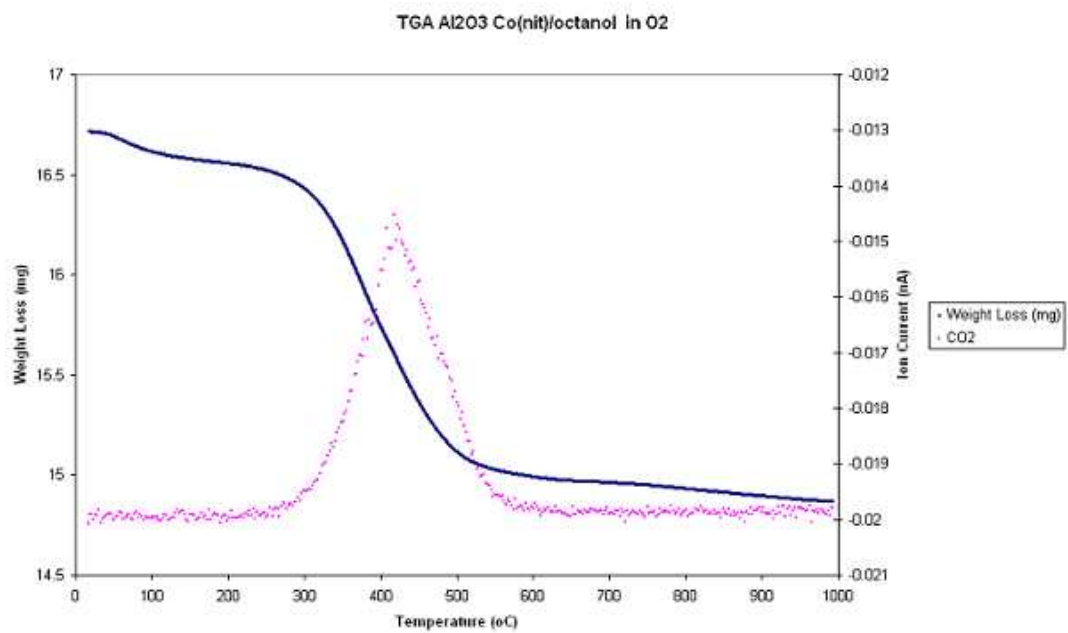


Figure 4-52 MS post reaction TGA on alumina support under oxygen gas

4.1.4 Reaction with addition of decanol then a mixture of naphthalene and dodecane

The FT activity of this catalyst was investigated at 210°C with the addition of a decanol feed then a further addition of 0.063 molar naphthalene in dodecane solution using the following conditions:

- Reaction Temperature (°C) 210
- Pressure (barg) 20
- Gas Flow (ml min⁻¹) 46.42
- Catalyst Volume (ml) 0.5570
- Catalyst weight (g) 0.395
- GHSV (hr⁻¹) ~5,000
- Residence time 0.72 s⁻¹
- Decanol introduced 0.02 ml / min
- Naphthalene solution introduced 0.02 ml / min

The synthesis feed gas composition employed was 31.44ml min⁻¹ H₂ and 14.96ml min⁻¹ CO. This equated to a molar ratio of 2.1:1 H₂:CO which was ideal for FTS.

Prior to reaction, the catalyst was reduced *in situ* in the reactor under 46.42ml min⁻¹ flowing hydrogen using the reduction conditions stated earlier in section two. Once the reduction programme was complete the catalyst was brought on-line very slowly and gently, as this F-T catalyst is easily damaged if brought on-line too harshly. During the reaction decanol was co-fed into the reactor for a period of time then stopped. Once the reaction had regenerated a 0.063 molar naphthalene in dodecane solution was co-fed to investigate the effect this had on the reaction profile.

4.1.4.1 Before decanol addition

The catalyst was brought online and behaved as expected. The conversion dropped from ~43% to ~30% over the first ~288 hrs TOS. This was slightly higher than with the previous two runs where the conversion drops over the same time period were ~23% to ~12% and ~35% to ~21% respectively. The main difference

was a higher 1st order deactivation constant that was observed of 0.0662hr^{-1} compared with the first two runs of 0.0032hr^{-1} and 0.0016hr^{-1} over the same time period.

From the light organic phase results, before decanol addition, the selectivity peaks at carbon numbers nine-to-eleven which is similar to the previous reactions at 210°C . As the reaction proceeds the volume of liquid organics produced again decreases as expected from the deactivation profile.

From the wax phase results before decanol addition the selectivity peaks in the same hydrocarbon number region to the previous runs at 210°C . Similarly to the light hydrocarbon phase, as the reaction proceeds the mass of heavy hydrocarbons produced decreases again supporting the deactivation profile.

The selectivity of the hydrocarbon products shifts slightly to higher hydrocarbons as TOS increases. The Anderson-Shultz-Flory plots are in agreement with earlier experiments with the alpha value at 312 hrs TOS calculated as 0.909 for carbon numbers 25-35. The overall average alpha value for the reaction before the introduction of octanol was 0.900 ± 0.009 (C25-35) which is within experimental error as the previous reactions at 210°C . The selectivity and alpha values confirm that the catalyst is behaving as previously observed.

4.1.4.2 During decanol addition

The graph below represents carbon monoxide conversion during the co-feeding of decanol. The conversion dropped from ~30% to ~12% in this time period. Clear deactivation has occurred and the deactivation profile suggests linear decay has taken place. The 1st order deactivation constant was calculated over this time period as 0.0027hr^{-1} .

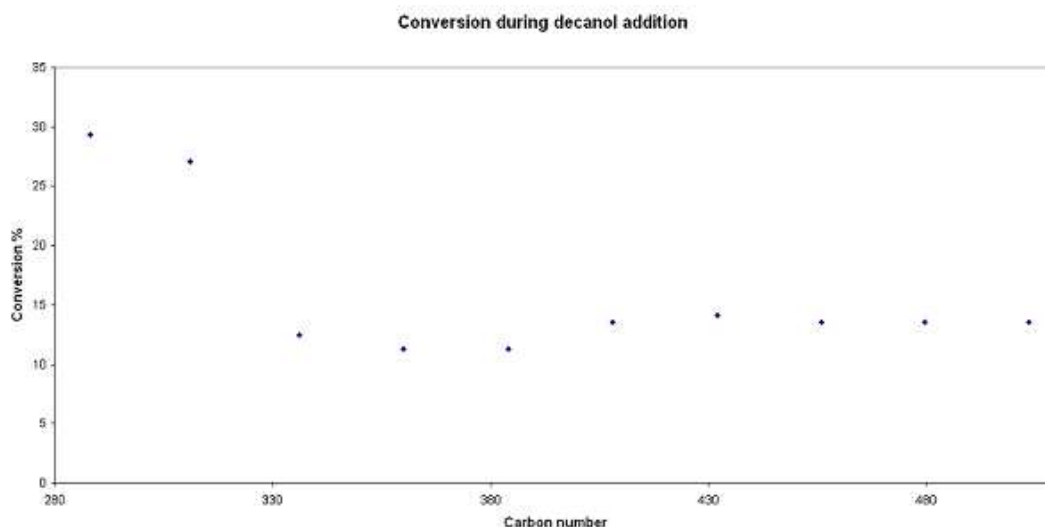


Figure 4-53 Conversion during decanol addition

The graph below represents the number moles in the light organic phase, during decanol addition at 311 hrs TOS, of each hydrocarbon formed during the reaction. From the graph it can be seen that a broad range of hydrocarbons are formed. The selectivity peaks at carbon number ten which is similar to before the addition of decanol.

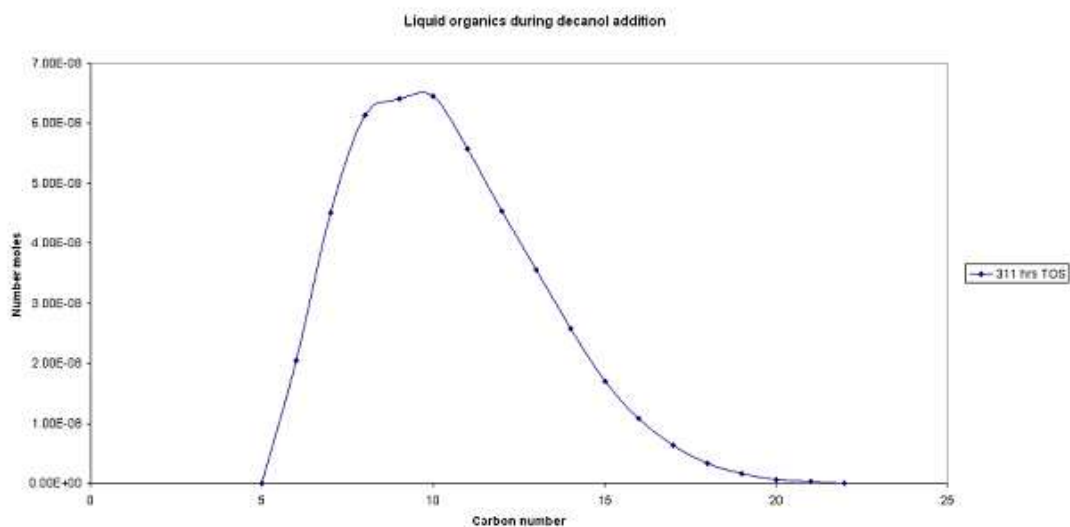


Figure 4-54 Moles of carbon products in liquid phase during decanol addition at 311 hrs TOS

The figure below represents the gas chromatogram trace for the light organic phase during decanol addition at 311 hrs TOS. From the trace it can be seen

that linear alkanes are still present but there are two very distinct large peaks that appear that were not present before the addition of decanol. There also seems to be more oxygenates or alkenes present.

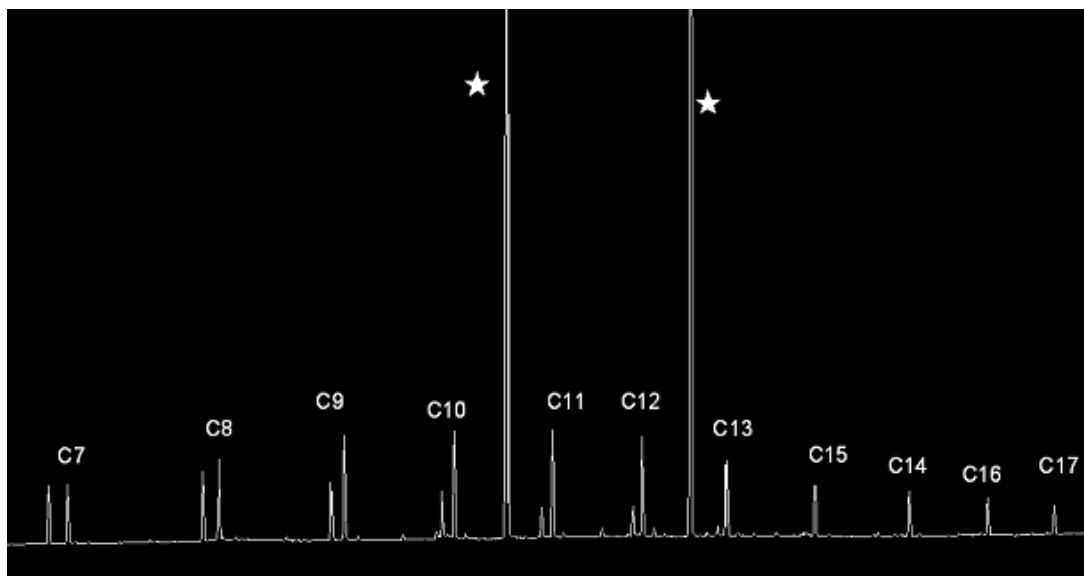


Figure 4-55 Gas chromatogram trace of light hydrocarbons during decanol addition

The figure below represents the overlay of the gas chromatogram traces for the light organic phase, during decanol addition, and a mixture of C8, C10, C12, C14 and C16 alcohols. From the trace it can clearly be seen that the two extra peaks represent octanol and decanol. The peak representing octanol (1st peak) disappears after 384 hrs TOS and this is due to some octanol still present in the HPLC line leading to the reactor from the previous run.

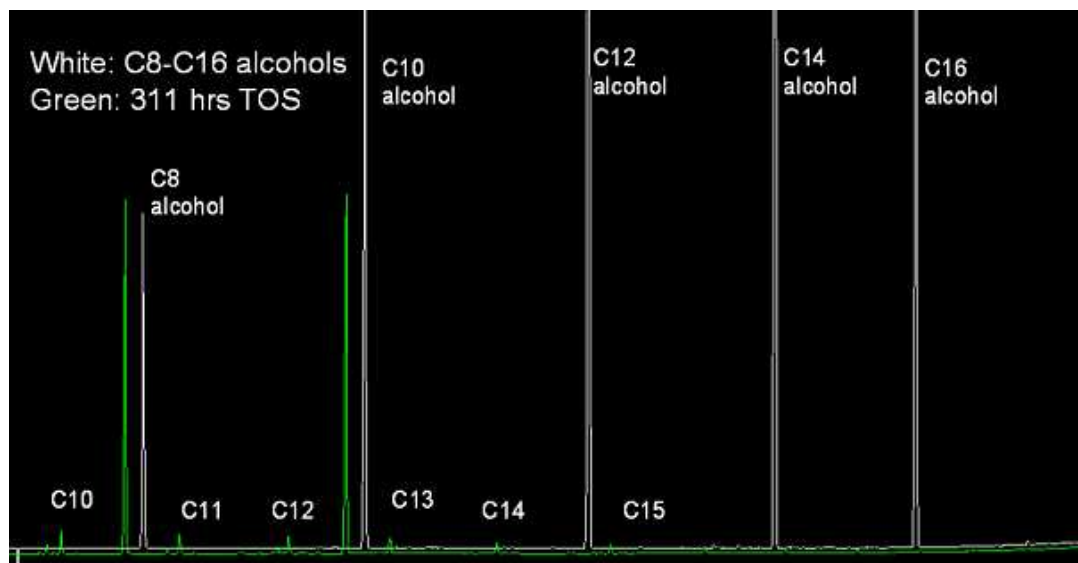


Figure 4-56 Overlay of chromatograms of light hydrocarbons during decanol addition and C8, C10, C12, C14 and C16 alcohol mix

The table below represents the quantification of octanol and decanol within the light organic phase during octanol addition:

| TOS hrs | Moles octanol | Moles decanol |
|---------|---------------|---------------|
| 311 | 5.38E-2 | 4.03E-2 |
| 336 | 1.62E-2 | 5.56E-2 |
| 360 | 8.41E-3 | 8.67E-2 |
| 384 | | 5.08E-2 |
| 408 | | 6.18E-2 |
| 432 | | 6.45E-2 |
| 456 | | 6.05E-2 |
| 479.5 | | 4.34E-2 |
| 503.5 | | 6.00E-2 |

Table 4-5 Quantification of moles of octanol and decanol in light organic phase

The graph below represents the number moles in the wax phase, during decanol addition at 311 hrs TOS, of each hydrocarbon formed during the reaction. It is clear that a totally different profile is observed to the profile without decanol addition.

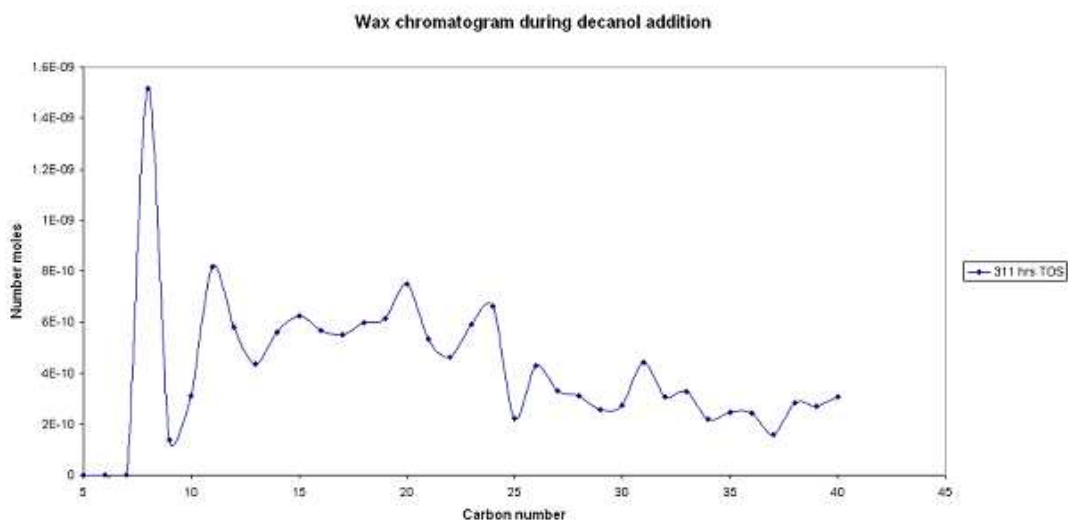


Figure 4-57 Moles of carbon products in wax phase during decanol addition at 311 hrs TOS

The figure below represents the gas chromatogram trace for the wax phase during decanol addition at 311 hrs TOS. From the trace it can be clearly seen that linear alkanes are still present but again there are two very distinct large peaks that appear that were not present before the addition of octanol.

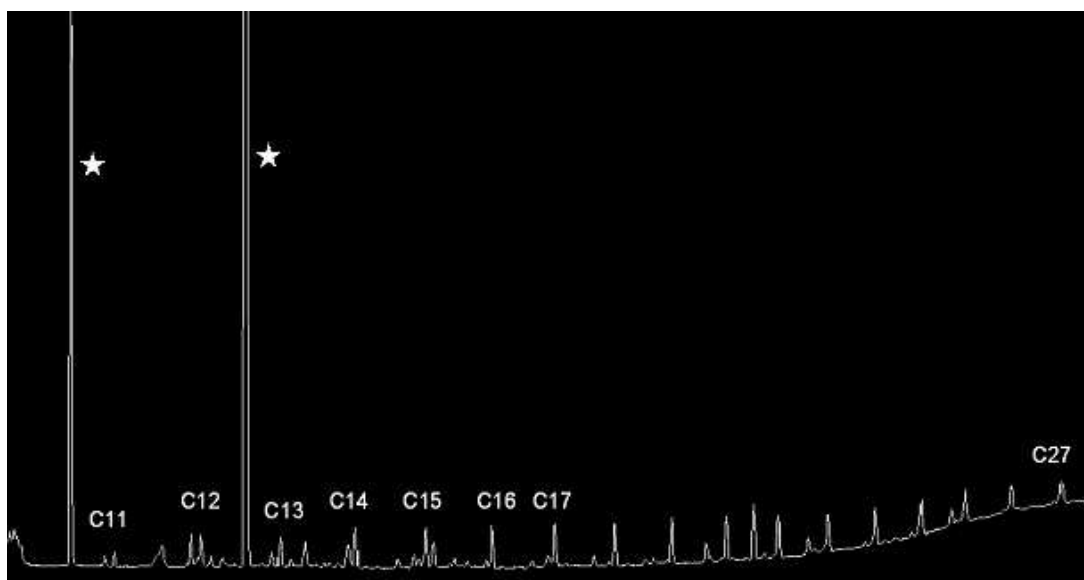


Figure 4-58 Typical chromatogram of heavy hydrocarbons during decanol addition

The figure below represents the overlay of the gas chromatogram traces for the wax phase, during octanol addition, and a mixture of C8, C10, C12, C14 and C16 alcohols. From the trace it can clearly be seen that the two extra peaks represent octanol and decanol. Similarly to the light organic phase results, the

peak representing octanol (1st peak) disappears after 336 hrs TOS and this is due to some octanol still present in the HPLC line leading to the reactor from the previous run.

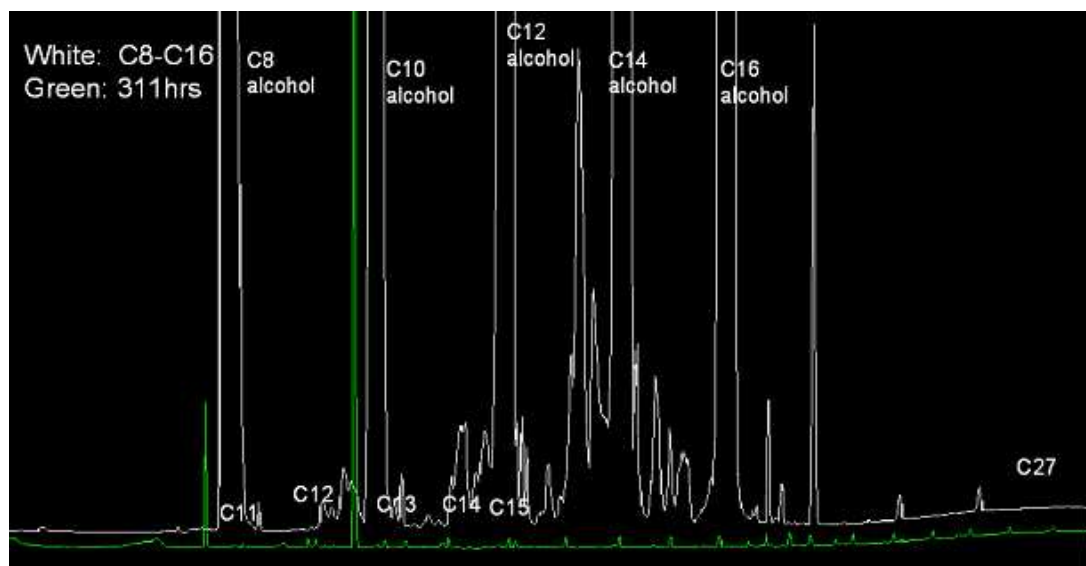


Figure 4-59 Overlay of chromatograms of heavy hydrocarbons during decanol addition and C8, C10, C12, C14 and C16 alcohol mix

The table below represents the quantification of octanol and decanol within the wax phase during octanol addition:

| TOS hrs | Moles octanol | Moles decanol |
|---------|---------------|---------------|
| 311 | 3.10E-4 | 3.16E-3 |
| 336 | 1.31E-5 | 3.26E-3 |
| 360 | | 3.37E-3 |
| 384 | | 3.33E-3 |
| 408 | | 4.00E-3 |
| 432 | | 2.63E-3 |
| 456 | | 2.94E-3 |
| 479.5 | | 3.57E-3 |
| 503.5 | | 3.78E-3 |

Table 4-6 Quantification of moles of octanol and decanol in wax phase

The graph below represents the change in selectivity of the hydrocarbon products as TOS increases. What appears to be happening is a situation where the initial effect of decanol inhibits polymerisation and over time the polymerisation seems to increase which is comparable to the reaction with octanol addition.

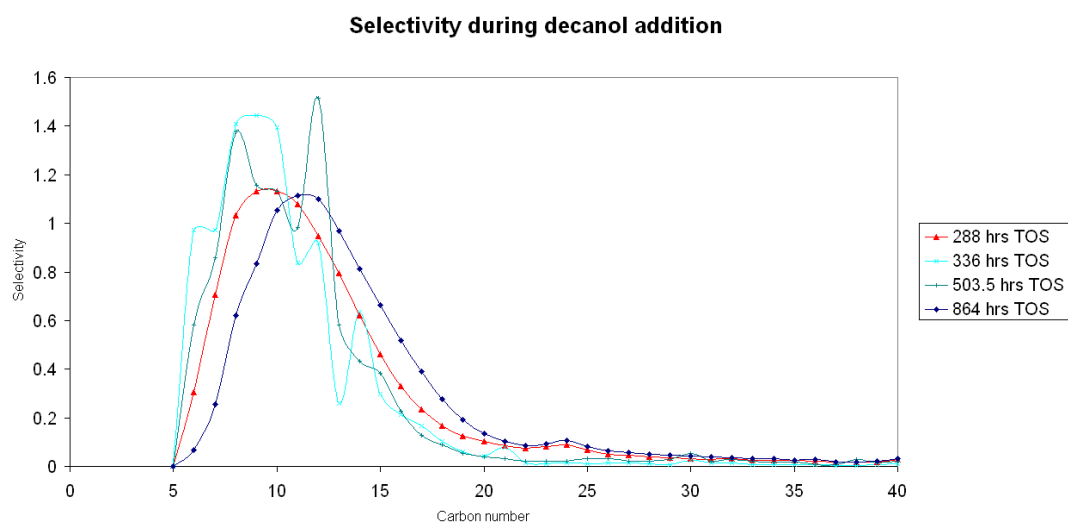


Figure 4-60 Change in selectivity during decanol addition

The graph below represents the Anderson-Shultz-Flory plot for the reaction during decanol addition at 408 hrs TOS. The alpha value at 408 hrs TOS was calculated at 0.913 for carbon numbers 25-35. The overall average alpha value for the reaction during the introduction of octanol was 0.94 ± 0.033 (C25-35).

There is no statistical difference between the α value for the reactions before and during the addition of decanol.

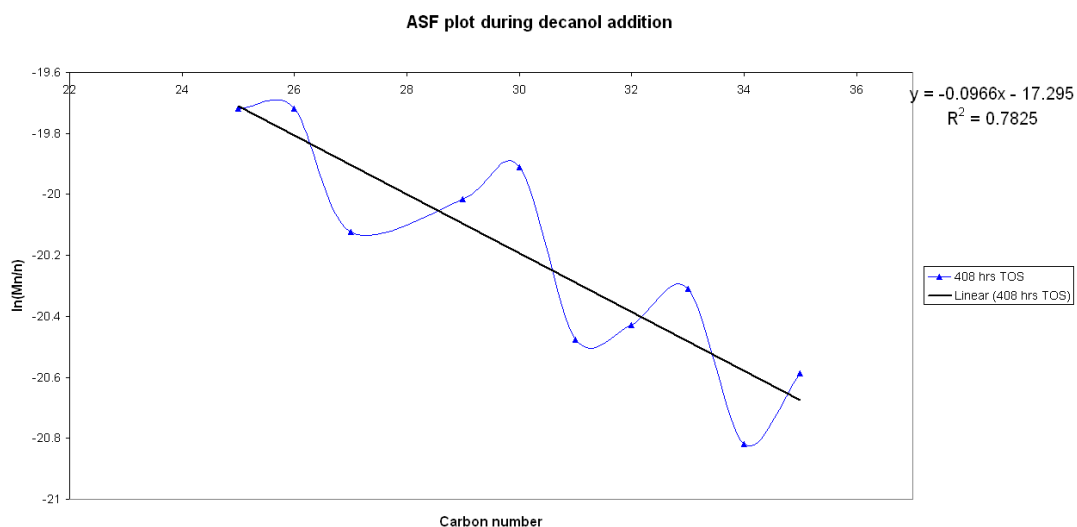


Figure 4-61 Typical ASF plot during addition of decanol

4.1.4.3 After decanol feed turned off

After a period of 360 hrs TOS with decanol being co-fed into the reactor the liquid feed was turned off to see if this had a positive effect on the catalyst activity. The conversion dropped from ~13% to ~9.5% and the deactivation slowed. The 1st order deactivation constant decreased to 0.0006hr^{-1} .

From the light organic phase results, after decanol addition had ceased, the selectivity of hydrocarbons shows a similar trend to the previous reactions at 210°C . As the reaction proceeds the volume of liquid organics produced again decreases as expected from the deactivation profile.

From the wax phase results, after decanol addition had ceased, the selectivity of hydrocarbons revert back to the expected profile but the selectivity peaks at a higher hydrocarbon number range compared with previous runs at 210°C . Similarly to the light hydrocarbon phase, as the reaction proceeds the mass of heavy hydrocarbons produced decreases again supporting the deactivation profile.

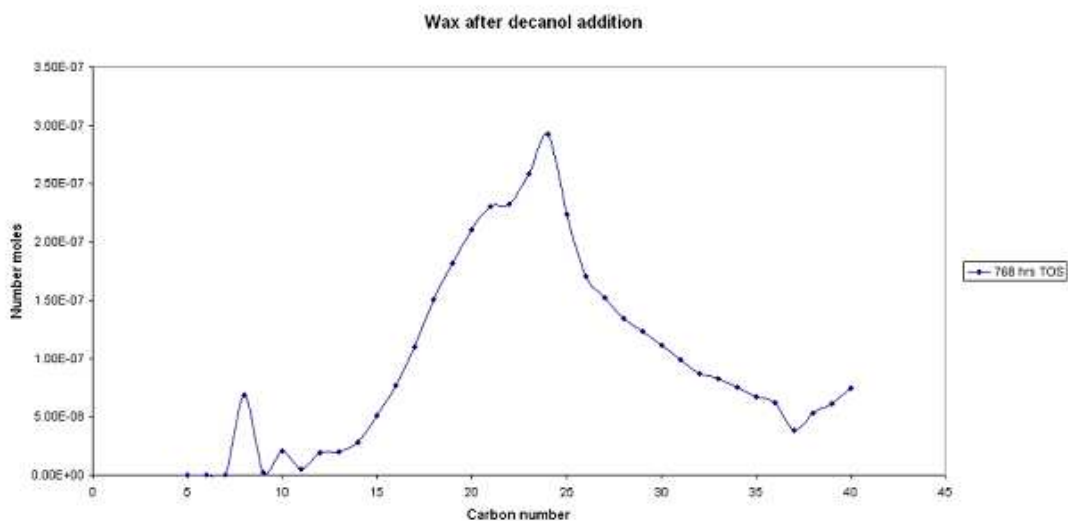


Figure 4-62 Moles of carbon products in liquid phase after decanol addition at 768 hrs TOS

The selectivity of the hydrocarbon products shifts slightly to higher hydrocarbons as TOS increases. The Anderson-Shultz-Flory plots are in agreement with earlier experiments with the alpha value at 839 hrs TOS calculated as 0.894 for carbon numbers 25-35. The overall average alpha value for the reaction before the introduction of octanol was 0.900 ± 0.016 (C25-35) which is within experimental error as the previous reactions at 210°C. The selectivity and alpha values confirm that the catalyst is behaving as previously observed.

4.1.4.4 Naphthalene and dodecane addition

A dramatic negative effect on the catalyst activity was seen with the introduction of 0.063 molar naphthalene in dodecane solution. The reaction deactivated rapidly and after 48 hrs TOS co-feeding this solution into the reactor, the reaction was fully deactivated.

4.1.4.5 Post reaction analysis

The graphs below, Figures 4-63 and 4-64, represent soxhlet analysis of the post-reaction catalyst and gamma alumina. From the graphs it can be seen that a broad range of hydrocarbons are deposited on both these materials with selectivity towards higher molecular weight hydrocarbons.

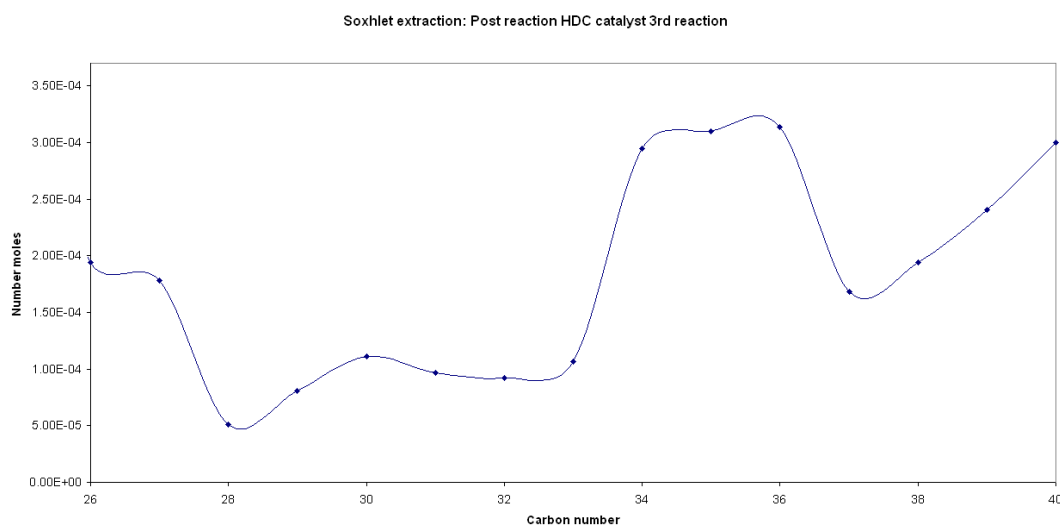


Figure 4-63 Soxhlet post reaction on a sample of catalyst 3rd reaction

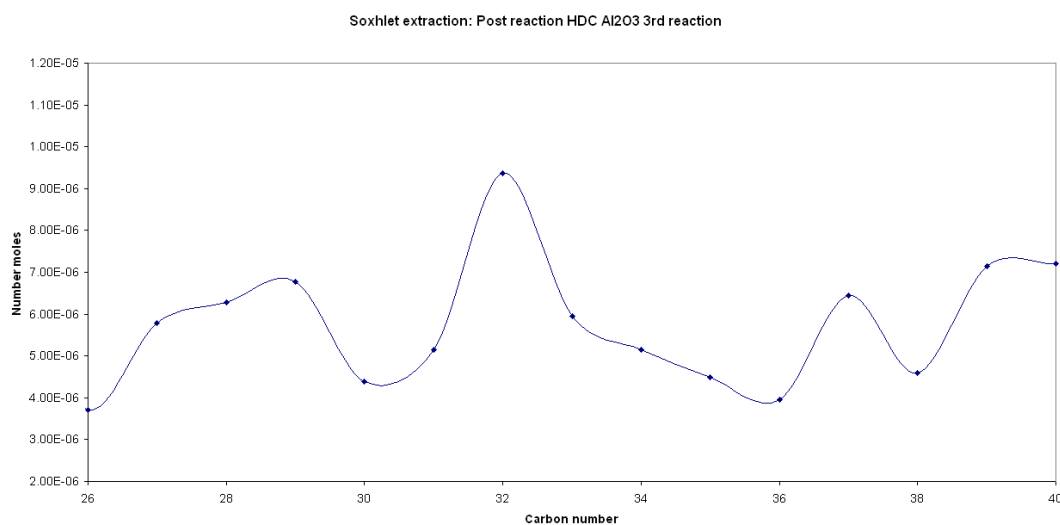


Figure 4-64 Soxhlet post reaction on a sample of alumina support 3rd reaction

To determine as to whether carbon laydown had occurred on the surface of the catalyst, a temperature programmed oxidation (TPO) was performed on a sample of the post reaction catalyst. Any carbonaceous species deposited on the surface of the catalyst would be removed in the form of CO₂.

The graph, Figure 4-65, shows that the weight loss occurred over 2 broad events: one broad peak between 35°C-200°C, and the next between 200°C-600°C. There was even a small weight loss at higher temperature of 947°C. From the weight

loss curve it was calculated that the weight loss of the catalyst was ~7%. Graph, Figure 4-66, shows that CO₂ evolution occurred over a broad temperature range of 200°C-515°C. A DSC trace showed that the evolutions were exothermic, confirming that the burn off of carbonaceous species was likely.

An unusual feature of the temperature programmed oxidation was that there was a slight weight increase upon exposure to the 2%O₂/Ar gas. This was most likely due to the high levels of cobalt oxide that were present in the catalyst prior to reaction. Upon reduction of the catalyst and under the CO/H₂ feed employed during the experiment, the cobalt oxide will have been reduced to metallic cobalt. Upon performing the TPO the cobalt in the catalyst re-oxidised to cobalt oxide. The weight increase in the sample indicates that only ~0.7% of the cobalt was re-oxidised. However prior to the TPO being performed the catalyst was exposed to air upon opening of the reactor lid and therefore its probable that the majority of the cobalt had been oxidised during this instance.

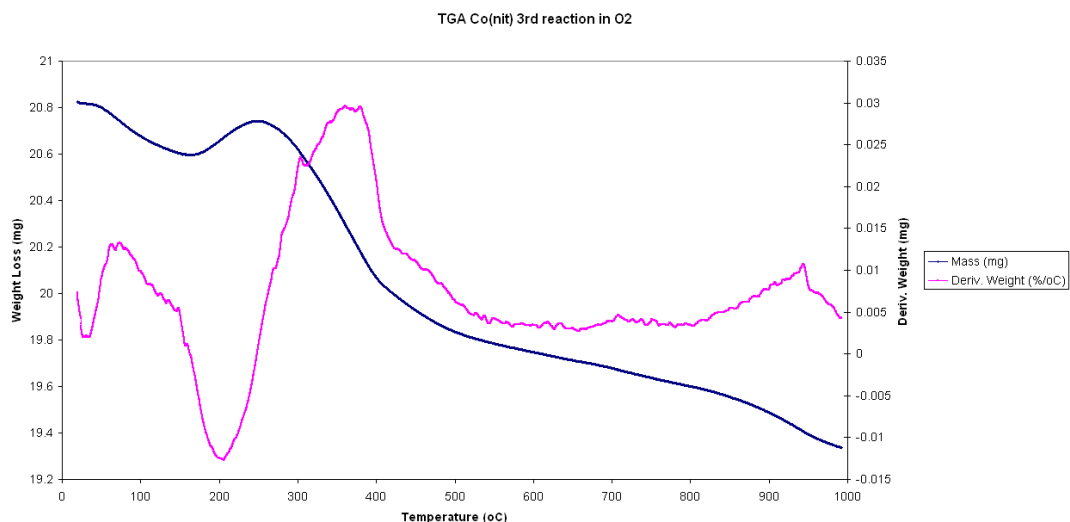


Figure 4-65 Post reaction TGA (3rd reaction) catalyst under oxygen gas

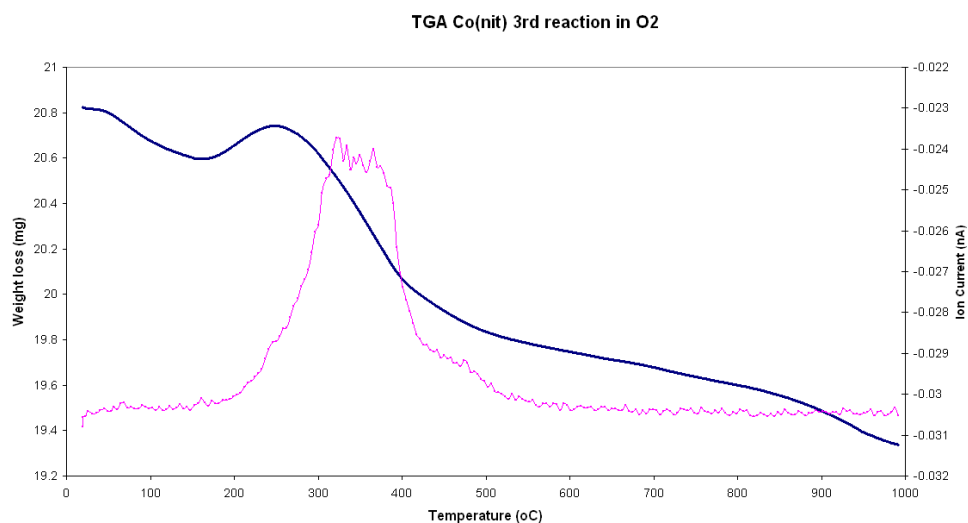


Figure 4-66 MS post reaction TGA (3rd reaction) catalyst under oxygen gas

To determine as to whether carbon laydown had occurred on the surface of the gamma alumina packing material, a temperature programmed oxidation (TPO) was performed on a sample of the post reaction gamma alumina packing material. Any carbonaceous species deposited on the surface of the catalyst would be removed in the form of CO₂.

The graph, Figure 4-67, shows there was a small weight loss at 66°C and the main weight loss occurred over a broad temperature range between 210°C-680°C. From the weight loss curve it was calculated that the weight loss of the alumina was ~8.3%. Graph, Figure 4-68, shows that CO₂ evolution occurred over a broad temperature range with two maxima at 287°C and 436°C. A DSC trace showed that the evolution was exothermic, confirming that the burn off of carbonaceous species was likely.

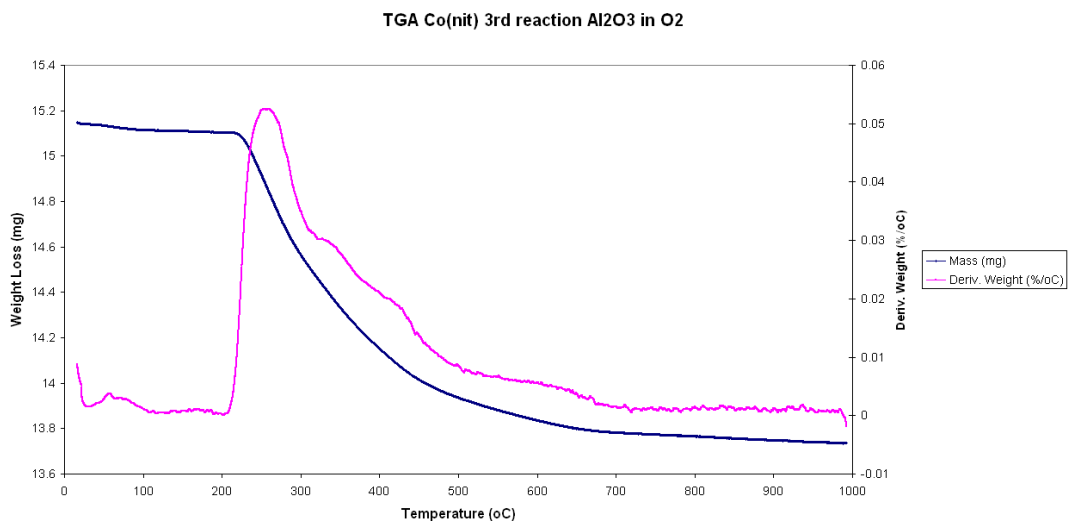


Figure 4-67 Post reaction TGA (3rd reaction) Al₂O₃ under oxygen gas

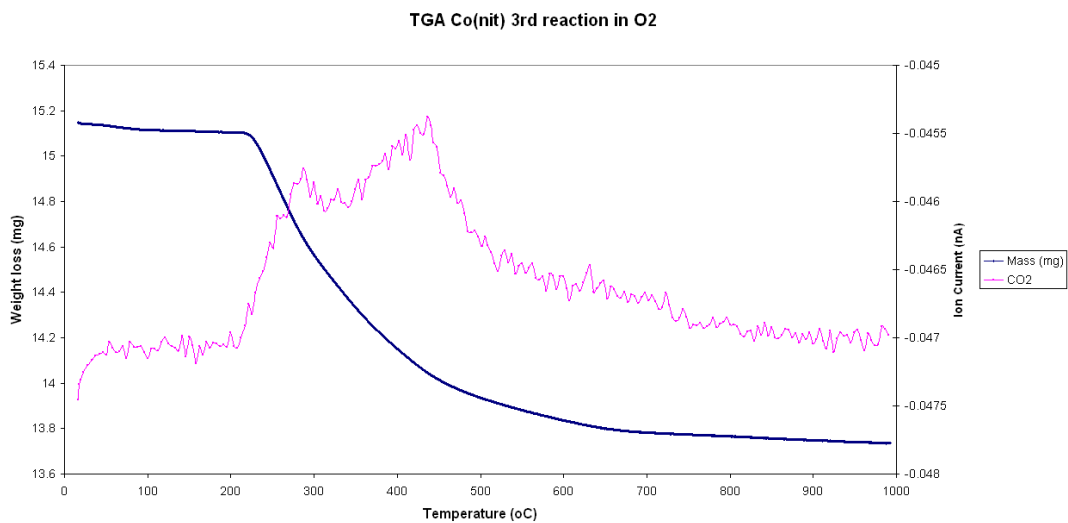


Figure 4-68 MS post reaction TGA (3rd reaction) Al₂O₃ under oxygen gas

4.2 Cobalt/alumina catalyst prepared via High Dispersion Cobalt (HDC) catalyst method

4.2.1 Characterisation

4.2.1.1 Thermo-gravimetric Analysis (TGA)

TGA analysis in oxygen

Usually the temperature at which to calcine and activate the catalyst needs to be determined and for this you can use TGA. However, as this was an industrial catalyst produced at Johnson Matthey, they had already determined the calcination temperature of the catalyst to be 105°C.

From the weight and derivative weight profiles, shown in Figure 4-69, it appeared that calcination of the catalyst at 105°C does not fully decompose the nitrate precursor. The decomposition of cobalt nitrate has been investigated previously [110] and shows a similar decomposition profile to that shown in Fig 4-69. The cobalt nitrate decomposition in oxygen mainly occurs as several broad events at 90°C, 218°C, 320°C, and a high temperature weight loss at 677°C. From the heat flow data, Figure 4-70, it can be seen that the weight loss occurs as a very broad exothermic event, which suggests the nitrate precursor, was breaking down to form the oxide.

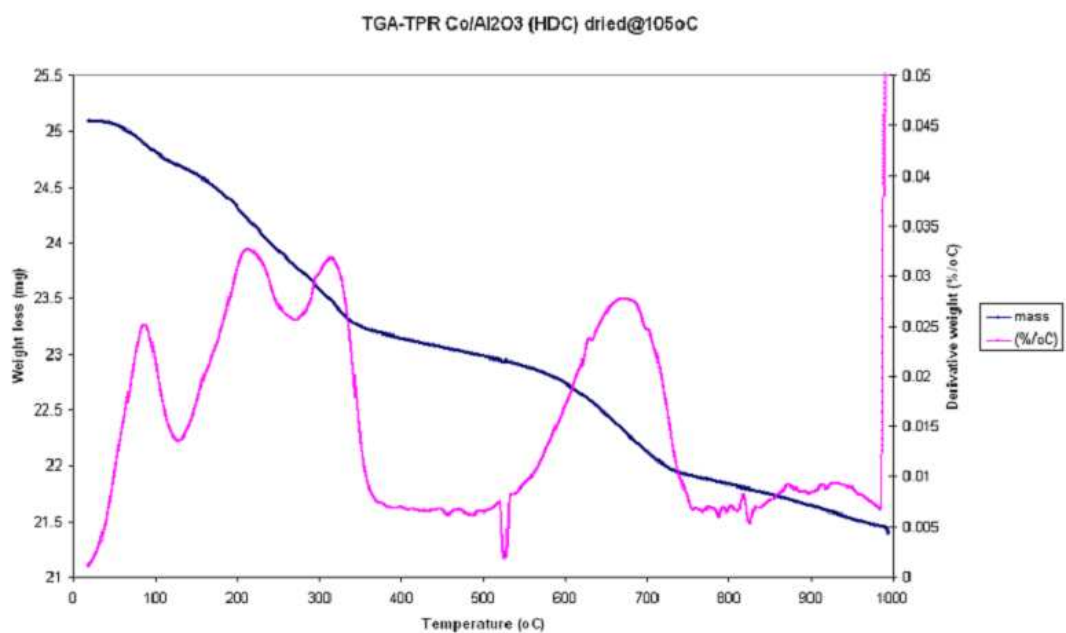


Figure 4-69 TGA analysis (weight loss/derivative weight vs temperature) of Co/Al₂O₃ (HDC) catalyst under 2%O₂/Ar feed

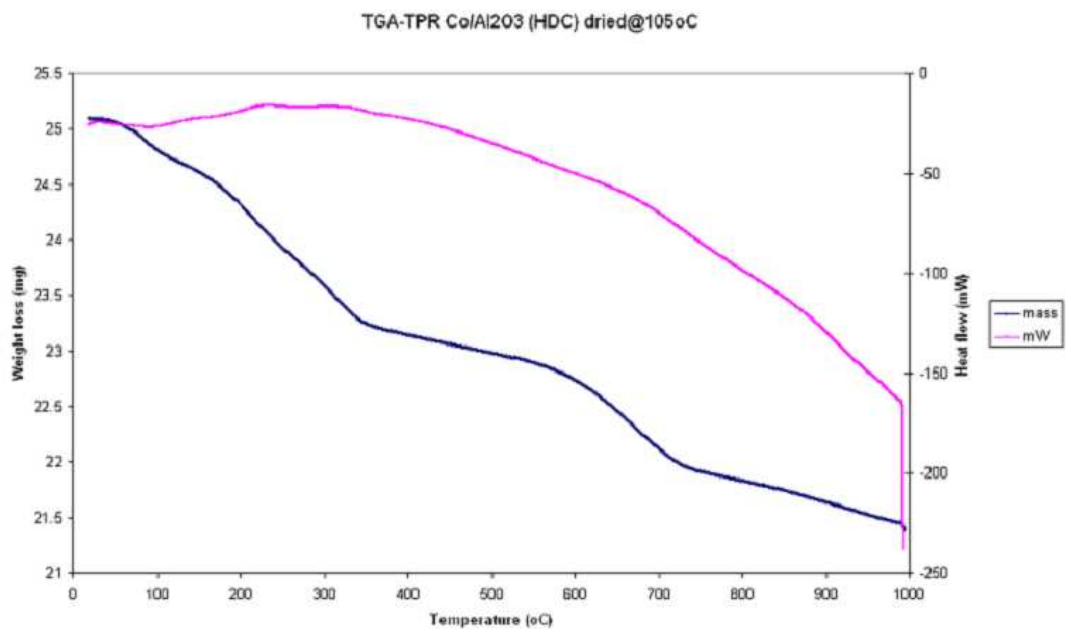


Figure 4-70 TGA analysis (weight loss/heat flow vs temperature) of Co/Al₂O₃ (HDC) catalyst under 2%O₂/Ar feed

TGA analysis in hydrogen

The graph below shows the weight loss and derivative weight profile for the Co/Al₂O₃ (HDC) catalyst under a reducing atmosphere. From Figure 4-71, it can be seen that the weight loss occurs over four events at 88°C, 212°C, 318°C and 679°C.

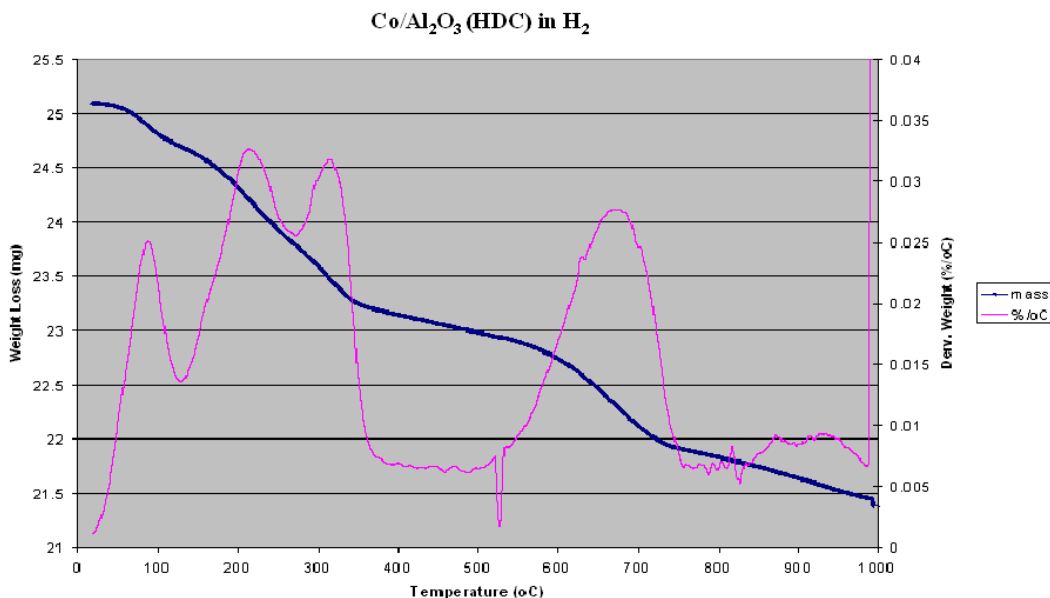


Figure 4-71 TGA analysis (weight loss/derivative weight vs temperature) of Co/Al₂O₃ (HDC) catalyst under 5%H₂/N₂ feed

Mass spectrometry data, Figure 4-72, showed that the weight losses at 88°C, 212°C, 318°C and 679°C correspond to the loss of water and the peak at 88°C represents physisorbed water on the catalyst surface. The uptake of hydrogen shown by Figure 4-73, occurred at 232°C, 321°C, and 675°C and correspond with the three later evolutions of water. The uptake of H₂ and release of H₂O however is most likely due to the reduction of the cobalt oxide. Like the cobalt/alumina (nitrate) catalyst, an evolution of nitric oxide occurred at 214°C, Figure 4-74, indicating that not all of the nitrate precursor had been converted to the oxide in the calcination stage in agreement with the O₂ TGA. The catalyst was calcined at higher temperatures, 250°C, 300°C, 350°C, and 400°C to see if this increase in temperature would decompose all of the nitrate precursor. Similarly to the cobalt alumina (nitrate) catalyst, it was found that temperatures

of 350°C and above are needed to remove any nitrates still present and the higher the calcination temperature, the higher the temperature needed to reduce cobalt oxide.

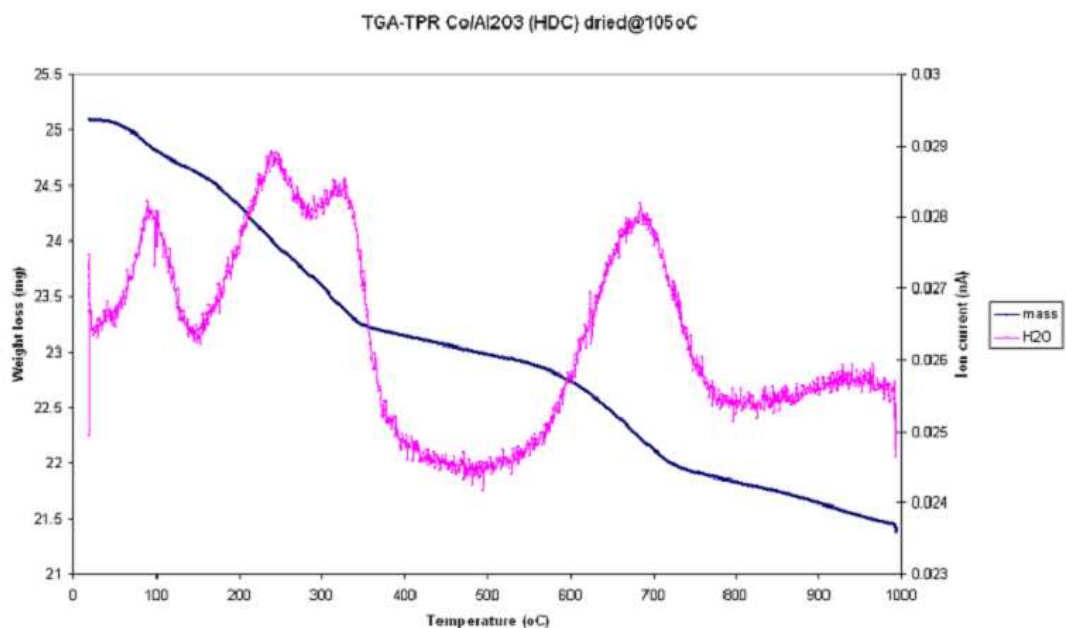


Figure 4-72 TGA analysis (evolution of water) of Co/Al₂O₃ (HDC) catalyst under 5%H₂/N₂ feed

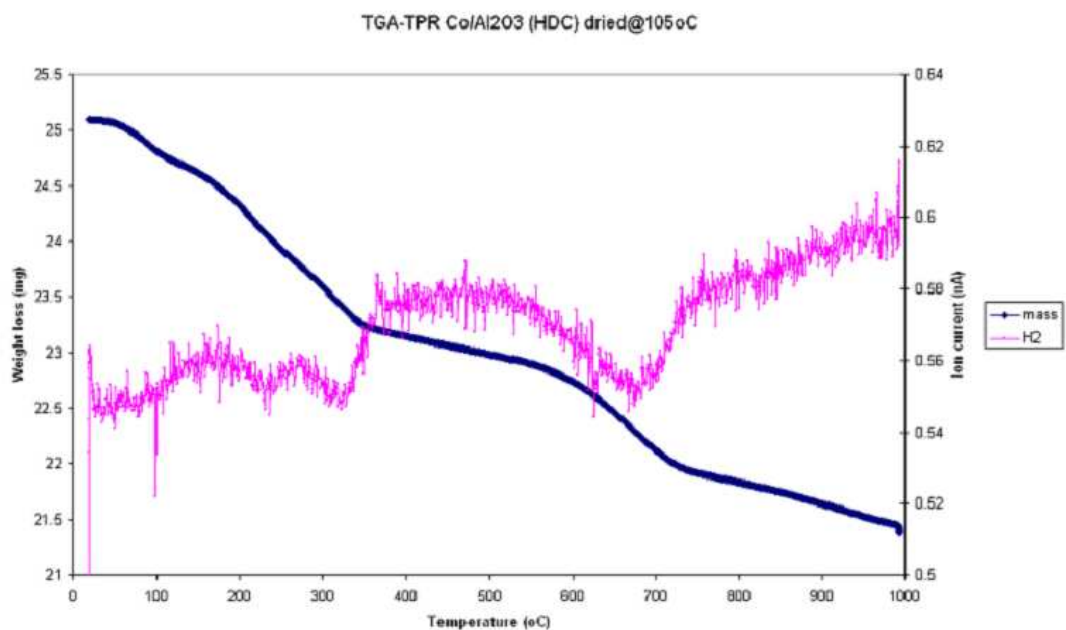


Figure 4-73 TGA analysis (uptake of hydrogen) of Co/Al₂O₃ (HDC) catalyst under 5%H₂/N₂ feed

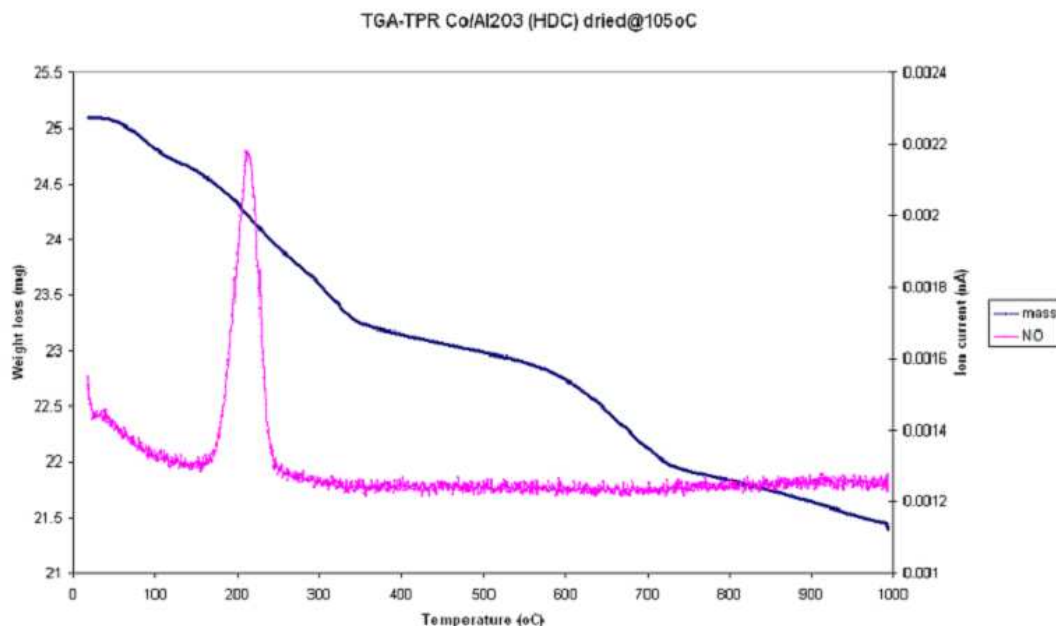


Figure 4-74 TGA analysis (evolution of NO) of Co/Al₂O₃ (HDC) catalyst under 5%H₂/N₂ feed

Studying the TGA data it can be seen that the peaks are reasonably broad which indicates the catalyst reduction is over a broad temperature range.

The graph below represents a TPR/TPD measurement of the Co/Al₂O₃ (HDC) catalyst. Adel Neale from Johnson Matthey carried out this procedure. It is widely acknowledged that reduction of unsupported cobalt oxide (Co₃O₄) occurs as a two stage process [111, 112] which can be ascribed to successive reduction of Co₃O₄ to CoO and then to Co [113, 114]. The first low temperature peak at 226°C corresponds to any nitrate precursor that is still present after calcination and this is in agreement with the TGA data showing the release of nitric oxide at 214°C. The second low temperature peak at 306°C represents Co₃O₄ being reduced to CoO and then to Co with the third peak at 614°C representing the final reduction CoO to Co metal and any alumina interaction species. The final broad high temperature peak at 845°C represents any cobalt aluminate which always occur with alumina supported cobalt catalysts [43]. These species are very difficult to reduce even at temperatures of >1000°C[43]. These peaks are in agreement with the derivative weight plot, Figure 4-72, and also with literature. Jacobs et al [25] and Bechara et al. [115] have typically assigned the reduction of surface Co₃O₄ phase (Co³⁺ to Co²⁺ to Co) between 260-450°C. The

high temperature peaks between 450-750°C are attributed to the reduction of cobalt oxide and alumina interaction species.

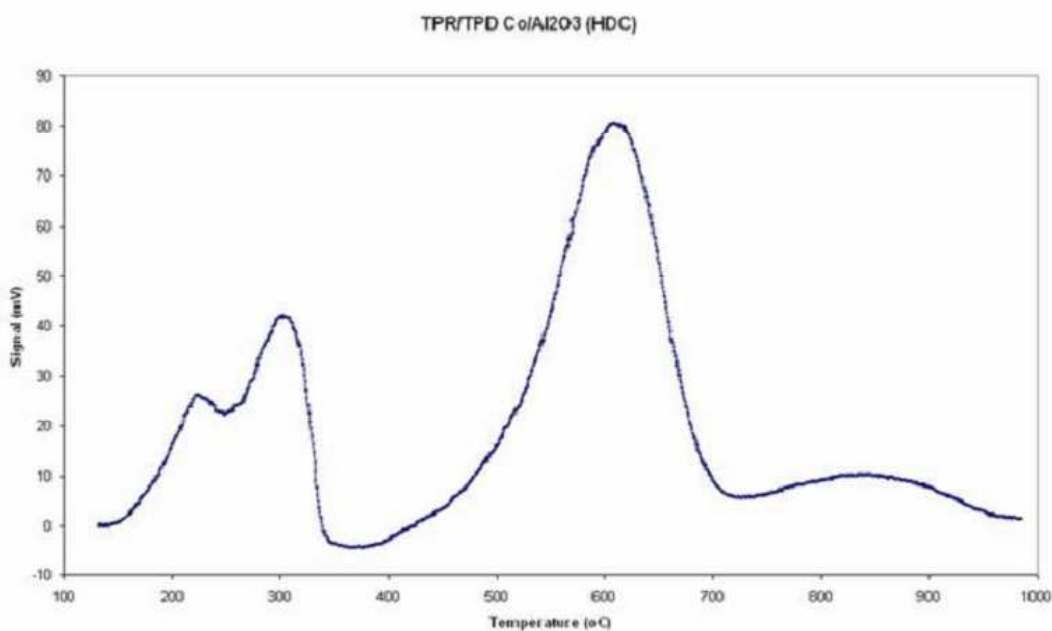


Figure 4-75 TGA measurement (TPR/TPD) of Co/Al₂O₃ (HDC) catalyst

4.2.1.2 BET Surface area analysis

The table below represents surface area analysis of Co/Al₂O₃ (HDC) catalyst. The analysis was carried out by the procedure covered in section two.

| Catalyst | Surface Area (m ² / g) | Pore Diameter (Å) | Pore Volume (cm ³ / g) |
|---|-----------------------------------|-------------------|-----------------------------------|
| Co/Al ₂ O ₃ (HDC) | 188 | 127 | 0.60 |

Table 4-7 Surface area analysis of lab prepared Co/Al₂O₃ (HDC) catalyst

From surface area analysis, it is shown that the cobalt/alumina (HDC) catalyst has a larger surface area, smaller pore diameter and slightly smaller pore volume compared with the cobalt alumina (nitrate) catalyst.

4.2.1.3 Hot stage powder X-ray diffraction (XRD)

X-ray diffraction can provide information regarding a materials crystal structure, degree of crystallinity and crystallite size. Although unable to determine the complete active phase of a catalyst, XRD can be used to gain information about materials with long range order. It is particularly useful for characterising materials with well ordered structures such as zeolites[116, 117]. Although materials such as alumina (the support for the catalysts) can be amorphous, XRD can still be used to gain information regarding the active species on the support if it exists in a crystalline phase.

Powder XRD was used to determine if any phase changes occurred upon reduction. Identification of the species present on the support was made by comparison with the Powder Diffraction Database[118]. The reduction of the samples took place inside the catalyst reactor using the conditions defined in the previous section. The graph below represents the XRD pattern for the calcined cobalt/alumina (HDC) catalyst. It can be seen that the crystalline phases present are Co_3O_4 and gamma alumina support. The peak at 37 (2θ) represents Co_3O_4 spinel. The crystal size of this particle could not be calculated using the Scherrer equation as the XRD peak at 37 (2θ) was very broad and the sample was amorphous.

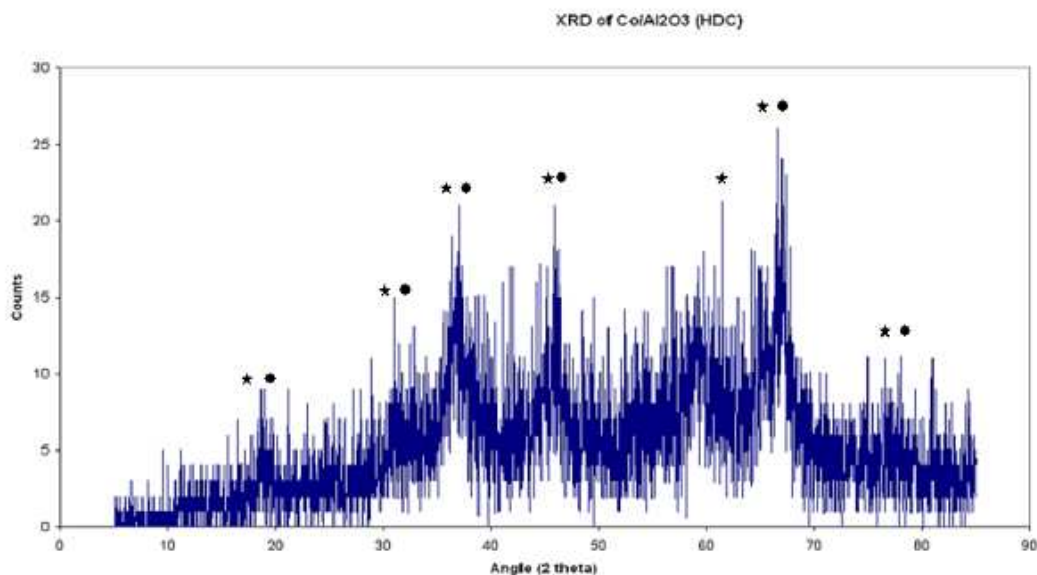


Figure 4-76 XRD graph of $\text{Co}/\text{Al}_2\text{O}_3$ (HDC)

Phases denoted are (★) Co_3O_4 and (●) $\gamma\text{-Al}_2\text{O}_3$

Figure 4-77 shows the hot-stage XRD pattern for cobalt alumina (HDC) catalyst under reducing conditions. The reduction of the sample took place *in-situ* inside the XRD diffractometer using the conditions defined in the section two.

The graph below shows the reduction of Co_3O_4 (Co^{3+}) to CoO (Co^{2+}) to Co metal (Co^0). As the temperature increases, the cobalt oxide is being reduced to cobalt metal but even at 800°C there is still cobalt oxide present which is similar to cobalt alumina (nitrate) catalyst. Not all of the oxide is being reduced to metal. There is also CoAl_2O_4 (cobalt aluminate) spinel present, which is virtually irreducible even at high temperatures [43]. The peaks at higher temperatures are sharper than those at lower temperatures which indicates an increase in crystallinity upon reduction. The peak at 43 (2θ) at 800°C represents cobalt metal phase and the crystal size was calculated at $\sim 10\text{nm}$ using the Scherrer equation. The cobalt crystal size in this catalyst is slightly smaller than that of the cobalt nitrate catalyst and this is due to the preparation method.

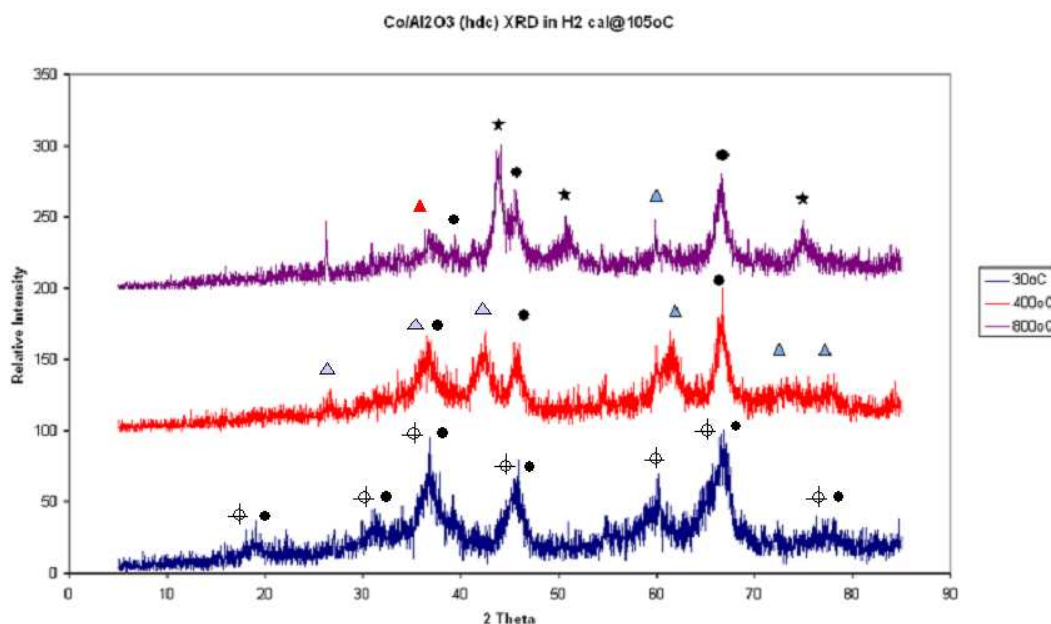


Figure 4-77 Hot-Stage XRD graph of $\text{Co}/\text{Al}_2\text{O}_3$ (HDC) under H_2

Phases denoted are (\star) Co , (\triangle) CoO , (\oplus) Co_3O_4 , (\blacktriangle) $\text{Co}/\text{Al}_2\text{O}_4$ and (\bullet) Al_2O_3

4.2.1.4 TPR-UV-vis-NIR spectroscopy

The graph below represents the UV-spectrum of cobalt/alumina (HDC) catalyst under reducing conditions at different temperatures. At 335°C we get an absorption band starting at 510nm which is attributed to a ${}^4T_{1g}(F) \longrightarrow {}^4T_{1g}(P)$ transition in octahedral high-spin Co^{2+} complexes [119]. This corresponds with the TPR/TRP graph, Figure 4-75, which shows Co^{3+} being reduced to Co^{2+} in that temperature region.

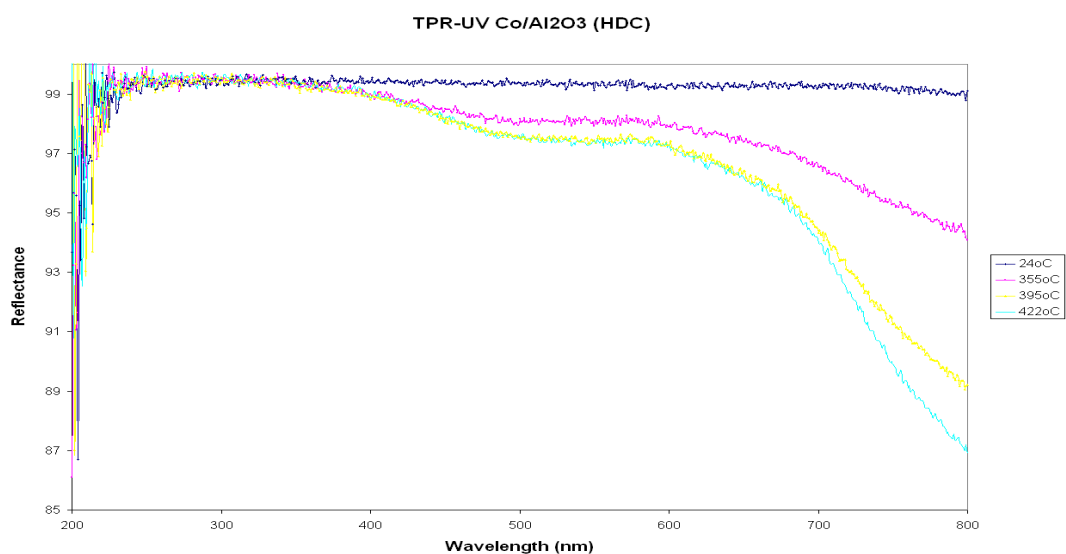


Figure 4-78 TPR-UV-vis-NIR spectroscopy graph of Co/Al_2O_3 (HDC) under H_2

4.2.1.5 Transmission Electron Microscopy (TEM)

Figure 4-79 represents a TEM image of the calcined Co/Al_2O_3 (HDC) catalyst. In literature there has been a number of studies using TEM on silica and titania supported cobalt catalysts [120-123] but not as much on alumina supported cobalt catalysts. It has been found that with an increase in metal loading there is an increase in aggregation of cobalt oxide clusters and the cobalt species are not homogeneously distributed on silica support [123]. They appear as near spherical aggregates of Co_3O_4 particles inside the pores and on the surface of the support. The aggregates can form different sizes from single Co_3O_4 particles to larger clusters [123]. The dark areas in Figure 4-79 represent Co_3O_4 particles or clusters with the lighter areas representing alumina support. From the image it can be seen that the structure consists mostly of clusters of cobalt oxide (Co_3O_4)

on the alumina support with some smaller clusters or single particles. The size of cobalt clusters or particles range from roughly 10-20nm to larger clusters of 100nm in diameter.

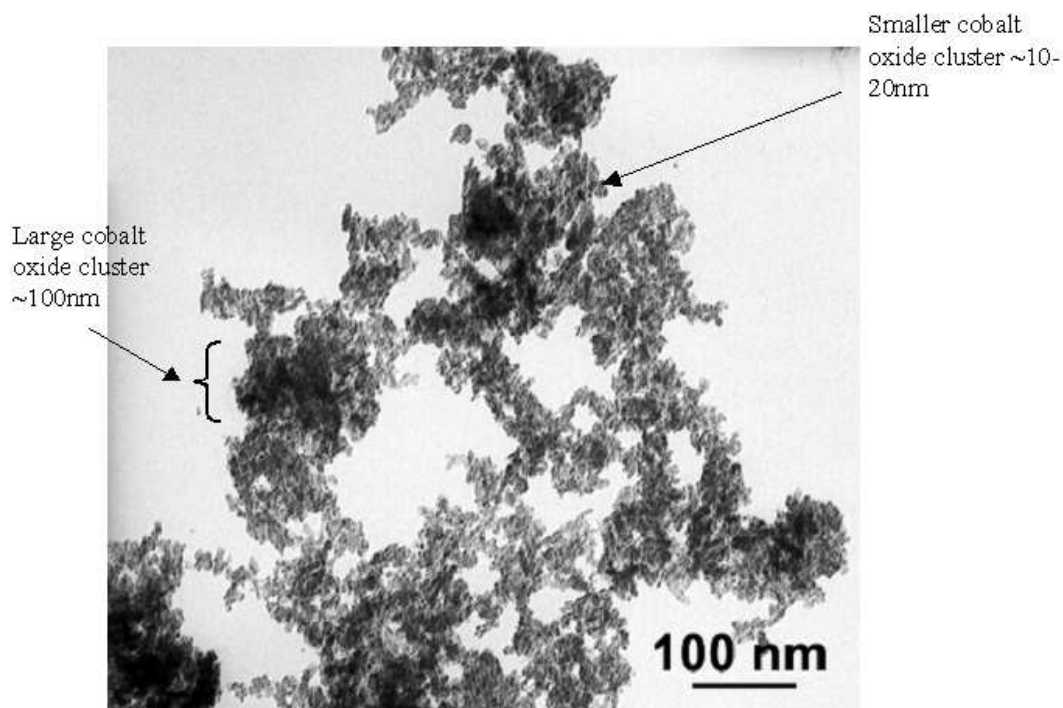


Figure 4-79 TEM image for Co/Al₂O₃ (HDC) catalyst

4.2.2 Reaction at 210°C

The FT activity of this catalyst was investigated at 210°C using the following conditions:

| | |
|------------------------------------|----------------------|
| • Reaction Temperature (°C) | 210 |
| • Pressure (barg) | 20 |
| • Gas Flow (ml min ⁻¹) | 45.20 |
| • Catalyst Volume (ml) | 0.5424 |
| • Catalyst weight (g) | 0.4018 |
| • GHSV (hr ⁻¹) | ~5,000 |
| • Residence time | 0.72 s ⁻¹ |

The synthesis feed gas composition employed was $30.62 \text{ ml min}^{-1} \text{ H}_2$ and $14.58 \text{ ml min}^{-1} \text{ CO}$. This equated to a molar ratio of 2.1:1 $\text{H}_2:\text{CO}$ which was ideal for FTS.

Prior to reaction, the catalyst was reduced *in situ* in the reactor under $45.20 \text{ ml min}^{-1}$ flowing hydrogen using the reduction conditions stated earlier in section two. Once the reduction programme was complete the catalyst was brought on-line very slowly and gently, as this F-T catalyst is easily damaged if brought on-line too harshly.

The graph below represents carbon monoxide conversion over 480hrs TOS. The conversion dropped from ~20% to ~12% in this time period and clear deactivation has occurred however the reaction has not reached steady state yet. The deactivation profile suggests linear decay has taken place. The 1st order deactivation constant was calculated over this time period as 0.0011 hr^{-1} .

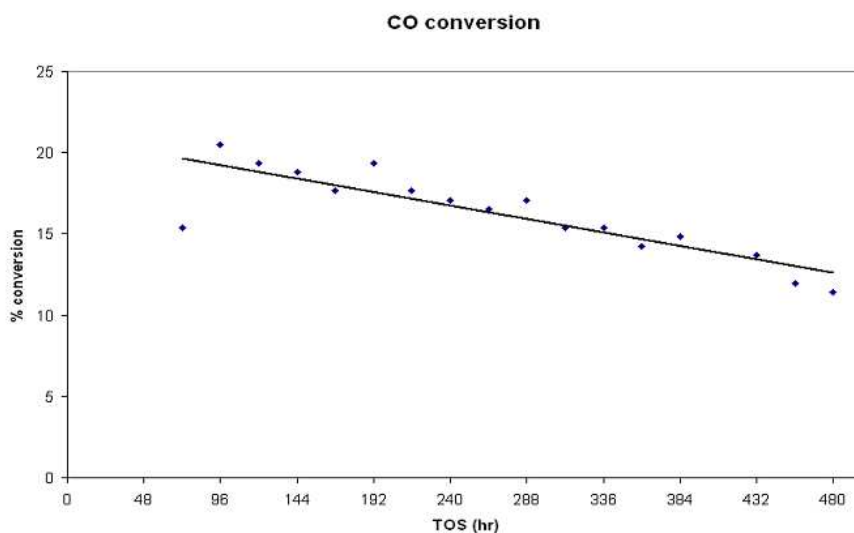


Figure 4-80 Conversion of reaction at 210°C

The graph below represents the number moles in the light organic phase, at 216 hrs TOS, of each hydrocarbon formed during the reaction. From the graph it can be seen that a broad range of hydrocarbons are formed and the selectivity peaks carbon numbers ten which is similar to $\text{Co}/\text{Al}_2\text{O}_3$ (nitrate) catalyst. As the reaction proceeds the volume of liquid organics produced decreases as expected from the deactivation profile.

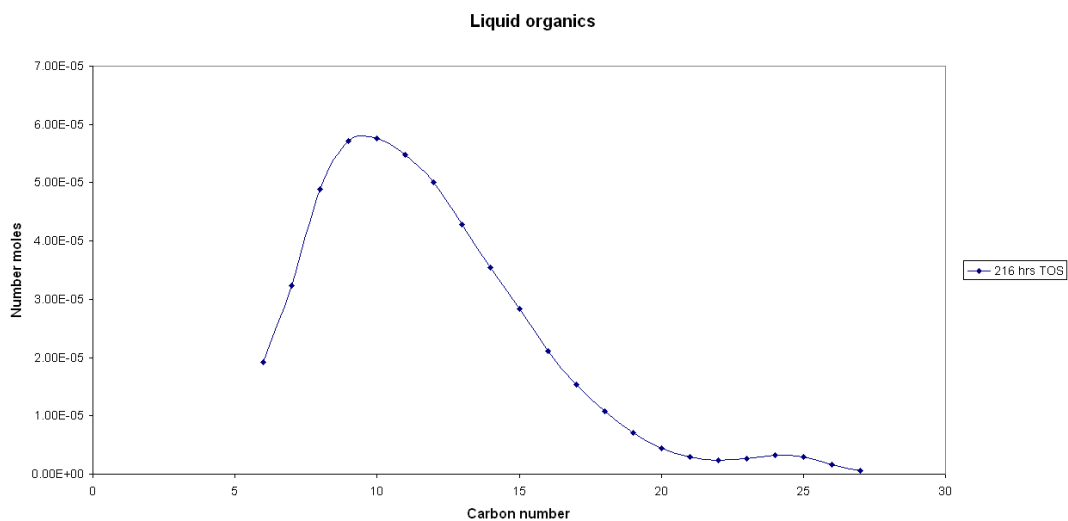


Figure 4-81 Moles of carbon products in liquid organic phase at 216 hrs TOS

The graph below represents the number moles in the wax phase, at 216 hrs TOS, of each hydrocarbon formed during the reaction. The wax phase contains an even broader range of hydrocarbons than in the light phase. The selectivity peaks at carbon number twenty-one which is a higher carbon number than with the light phase. Similarly to the light hydrocarbon phase, as the reaction proceeds the mass of heavy hydrocarbons produced decreases again supporting the deactivation profile.

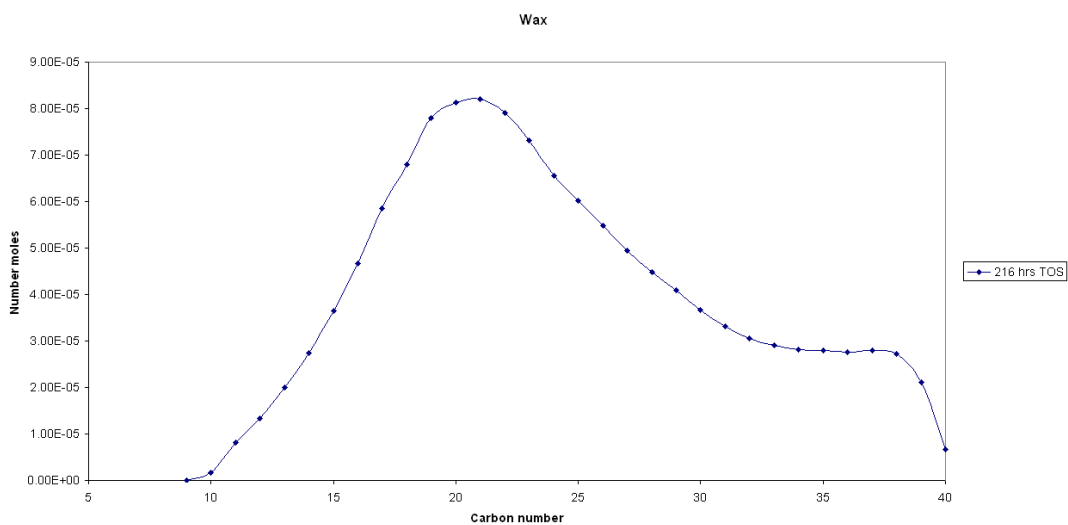


Figure 4-82 Moles of carbon products in wax phase at 216 hrs TOS

The graphs below represent the change in selectivity of the hydrocarbon products as TOS increases. It can be seen that as the reaction proceeds, the selectivity shifts slightly to higher carbon numbers.

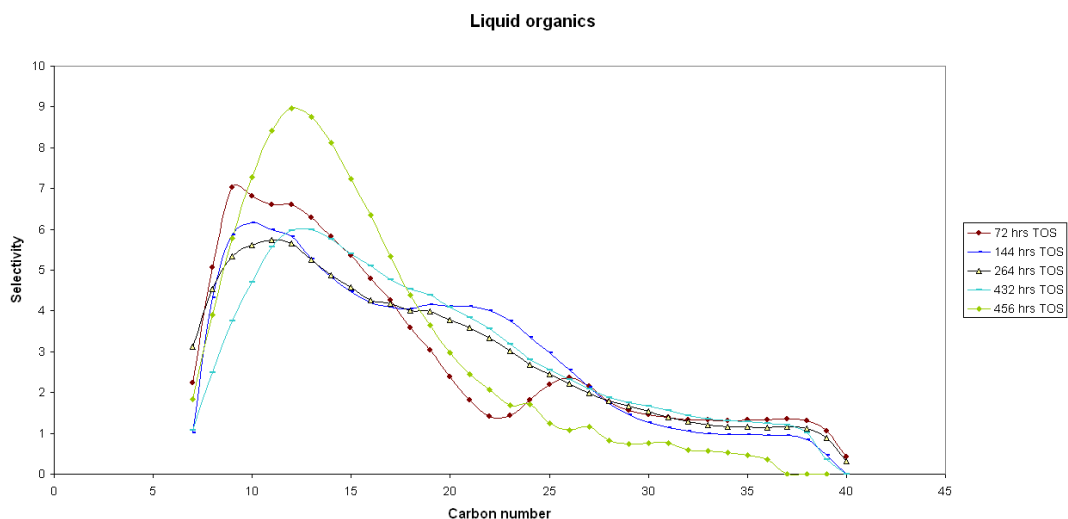


Figure 4-83 Selectivity over whole reaction

The graph below represents the Anderson-Shultz-Flory plot for the reaction at 210°C at 72 hrs TOS. The alpha value at 72 hrs TOS was calculated at 0.907 for carbon numbers 25-35. The overall average alpha value for the reaction at 210°C was 0.89 ± 0.02 (C25-35). The alpha value increased as TOS increased.

There is no statistical difference between the α value for the reactions involving both cobalt/alumina catalysts.

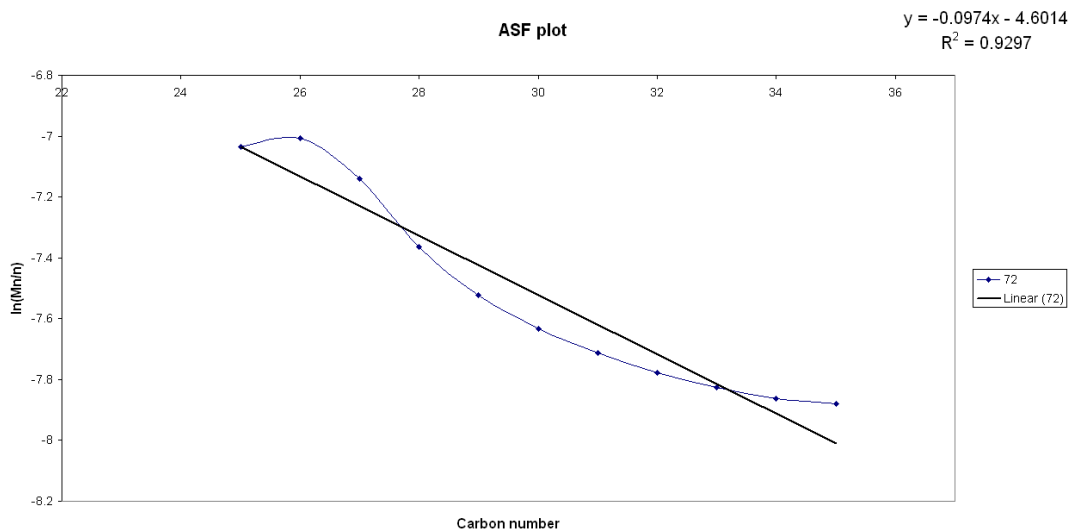


Figure 4-84 Typical ASF plot for Co(HDC) reaction at 210°C

4.2.2.1 Post reaction analysis

To get full post reaction analysis on the catalysts it was decided not to use the online mass spectrometer for temperature-programme-oxidations. If the mass spectrometer was used all of the catalyst samples would be fully oxidised online and this limited any other post reaction analysis to be carried out.

The graphs below, Figures 4-85 and 4-86, represent soxhlet analysis of the post-reaction catalyst and gamma alumina. From the graphs it can be seen that a broad range of hydrocarbons are deposited on both these materials with selectivity towards higher molecular weight hydrocarbons. Although not shown below, both materials contain hydrocarbons of C40+ with the gamma alumina containing heavier molecular weight hydrocarbons than the catalyst.

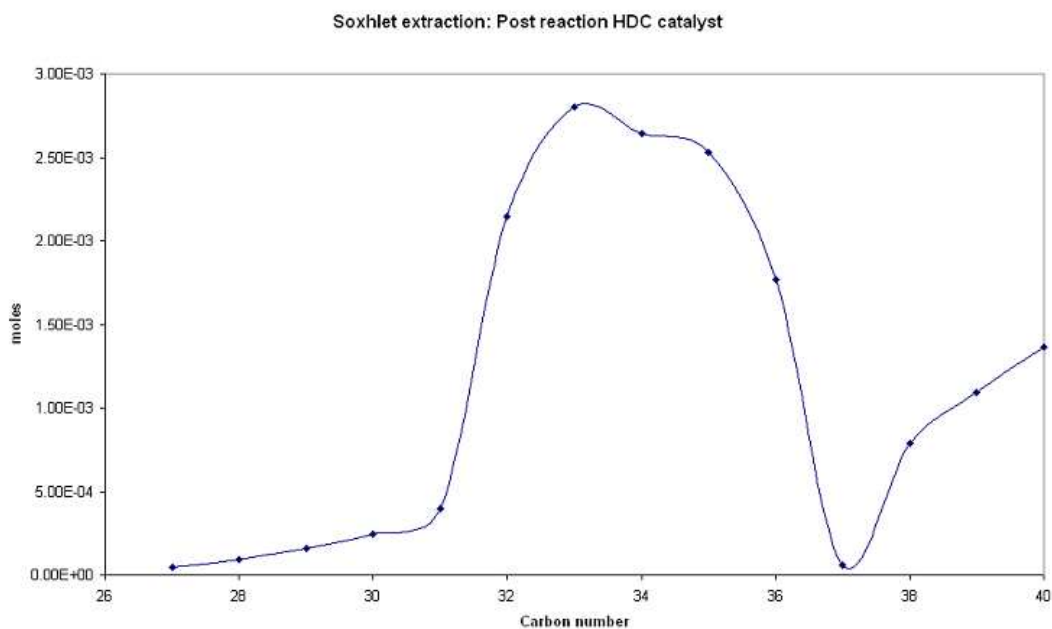


Figure 4-85 Soxhlet results post reaction on a sample of catalyst

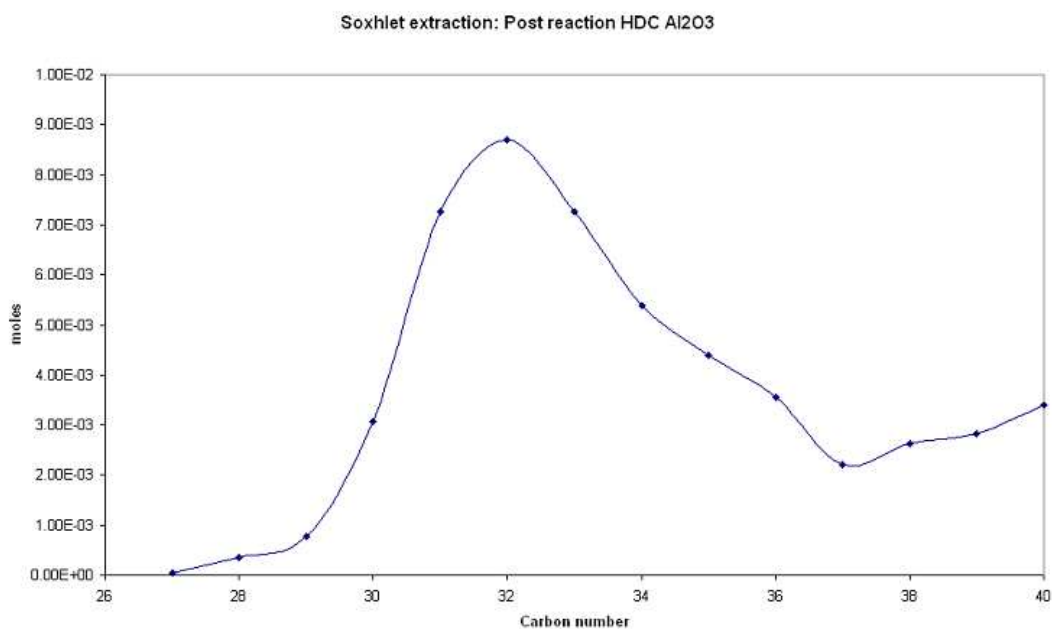


Figure 4-86 Soxhlet results post reaction on a sample of alumina support

To determine as to whether carbon laydown had occurred on the surface of the catalyst, a temperature programmed oxidation (TPO) was performed on a sample of the post reaction catalyst. Any carbonaceous species deposited on the surface of the catalyst would be removed in the form of CO₂.

The graph, Figure 4-87, shows that the weight loss occurred over 3 distinct events: one broad peak between 35°C-200°C, and two further higher temperature peaks at 363°C and 477°C. From the weight loss curve it was calculated that the weight loss of the catalyst was ~35%. Graph, Figure 4-89, shows that CO₂ evolutions occur over two temperature ranges peaking at 379°C and 485°C. A DSC trace showed that the evolutions were exothermic, confirming that the burn off of carbonaceous species was likely.

Unlike the cobalt/alumina (nitrate) catalyst this cobalt/alumina (HDC) catalyst does not show any re-oxidation or increase in weight.

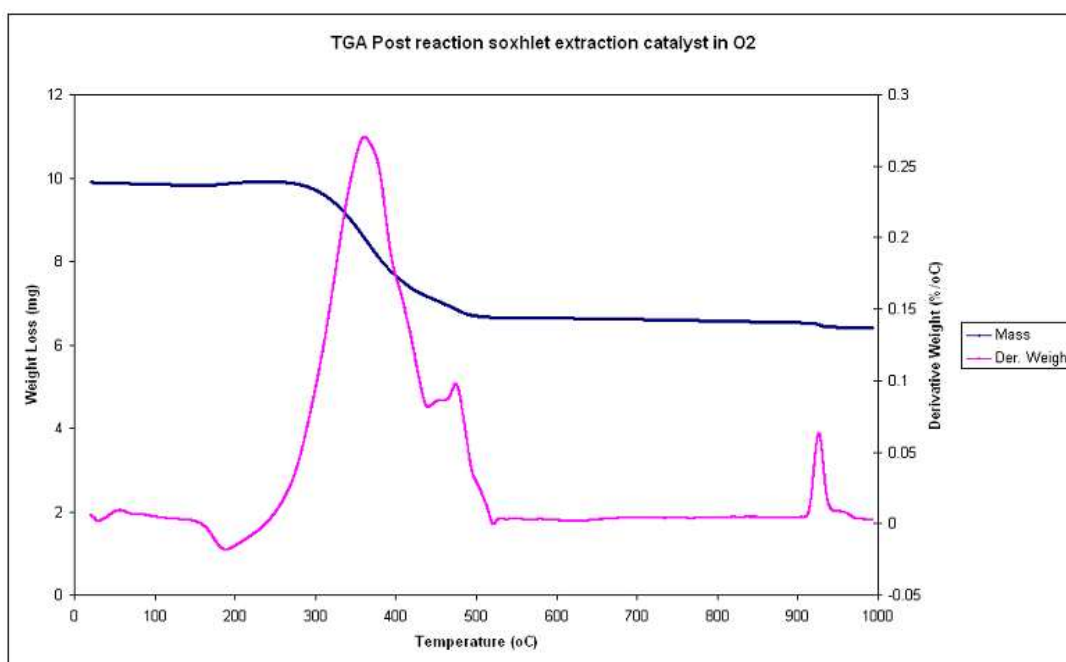


Figure 4-87 Post-reaction TGA on catalyst under oxygen gas

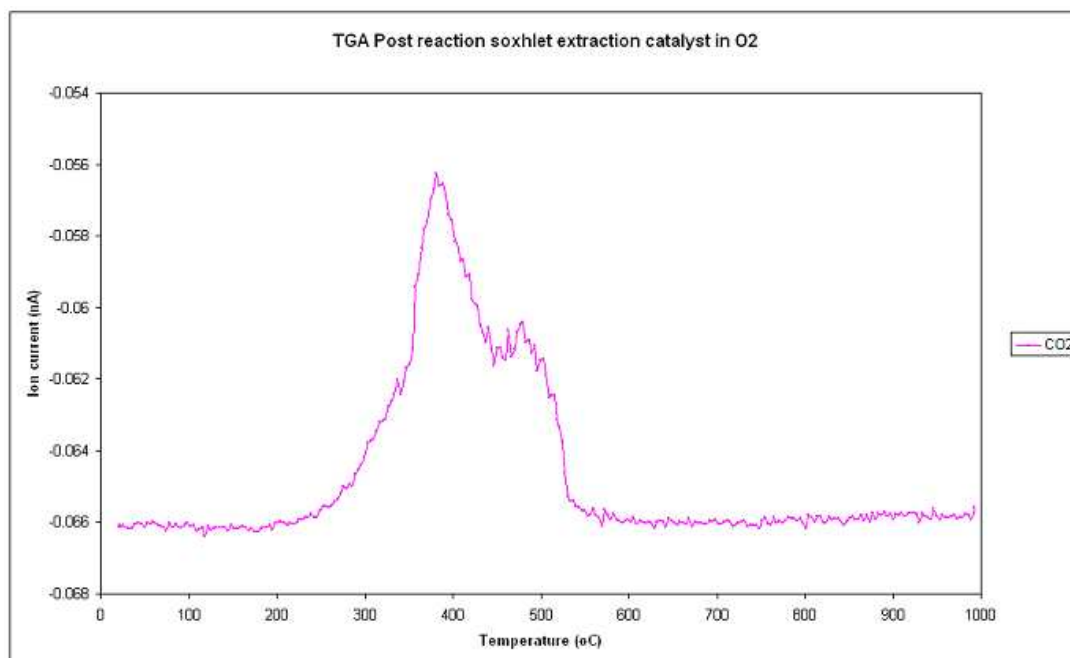


Figure 4-88 MS post-reaction TGA on catalyst under oxygen gas

To determine as to whether carbon laydown had occurred on the surface of the gamma alumina packing material, a temperature programmed oxidation (TPO) was performed on a sample of the post reaction gamma alumina packing material. Any carbonaceous species deposited on the surface of the catalyst would be removed in the form of CO₂.

The graph, Figure 4-89, shows that the main weight loss occurred over one broad temperature range between 250°C- 450°C with two small weight losses at higher temperatures between 470°C-580°C and 930°C. From the weight loss curve it was calculated that the weight loss of the alumina was ~39%. Graph, Figure 4-90, shows that CO₂ evolution occurred over a broad temperature range 250°C-580°C. A DSC trace showed that the evolution was exothermic, confirming that the burn off of carbonaceous species was likely.

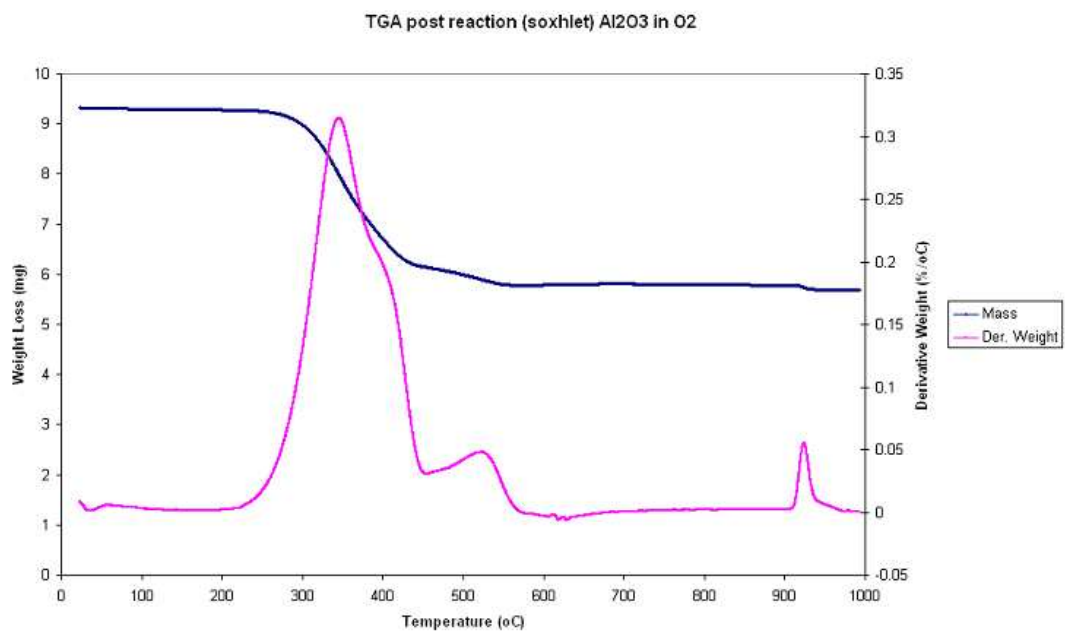


Figure 4-89 Post-reaction TGA on alumina support under oxygen gas

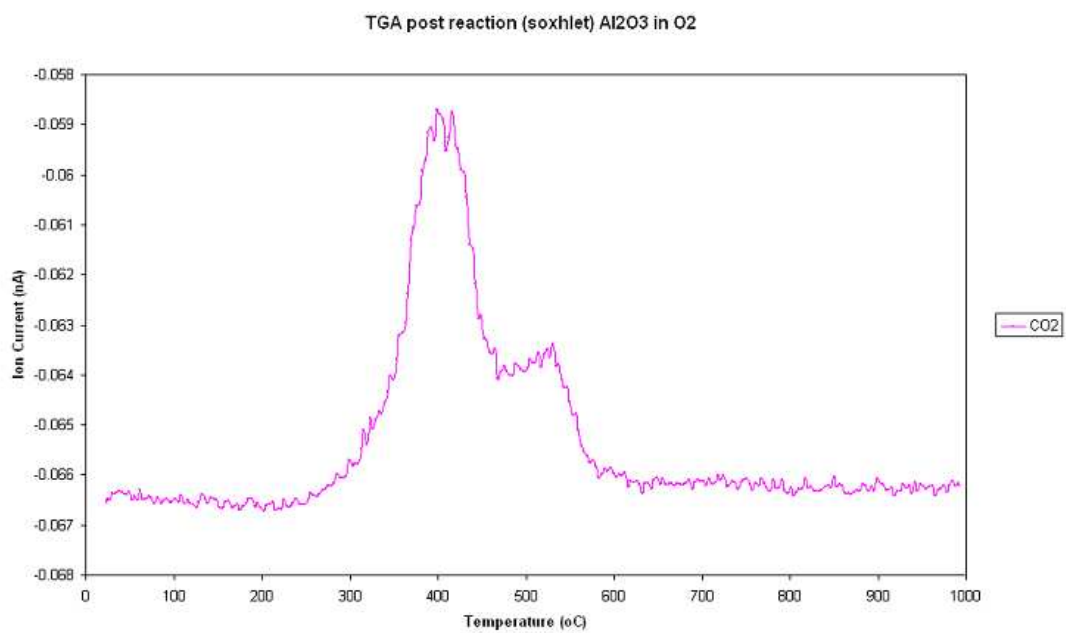


Figure 4-90 MS post-reaction TGA on alumina support under oxygen gas

4.2.3 Reaction with addition of octanol

The FT activity of this catalyst was investigated at 210°C with the addition of an octanol feed using the following conditions:

| | |
|------------------------------------|----------------------|
| • Reaction Temperature (°C) | 210 |
| • Pressure (barg) | 20 |
| • Gas Flow (ml min ⁻¹) | 45.60 |
| • Catalyst Volume (ml) | 0.5472 |
| • Catalyst weight (g) | 0.4053 |
| • GHSV (hr ⁻¹) | ~5,000 |
| • Residence time | 0.72 s ⁻¹ |
| • Octanol introduced | 0.02 ml / min |

The synthesis feed gas composition employed was 30.89ml min⁻¹ H₂ and 14.71ml min⁻¹ CO. This equated to a molar ratio of 2.1:1 H₂:CO which was ideal for FTS.

Prior to reaction, the catalyst was reduced *in situ* in the reactor under 45.60ml min⁻¹ flowing hydrogen using the reduction conditions stated earlier in section two. Once the reduction programme was complete the catalyst was brought on-line very slowly and gently, as this F-T catalyst is easily damaged if brought on-line too harshly. During the reaction octanol was co-fed into the reactor to investigate the effect this had on the reaction profile.

This reaction however, did not behave in a similar fashion to the 1st run at 210°C. Instead of a two-phase system (light organic and heavy organic phases) the reaction only produced a one-phase system. No heavy molecular weight hydrocarbons were collected in the 2nd knockout trap before the addition of octanol into the reactor and this observation was found on a previous experimental run.

4.2.3.1 Before octanol addition

The graph below represents carbon monoxide conversion before the addition of octanol. The conversion dropped from ~14% to ~5% in this time period compared with the drop of ~14%-12% with the 1st reaction at 210°C. Clear deactivation has occurred and the 1st order deactivation constant was calculated as 0.0014hr^{-1} which is comparable to the 1st reaction value of 0.0011hr^{-1} .

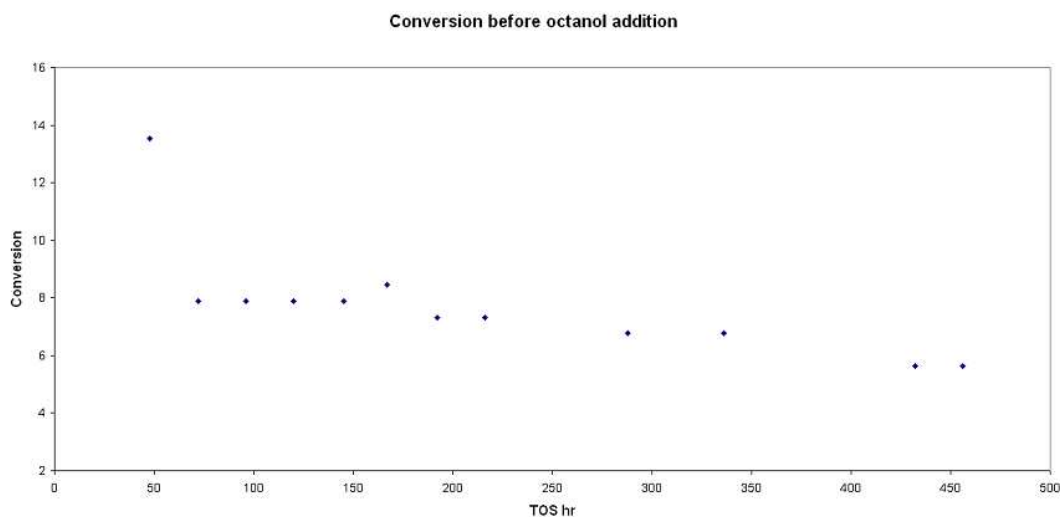


Figure 4-91 Conversion before octanol addition

The graph below represents the number moles in the light organic phase before octanol addition, at 288 hrs TOS, of each hydrocarbon formed during the reaction. From the graph it can be seen that a broad range of hydrocarbons are formed and the selectivity follows a similar profile to 1st reaction at 210°C. As the reaction proceeds the volume of liquid organics produced again decreases supporting the deactivation profile. The high C12 peak can be explained by residual dodecane still being present in the system from a previous run.

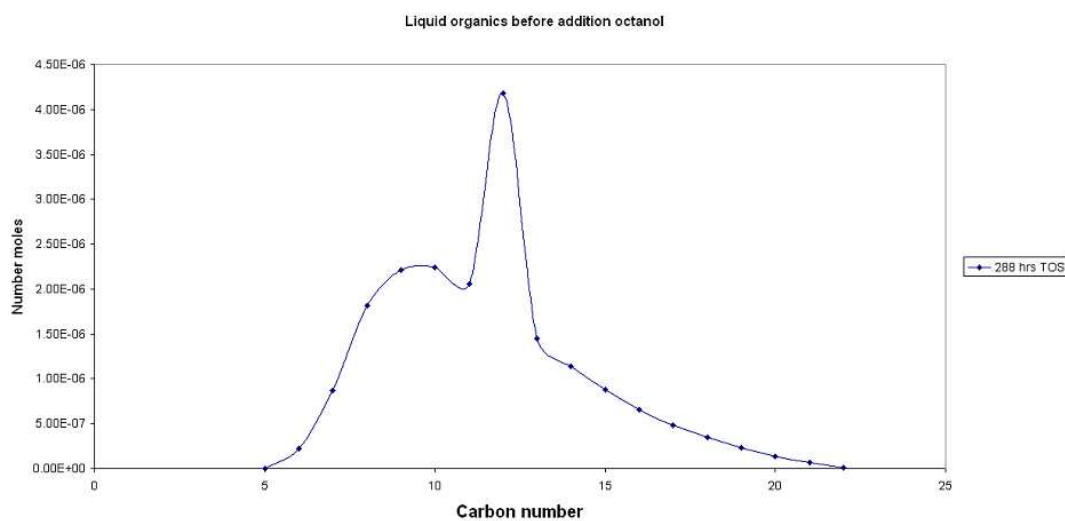


Figure 4-92 Moles of carbon products in liquid phase before octanol addition at 288 hrs TOS

The graph below represents the change in selectivity of the hydrocarbon products as TOS increases. It can be seen that as the reaction proceeds, the selectivity shifts slightly to higher carbon numbers. From the selectivity graph below it can be seen that C12 peak is large, as explained above, however, as TOS increases the concentration of dodecane decreases as it is being flushed from the reactor and this trend is seen in the graph below.

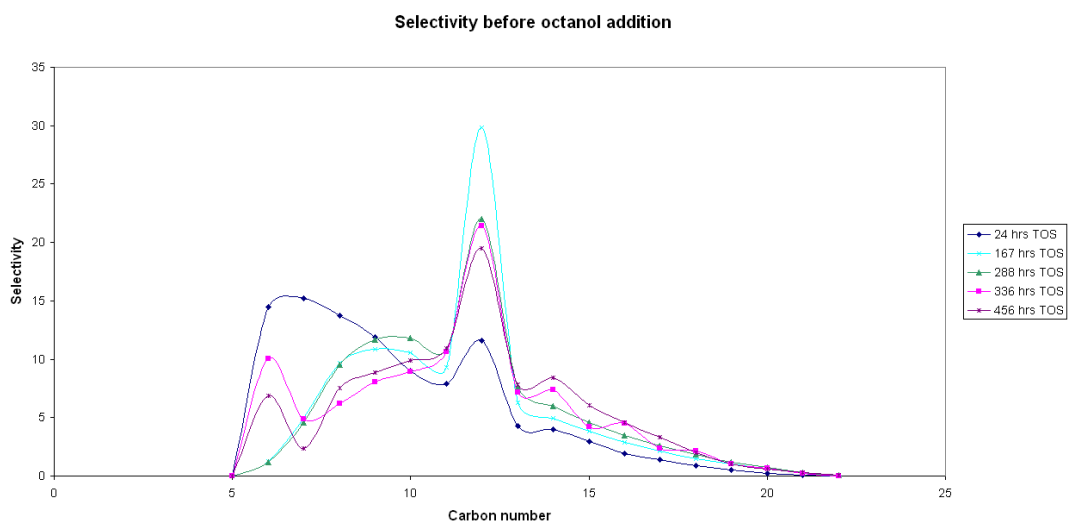


Figure 4-93 Change in selectivity before octanol addition

The graph below represents the Anderson-Shultz-Flory plot for the reaction at before octanol addition at 456 hrs TOS. The alpha value at 456 hrs TOS was calculated at 0.744 for a different set of carbon numbers than before (C10-C20). The alpha value increased as TOS increased. The overall average alpha value for the reaction before the introduction of octanol was 0.724 ± 0.02 (C10-20). This low alpha value was due to no heavy molecular weight hydrocarbons being seen in the 2nd knockout pot before octanol addition.

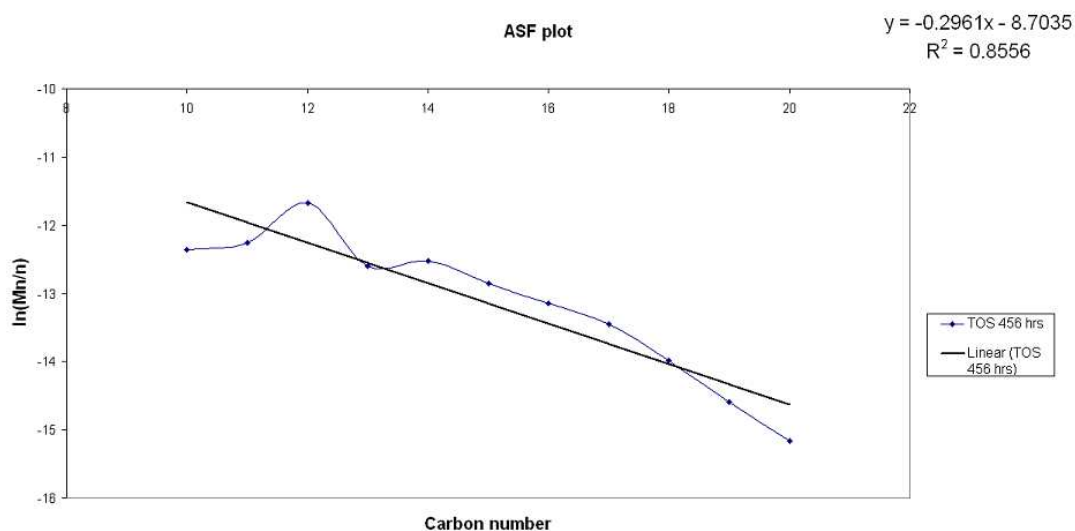


Figure 4-94 Typical ASF plot before addition of octanol

4.2.3.2 During octanol addition

After introduction of octanol into the system, the light organic phase samples became very frothy and resembled an emulsifier. The result of this was that no conversion or deactivation constant could be calculated for this section of the reaction because the light organic and aqueous phases seemed to be mixed together, thus no volume of water could be measured.

On testing the liquid samples that were collected in the light organic phase trap, it was seen that linear hydrocarbons were still being produced. These hydrocarbons were dissolved in the unreacted octanol that was exiting the reactor.

The graph below represents the number moles, in the light phase during octanol addition at 480 hrs TOS, of each hydrocarbon formed during the reaction. From the graph it can be seen that a broad range of hydrocarbons are formed and the selectivity profile resembles that of the previous reaction at 210°C. The large peak at C12 can be explained by dodecane still present in the system from a previous reaction.

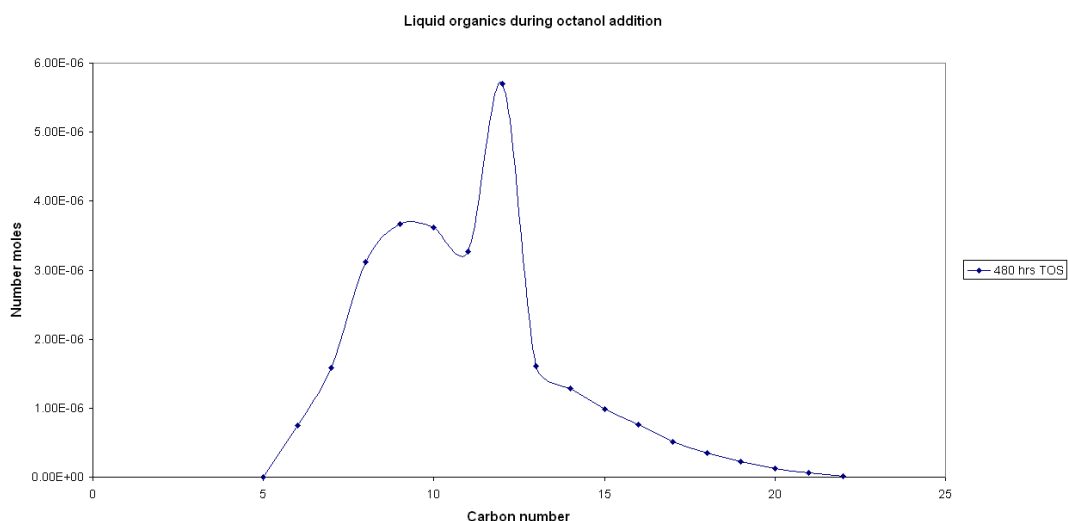


Figure 4-95 Moles of carbon products in liquid phase during octanol addition at 480 hrs TOS

The figure below represents the gas chromatogram trace for the light organic phase during octanol addition at 480 hrs TOS. From the trace it can be seen that

linear alkanes are still present but there are two very distinct large peaks that are apparent. The second large peak (C12-dodecane) disappears after 576hrs TOS. The large concentration of dodecane is residual dodecane present in the system from a previous run.

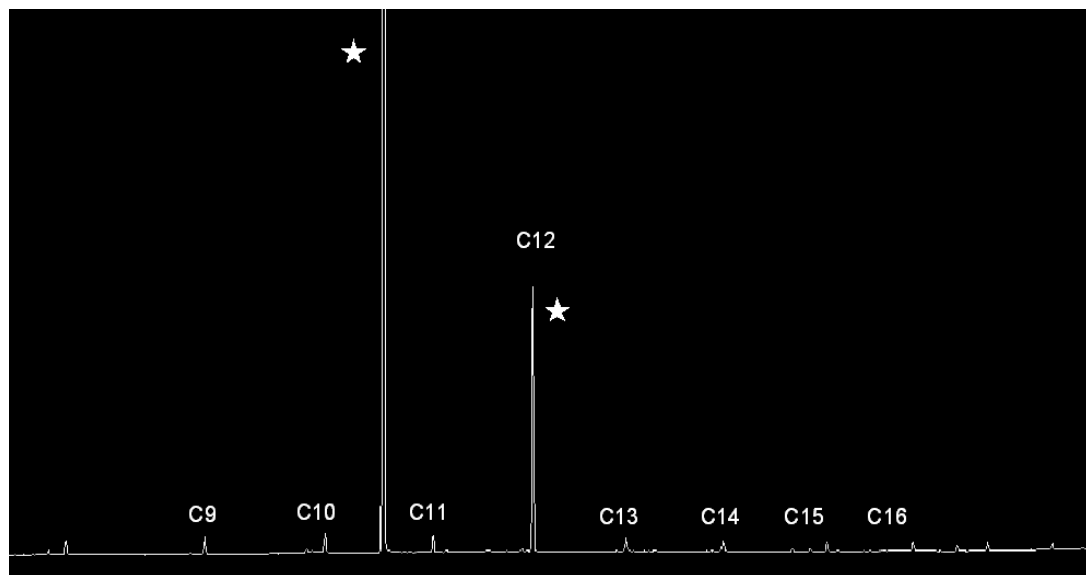


Figure 4-96 Typical chromatogram of light hydrocarons during octanol addition

The figure below represents the overlay of the gas chromatogram traces for the light organic phase during octanol addition and a mixture of C8, C10, C12, C14 and C16 alcohols. From the trace it can clearly be seen that the first peak represent octanol the second peak represents dodecane.

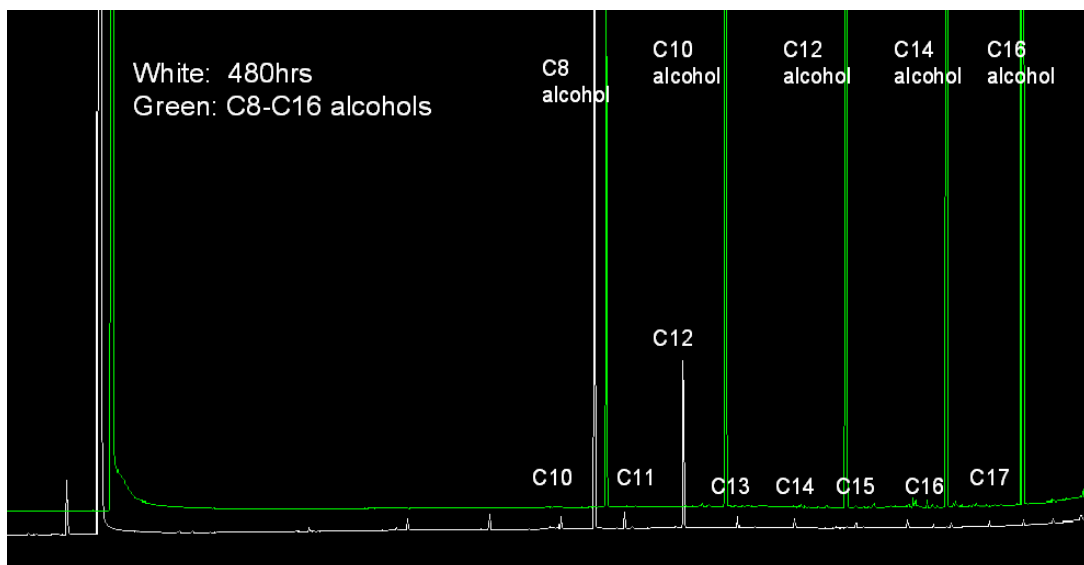


Figure 4-97 Overlay of chromatograms of light hydrocarbons during octanol addition and C8, C10, C12, C14 and C16 alcohol mix

The table below represents the quantification of octanol and dodecane within the light organic phase during octanol addition:

| TOS (hrs) | Moles of octanol | Moles of dodecane |
|-----------|------------------|-------------------|
| 480 | 8.82E-2 | 1.06E-2 |
| 505 | 9.31E-2 | 5.93E-3 |
| 528 | 9.78E-2 | 4.00E-3 |
| 552 | 1.01E-1 | 3.52E-3 |
| 576 | 1.10E-1 | 3.47E-3 |
| 600 | 1.09E-1 | 3.36E-3 |
| 624 | 1.04E-1 | 3.36E-3 |
| 648 | 9.51E-2 | 3.36E-3 |

Table 4-8 Quantification of moles of octanol and dodecane in light organic phase

The graph below represents the number moles, in the wax phase during octanol addition at 480 hrs TOS, of each hydrocarbon formed during the reaction. Again the wax phase contains a larger range of hydrocarbons than in the light phase. It is clear that a totally different profile is observed to the profile without octanol addition from the 1st reaction at 210°C.

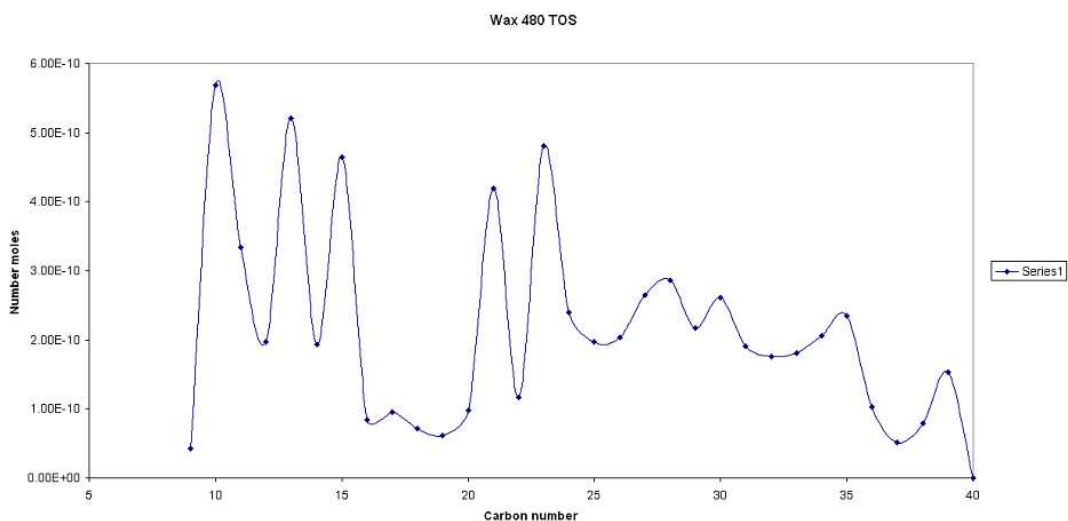


Figure 4-98 Moles of carbon products in wax phase during octanol addition at 480 hrs TOS

The figure below represents the gas chromatogram trace for the wax phase during octanol addition at 480 hrs TOS. From the trace it can be clearly seen that linear alkanes are still present but now there are three very distinct large peaks and two that were not present before the addition of octanol.

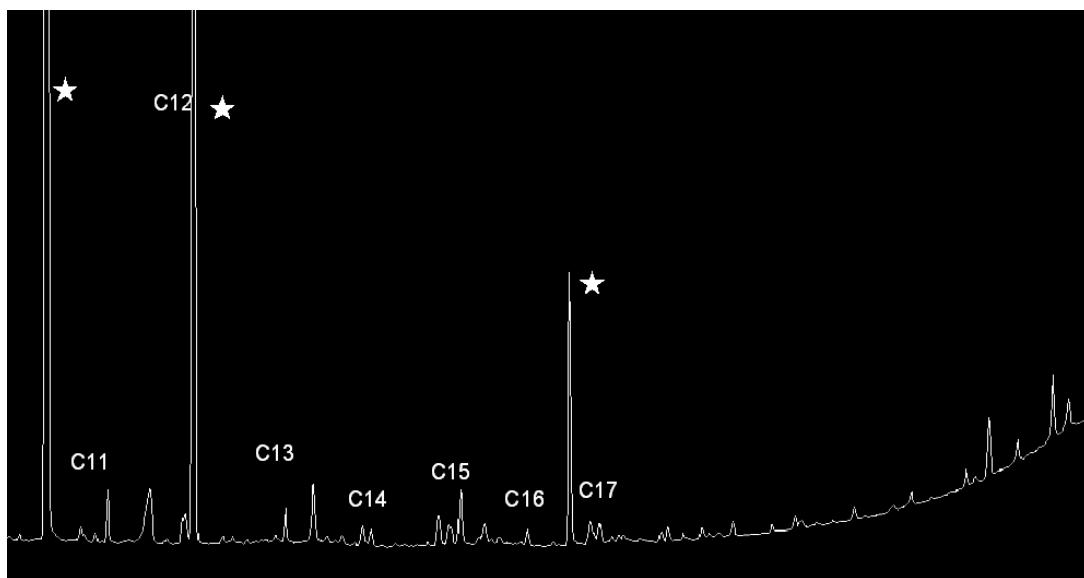


Figure 4-99 Typical chromatogram of heavy hydrocarbons during octanol addition

The figure below represents the overlay of the gas chromatogram traces for the wax phase during octanol addition and a mixture of C8, C10, C12, C14 and C16 alcohols. From the trace it can clearly be seen that the first peak represents

octanol with the last peak representing tetradecanol. The peak in the middle is dodecane and its presence has been described earlier.

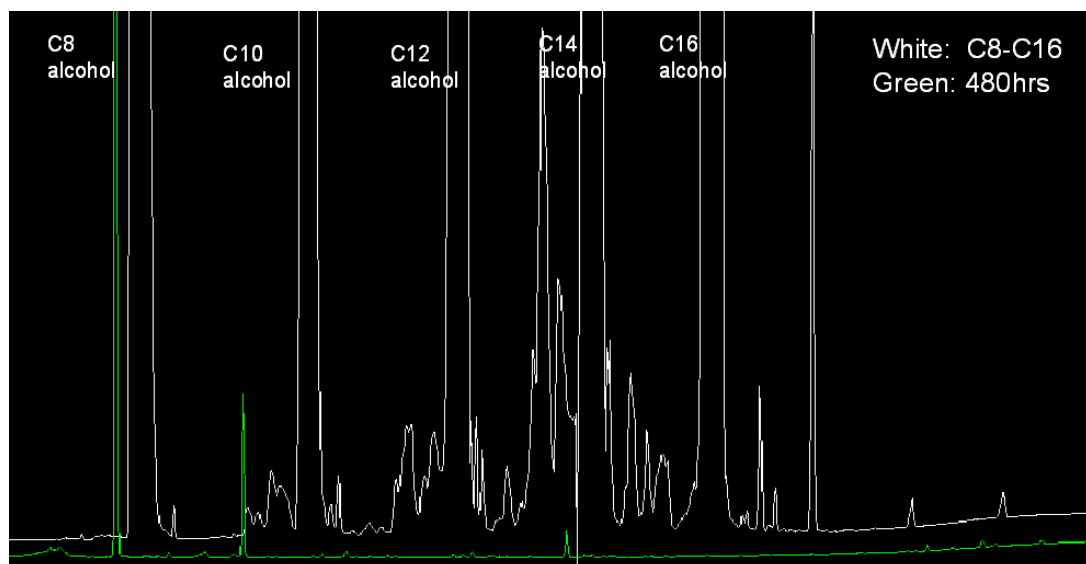


Figure 4-100 Overlay of chromatograms of heavy hydrocarbons during octanol addition and C8, C10, C12, C14 and C16 alcohols

The table below represents the quantification of octanol, dodecane and tetradecanol within the wax phase during octanol addition:

| TOS (hrs) | Moles of octanol | Moles of tetradecanol | Factor | |
|-----------|------------------|-----------------------|----------------------------------|-------------------|
| | | | between octanol and tetradecanol | Moles of dodecane |
| 480 | 4.54E-3 | 3.11E-5 | 145 | 2.55E-4 |
| 505 | 9.20E-3 | 1.26E-5 | 73 | 3.49E-5 |
| 528 | 7.32E-3 | 6.94E-5 | 105 | |
| 552 | 7.96E-3 | 4.17E-5 | 191 | |
| 576 | 7.27E-3 | 5.99E-5 | 121 | |
| 600 | 7.70E-3 | 9.98E-5 | 77 | |
| 624 | 8.38E-3 | 6.00E-5 | 140 | |
| 648 | 7.58E-3 | 5.57E-5 | 136 | |

Table 4-9 Quantification of moles of octanol, tetradecanol and dodecane in wax phase

The graph below represents the change in selectivity of the hydrocarbon products as TOS increases. It can be seen that as the reaction proceeds, the selectivity shifts slightly to higher carbon numbers.

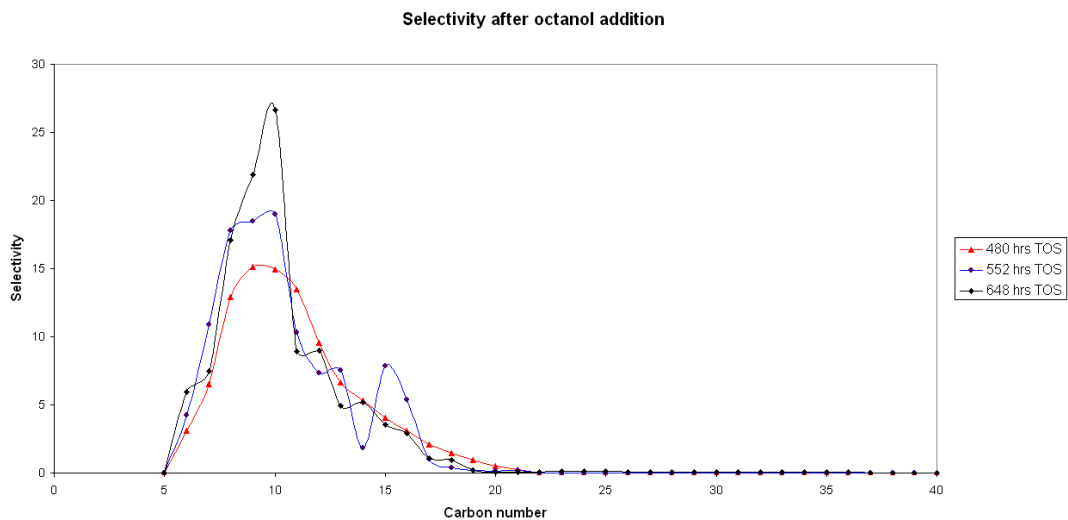


Figure 4-101 Change in selectivity during octanol addition

The graph below represents the Anderson-Shultz-Flory plot for the reaction during the addition of octanol at 600 hrs TOS. The alpha value at 600 hrs TOS was calculated at 0.953 for carbon numbers 25-35. The overall average alpha value for the reaction during octanol addition was 0.996 ± 0.02 (C25-35).

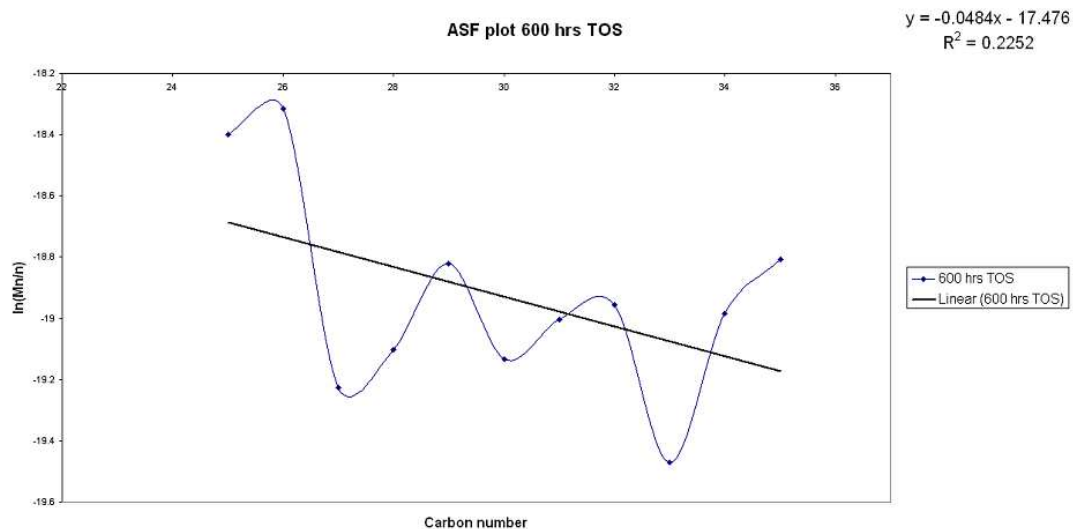


Figure 4-102 Typical ASF plot during addition of octanol

4.2.3.3 Post reaction analysis

The graphs below, Figures 4-103 and 4-104, represent soxhlet analysis of the post-reaction catalyst and gamma alumina. From the graphs it can be seen that a broad range of hydrocarbons are deposited on both these materials with selectivity towards higher molecular weight hydrocarbons.

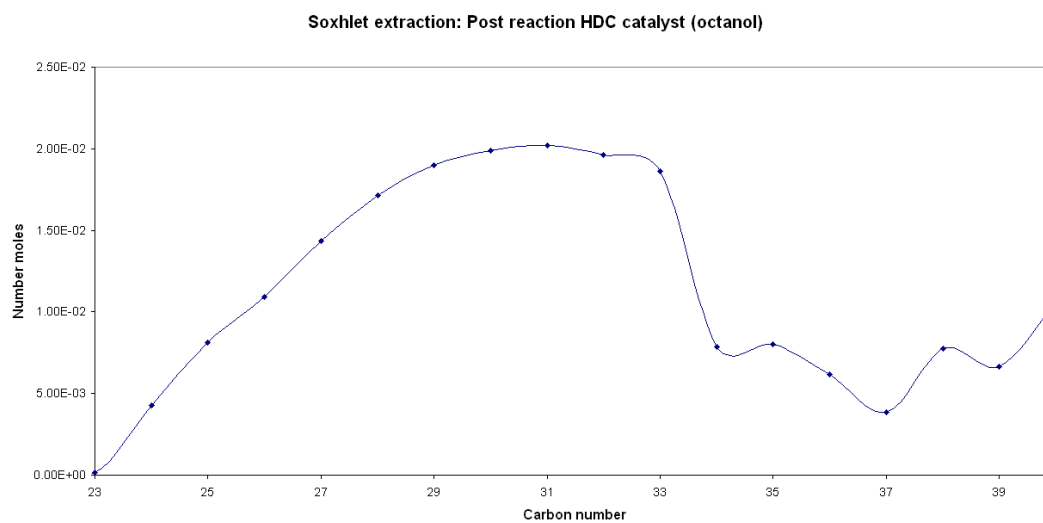


Figure 4-103 Soxhlet results post reaction on a sample of catalyst (octanol run)

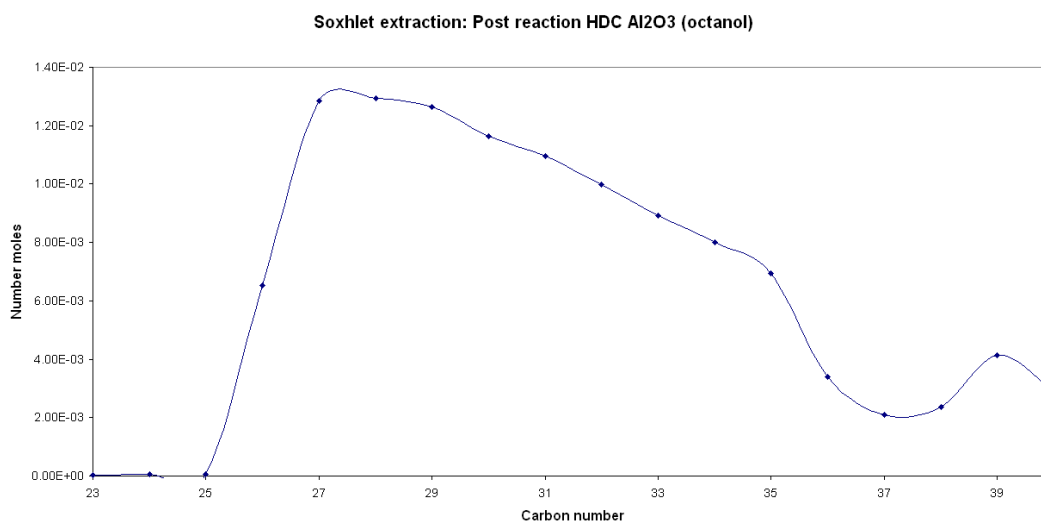


Figure 4-104 Soxhlet results post reaction on a sample of alumina (octanol run)

To determine as to whether carbon laydown had occurred on the surface of the catalyst, a temperature programmed oxidation (TPO) was performed on a sample of the post reaction catalyst. Any carbonaceous species deposited on the surface of the catalyst would be removed in the form of CO₂.

The graph, Figure 4-105, shows that the weight loss occurred over one broad peak between 210°C-360°C with two maxima at 303°C and 344°C. From the weight loss curve it was calculated that the weight loss of the catalyst was ~20.5%. Graph, Figure 4-106, shows that CO₂ evolution occurs over a broad temperature range of 200°C-590°C. A DSC trace showed that the evolution was exothermic, confirming that the burn off of carbonaceous species was likely.

Unlike the cobalt/alumina (nitrate) catalyst this cobalt/alumina (HDC) catalyst does not show any re-oxidation or increase in weight.

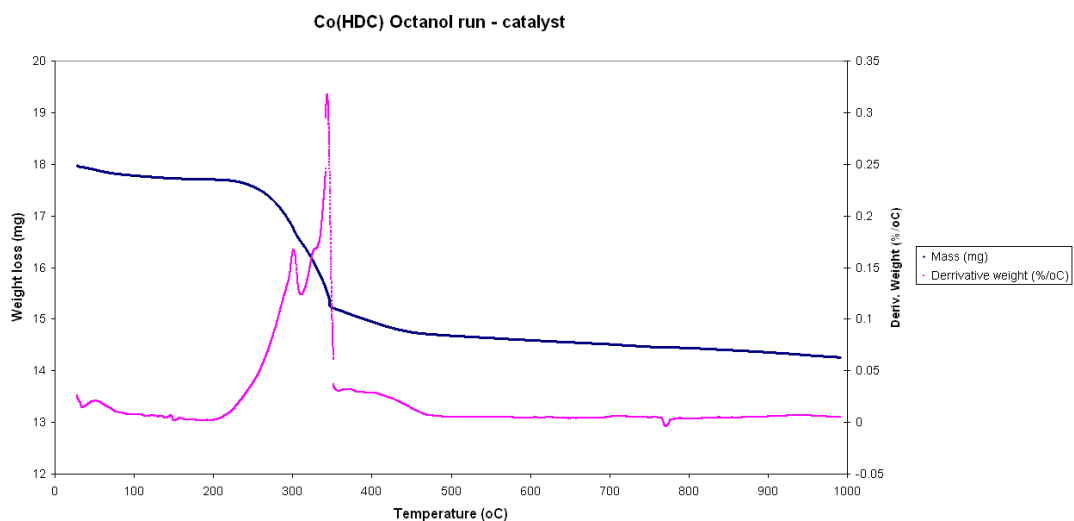


Figure 4-105 Post-reaction TGA on catalyst under oxygen gas (octanol run)

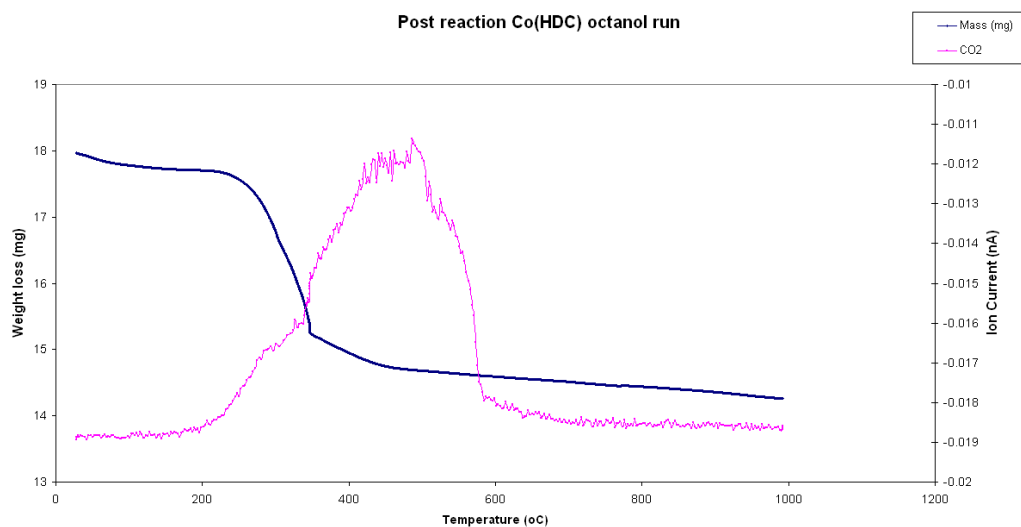


Figure 4-106 MS post-reaction TGA on catalyst under oxygen gas (octanol run)

To determine as to whether carbon laydown had occurred on the surface of the gamma alumina packing material, a temperature programmed oxidation (TPO) was performed on a sample of the post reaction gamma alumina packing material. Any carbonaceous species deposited on the surface of the catalyst would be removed in the form of CO₂.

The graph, Figure 4-107, shows that the weight loss occurred over two broad temperature ranges with maxima of 258°C and 377°C with a small weight loss at a higher temperature of 573°C. From the weight loss curve it was calculated

that the weight loss of the alumina was ~28%. Graph, Figure 4-108, shows that CO₂ evolution occurred over a broad temperature range between 208°C-720°C. A DSC trace showed that the evolution was exothermic, confirming that the burn off of carbonaceous species was likely.

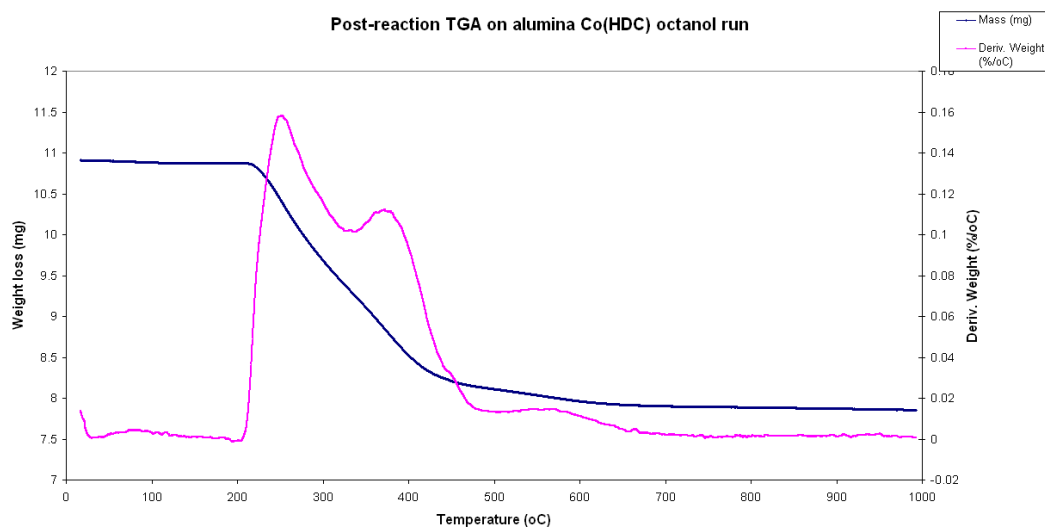


Figure 4-107 Post-reaction TGA on alumina under oxygen gas (octanol run)

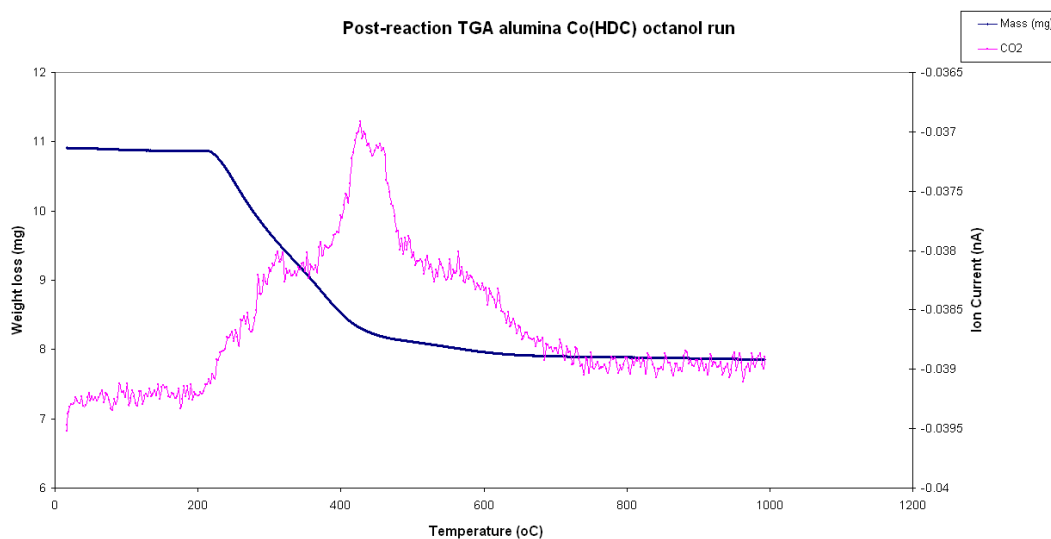


Figure 4-108 MS post-reaction TGA on alumina under oxygen gas (octanol run)

5 Discussion

5.1 Characterisation

5.1.1 TGA

The two catalysts were prepared at Johnson Matthey and are in line with industrial methodology. The Co/Al₂O₃ (nitrate) catalyst was calcined at 200°C with the Co/Al₂O₃ (HDC) catalyst calcined at the lower temperature of 105°C. The oxidative decomposition of cobalt/alumina (nitrate) and cobalt/alumina (HDC) catalysts were investigated by TGA-DSC and online MS analysis of gaseous products as a function of temperature, with the results shown in section 4. Both catalysts showed decomposition occurring over several events rather than a single decomposition. Cobalt/alumina (nitrate) catalyst decomposed over 4 distinct phases with a broad peak below 100°C, a sharp evolution at 248°C, a smaller broad evolution at 310°C and a further high temperature weight loss at 749°C. A similar profile was also seen with the cobalt/alumina (HDC) catalyst where the oxidative decomposition occurred at 90°C, 218°C, 320°C and a broader high temperature peak at 677°C. There were also a series of small decompositions above 800°C for both catalysts. The two lowest temperature peaks for both catalysts correspond to loss of physisorbed water on the catalysts surfaces with the next temperature evolutions at 248°C and 218°C both corresponding to water and nitrogen oxide. A DSC trace showed the weight loss at 258°C for the cobalt/alumina (nitrate) catalyst was exothermic suggesting the nitrate precursor was breaking down to form the oxide. Although the cobalt/alumina (HDC) catalyst did not exhibit a sharp exotherm, it did show a broad exotherm with a slight peak in the region of 220°C, suggesting the nitrate precursor was breaking down to form the oxide over a larger temperature range. These results reveal that the calcination temperatures of 200°C and 105°C were insufficient to convert the cobalt nitrate to cobalt oxide. The next higher temperature evolutions at 320°C and 677°C for cobalt/alumina (HDC) catalyst and 310°C for cobalt/alumina (nitrate) catalyst correspond to water being driven from the material. The highest temperature evolutions at 749°C and 800+°C for both catalysts are due to Co₃O₄ spinel being decomposed to the more thermodynamically stable CoO involving the release of oxygen.

The reductive decomposition of calcined cobalt/alumina (nitrate) and cobalt/alumina (HDC) catalysts were investigated by TGA-DSC and online MS analysis of gaseous products as a function of temperature, with the results shown in section 4. The reductive profiles are similar to the oxidative profiles. Cobalt/alumina (nitrate) catalyst decomposed over 4 distinct phases with a broad peak below 100°C, a sharp evolution at 256°C, a smaller broad evolution at 357°C and a further high temperature weight loss at 749°C. A similar profile was also seen with the cobalt/alumina (HDC) catalyst where the reductive decomposition occurred at 88°C, 212°C, 318°C and a broader high temperature peak at 679°C. There were also a series of small decompositions above 800°C for both catalysts. The two lowest temperature peaks for both catalysts correspond to loss of physisorbed water on the catalysts surfaces. The evolutions at 256°C, 307°C and the broad peak at ~630°C for cobalt/alumina (nitrate) catalyst and the peaks at 232°C, 326°C and 681°C for cobalt/alumina (HDC) represent the release of water and these evolutions mirror that of the hydrogen uptake, from the reduction of cobalt oxide. As mentioned earlier both catalysts showed an evolution of nitric oxide showing the nitrate precursor had not been fully decomposed with calcination. Overall the evolution of nitric oxide was not expected as Johnson Matthey reported that the calcination temperatures used for the two catalysts were sufficient to convert all the nitrate precursor to the oxide. The cobalt/alumina (nitrate) catalyst was prepared by impregnating the gamma alumina support to incipient wetness with an aqueous solution containing the cobalt nitrate precursor salt and it has been proven that there is still nitrate precursor present after calcination however, the nitric oxide evolution was even more surprising regarding the cobalt/alumina (HDC) catalyst because the catalyst was prepared by a single deposition step by deposition-precipitation of cobalt compound at high pH via cobalt amine complex. This procedure is thought to be a nitrate-free process [124]. Under oxygen rich conditions any amine would be expected to be converted to NO_x and this was the case. However, the TGA-DSC data under reducing conditions show nitric oxide rather than NH₃ being released suggesting that the amine complex could be interacting with the surface hydroxyl groups of the alumina support. It was discovered that temperatures of 350+°C were needed to decompose all the nitrates still present in both catalysts and that the higher the calcination temperature, the higher the temperature needed to reduce the cobalt oxide.

5.1.2 TPR/TPR

The TPR/TPD data, shown in section 4, show the same profile for both catalysts. The 1st peaks in both graphs represent any nitrates still present after calcinations and the TGA-DSC experiments confirm this. In literature it is widely agreed that the reduction of unsupported cobalt oxide (Co_3O_4) occurs as a two stage process [111, 112] which can be ascribed to successive reduction of Co_3O_4 to CoO and then to Co [113, 114]. The two middle peaks in both TPR/TPD graphs represent these reductions and the TGA-DSC data again validates this. Jacobs et al. [25] and Bechara et al. [115] assigned the reduction of surface Co_3O_4 spinel between 260-450°C with the higher temperature peaks between 450-750°C being attributed to the reduction of cobalt oxide and alumina interaction species. The high temperature peaks at 914°C for cobalt/alumina (nitrate) catalyst and 845°C for cobalt/alumina (HDC) catalyst represent cobalt aluminate species which are always present in alumina supported cobalt catalysts [43]. The formation of these species are seen above 800+°C in the TGA-DSC analysis.

The main difference between the two catalysts is that the reduction band for CoO to Co is far broader for cobalt/alumina (nitrate) catalyst suggesting that it is more difficult to reduce to Co metal. This is down to the preparation method for cobalt/alumina (HDC) catalyst which was specifically designed to produce evenly and high-dispersed catalysts. Traditionally cobalt catalysts produced by incipient wetness impregnation using an aqueous cobalt nitrate solution at low pH of 2-3 [125, 126] can only achieve modest interaction between the positively charged alumina carrier and the similarly charged Co cations. Therefore, cobalt can be deposited as relatively large clusters of crystallites of up to a few 100nm [127] making them more difficult to reduce.

5.1.3 BET Surface area analysis

The BET surface area of cobalt/alumina (HDC) catalyst ($188 \text{ m}^2/\text{g}$) is larger than that of the cobalt/alumina (nitrate) catalyst ($108 \text{ m}^2/\text{g}$) but the pore diameter is smaller 127\AA compared with 240\AA which again supports the idea that catalysts produced by the HDC method yield higher dispersed catalysts than catalysts produced by impregnation methods. Using the HDC method the cobalt surface area almost increases linearly with cobalt content to about $30\text{-}40 \text{ m}^2/\text{g}$ catalyst for 50wt% Co in the reduced catalyst compared to the $12\text{-}16 \text{ m}^2/\text{g}$ generally attainable for a 20wt% Co catalyst made by nitrate impregnation [125]. The dispersion of HDC catalysts do decline from 0.15 for 20wt% Co to ~ 0.1 for 50wt% Co catalyst and subsequently to lower values but the dispersion is maintained better than in cobalt nitrate impregnation where an earlier levelling off of the cobalt surface area or activity is observed [125, 126]. More over repeated cobalt nitrate impregnation is required to reach high Co levels.

5.1.4 Transmission Electron Microscopy (TEM)

From the TEM images shown in section 4 it can be seen that the cobalt oxide crystallites are more homogeneously distributed on the cobalt/alumina (HDC) catalyst compared with the cobalt/alumina (nitrate) catalyst. The crystallites in the $\text{Co}/\text{Al}_2\text{O}_3$ (nitrate) catalyst form in large clusters ($150\text{nm}+$), also reported by Marion et al. [127] compared with the smaller clusters ($<100\text{nm}$) seen for the cobalt/alumina (HDC) catalyst. This again shows the difference the catalyst preparation method can make to the catalyst surface structure.

5.1.5 Powder and hot-stage powder X-ray diffraction (XRD)

From the powder XRD graphs in section 4 it can be seen that the calcined catalysts both show crystalline phases for Co_3O_4 spinel and gamma alumina as expected with the cobalt/alumina (nitrate) catalyst having more defined peaks compared with the more amorphous cobalt/alumina (HDC) catalyst.

Hot-stage XRD experiments under reducing conditions showed the reduction of the two catalysts. The cobalt/alumina (nitrate) catalyst Co_3O_4 spinel (Co^{3+})

reduced to CoO (Co^{2+}) between 300°C-350°C then to Co (Co^0) from 400°C and above. The cobalt crystal size was calculated at ~20nm at 800°C. These findings were consistent with literature [110] and with data from TPR/TPD and TGA-DSC experiments. The cobalt/alumina (HDC) catalyst Co_3O_4 spinel (Co^{3+}) reduced to CoO (Co^{2+}) between the same temperature range (300°C-350°C) then to Co (Co^0) from 500°C and above. This higher reduction temperature could be due to Co having a stronger interaction with the gamma alumina support. The formation of Co metal did not appear until higher temperatures compared with cobalt/alumina (nitrate) catalyst which again is consistent with data from TPR/TPD and TGA-DSC experiments. In literature [124] it has been shown that the HDC catalyst should reduce from Co^{3+} to Co^{2+} at 200-300°C, followed by the reduction of Co^{2+} to the metallic state at 350-450°C but it is seen from the data presented that it occurs at slightly higher temperatures in this case. The cobalt crystal size was calculated at ~10nm at 800°C which is larger than the quoted 3nm in literature [124]. This could be due to the amorphous nature of the HDC catalyst or the gamma alumina peak that is overlapping onto the metallic cobalt peak or most likely that using the Scherrer equation to calculate the crystal size. This is only an approximate method since the results can be influenced by various factors such as lattice distortion as well as instrumental parameters. The smaller crystallite size for HDC catalyst is again in agreement with BET, TEM data and literature [124].

5.1.6 TPR-UV-vis-NIR spectroscopy

The TPR-UV-vis-NIR spectroscopy experiments carried out for both catalysts show absorption bands that are attributed to ${}^4\text{T}_{1g}(\text{F}) \longrightarrow {}^4\text{T}_{1g}(\text{P})$ transitions in octahedral high-spin Co^{2+} complexes [119]. Both the TPR-UV experiments show Co^{3+} being reduced to Co^{2+} and they are in the same temperature ranges as shown in the TRP/TPD and TGA-DSC experiments from section 4.

5.2 Reaction chemistry

5.2.1 Reactions at 210°C (and 220°C in the case of Co/Al₂O₃ (nitrate) catalyst)

Both catalysts were studied for F-T activity under similar reaction conditions of 210°C and 5000 GHSV over an extended number of hours TOS with the cobalt/alumina (nitrate) catalyst being further examined at the elevated reaction temperature of 220°C.

5.2.1.1 Conversion

The conversion for the 1st reaction at 210°C for the Co/Al₂O₃ (nitrate) catalyst over 900 hrs TOS was 23-8% with a 1st order deactivation constant of 0.0014 hr⁻¹. The conversion for the 1st reaction at 210°C for Co/Al₂O₃ (HDC) catalyst over a shorter time period (480 hrs TOS) was 20-12% with a 1st order deactivation constant of 0.0011 hr⁻¹. If we compare the data for the Co/Al₂O₃ (nitrate) catalyst to the Co/Al₂O₃ (HDC) catalyst over the same time period (480 hrs TOS) we now get a conversion drop of 23-9% with a 1st order deactivation constant of 0.0311 hr⁻¹. From this data it can be concluded that the Co/Al₂O₃ (nitrate) catalyst has a higher initial conversion value but deactivates more rapidly than the Co/Al₂O₃ (HDC) catalyst, as seen from roughly a factor of three difference in the deactivation constants. Although it is widely accepted that the oxidation of cobalt metal to cobalt oxide or cobalt aluminate by the product of water is an important method for deactivation, it is mainly believed to be related to cobalt crystallite size distribution [128]. The cobalt/alumina nitrate catalyst showed faster deactivation compared with the cobalt/alumina HDC catalyst for these reactions at 210°C. A possible reason for this faster deactivation was that the nitrate catalyst was the 1st catalyst that was used in the rig and impurities inside the rig caused this fast initial deactivation as the subsequent reactions of both catalysts followed similar trends.

When the reaction temperature is increased to 220°C for the Co/Al₂O₃ (nitrate) catalyst the conversion shows a slight increase from 8-12% and then a slow deactivation to 9% over the next ~600 hrs TOS and this is confirmed with the

much smaller deactivation constant of 0.0004 hr^{-1} . The reason for this increase in conversion could be the higher temperature forcing hydrocarbons out of the pores and off the surface of the catalyst increasing the rate of diffusion in and out of the catalyst particles. The slower deactivation could be due to the reaction reaching steady state.

5.2.1.2 Selectivity

Under the same reaction conditions the selectivity's of both cobalt catalysts behave in a similar fashion. In the light organic phase the selectivity's peak around the C9-C11 region with peaks in the wax phase around C18-C21. As the TOS increases both catalysts are selective in producing hydrocarbons that have higher molecular weights. Low temperatures result in F-T products with higher average carbon numbers [32] due to high chain growth probability (thermodynamically expected in an exothermic reaction). Longer chain products are generally found at low temperatures in polymerisation reactions, which can mechanistically be interpreted as an inhibition of the desorption step relative to the chain growth step [32].

When the reaction temperature is increased to 220°C for the $\text{Co}/\text{Al}_2\text{O}_3$ (nitrate) catalyst the change in selectivity is very minimal. This could be due to the reaction reaching steady state, as seen by the conversion profile and small deactivation constant at 220°C , and therefore a change in selectivity is not expected.

5.2.1.3 Alpha value

The average alpha (α) values for both cobalt catalysts, under equivalent reaction conditions, are comparable. There is no statistical difference between the (α) values of the two catalysts. Even when the reaction temperature is increased to 220°C there is still not a shift in the (α) value. This is not unexpected because it is quite difficult to increase α -value once the reaction is online. The parameters that can increase the α -value are: choice of active phase, addition of promoter, increase of pressure and decrease of temperature and $\text{H}_2:\text{CO}$ ratio.

5.2.1.4 Post reaction soxhlet extractions and TGA-DSC analysis

Post-reaction soxhlet extractions for both catalysts show a broad range of hydrocarbons deposited on both catalysts and gamma alumina packing material. The Co/Al₂O₃ (nitrate) catalyst shows selectivity of the deposited compounds towards higher molecular weight hydrocarbons (C35+) compared to Co/Al₂O₃ (HDC) catalyst where the selectivity is towards C30-C37 hydrocarbons. This could be explained by the filling of catalyst pores with high molecular mass waxes. Although, not shown in section 4, both the catalysts and gamma alumina packing material contain deposited hydrocarbons greater than C40 with the alumina showing heavier molecular weight hydrocarbons compared to the catalysts. This could be explained by slow diffusion of larger hydrocarbons through the system. These compounds lower the F-T conversion by reducing the rate of diffusion in and out of the catalyst particles. This can occur with time on stream if there is a continuous build-up of these products in the catalyst pores. As the alumina packing material has a long bed length this could explain why heavier hydrocarbons are trapped on the alumina. The Co/Al₂O₃ (nitrate) catalyst accumulated more carbonaceous material compared with the Co/Al₂O₃ (HDC) catalyst as seen by the number of moles detected from the soxhlet extractions. This could be due to the larger pore volume of the nitrate catalyst.

TGA-DSC experiments were ran on the post-reaction catalysts and alumina packing material to determine whether carbon laydown had occurred on the surface of materials. TPO's were performed on the materials and any carbonaceous species were removed in the form of CO₂. From the TGA data it can be seen that the Co/Al₂O₃ (nitrate) catalyst under oxidative conditions shows a smaller weight loss of ~15% compared with ~35% weight loss of the Co/Al₂O₃ (HDC) catalyst. The DSC traces showed the evolutions were exothermic confirming that the burn off of carbonaceous species was likely. The Co/Al₂O₃ (nitrate) catalyst shows a slight weight increase upon exposure to 2% O₂/Ar gas. This was due to cobalt metal being exposed to air after reaction therefore, re-oxidising to cobalt oxide. This feature was not observed for Co/Al₂O₃ (HDC) catalyst. The CO₂ evolutions were all below 540°C suggesting no graphitic material was present. Both catalysts showed weight losses at very high temperatures. These evolutions can be assigned to the formation of cobalt

aluminate species (CoAl_2O_4) [119]. From the TGA-DSC data for the post-reaction alumina it can be seen that weight losses for both alumina are similar and that CO_2 evolutions occur before 600°C again suggesting no graphitic material was present. The DSC traces showed the evolutions were exothermic again confirming that the burn off of carbonaceous species was likely. There was an unexpected evolution over 900°C . This is believed to be due to migration of Co species onto the gamma alumina packing material thus forming CoAl_2O_4 or some catalyst was present in the alumina sample that was tested. This weight loss at high temperatures on the alumina, under oxidative conditions, did not occur with subsequent reactions.

5.2.2 Reactions involving the co-feeding of octanol into the reactor

Both catalysts were studied for F-T activity at 210°C and 5000 GHSV over an extended number of hours TOS with the introduction of octanol into the feed stream at 0.02 ml/min.

5.2.2.1 Conversion

The conversion for the reaction at 210°C before octanol addition, for the $\text{Co}/\text{Al}_2\text{O}_3$ (nitrate) catalyst over 336 hrs TOS, was 35-21% with a 1st order deactivation constant of 0.0015 hr^{-1} . The conversion was slightly higher for this run than for the 1st run at 210°C but the deactivation constants are comparable. The conversion for the reaction at 210°C before octanol addition, for $\text{Co}/\text{Al}_2\text{O}_3$ (HDC) catalyst, was 14-5% with a 1st order deactivation constant of 0.0014 hr^{-1} . Again the conversion was slightly different for this run but, in this case it was smaller compared with the 1st run at 210°C , and like the cobalt/alumina (nitrate) catalyst the deactivation constants have no statistical difference. Unlike the 1st experiments carried out for both catalysts at 210°C , these sets of experiments show very similar deactivation constants over the same time period although the same trend is seen regarding conversion, where the $\text{Co}/\text{Al}_2\text{O}_3$ (nitrate) catalyst has a higher starting conversion value compared with the $\text{Co}/\text{Al}_2\text{O}_3$ (HDC) catalyst.

The conversion during octanol addition for the Co/Al₂O₃ (nitrate) catalyst was ~21%-7% with an increased deactivation constant of 0.0032 hr⁻¹. On introduction of octanol the deactivation constant doubled suggesting that octanol had a negative effect on the catalyst. The conversion and deactivation constant could not be calculated for the Co/Al₂O₃ (HDC) catalyst as the light organic phase samples became very frothy and resembled an emulsifier. The conversion was calculated using the volume of water produced but as the samples were in one phase and not in the 2 phases like before, the volume of water could not be measured. This was not an error with this reaction as when the reaction was repeated, the same outcome was observed.

5.2.2.2 Selectivity

The selectivity of the Co/Al₂O₃ (nitrate) catalyst was very similar to the 1st run. Both the light organic and wax products peaked in the same regions as before. As TOS increased the selectivity shifts to higher hydrocarbons. However, the Co/Al₂O₃ (HDC) catalyst did not behave in the same manner as before. The 1st difference was that the light organic phase produced samples that were emulsified compared with before but a more surprising observation was that no heavy molecular weight hydrocarbons were seen in the 2nd knockout trap. However, on repeating the experiment the same observations were seen, so it is clear that these observations are not trivial. Similarly to the 1st reaction as TOS increased the selectivity shifts to higher hydrocarbons.

The introduction of octanol into the systems had an effect on selectivity. The Co/Al₂O₃ (nitrate) catalyst light organics profile was significantly different compared with before the addition of octanol, where as the Co/Al₂O₃ (HDC) catalyst light organics profile, showed no difference. The Co/Al₂O₃ (nitrate) catalyst wax profile was unchanged compared with before the addition of octanol, where as the Co/Al₂O₃ (HDC) catalyst wax profile was significantly different compared with the 1st run. On the initial introduction of octanol into the Co/Al₂O₃ (nitrate) system the polymerisation seemed to be inhibited then over time polymerisation started to recover however this was not observed for the Co/Al₂O₃ (HDC) catalyst as the introduction of octanol did not seem to effect the overall selectivity.

The main difference between selectivity's on the addition of octanol was the formation of tetradecanol in both cases. Both catalysts react qualitatively the same way but quantitatively they are much different. In the light organic phase, for the Co/Al₂O₃ (nitrate) catalyst, the number of moles of tetradecanol produced was roughly a factor of 19 smaller than the unreacted octanol. In the wax phase this increased to a factor ~3 smaller than the unreacted octanol.

| Time period (hrs) | Moles octanol in light organic phase | Moles octanol in wax phase | Moles tetradecanol in light organic phase | Moles tetradecanol in wax phase | Total moles | Moles octanol in - per 24 hrs | Mass balance |
|-------------------|--------------------------------------|----------------------------|---|---------------------------------|-------------|-------------------------------|--------------|
| 24 | 6.99E-2 | 4.42E-3 | 1.42E-2 | 3.46E-3 | 9.20E-2 | 1.83E-1 | 50.27% |
| 48 | 7.06E-2 | 4.71E-3 | 1.43E-2 | 4.72E-3 | 9.43E-2 | 1.83E-1 | 51.53% |
| 72 | 1.06E-1 | 5.39E-3 | 1.60E-2 | 5.32E-3 | 1.33E-1 | 1.83E-1 | 72.68% |
| 96 | 1.47E-1 | 6.00E-3 | 1.731E-2 | 5.35E-3 | 1.75E-1 | 1.83E-1 | 95.63% |

Table 5-1 Mass balance data for Co/Al₂O₃ (nitrate) catalyst

The mass balance of this reaction will be discussed at the end of this section.

With the Co/Al₂O₃ (HDC) catalyst no tetradecanol was observed in the light organic phase however in the wax phase tetradecanol was observed but in much smaller quantities compared with the Co/Al₂O₃ (nitrate) catalyst. The number of moles of tetradecanol produced was roughly a factor of 120 smaller than the unreacted octanol so this suggests the HDC catalyst is poorer in forming tetradecanol compared with nitrate catalyst. The difference between two reactions is ~2 orders of magnitude between the HDC and nitrate catalysts regarding the number of moles of tetradecanol produced.

| Time period (hrs) | Moles octanol in light organic phase | Moles octanol in wax phase | Moles tetradecanol in wax phase | Total moles | Moles octanol in - per 24 hrs | Mass balance |
|-------------------|--------------------------------------|----------------------------|---------------------------------|-------------|-------------------------------|--------------|
| 24 | 8.82E-2 | 4.54E-3 | 3.11E-5 | 9.28E-2 | 1.83E-1 | 50.71% |
| 48 | 9.31E-2 | 9.20E-3 | 1.26E-5 | 1.02E-1 | 1.83E-1 | 55.74% |
| 72 | 9.78E-2 | 7.32E-3 | 6.94E-5 | 1.05E-1 | 1.83E-1 | 57.38% |
| 96 | 1.01E-1 | 7.96E-3 | 4.17E-5 | 1.09E-1 | 1.83E-1 | 59.56% |
| 120 | 1.10E-1 | 7.27E-3 | 5.99E-5 | 1.17E-1 | 1.83E-1 | 63.93% |
| 144 | 1.09E-1 | 7.70E-3 | 9.98E-5 | 1.17E-1 | 1.83E-1 | 63.93% |
| 168 | 1.04E-1 | 8.38E-3 | 6.00E-5 | 1.12E-1 | 1.83E-1 | 61.20% |
| 192 | 9.51E-2 | 7.58E-3 | 5.57E-5 | 1.03E-1 | 1.83E-1 | 56.28% |

Table 5-2 Mass balance data for Co/Al₂O₃ (HDC) catalyst

The mass balance again will be discussed at the end of this section.

It is widely accepted that cobalt particle size has an important role to play in the performance in Fischer-Tröpsch synthesis. Many groups have reported that the TOF suddenly decreased for catalysts with cobalt particle sizes <10nm [25, 129-132]. However other groups did not observe this so-called particle size effect, while measuring catalysts with similar sizes [47, 124, 133, 134]. Small particles seem to be more susceptible to oxidation than large particles, and oxidation during high-pressure catalytic testing has been reported to occur for catalysts with sizes <6nm [47]. The group van Steen et al. [12] also showed that cobalt particles smaller than 4nm can be oxidised during F-T operation with Bezemer et al. [128] also reporting a large drop in C5+ selectivity with cobalt particle sizes smaller than 6nm. Although the cobalt particle size for the Co/Al₂O₃ (HDC) catalyst was calculated by *in-situ* XRD to be ~10nm, it is reported in literature [124] that the cobalt particle size is much smaller and was calculated as 3nm. The smaller particle size of the HDC catalyst could explain why the catalyst did not perform well for FTS.

As shown, in section 4 and above, both catalysts produce tetradecanol from octanol selectively. There are two possible methods in which tetradecanol can be formed:

- 1) The first possible method involves 8 carbons from 1 molecule of octanol and the remaining 6 carbons come from the F-T reaction. The octanol molecule and 6 carbons react together to form tetradecanol. If this was the case then C6 molecules play an important role on the surface of the catalyst which is unlikely because longer chains incorporate less into the F-T products than shorter chains [102]. Instead of C6 molecules being a key intermediate, carbon chains of different lengths could act as intermediates in the F-T reaction to produce tetradecanol. This seems unlikely because if this were the case then a range of hydrocarbon/oxygenated species with ranging chain lengths would be seen and they are not, only tetradecanol was produced selectively.
- 2) Therefore logic tells us that the more likely method to produce tetradecanol from octanol involves two octanol molecules reacting together to form tetradecanol. Although an explanation on how this happens mechanistically is not proposed, it does seem the most probable method of tetradecanol production in this case.

Possible routes of tetradecanol formation are:

- 1) 2 * octanol molecules \longrightarrow tetradecanol + C₂H₄ + H₂O or
- 2) 2 * octanol molecules \longrightarrow tetradecanol + C₂H₅OH

The volume of water produced is very small so the increase wouldn't be seen and because there is no GC analysis for lights, ethene again wouldn't be seen. The solvents used for GC analysis have similar boiling points to ethanol so they would mask any ethanol peaks in the GC trace. Note: there were no other extra peaks in the GC traces.

The mass balance for the reaction involving cobalt/alumina (nitrate) catalyst, Table 5-1, showed mass loss no matter if 1 or 2 molecules of octanol were used to make tetradecanol. Even the last point is within experimental error of 100 \pm 5%. The mass balance for the reaction involving cobalt/alumina (HDC) catalyst, Table 5-2, shows a lower mass balance. This could be due to carbon deposition

from the octanol with the possibility of olefin/ethanol formation. A key parameter for this reaction, with the addition of octanol, is that the HDC catalyst has more carbon lay down compared with the nitrate catalyst.

5.2.2.3 Alpha value

The average alpha (α) value for the Co/Al₂O₃ (nitrate) catalyst before octanol addition was consistent with previous experiments. However, the average alpha (α) value for the Co/Al₂O₃ (HDC) catalyst before octanol addition was significantly lower and this is due to no heavy molecular hydrocarbons being seen in the 2nd knockout trap. Again this supports the theory that the smaller cobalt particle size for the HDC catalyst is the reason for poor F-T activity with a decrease in C₅+ selectivity likely [128].

The addition of octanol into the Co/Al₂O₃ (nitrate) system did not have an effect on the alpha (α) value however it can be seen from comparing the C₁₂+ and C₂₀+ selectivity values that the selectivity is significantly shifted to lower hydrocarbons with the addition of octanol. The introduction of octanol into the Co/Al₂O₃ (HDC) system did have an effect on the alpha (α) value. The average α -value increased to 0.996 \pm 0.02 (C₂₅-35) that is significantly higher than the previous experiment where the α -value was 0.89 \pm 0.02 (C₂₅-35). This could be due to no wax products being seen before octanol addition. On the introduction of octanol the wax products that have accumulated are washed off in large volumes giving this high alpha value.

5.2.2.4 Post reaction soxhlet extractions and TGA-DSC analysis

Post-reaction soxhlet extractions for both catalysts show a broad range of hydrocarbons deposited on both catalysts and gamma alumina packing material. Both catalysts show selectivity of the accumulated compounds towards higher molecular weight hydrocarbons which is similar to before. Again both the catalysts and gamma alumina packing material contain deposited hydrocarbons greater than C₄₀ with the alumina showing heavier molecular weight hydrocarbons compared to the catalysts. Again the Co/Al₂O₃ (nitrate) catalyst accumulated more carbonaceous material compared with the Co/Al₂O₃ (HDC)

catalyst as seen by the number of moles detected from the soxhlet extractions. This could be due to the larger pore volume of the nitrate catalyst.

TGA-DSC experiments were ran on the post-reaction catalysts and alumina packing material to determine whether carbon laydown had occurred on the surface of materials. TPO's were performed on the materials and any carbonaceous species were removed in the form of CO_2 . From the TGA data it can be seen that the $\text{Co}/\text{Al}_2\text{O}_3$ (nitrate) catalyst under oxidative conditions shows a smaller weight loss of $\sim 6.5\%$ compared with $\sim 20.5\%$ weight loss of the $\text{Co}/\text{Al}_2\text{O}_3$ (HDC) catalyst. Although the weight losses are smaller than before the trend is the same. The smaller weight losses are due to the octanol flushing hydrocarbons from the surface and pores of the catalysts. The DSC traces showed the evolutions were exothermic confirming that the burn off of carbonaceous species was likely. The $\text{Co}/\text{Al}_2\text{O}_3$ (nitrate) catalyst shows a slight weight increase upon exposure to $2\% \text{O}_2/\text{Ar}$ gas. This was due to cobalt metal being exposed to air after reaction therefore, re-oxidising to cobalt oxide. This feature was not observed for $\text{Co}/\text{Al}_2\text{O}_3$ (HDC) catalyst. The CO_2 evolutions were all below 590°C suggesting no graphitic material was present. Unlike the previous reactions, only the $\text{Co}/\text{Al}_2\text{O}_3$ (nitrate) catalyst showed a weight loss at very high temperatures. This weight loss can be assigned to the formation of cobalt aluminate species (CoAl_2O_4) [119]. From the TGA-DSC data for the post-reaction alumina it can be seen that weight losses for both alumina are smaller than before and again this is due to the octanol stripping hydrocarbons from the material. CO_2 evolutions occur before 720°C again suggesting no graphitic material was present. The DSC traces showed the evolutions were exothermic again confirming that the burn off of carbonaceous species was likely.

5.2.3 Reaction involving the co-feeding of decanol and 0.063M naphthalene solution into the reactor

The F-T activity for cobalt/alumina (nitrate) catalyst was studied at 210°C and 5000 GHSV over an extended number of hours TOS with the introduction of decanol and then 0.063M naphthalene solution into the feed stream at 0.02 ml/min.

5.2.3.1 Conversion

The conversion for the reaction at 210°C before decanol addition, for the Co/Al₂O₃ (nitrate) catalyst over 288 hrs TOS, was 43-30% with a 1st order deactivation constant of 0.0662 hr⁻¹. The conversion for this reaction was higher than the previous reactions and the deactivation constant was significantly larger than the previous reactions. This larger deactivation constant is due to the catalyst being more active at first. As the reaction proceeds the catalyst quickly settles to steady state just like the other reactions that were ran.

The conversion during decanol addition for the Co/Al₂O₃ (nitrate) catalyst was ~30%-12% with and smaller deactivation constant of 0.0027 hr⁻¹. This smaller deactivation constant was due to the reaction reaching steady state.

After a period of 360 hrs TOS with decanol being co-fed into the reactor the liquid feed was switched off to see what affect this had on the catalyst. The conversion slowly dropped from ~13%--9.5% with a drop in the deactivation constant also seen - 0.0006 hr⁻¹ therefore suggesting that removing the decanol from the reaction had a positive effect on the catalyst.

The introduction of 0.063M naphthalene solution had a dramatic negative effect on the catalyst. The reaction quickly deactivated and after a period of 48 hrs TOS the reaction was fully deactivated.

5.2.3.2 Selectivity

The selectivity of the Co/Al₂O₃ (nitrate) catalyst before decanol addition was very similar to the previous runs. Both the light organic and wax products peaked in the same regions as before. As TOS increased the selectivity shifts to higher hydrocarbons.

The introduction of decanol into the system had a small effect on selectivity. The light organics profile showed no difference however the wax phase profile was significantly different compared with before the addition of decanol. This was the opposite of what happened when octanol was co-fed into the system. In this case carbon lay down affected the wax phase more than the light phase and

this is similar to the HDC catalyst where carbon lay down affected the wax phase more than the light phase. On the initial introduction of decanol into the system the polymerisation seemed to be inhibited then over time polymerisation started to recover and this was a similar trend to the result of co-feeding octanol into the Co/Al₂O₃ (nitrate) system.

When octanol was co-fed into the system tetradecanol was formed so it could be expected that with the addition of decanol into the system then octadecanol would be produced but this is not the case. No octadecanol or higher molecular weight alcohols were formed, the decanol passed through unreacted.

| Time period (hrs) | Moles decanol in light organic phase | Moles decanol in wax phase | Total moles | Moles decanol in - per 24 hrs | Mass balance |
|-------------------|--------------------------------------|----------------------------|-------------|-------------------------------|--------------|
| 24 | 4.03E-2 | 3.16E-3 | 4.35E-2 | 1.49E-1 | 29.19% |
| 48 | 5.56E-2 | 3.26E-3 | 5.89E-2 | 1.49E-1 | 39.53% |
| 72 | 8.67E-2 | 3.37E-3 | 9.01E-2 | 1.49E-1 | 60.47% |
| 96 | 5.08E-2 | 3.33E-3 | 5.41E-2 | 1.49E-1 | 36.31% |
| 120 | 6.18E-2 | 4.00E-3 | 6.58E-2 | 1.49E-1 | 44.16% |
| 144 | 6.45E-2 | 2.63E-3 | 6.71E-2 | 1.49E-1 | 45.03% |
| 168 | 6.05E-2 | 2.94E-3 | 6.34E-2 | 1.49E-1 | 42.55% |
| 192 | 4.34E-2 | 3.57E-3 | 4.70E-2 | 1.49E-1 | 31.54% |
| 216 | 6.00E-2 | 3.78E-3 | 6.38E-2 | 1.49E-1 | 42.82% |

Table 5-3 Mass balance data for Co/Al₂O₃ (nitrate) catalyst during addition decanol

The mass balance is low and this could be due to carbon lay down on the catalyst. When the decanol feed was switched off the selectivity again shifted slowly towards higher molecular weight hydrocarbons.

5.2.3.3 Alpha value

The addition of decanol into the Co/Al₂O₃ (nitrate) system did not have an effect on the average alpha (α) value. Before decanol addition the α -value was calculated at 0.900 ± 0.009 (C25-35), which is similar to previous α -values, and

during decanol addition the α -value was calculated at 0.94 ± 0.033 (C25-35). When the decanol feed was switched off the α -value was calculated at 0.900 ± 0.016 (C25-35) so they are no statistical differences between the α -values. Because the reaction deactivated rapidly with the addition of naphthalene solution, no α -value could be calculated.

5.2.3.4 Post reaction soxhlet extractions and TGA-DSC analysis

Post-reaction soxhlet extractions for both the catalyst and gamma alumina packing material show a broad range of hydrocarbons are deposited on the materials. Both the catalyst and alumina show selectivity of the accumulated compounds towards higher molecular weight hydrocarbons which is similar to before and again both these materials contain deposited hydrocarbons greater than C40 with the alumina showing heavier molecular weight hydrocarbons compared to the catalysts.

TGA-DSC experiments were ran on the post-reaction catalyst and alumina packing material to determine whether carbon laydown had occurred on the surface of materials. TPO's were performed on the materials and any carbonaceous species were removed in the form of CO_2 . From the TGA data it can be seen that the catalyst under oxidative conditions shows a similar weight loss of $\sim 7\%$, which similar to the previous reaction with the addition of octanol. The smaller weight loss is due to the decanol flushing hydrocarbons from the surface and pores of the catalyst. The DSC traces showed the evolutions were exothermic confirming that the burn off of carbonaceous species was likely. The catalyst showed a slight weight increase upon exposure to $2\% \text{O}_2/\text{Ar}$ gas. This was due to cobalt metal being exposed to air after reaction therefore, re-oxidising to cobalt oxide. The CO_2 evolutions were all below 550°C suggesting no graphitic material was present. Like the previous reactions, the $\text{Co}/\text{Al}_2\text{O}_3$ (nitrate) catalyst showed a weight loss at very high temperatures. This weight loss can be assigned to formation of CoAl_2O_4 [119]. From the TGA-DSC data for the post-reaction alumina it can be seen that there is a smaller weight loss of $\sim 8.3\%$ that again is due to the decanol stripping hydrocarbons form the material. CO_2 evolutions occur before 680°C again suggesting no graphitic material was

present. The DSC traces showed the evolutions were exothermic again confirming that the burn off of carbonaceous species was likely.

5.3 Summary

Overall it was shown that cobalt/alumina (HDC) catalyst performed poorer under F-T conditions compared with cobalt/alumina (nitrate) catalyst and this again supports the theory that smaller cobalt particle sizes are not necessarily good for F-T.

When octanol is introduced into F-T systems with cobalt/alumina catalysts tetradecanol is selectively produced. Decanol however does not show any reactivity when co-fed into systems under the same reaction conditions.

5.4 Future work

- If more time were available for the project then to get a complete set of reactions that are comparable with each catalyst, decanol would be co-fed into the reactor system over the Co/alumina (HDC) catalyst under the same conditions, to see what effect this had on the activity of the catalyst to see if decanol would become involved in the F-T reaction unlike with the Co/alumina (nitrate) catalyst.
- In order to get a better understanding of the pathway of tetradecanol formation, ^{13}C labelled experiments could be ran using ^{13}C labelled octanol. This technique could be used to follow the path of a labelled ^{13}C from octanol to see if this labelled carbon becomes involved in the F-T reaction and to see if the labelled carbon is then seen in the tetradecanol products.

6 References

- [1] Institute for the analysis of global security, "The future of oil", [<http://www.iags.org/futureofoil.html>]
- [2] Energy Bulletin, "Back to the post-oil future", [<http://energybulletin.net>]
- [3] The Catalyst Review Newsletter, "Gas-to-Liquids: Peering into the crystal ball", April 2005, p. 4.
- [4] Health and Energy, "The era of expensive oil", [<http://www.healthandenergy.com>]
- [5] Egypt Oil & Gas, "Gas to Liquid (GTL): is it an attractive route for gas monetization? GTL vs. LNG Economics", [<http://www.egyptoil-gas.com>]
- [6] BP: Statistical Review of World Energy, Report, 2007.
- [7] I.I. Rahmim, *Oil & Gas Journal*. 2009, 109.
- [8] Oilnergy, [<http://www.oilnergy.com>]
- [9] R.J.Farrauto and C.H. Bartholomew, "Fundamentals of Industrial Catalytic Processes", 1998.
- [10] Fischer, F.; Tropsch, H. *Brennst. Chem.* 1923, 4, 276.
- [11] P.J. van Berge, J. van de Loosdrecht, S. Barradas, and A.M. van der Kraan, *Catalysis Today*. 2000, 58, 321-334.
- [12] E. van Steen, M. Claeys, M.E. Dry, J. van de Loosdrecht, E.L. Viljoen, and J.L. Visagie, *Journal of Physical Chemistry B*. 2005, 109, 3575-3577.
- [13] E. van Steen, H. Shultz, *Applied Catalysis a-General*. 1999, 186, 309-320.
- [14] I. Wender, *Fuel Processing Technology*. 1996, 48, 189-297.
- [15] A.P. Steynberg, R.L. Espinoza, B. Jager, and A.C. Vosloo, *Applied Catalysis a-General*. 1999, 186, 41-54.
- [16] M.E. Dry, *Journal of Chemical Technology and Biotechnology*, 2002, 77, 43-50.
- [17] M.E. Dry, *Catalysis Today*, 2002, 71, 227-241.
- [18] H. Schulz, *Applied Catalysis a-General*, 1999, 186, 3-12.
- [19] J.A. Kritzinger, *Catalysis Today*, 2002, 71, 307-318.
- [20] W. Ngantsoue-Hoc, Y.Q. Zhang, R.J. O'Brien, M.S. Luo, and B.H. Davis, *Applied Catalysis a-General*, 2002, 236, 77-89.
- [21] S.A. Eliason, and C.H. Bartholomew, *Applied Catalysis a-General*, 1999, 186, 229-243.
- [22] S. Li, A. Li, S. Krishnamoorthy, and E. Iglesia, *Catalysis Letters*, 2001, 77, 197-205.
- [23] D.J. Wilhelm, D.R. Simbeck, A.D. Karp, and R.L. Dickenson, *Fuel Processing Technology*, 2001, 71, 139-148.
- [24] S. Bessell, *Applied Catalysis a-General*, 1993, 96, 253-268.
- [25] G. Jacobs, T.K. Das, Y.Q. Zhang, J.L. Li, G. Racoillet, and B.H. Davis, *Applied Catalysis a-General*, 2002, 233, 263-281.
- [26] G. Jacobs, P.M. Patterson, Y.Q. Zhang, T. Das, J.L. Li, and B.H. Davis, *Applied Catalysis a-General*, 2002, 233, 215-226.
- [27] N.N. Madikizela, and N.J. Coville, *Journal of Molecular Catalysis a-Chemical*, 2002, 181, 129-136.
- [28] S. Sun, K. Fujimoto, Y. Yoneyama, and N. Tsubaki, *Fuel*, 2002, 81, 1583-1591.
- [29] R.J. Obrien, L.G. Xu, R.L. Spicer, and B.H. Davis, *Energy & Fuels*, 1996, 10, 921-926.
- [30] B.H. Davis, *Catalysis Today*, 2003, 84, 83-98.

- [31] C.J. Bertole, C.A. Mims, and G. Kiss, *Journal of Catalysis*, **2004**, *221*, 191-203.
- [32] A.P. Stynberg, and M.E. Dry, "Fischer-Tropsch Technology", **2004**.
- [33] F. Fischer, *Brennt. Chem.* **1935**, *16*, 1.
- [34] M.E. Dry, "Catalysis: Science and Technology", *Springer-Verlag.*, **1981**.
- [35] T.H. Fleisch, R.A. Sills, and M.D. Briscoe, *Journal of Natural Gas Chemistry*, **2002**, *11*, 1-14.
- [36] R.L. Espinoza, A.P. Steynberg, B. Jager, and A.C. Vosloo, *Applied Catalysis a-General*, **1999**, *186*, 13-26.
- [37] C.H. Bartholomew, *Applied Catalysis a-General*, **2001**, *212*, 17-60.
- [38] D. Schanke, A.M. Hilmen, E. Bergene, K. Kinnari, E. Rytter, E. Adnanes, and A. Holmen, *Catalysis Letters*, **1995**, *34*, 269-284.
- [39] A.M. Hilmen, D. Schanke, K.F. Hanssen, and A. Holmen, *Applied Catalysis a-General*, **1999**, *186*, 169-188.
- [40] S. Krishnamoorthy, M. Tu, M.P. Ojeda, D. Pinna, and E. Iglesia, *Journal of Catalysis*, **2002**, *211*, 422-433.
- [41] C.J. Bertole, C.A. Mims, and G. Kiss, *Journal of Catalysis*, **2002**, *210*, 84-96.
- [42] G. Jacobs, P.M. Patterson, T.K. Das, M.S. Luo, and B.H. Davis, *Applied Catalysis a-General*, **2004**, *270*, 65-76.
- [43] J. Li, X. Zhan, Y. Zhang, G. Jacobs, T. Das, and B.H. Davis, *Applied Catalysis A: General*, **2002**, *228*, 203-212.
- [44] J. Zhang, J. Chen, J. Ren, Y. Li, and Y. Sun, *Fuel*, **2003**, *82*, 581-586.
- [45] G. Kiss, C.E. Kliewer, G.J. DeMartin, C.C. Culross, and J.E. Baumgartner, *Journal of Catalysis*, **2003**, *217*, 127-140.
- [46] J.J.H.M. Font Freide, T.D. Gamlin, J.R. Hensman, B. Nay, and C. Sharp, *Journal of Natural Gas Chemistry*, **2004**, *13(1)*, 1-9.
- [47] E. Iglesia, *Applied Catalysis a-General*, **1997**, *161*, 59-78.
- [48] J. van de Loosdrecht, B. Bazhinimaev, J.A. Dalmon, J.W. Niemantsverdriet, S.V. Tsybulya, A.M. Saib, P.J. van Berge, and J.L. Visagie, *Catalysis Today*, **2007**, *123*, 293-302.
- [49] R.B. Anderson, "Catalysis", New York: Reinhold Publishing Corporation, **1956**.
- [50] C.J. Kim, *Process for Hydrocarbon Synthesis Catalyzed by Cobalt on Titania*, European Patent, **1989**.
- [51] C.J. Kim, *Water addition for increased CO/H₂ hydrocarbon synthesis activity over catalysts comprising cobalt, ruthenium and mixtures thereof which may include a promoter metal*, United States Patent, **1993**.
- [52] C.J. Bertole, "Studies in Surface Science and Catalysis", **2004**.
- [53] G.P. Huffman, N. Shah, J.M. Zhao, F.E. Huggins, T.E. Hoost, S. Halvorsen, and J.G. Goodwin, *Journal of Catalysis*, **1995**, *151*, 17-25.
- [54] D. Schanke, A.M. Hilmen, E. Bergene, K. Kinnari, E. Rytter, E. Adnanes, and A. Holmen, *Energy & Fuels*, **1996**, *10*, 867-872.
- [55] A.M. Hilmen, "Stud. Surf. Sci and Catal.", **2001**.
- [56] A.M. Hilmen, *Surf. Sci, Catal.*, **1997**.
- [57] M. Rothaemel, K.F. Hanssen, E.A. Blekkan, D. Schanke, and A. Holmen, *Catalysis Today*, **1997**, *38*, 79-84.
- [58] J. van de Loosdrecht, P.J. van Berge, M.W.J. Craje, A.M. van der Kraan, *Hyperfine Interactions*, **2002**, *139/140*, 3.
- [59] M.W.J. Craje, A.M. van der Kraan, J. van de Loosdrecht, and P.J. van Berge, *Catalysis Today*, **2002**, *71*, 369-379.

- [60] P.J. van Berge, 14th International Congress on Catalysis: "The development and commercialization of a supported cobalt Fischer-Tropsch synthesis catalyst for the Sasol gas-to-liquids process", **2008**.
- [61] G. Jacobs, "Studies in Surface Science and Catalysis", **2001**.
- [62] G. Jacobs, T.K. Das, P.M. Patterson, J.L. Li, L. Sanchez, and B.H. Davis, *Applied Catalysis a-General*, **2003**, 247, 335-343.
- [63] A. Kogelbauer, J.C. Weber, and J.G. Goodwin, *Catalysis Letters*, **1995**, 34, 259-267.
- [64] W. Huber, "Studies in Surface Science and Catalysis", **2001**.
- [65] G.Z. Bian, N. Fujishita, T. Mochizuki, W.S. Ning, and M. Yamada, *Applied Catalysis a-General*, **2003**, 252, 251-260.
- [66] J.L. Li, G. Jacobs, T. Das, Y.Q. Zhang, and B. Davis, *Applied Catalysis a-General*, **2002**, 236, 67-76.
- [67] S. Storsaeter, O. Borg, E.A. Blekkan, and A. Holmen, *Journal of Catalysis*, **2005**, 231, 405-419.
- [68] J.L. Li, G. Jacobs, T. Das, and B.H. Davis, *Applied Catalysis a-General*, **2002**, 233, 255-262.
- [69] C.H. Bartholomew, and R.M. Bowman, *Applied Catalysis*, **1985**, 15, 59-67.
- [70] Z.T. Liu, J.L. Zhou, and B.J. Zhang, *Journal of Molecular Catalysis*, **1994**, 94, 255-261.
- [71] Z.T. Liu, Y.W. Li, J.L. Zhou, Z.X. Zhang, and B.J. Zhang, *Applied Catalysis a-General*, **1997**, 161, 137-151.
- [72] M.S. Kim, N.M. Rodriguez, and R.T.K. Baker, *Journal of Catalysis*, **1993**, 143, 449-463.
- [73] V. Curtis, C.P. Nicolaidis, N.J. Coville, D. Hildebrandt, and D. Glasser, *Catalysis Today*, **1999**, 49, 33-40.
- [74] T.K. Das, G. Jacobs, P.M. Patterson, W.A. Conner, J. Li, and B.H. Davis, *Fuel*, **2003**, 82, 805-815.
- [75] J.G. Chen, H.W. Xiang, H.Y. Gao, and Y.H. Sun, *Reaction Kinetics and Catalysis Letters*, **2001**, 73, 169-177.
- [76] G.P. Van der Laan, and A. Beenackers, *Catalysis Reviews-Science and Engineering*, **1999**, 41, 255-318.
- [77] F. Fischer, and H. Tropsch, *Brennstoff-Chemie*, **1926**, 97.
- [78] R.C. Brady, and R. Pettit, *Journal of the American Chemical Society*, **1981**, 103, 1287-1289.
- [79] O.C. Elvins, and A.W. Nash, *Nature*, **1926**, 118, 154.
- [80] H. Pichler, and H. Schulz, *Chemie Ingenieur Technik*, **1970**, 42, 1162.
- [81] S.R. Craxford, and E.K. Rideal, *Journal of the Chemical Society*, **1939**, 1604-1614.
- [82] F.R. van den Berg, M.W.J. Craje, A.M. van der Kraan, and J.W. Geus, *Applied Catalysis a-General*, **2003**, 242, 403-416.
- [83] P. Biloen, J.N. Helle, and W.M.H. Sachtler, *Journal of Catalysis*, **1979**, 58, 95-107.
- [84] G.B. Young, and G.M. Whitesides, *Journal of the American Chemical Society*, **1978**, 100, 5808-5815.
- [85] Y.T. Eidus, *Bureau of Mine Information: Circular*, **1958**, 7821.
- [86] J.T. Kummer, T.W. Dewitt, and P.H. Emmett, *Journal of the American Chemical Society*, **1948**, 70, 3632-3643.
- [87] R.C. Brady, and R. Pettit, *Journal of the American Chemical Society*, **1980**, 102, 6181-6182.
- [88] R.J. Kokes, W.K. Hall, and P.H. Emmett, *Journal of the American Chemical Society*, **1957**, 79, 2989-2996.

- [89] J.T. Kummer, and P.H. Emmett, *Journal of the American Chemical Society*, **1953**, *75*, 5177-5183.
- [90] G. Blyholder, and P.H. Emmett, *Journal of Physical Chemistry*, **1959**, *63*, 962-965.
- [91] M.E. Dry, *Applied Catalysis A-General*, **1996**, *138*, 319-344.
- [92] M.E. Dry, *Catal. Today*, **1990**, 183-206.
- [93] J. Gaube, and H.F. Klein, *Journal of Molecular Catalysis a-Chemical*, **2008**, *283*, 60-68.
- [94] M.L. Turner, N. Marsih, B.E. Mann, R. Quyoum, H.C. Long, and P.M. Maitlis, *Journal of the American Chemical Society*, **2002**, *124*, 10456-10472.
- [95] L.M. Tau, H.A. Dabbagh, and B.H. Davis, *Energy & Fuels*, **1991**, *5*, 174-179.
- [96] Y.G. Wang, and B.H. Davis, *Catalysis a-General*, **1999**, *180*, 277-285.
- [97] H. Adkins, W. Kutz, and D.D. Coffman, *Journal of the American Chemical Society*, **2002**, *52*, 3212-3221.
- [98] E. Gibson, *CHEMISTRY & INDUSTRY*, **1949**, 649.
- [99] J. Barrault, C. Forquy, and V. Perrichon, *Journal of Molecular Catalysis*, **1982**, *17*, 195-203.
- [100] A.A. Adesina, R.R. Hudgins, and P.L. Silveston, *Applied Catalysis*, **1990**, *62*, 295-308.
- [101] R. Snel, and R.L. Espinoza, *Journal of Molecular Catalysis*, **1987**, *43*, 237-247.
- [102] H. Schulz, and M. Claeys, *Applied Catalysis a-General*, **1999**, *186*, 71-90.
- [103] J.H. Boelee, J.M.G. Custers, and K. Vanderwiele, *Applied Catalysis*, **1989**, *53*, 1-13.
- [104] H.C. Long, M.L. Turner, P. Fornasiero, J. Kaspar, M. Graziani, and P.M. Maitlis, *Journal of Catalysis*, **1997**, *167*, 172-179.
- [105] A. Guiner, "X-Ray Diffraction", San Francisco and London: W.H. Freeman and Company, **1963**.
- [106] R. Krishna, and S.T. Sie, *Fuel Processing Technology*, **2000**, *64*, 73-105.
- [107] **Zero Emission Resource Organisation (ZERO)**,
[\[http://www.zero.no/transport/bio/ft3.gif\]](http://www.zero.no/transport/bio/ft3.gif).
- [108] M. Watanabe, and P. Wissmann, *Catalysis Letters*, **1991**, *7*, 15-25.
- [109] C.N. Satterfield, "Heterogeneous Catalysis in Practice", McGraw - Hill Engineering Series, **1980**.
- [110] F.A. Wigzell, M.Sc., "The characterisation of supported cobalt catalysts", *University of Glasgow*, **2007**.
- [111] R. Brown, M.E. Cooper, and D.A. Whan, *Applied Catalysis*, **1982**, *3*, 177-186.
- [112] H.F.J. Vantblik, and R. Prins, *Journal of Catalysis*, **1986**, *97*, 188-199.
- [113] B.A. Sexton, A.E. Hughes, and T.W. Turney, *Journal of Catalysis*, **1986**, *97*, 390-406.
- [114] B. Viswanathan, and R. Gopalakrishnan, *Journal of Catalysis*, **1986**, *99*, 342-348.
- [115] R. Bechara, D. Balloy, J.Y. Dauphin, and J. Grimblot, *Chemistry of Materials*, **1999**, *11*, 1703-1711.
- [116] B. Imelik, and J.C. Vedrine, "Catalyst Characterization: Physical Techniques for Solid Materials", New York: Plenum Press, **1994**.
- [117] H. van Beklam, E.M. Flanigen, and J.C. Jansen, "Introduction to Zeolite Science and Practise", Amsterdam: Elsevier Science Publishers B.V., **1991**.
- [118] Powder Diffraction File (CD-ROM). International Centre for Diffraction Data: Newton Square, **2000**.

- [119] A.Y. Khodakov, W. Chu, and P. Fongarland, *Chemical Reviews*, **2007**, *107*, 1692-1744.
- [120] B. Jongsomjit, T. Wongsalee, and P. Praserttham, *Materials Chemistry and Physics*, **2006**, *97*, 343-350.
- [121] S.L. Sun, N. Tsubaki, and K. Fujimoto, *Applied Catalysis a-General*, **2000**, *202*, 121-131.
- [122] R. Riva, H. Miessner, R. Vitali, and G. Del Piero, *Applied Catalysis a-General*, **2000**, *196*, 111-123.
- [123] V.A. de la Peña O'Shea, M.C. Alvarez-Galvan, J. Campos-Martin, and J. Fierro, *Catalysis Letters*, **2005**, *100*, 105-116.
- [124] C.M. Lok, editor. "Novel highly dispersed cobalt catalysts for improved Fischer-Tropsch productivity". **2004**.
- [125] W.J. Wang, and Y.W. Chen, *Applied Catalysis*, **1991**, *77*, 223-233.
- [126] T. Riis, S. Eri, G. Marcelin, and J. Goodwin, US Patent: 4880763, **1989**.
- [127] M-C. Marion, and M. Roy, US Patent: 6235798, **2001**.
- [128] G.L. Bezemer, J.H. Bitter, H. Kuipers, H. Oosterbeek, J.E. Holewijn, X.D. Xu, F. Kapteijn, A.J. van Dillen, and K.P. de Jong, *Journal of the American Chemical Society*, **2006**, *128*, 3956-3964.
- [129] R.C. Reuel, and C.H. Bartholomew, *Journal of Catalysis*, **1984**, *85*, 78-88.
- [130] A. Martinez, C. Lopez, F. Marquez, and I. Diaz, *Journal of Catalysis*, **2003**, *220*, 486-499.
- [131] L. Fu, and C.H. Bartholomew, *Journal of Catalysis*, **1985**, *92*, 376-387.
- [132] S.L. Soled, E. Iglesia, R.A. Fiato, J.E. Baumgartner, H. Vroman, and S. Miseo, *Topics in Catalysis*, **2003**, *26*, 101-109.
- [133] E. Iglesia, S.L. Soled, and R.A. Fiato, *Journal of Catalysis*, **1992**, *137*, 212-224.
- [134] A.Y. Khodakov, A. Griboval-Constant, R. Bechara, and V.L. Zholobenko, *Journal of Catalysis*, **2002**, *206*, 230-241.